Investigation of the Performance of Cracked Steel Members Strengthened with Carbon Fibre Reinforced Polymers under Impact Loads

By

Alaa Al-Mosawe

A thesis submitted in fulfilment of the requirements for the degree of Doctor of Philosophy

Faculty of Science, Engineering and Technology,
Swinburne University of Technology

SWINBURNE UNIVERSITY OF TECHNOLOGY

2016

Declaration

This thesis is submitted to Swinburne University of Technology, Melbourne, Australia, for the Degree of Doctor of Philosophy. All experimental and analytical work reported in this thesis was carried out by the candidate during the years 2011-2015 in the Faculty of Science, Engineering and Technology at Swinburne University of Technology, and in the Department of Civil Engineering at Monash University. This research was under the supervision of Professor Riadh Al-Mahaidi.

The candidate declares that this thesis contains no material accepted for any other degree or diploma in any university. No experimental and analytical work presented in this thesis was previously written or published by any other person except where due reference is made. All experimental and analytical programs reported in this thesis are original work.

Alaa Al-Mosawe

2016

List of Publications

During the candidature, nine reviewed journal and conference papers based on the work presented in this thesis were published or submitted for publication with Professor Riadh Al-Mahaidi and Professor Xiao-Ling Zhao.

Journal Papers

Al-Mosawe, A., Al-Mahaidi, R. & Zhao, X.-L. 2015. Effect of CFRP properties, on the bond characteristics between steel and CFRP laminate under quasi-static loading. Construction and Building Materials, 98, 489-501.

Al-Mosawe, A., Al-Mahaidi, R. & Zhao, X.-L. 2016. Experimental and Numerical Study on Strengthening of Steel Members Subjected to Impact Loading Using Ultra-High Modulus CFRP. Composites for Construction, (Accepted).

Al-Mosawe, A., Al-Mahaidi, R. & Zhao, X.-L. 2015b. Bond Behaviour between CFRP Laminates and Steel Members under Different Loading Rates. Composite structures, (under review)

Al-Mosawe, A., Kalfat, R. & Al-Mahaidi, R. 2015c. A New Formulation of CFRP-Steel Double Strap Joints using Genetic Programing. Composites Part B (under review)

Conference Papers

Al-Mosawe, A., Al-Mahaidi, R. & Zhao, X-L., A review of the bond characteristics between steel and CFRP laminate under static and impact loads. Fourth Asia-Pacific Conference on FRP in Structures (APFIS 2013), 11-13 December 2013. Melbourne, Australia: International Institute for FRP in Construction.

Al-Mosawe, A., Al-Mahaidi, R., Bond characteristics between steel and CFRP laminate under impact loads. 23rd Australasian Conference on the Mechanics of Structures and Materials (ACMSM23), 2014 Byron Bay, Australia.

Al-Mosawe, A., Al-Mahaidi, R. Strengthening of steel members subjected to impact loading using ultra high modulus CFRP. Accepted for presentation and publication at the 2nd International Conference on Buildings, Construction and Environmental Engineering (bcee2). Beirut, Lebanon 2015.

Al-Mosawe, A., Al-Mahaidi, R. & Zhao, X-L., Bond behaviour between CFRP laminates and steel members under different loading rates. Accepted for presentation and publication at The 12th International Symposium on Fiber Reinforced Polymers for Reinforced Concrete Structures (FRPRCS-12) & the 5th Asia-Pacific Conference on FRP in Structures (APFIS 2015), 14-16 December 2015, Nanjing, China.

Al-Mosawe, A., Al-Mahaidi, R. & Zhao, X-L., Finite element analysis of bond behaviour between CFRP laminates and steel members under impact load. Accepted for presentation and publication at The 12th International Symposium on Fiber Reinforced Polymers for Reinforced Concrete Structures (FRPRCS-12) & the 5th Asia-Pacific Conference on FRP in Structures (APFIS 2015), 14-16 December 2015, Nanjing, China.

Acknowledgments

I would like to express my sincere thanks to my supervisor Professor Riadh Al-Mahaidi for his expert advice, very clear guidance and continuous encouragement. Professor Al-Mahaidi has been supportive since the day I met him. I will never forget his advice, humility and simplicity in solving many huge problems, which encouraged me to complete my PhD. Professor Al-Mahaidi has supported me not only in providing research advice over the four years of study, but academically and emotionally through the journey of working together. I am proud of having worked with him in research, in academic roles, and in the development of some academic programs.

I would like acknowledge Swinburne University of Technology for providing a tuition fee scholarship throughout my study. I also acknowledge the financial support to this project provided by the Australian Research Council (ARC). I also extend my thanks to the Faculty of Science, Engineering and Technology at Swinburne University of Technology, which provided funds for local and overseas travel to participate in some international conferences. I also acknowledge the generosity of my supervisor for presenting my work at other international conferences.

The PhD journey is perilous, adventurous, and engaged with complex problems. Many people helped to eliminate this complexity by providing their advice and physical help. I wish to thank the technical staff at the Swinburne Smart Structures Laboratory (SSL), particularly Mr Michael Culton, Mr Graeme Burnett, Mr Kia Rasekhi, and Mr Sanjeet Chandra. Special thanks are extended to the Swinburne SSL Technician Mr Kevin Nievaart for his great contribution in running the dynamic tests at Monash University. I would also like to acknowledge Mr Long Goh and other laboratory staff at the Civil Engineering Laboratory at Monash University for their help and advice.

I would also like to thank all staff, PhD students and friends at Swinburne University of Technology for their friendship, encouragement and support.

Finally I wish to mention the great family that I have, who guided and helped me to complete my PhD. Even though they are overseas, I feel that my parents they are living with me at each step in my life. There is not enough space here to describe what they have done for me, but one call from them relieves all worries and anxiety that I face during my life. I am greatly indebted to my wife for her endless patience and support during my PhD journey, I would never have been able to finish my project without her support and help in taking care of our little lovely baby Ameer, whose smiling face is the source of our gladness and happiness. I would also like to extend my grateful thanks to my two brothers and my sister for their constant support during my study.

Abstract

Generally, steel structures are subjected to different types of loadings during their life-time. Over time these structures sustain fewer loads than those for which they were designed. The reduction in structural capacity might occur as a result of various parameters, including ageing, changes in use, increases in applied loads, and as a result of environmental effects causing corrosion. These structures need to be strengthened or repaired in order to be able to carry the different applied loads.

Carbon fibre reinforced polymers (CFRPs) are a new method of strengthening, the use of which has grown in the last few decades. This method of strengthening has attracted structural engineers due to its ease of application, light weight and very high tensile strength. The bond between CFRP and steel members is the main issue in understanding the bond behaviour. This thesis presents the effect of impact loading on the bond behaviour of CFRP-steel double strap joints.

The results of comprehensive experimental tests are presented in this project on the basis of testing large numbers of CFRP-steel double strap joints under both static and dynamic loadings. Another series of tests was conducted to investigate the mechanical properties of the composite material itself. The mechanical properties were investigated under different loading rates, starting from quasi-static loading at 2mm/min, to impact loadings of 201×10^3, 258×10^3 and 300×10^3 mm/min. The experimental results showed that loading rate has a significant effect on the material properties, and a significant increase was shown in tensile strength and modulus of elasticity.

The results of another series of tests are presented in this thesis. A number of CFRP-steel double strap joints were prepared and tested under quasi-static loads. Three different types of CFRP modulus (low modulus 165 GPa, normal modulus 205GPa and ultra-high CFRP modulus 460 GPa) were used, to study the effect of CFRP modulus on the bond behaviour between steel and CFRP laminates. In order to investigate the effect of CFRP geometry on the bond properties, two different CFRP sections were used (20 × 1.4mm and 10 × 1.4mm). The results showed a significant influence on the bond strength, strain distribution along the bond, effective bond length and failure mode for specimens with different CFRP modulus. The results also showed that a small CFRP section is sensitive to any little movement.

Further tests were also conducted on CFRP-steel double strap specimens with different CFRP moduli under high impact loading rates. The load rates used in this project were 201×10^3, 258×10^3 and 300×10^3 mm/min. The aim of this test was to find the degree of joint enhancement under dynamic loadings compared to quasi-static loads. The results showed a significant increase in load-carrying capacity, and strain distribution along the bond. However, a significant decrease in the effective bond length under impact loads was observed compared to quasi-static testing. Different failure modes were shown compared to specimens tested under quasi-static loadings.

Finite element analysis was conducted in this research to model the CFRP-steel double strap joint under both quasi-static and dynamic loads. The individual components of the joint (CFRP laminate, Araldite 420 adhesive and steel plates) were first modelled and analysed under the four loading rates. The CFRP-steel double strap joints were modelled using non-linear finite element analysis using the commercial software ABAQUS 6.13. The results showed good prediction of material properties and joint behaviour using non-linear finite element analysis, and the results of tensile joint strength, strain distribution along the bond, effective bond length and failure modes were close to those tested experimentally.

This thesis also shows a new formulation of CFRP-steel double strap joints using genetic programming; the data from the experimental and numerical analysis were analysed using genetic programming software. Three different parameters were used: bond length, loading rate and the CFRP modulus. The outcomes of this analysis are showing an expression tree and a new equation to express the bond strength of these types of joints. The results are assumed to be used for the range of parameters used as input data in the programming.

Finally, some suggestions on future work to continue the investigation of the bond behaviour between CFRP and steel in the double strap joints are provided.

Table of Contents

List of Figures

CHAPTER ONE INTRODUCTION

BACKGROUND

Large numbers of steel structures around the world are sustaining fewer loads than the design loads; these structures no longer satisfy the design standards. Steel structural elements such as bridges and buildings may become deficient and deteriorated because of ageing, or changes in use or increasing daily traffic, which exceed the design capacity. Corrosion also causes deformation in structures, which leads to loss of load-carrying capacity.

Bocciarelli et al. (2009) state that many structures are old and there is a reduction in their resistance to loads; 50% of the existing bridges in Europe need to be repaired for these reasons. After the Second World War the use of composite materials was limited to military, aerospace, automotive and marine applications, but composite materials were explored and then adopted for use in structural and semi-structural members (Zhao and Zhang, 2007). Advanced composite material is defined as a material that obtains its physical and mechanical characteristics through the integration of other materials. CFRP is one of the most commonly used composite materials. Carbon fibre reinforced polymers (CFRPs) have wide use in structural applications due to their particular properties. A composite material is a hybrid material produced by mixing two materials together, and these two materials exhibit their individual properties in the third material that is generated. In structural applications, the properties that are improved by combining composite materials include strength, weight, fatigue life, impact resistance, corrosion resistance, stiffness, attractiveness and temperature resistance (Bocciarelli et al., 2009; Karbhari and Shulley, 1995). The aim is to design a material with a feature suitable for the task that it is designed for.

Deteriorated structures can be repaired and strengthened using many methods of repair, such as external post-tensioning, using steel jackets, replacing the damaged or degraded elements, adding new elements to relieve overloaded parts, or enhancing the load-carrying capacity by welding or bolting steel plates. These strengthening methods are traditional and time-consuming, and may not be adequate because they increase the dead load of structures. Therefore, there is a need to find a material or method to strengthen structures without these disadvantages.

Carbon fibre reinforced polymer (CFRP) is a good modern alternative material for the rehabilitation and strengthening of structures, and it appears to be an excellent solution. CFRP is attractive to structural researchers and is increasingly being used in structural applications. It is easy to handle due to its light weight, which eliminates the need for mechanical lifting or anchoring devices, hence minimising disruption to services for the duration of the strengthening and maintenance process. Figure

The Little River Bridge in Victoria is 84 years old. Carbon fibre fabric material was used to strengthen the bridge beams for positive moments due to widening the freeway from 4 lanes to 6 lanes (Aravinthan and Manalo, 2012).

A number of researchers have focussed on the bond properties between different CFRP-steel structures under different types of loading and different parameters. Some researchers have studied the effect of fatigue loading on CFRP-bonded steel structures (Imanaka et al., 1995; Jones and Civjan, 2003; Kim and Harries, 2011a; Liu et al., 2005b; Schnerch, 2005; Buyukozturk et al., 2004; Miller et al., 2001; Cantwell and Morton, 1991; Karbhari and Zhao, 2000; Kim and Harries, 2011b) while others have studied the behaviour of CFRP-to-steel structures under static loading. There have also been extensive studies of the static load behaviour of CFRP sheets bonding steel or concrete (André et al., 2012; Fawzia et al., 2006a; Fawzia et al., 2010; Haghani, 2010; Buyukozturk et al., 2004; Czaderski and Motavalli, 2007; Benzarti et al., 2011; Capozucca, 2007; Rafi et al., 2008; Astorga et al., 2013; Ganesh Prabhu and Sundarraja, 2013; Hadi and Le, 2014; Fernandes et al., 2015; Nagai et al., 2012; Liu et al., 2009).

The bond characteristics between CFRP laminates and steel structures have not been studied yet. Due to the difficulties facing dynamic tests and numerical simulations, fewer studies have focused on the behaviour of CFRP strengthened structures under dynamic load than static loading. The difficulties facing dynamic tests and simulations are the limited availability of dynamic testing machines than those for static testing, the lack of accurate software and the limited availability of high-speed computers.

This study investigates the bond properties between CFRP laminates and steel members under impact tension load using epoxy, as this has not been studied to date. Tensile stress, bond length, failure mode and loading speed are the parameters studied in this research.

AIM OF THE RESEARCH

The main aim of this research is to investigate the dynamic behaviour of the bond between CFRP laminates and steel members under impact tensile load. It is proposed to investigate how to increase the tensile impact resistance of CFRP laminates bonded to steel structures. The specific objectives are:

- To experimentally investigate the mechanical properties of the materials used in the strengthening system, such as different types of CFRP laminate and epoxy under dynamic tensile loads. These results will be compared with those under static loads and the manufacturer's claimed figures.
- To experimentally investigate the bond behaviour and de-bonding mechanism between steel and different types of CFRP modulus under dynamic loads. The results will be compared with those of static loads.
- To investigate the effect of CFRP properties on the bond between CFRP laminates and steel members.
- To use finite element analysis to simulate a model of the dynamic bond behaviour between steel and CFRP laminates in double strap joints

All the above investigations are to obtain the mechanical bond characteristics between CFRP laminates and steel structures, and the outcomes focus on bond strength, failure modes, strain distribution along the bond and effective bond length. For the dynamic testing, three loading rates were used in the experimental tests: 201×10^3, 258×10^3 and 300×10^3 mm/min.

THESIS OUTLINE

This thesis has six chapters describing all the experimental tests and analytical models. The introduction provides a general statement of the reasons for and the best methods of strengthening structures. Today, CFRP strengthening is the most commonly used method for the enhancement of structures.

A large number of research studies are summarised in Chapter Two. The literature review includes methods of surface preparation before applying CFRP to the deteriorated structures, the bond behaviour between CFRP and steel under different types of loading, the bond behaviour of CFRP-bonded steel members subjected to tension loading, and a summary of the analytical modelling of CFRP-to-steel structures subjected to tensile loads.

Chapter Three describes the comprehensive experimental tests and presents the results of the bond characteristics between CFRP laminate and steel members. A number of CFRP-steel double strap joints were prepared and tested under a loading rate of 2mm/min. Araldite 420 was used to bond the CFRP to the steel joints; different CFRP sections and modulus were used to achieve a full understanding of the bond behaviour.

Chapter Four describes the experimental investigation of the bond characteristics between CFRP laminate and steel joints under dynamic loading. A number of CFRP-steel double strap joints were prepared and tested under three different loading rates: 201×10^3, 258×10^3 and 300×10^3 mm/min. Three types of CFRP modulus were used, and the results were then compared with those from the static tests to obtain the bond enhancement.

Chapter Five presents the numerical simulation of all specimens tested under quasi-static and dynamic loadings, and finite element analysis was used to model the specimens with different parameters using ABAQUS software. The results from finite element analysis are compared with the results from the experimental tests to validate the efficiency of finite element analysis in modelling the failure mechanisms and other mechanical properties.

Chapter four presents a genetic programming to generate an expression tree and equation model of the bond strength for CFRP-steel double strap joints. The input data were obtained from both experimental tests and analytical models.

Chapter Seven provides all the results and outcomes of this research, and makes some recommendations for future research.

CHAPTER TWO LITERATURE REVIEW

2.1 INTRODUCTION

Carbon fibre reinforced polymer (CFRP) composite material has been used for strengthening structures since the Second World War. It has been used in different applications in the military, and in the aerospace and automotive industries. The use of CFRPs for strengthening and repair is recognised as an excellent method for strengthening steel elements. CFRP is also used in civil engineering applications to strengthen different structural elements in bridges, buildings, off-shore platforms etc. However, CFRP strengthening and repair of structures has some challenges, and the mechanical properties of CFRP have some effect on the strengthening outcomes, such as bond strength and ultimate strain values. Furthermore, the bond between CFRP and structural elements is a key issue for different load applications with static and dynamic loadings. The preparation of bonded surfaces also has some effect on the efficiency of the bond properties between steel or concrete structural elements. It is important to choose the most suitable type of adhesive, depending on the structural application and type of loading. Adhesive debonding is the most common failure mechanism in adhesively bonded joints, and depends on the adhesive type used and other CFRP properties. To use CFRP composite material in strengthening structural elements, all the above aspects need to be fully understood. Consequently, a review of the relevant literature is presented in this chapter to focus on the effect of different parameters on the bond between CFRP and steel structural elements. Generally, the variables used in the literature are the mechanical properties of CFRP, the type of adhesive used to bond the composite material to the deteriorated structural element, the surface preparation of the structural element, and the effect of different velocities on the joint strength of FRP-structural elements.

2.2 PROPERTIES OF FRP COMPOSITE MATERIAL UNDER DIFFERENT STRAIN RATES

As steel or concrete structures are usually subjected to static and dynamic loads during their service life, these structures deteriorate and need to be strengthened. One of the possible methods of strengthening is the use of FRP composite materials to enhance the structural capacity. To have a good understanding of the bond between CFRP and steel or concrete structures, the properties of CFRP itself need to be examined. Many previous studies used the mechanical properties provided by the manufacturers, and some researchers have investigated the mechanical properties of FRP and other materials as per the load conditions used in tests. The manufacturer's technical sheets usually provide the static properties of a material, such as elastic modulus, tensile strength and ultimate strain, without showing the tensile or compressive dynamic properties of the material.

A large number of experimental investigations have been conducted to study the tensile mechanical properties of various types of FRP, and static and dynamic tensile loading are the main loadings used in the research literature. Jacob et al. (2004) presented a review of the strain rate effect on the material properties of some FRP composites. The main focus of Jacob et al. research is to review research on the effect of velocity to gauge length ratios, and then the effect of these ratios on different mechanical properties of FRP under different applied loads are studied.

There are different methods of performing impact testing on FRP composite materials. The Charpy pendulum, drop mass, hydraulic instruments and split Hopkinson pressure bar are techniques available to obtain the desired strain rate, each of these techniques can achieve a range of strain rates. These methods are summarised by Deshpande (2006). Harding and Welsh (1983) modified the split Hopkinson pressure bar technique for testing materials with unidirectional fibres such as FRPs under high tensile loading rates. Their research showed that the mechanical properties of glass fibre reinforce polymers (GFRP) are significantly affected by strain rate for both 0° and 45° fibre directions.

Another method of testing unidirectional fibres under high loading rate was presented by Adams and Adams (1989), who modified the Charpy or Izod impact tester to test materials under high loading using a pendulum impact tester. This pendulum impact machine has a maximum supply energy of 325 N.m and maximum velocity of 5.2 m/s. Carbon-epoxy, glass-epoxy and pure adhesive specimens were tested using this technique, and the results showed that the strain rate had no effect on the energy absorption of CFRP.

Glass-epoxy and carbon fibre-epoxy specimens were tested with different strain rates starting from 100 to 250 s^{-1} using the Hopkinson pressure machine. The results showed that the higher the strain rate, the more significant the effect on the mechanical properties of the composite materials. The tensile stress and elastic modulus of carbon fibre-epoxy were increased significantly with the increase of strain rates. Less strength increment was observed for glass-epoxy specimens for both Young's modulus and tensile strength ((Lifshitz and Leber, 1998).

Adams and Adams (1990) continued their investigation of the mechanical properties of composite materials under impact loads, and a range of loading rates (quasi-static, 2.1, 3.1 and 4.9 m/s) were applied to carbon-epoxy and glass-epoxy specimens. The results showed that with the strain rate increase, there was a decrease in elastic modulus and an increase in tensile strength for both carbon-epoxy and glass-epoxy.

In 1996, an investigation of the dynamic properties of GFRPs was reported by Barré et al. (1996). Different strain rates were used, starting from 10^{-1} to 10^{+1} s^{-1} using a drop-mass technique to produce impact load. The results showed that increasing the load rate has increased the tensile elastic modulus and strength .

Hou and Ruiz (2000) studied the mechanical properties of woven CFRP T300/914 at different velocities. Tension, compression and in-plane shear tests were applied to two types of CFRP specimens, and 0° and 90° were the orientations of the specimens. The split Hopkinson pressure bar machine was used for tension and compression tests, and Figure 2.1 shows the compression split Hopkinson pressure bar.

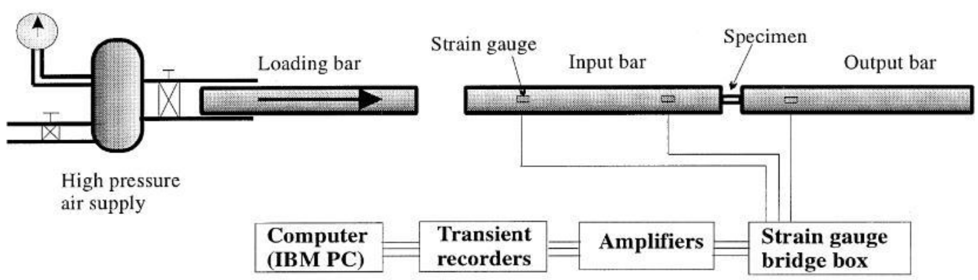

Figure 2.1: Compression split Hopkinson bar apparatus (Hou and Ruiz, 2000)

The results showed elastic behaviour for both types of specimens (0° and 90°) under tensile loading until failure. Linear elastic behaviour was observed for specimens tested under tension loading, while plastic deformation occurred for specimens tested under compression impact loading. The results also showed that CFRP laminates are strain rate-dependent, due to the fact that epoxy has higher shear and tensile strengths at high strain rates, while an insignificant effect was shown for pure fibre specimens.

The influence of high strain rates on the energy absorption of woven glass-fibre laminates was investigated by Okoli (2001). Three types of loading, tensile, shear and three-point bending were used in this study. The results showed linear behaviour between expended energy and strain rate. The mechanical properties were increased for each decade increment of strain rates. The tensile strength was increased by 17%, while shear stress was increased by 5.9 and the flexural energy was increased by 8.5%. The failure mode showed laminate brittle failure for high strain rates, initiated from matrix failure and propagated to final laminate fracture as shown in Figure 2.2.

Figure 2.2: Fibre brittle failure of woven glass-epoxy with fibre breakage (Okoli, 2001)

Fernie and Warrior (2002) used a drop-mass instrument to test composite materials under different strain rates. The aim of this study was to investigate the effect of high strain rates on the mechanical properties of glass polyester material, and to find the strain rate dependency of the material for both tension and compression loadings. The results showed an increment in ultimate strength of 115% in tension and 26% in compression for a strain rate of 5^{-1} ms^{-1}, while the increase in Young's modulus was recorded as 43% in tension and 9% in compression for the same strain rate.

Research was conducted by Majzoobi et al. (2005) to study the tensile mechanical properties of glass-epoxy composite materials under high strain rates. The R2000 glass-epoxy composite specimens were tested under a low strain rate (10^{-3} s^{-1}) and a high strain rate of 850 s^{-1}. Comparing the results of the two strain rates, a significant increase in the material tensile stress was observed under high strain rates compared to very low strain rates, while a reduction in ultimate strain was observed for specimens tested under high strain rates compared to those tested under low strain rates. The percentage of increment ranged from 300% to 500% for tensile strength, while the reduction percentage ranged between 60% and 75% for ultimate failure strain. The range of tensile strength increment was for different ply orientations.

Al-Zubaidy et al. (2011) investigated the mechanical properties of normal CFRP modulus and Araldite 420 adhesive under impact tensile loads. Quasi-static and impact tensile loads were conducted to determine the degree of increment in CFRP mechanical properties. The results showed 20-40% tensile strength increment, while the ultimate strain of CFRP was increased by 20%. The results of adhesive coupon tests showed increases in Young's modulus of 100% and 220% for the tensile strength. A 20% reduction in ultimate strain was observed for the adhesive under impact loading. Two strain rates were used for quasi-static testing (2.42×10^{-4} s^{-1} and 6.66×10^{-4} s^{-1}), while three high strain rates were used for impact tests (54.2, 67.2 and 87.4 s^{-1}).

2.3 SURFACE PREPARATION FOR BONDING CFRP TO STEEL STRUCTURES

The interface between CFRP and any structural element is the most important and sensitive part in the joints. The bond properties between CFRP and steel are affected by different factors such as the bond area, adhesive type, adhesive thickness and surface preparation. In order to achieve good interaction between the structural steel elements and the CFRP, the surfaces of the steel and CFRP need to be treated carefully. The major aspect of this treatment is the method of surface preparation, and a guide to surface preparation between metal and adhesive is provided in ASTM D2651-01(2008). The different methods of surface preparation proposed are most likely intended for small-scale applications. However, it is worth using a method that can be implemented in actual strengthening applications. The aim of surface preparation is to achieve a good degree of surface roughness to provide good interaction between the two layers. Grinders and sandblasters are the two main methods of surface preparation used by researchers. The two main requirements are direct contact between adhesive, CFRP and steel and the removal of weak layers or contaminations at the bonded area (Hutchinson, 1987). Meeting these two requirements has a positive effect on the CFRP utilization. Miller et al. (2001) suggest the use of grinders or sandblasters to prepare the flange surface of steel girders, and this preparation is to be carried out before the application of glass fibre fabrics within the adhesive layer between CFRP laminate and the flange of the steel girder. The aim of using glass fibre in the adhesive joints is to prevent corrosion of steel, which might occur by the galvanic reaction between steel and CFRP. The effect of the sizing agent on the galvanic corrosion rate was investigated by Tavakkolizadeh and Saadatmanesh (2001), who found that galvanic corrosion occurs when there is direct contact between CFRP and steel surface. The researchers used different solvents to check their efficiency in removing the sizing agents from the laminated fibres, and cleaning with epoxy was found to be most effective solvent for removing solvent agents. A fresh chemical active surface must be prepared to ensure that the bond has a good interaction with the adjacent layer, as reported by Hollaway and Cadei (2002). Their study also showed that the degree of bond efficiency between CFRP and steel or concrete is directly proportional to the method of surface preparation, starting from hand abrasion to mechanical abrading. The cleaner the surface, the higher the degree of bond efficiency. Other researchers have argued that any contamination left on the steel or concrete surfaces before applying the CFRP may cause reduction in the joint strength (Mays and Hutchinson, 2005; Hashim, 1999). The bond behaviour of FRP-bonded steel plates was studied by (Fawzia, 2008), who ground the steel surface using a grinder and then CFRP sheets were attached. Finally the double strap joints were tested under static loading in order to obtain the maximum joint capacity and failure modes. This research was continued by Al-Zubaidy (2012), the main difference between the two studies being the surface preparation method of the specimens. The study used sandblasting in order to examine the bond properties of CFRP-steel double strap joints under quasi-static loading, and the results showed some extra enhancement in joint strength when using sandblasting rather than grinding.

2.4 CFRP-BONDED STEEL STRUCTURES

Metal bridges, off-shore platforms and buildings need to be monitored and strengthened for different load types, but the conventional methods of strengthening are time-consuming, and mechanical lifters are required to attach the new elements to the degraded parts. Carbon fibre reinforced polymers (CFRPs) are now the most common method of strengthening, due to their light weight and high strength. As mentioned above, the most important part in the CFRP strengthening of steel or concrete structures is the bond. A number of studies have focussed on the bond characteristics between FRP and steel beams, columns, girders and steel boxes. A large number of parameters affect bond strength, most being related to the properties of the CFRP and the adhesive.

Colombi and Poggi (2006a) studied the effect of adhesive bonding CFRP laminates to H-shape steel beams. An identical steel beam was tested under three-point testing as a reference for those strengthened with CFRP strips. Different CFRP section properties were attached to the bottom flange of the steel beams with two types of adhesive, Sikadur 30 and Sikadur 330. The main objective of the research was to investigate the load transfer criteria and to find the enhancement in strength of the beam for the two types of adhesives. In order to have good understanding of strength enhancement, the beams were bonded with one and two plies of FRP laminates. A number of strain gauges were mounted on the CFRP surface to monitor the strain distribution along the bond area. A schematic view of the beam with CFRP attached to the tension flange is shown in Figure 2.3 below.

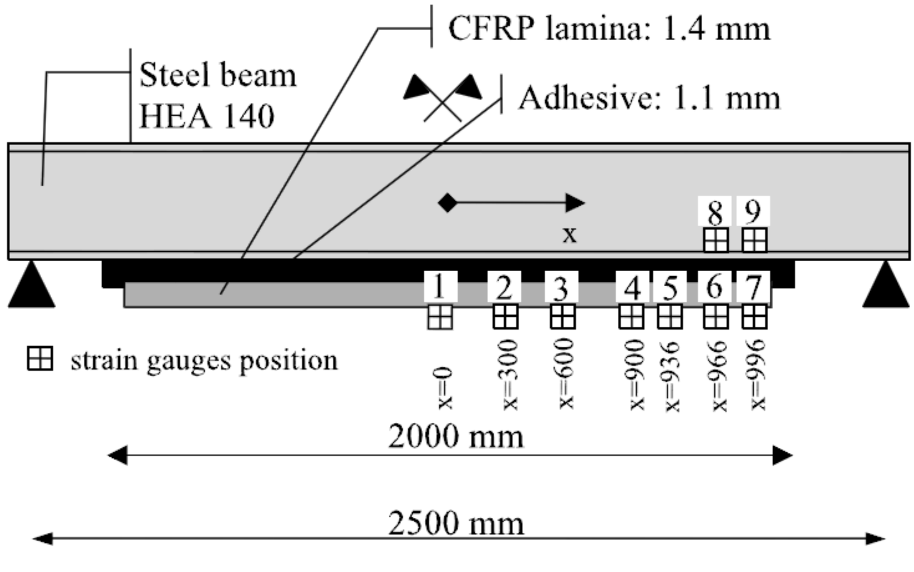

Figure 2.3 Schematic view of CFRP strengthened steel beams (Colombi and Poggi, 2006a)

The results showed that for specimens with one CFRP layer and Sikadur 30, the enhancement in load was 9.2%, which was close to that of the specimens with Sikadur

330, while the increment was about 23% for specimens with two layers of CFRP laminates and Sikadur 30 adhesive. In relation to the stiffness of the specimens, there was no increase in beam stiffness for specimens with one layer of CFRP, but it was increased by 13.8% for beams with two CFRP layers.

Another series of tests was carried out by Dawood and Rizkalla (2007) and Dawood et al(Dawood et al., 2009)(Dawood et al., 2009)., 2009. I-section steel beams were strengthened with main CFRP laminates and an additional splice of CFRP laminate, and the beams were subjected to 3-point bending tests. Different lengths of splice plates were used to find the effective length, with 200, 400 and 800mm being used in this research. The results of the three-point tests showed that all specimens experienced sudden debonding of the splice plate, the debonding starting from one of the splice ends and going towards the joint, then propagating to the interface between the CFRP main plate and the splice plate. The debonding failure is shown in Figure 2.4. The results also showed that increasing the splice length beyond 400mm produced an insignificant increase in ultimate beam strength.

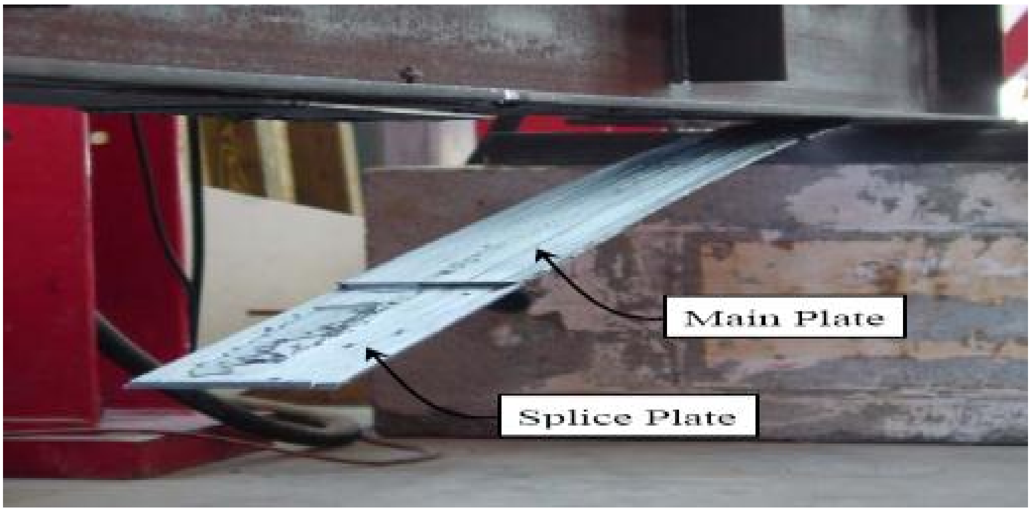

Figure 2.4: Failure of splice beam under four-point bending (Dawood and Rizkalla, 2007)

Three- and four-point load tests of CFRP strengthened steel beams were carried out Deng and Lee (2007). A mild steel beam was strengthened with CFRP laminate with a thickness of 0.3mm using Sikadur 31 adhesive. A servo-hydraulic Dennison 8032 testing machine with a capacity of 200 kN was used. The results showed an increase in load when the bond length of the CFRP increased from 300mm to 1000mm. In this study, a comparison of two strengthened beams with different CFRP thicknesses was made. The results showed that increasing CFRP thickness causes a reduction in strength enhancement, because of the high stress concentration at the end of the thicker laminate. A slight increase in strength (5%) for specimens with spew fillet at the end of laminate, showed that increasing bond length had no effect on beam stiffness, whereas increasing the CFRP thickness decreased the beam's stiffness. Figure 2.5 shows the load-deflection curves of two specimens, where S305 is the specimen with 3mm CFRP thickness, while S305D has 6mm CFRP thickness.

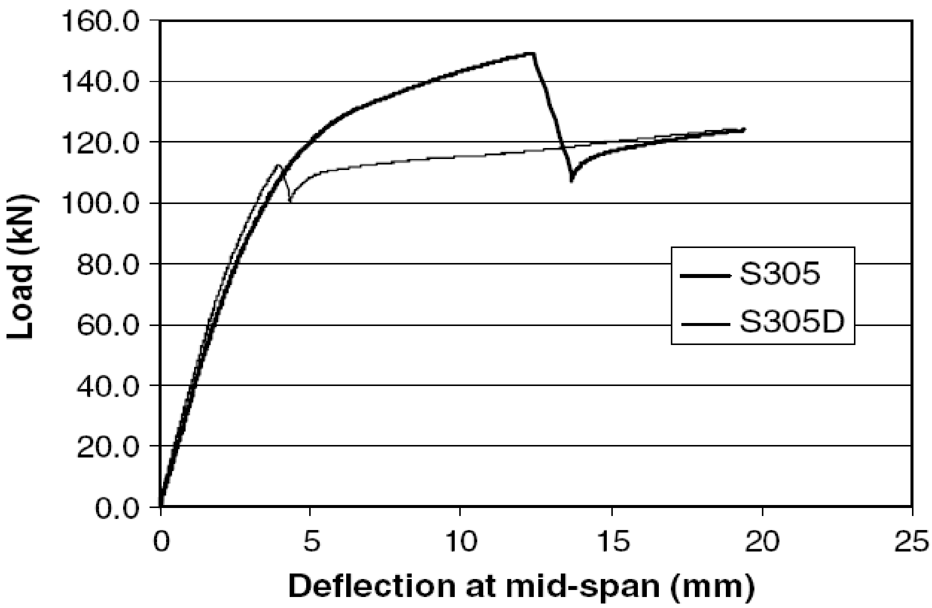

Figure 2.5: Load-deflection curves of different CFRP thicknesses (Deng and Lee, 2007)

In terms of failure modes, two main failure modes were observed. For beams with 3mm CFRP thickness, full debonding of CFRP laminate occurred, while debonding with some CFRP delamination was shown for beams with 6mm CFRP.

Another four-point test on full-scale FRP-strengthened steel beams as shown in Figure 2.6 was carried by Yu et al. (2011) . The authors used three parameters, laminate thickness, bond length and adhesive thickness. A full-scale non-strengthened steel beam was tested as a reference for those strengthened with FRP laminate. The results showed that the adhesive thickness has a significant effect on the total deflection, the larger adhesive thickness producing the lower beam deflection. Table 2.1 shows a summary of the test parameters and results.

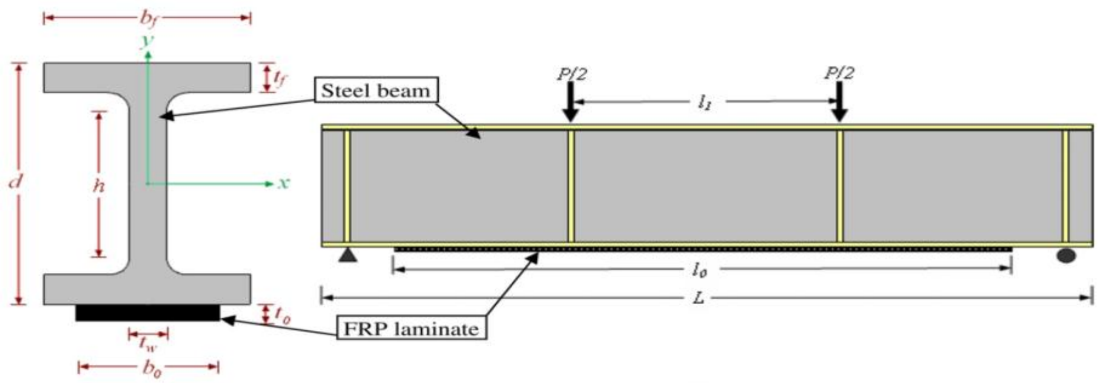

Figure 2.6: Schematic beam with flexural CFRP reinforcement (Yu et al., 2011).

Table 2.1: Test property results of CFRP-bonded steel beams (Yu et al., 2011).

Specimen	L(mm)	L_0 (mm)	t_0 (mm)	t_a (mm)	P (KN	Failure mode
B1	1800	-	-	-	177.1	B
B2	1800	700	1.5	0.5	185.5	A
B3	1800	700	4.5	0.5	200.0	A
B4	1800	700	7.5	0.5	206.9	A
B5	1800	700	1.5	1	183.6	A
B6	1800	700	1.5	2.5	178.9	A
B7	2400	-	-	-	120.8	B
B8	2400	750	1.5	0.5	122.9	A
B9	2400	850	1.5	0.5	127.7	A
B10	2400	1050	1.5	0.5	134.1	A
B11	2400	1450	1.5	0.5	140.8	B

B: Beam Yielding
A: Beam Yielding followed by debondng of FRP laminate

As the above table shows, beam strength was increased when the thickness of the CFRP increased from 1.5 to 4.5, but an insignificant increase was observed when the thickness increased to 7.5mm CFRP. The results also showed that adhesive thickness ha an insignificant effect on beam capacity. However, the load resistance increases as the bond length of the FRP laminate increases.

The axial capacity of a steel square hollow section (SHS) strengthened with CFRP sheet was investigated by Bambach et al. (2009). The SHSs were fabricated by spot-welding with different wall thicknesses (1.6mm and 2mm). MBrace CF-130 was bonded the exterior walls of the SHS using Araldite 420 resin. Two different fibre layouts were attached: one layer laid transversely, and the other longitudinally to the direction of axial load. as shown in Figure 2.7.

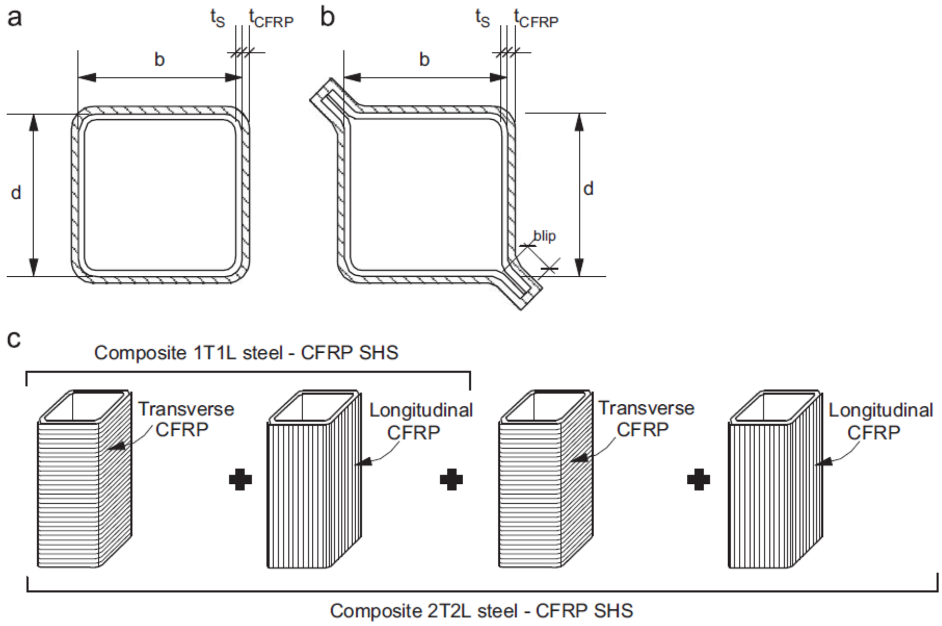

Figure 2.7: Specimens with CFRP strengthening. (a) SHS (commercially produced). (b) SHS (spot-welded). (c) Preparation method for bonded specimens (Bambach et al. 2009)

The specimens were tested under axial compression load. The axial capacity increased by 200% of the ultimate steel strength alone, and the stress-to-weight ratio increased up to 50%; buckling stress increased up to 4 times that of steel section alone.

2.5 BOND PROPERTIES OF FRP-BONDED AND STEEL MEMBERS

Tensile tests are among the most common basic tests conducted for testing composite materials. Many studies have focussed on the behaviours of different types of FRP composite materials with steel structures under static tensile loads. Studying this kind of load is important, as it represents many applications in civil engineering. The main outcomes observed from these tests are the bond strength, failure mode and the effective bond length. The effective bond length of adhesive joints bonded by FRP composites was first predicted by Hart-Smith (1973) , and the Hart-smith model was found to evaluate the effective bond length for single lap joints, the model being correlated with experimental tests. The effective bond length can be defined as the bond length beyond which no further increase in joint strength occurs. The effective bond length was then studied by number of researchers with different parameters. Matta (2003) studied the bond behaviour between steel and CFRP laminates, the research summarised all types of lap joints as shown in Figure 2.8.

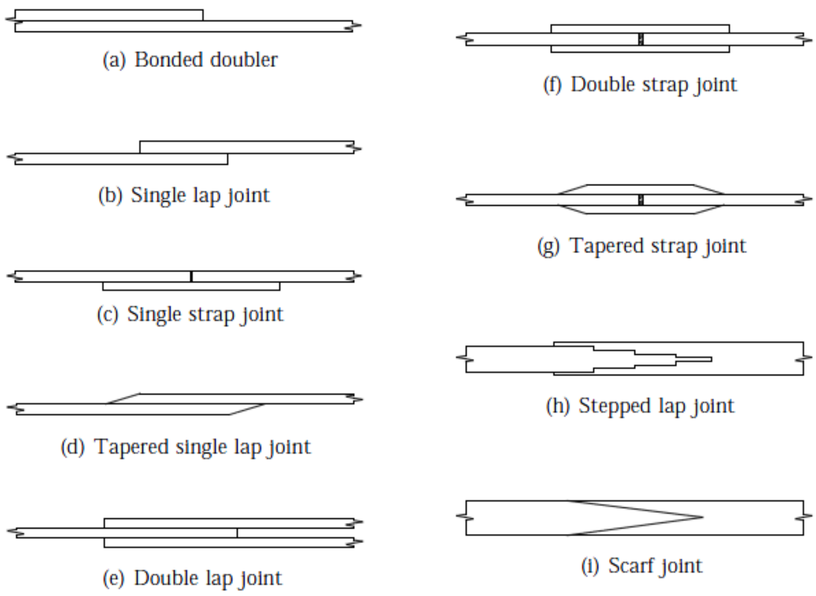

Figure 2.8: Typical configurations of structural adhesive joints (Matta, 2003)

Jiao and Zhao (2004) studied the strengthening of butt-welded very high strength circular steel tubes using CFRP sheets. Three types of epoxy resin (Sikadur-330, Araldite1 420 and Araldite1 Kit K138) were used to bond a total of 21 specimens of CFRP-steel butt-welded joints, and a Baldwin universal testing machine with a maximum capacity of 500 KN was used with a loading rate of 2 mm/min. The 21 specimens were tested under axial tensile load to obtain the bond shear strength. The researchers used SikaWrap Hex-230C CFRP, which has a typical unidirectional tensile strength of 3500 MPa and a Young's modulus of 230 GPa with an ultimate strain of 1.5%. The joint was bonded using 5 layers of CFRP fabrics; the thickness of one layer is 0.13mm. The main focus of this study was to find the influence of adhesive type on the bond properties between CFRP and steel members. Joints with Araldite 420 had the highest bond strength compared to other types of joints. Figure 2.9 shows the schematic view of the specimens tested under static tension load and the arrangement of joint layers.

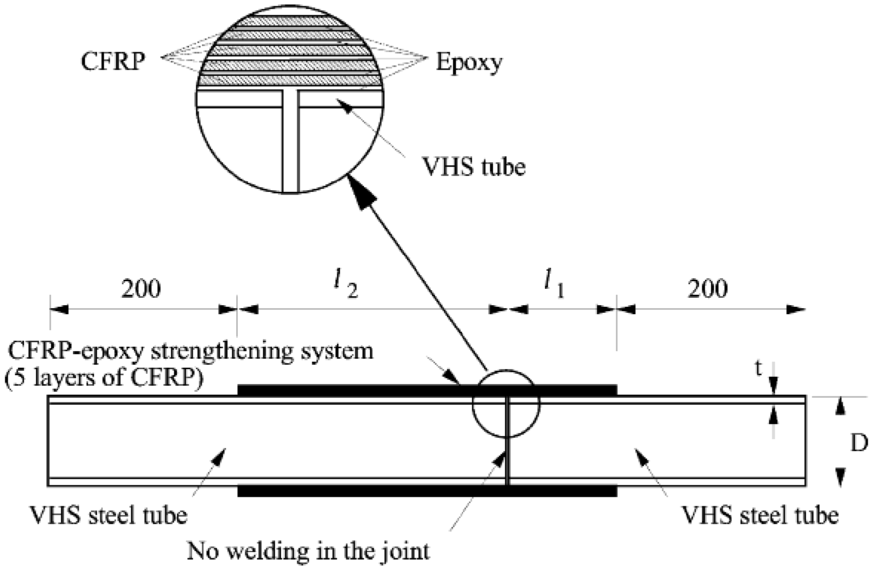

Figure 2.9: CFRP-steel double strap joints with 5 layers (Jiao and Zhao, 2004)

The results showed that the bond strength increases as the bond length increases, and there was an insignificant increase in bond strength when the bond length exceeded 75mm. Therefore, this bond length was considered to be the effective bond length for this type of joint. Figure 2.10 shows the relation between shear stress and bond length plotted from the experimental tests using the equation below:

$$V=\frac{P_{ult}}{\pi\, D\, L_1} \qquad \text{Equation 2-1}$$

where, P_{ult} is maximum joint force observed from the test; D is the external diameter of VHS tube; L_1 is the bond length, as shown in Figure 2.9. The graph shows high shear stress for specimens with short bond length and it decreases as the bond length increases.

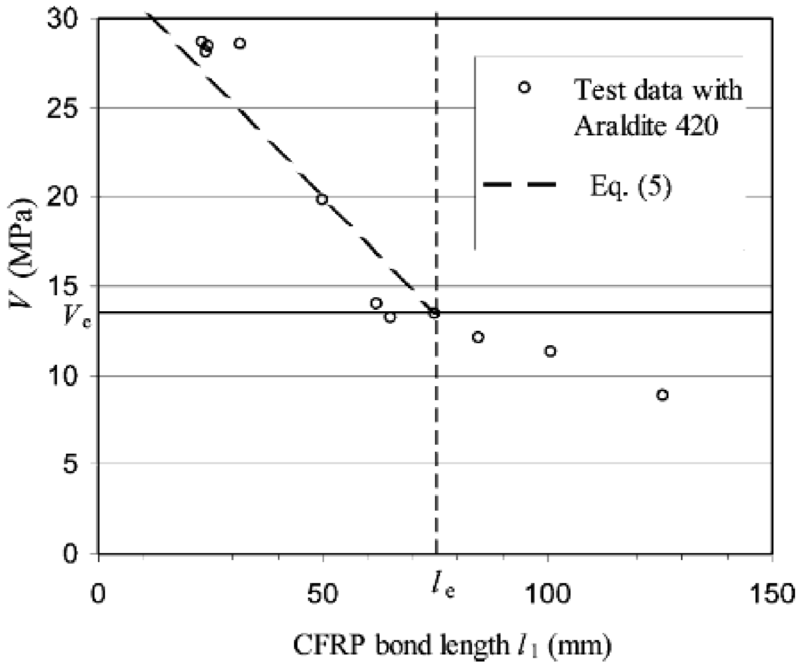

Figure 2.10: Shear stress vs. bond length for CFRP sheet-bonded VHS tube (Jiao and Zhao, 2004)

The failure mode was compared with the classification of seven failure modes mentioned in ASTM D5573, and different failure modes were observed with the different epoxies. In general, the most common failure modes for these specimens were adhesive failure and fibre-tear failure. Araldite 420 was found to be the most suitable epoxy for strengthening butt-welded VHS as it prevents fibre-tearing failure.

A pull-off test of CFRP-to-steel plate was conducted by Xia and Teng (2005) , where a tensile force was applied to the FRP laminate and the steel beam was fixed at the loaded end, as shown in Figure 2.11.

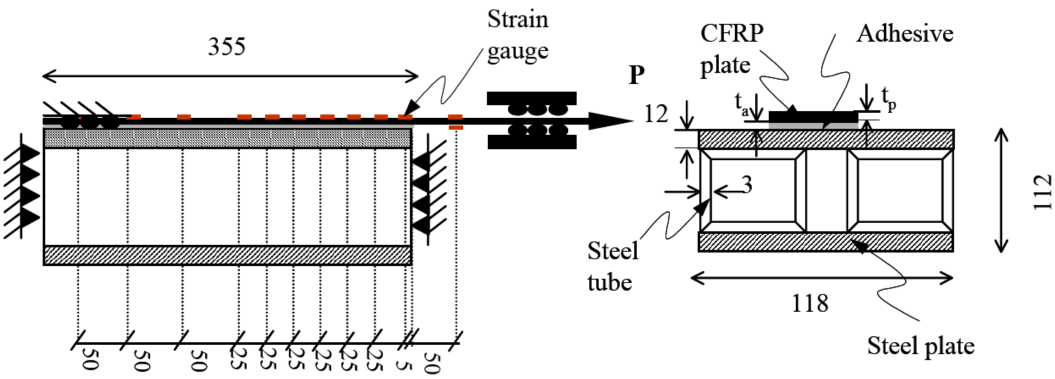

Figure 2.11: Pull-off test specimen and set-up (Xia and Teng, 2005)

Three different adhesive types were used in this experimental program, and the specimens were tested under static loading. The mechanical properties of the three adhesives are summarised in Table 2.2 below:

Table 2.2: Mechanical properties of the three adhesive types used by (Xia and Teng, 2005)

Adhesive	Tensile strength (MPa)	Young's modulus (MPa)	Poisson's ratio	Ultimate strain
A	22.53	4013	0.36	0.5614
B	20.48	10793	0.27	0.1898
C	13.89	5426	0.31	0.2560

The above adhesive types were applied with different thicknesses to evaluate the effect of adhesive thickness on the bond behaviour. The results showed that there was a significant effect on the failure mode for the different adhesive thickness. When the adhesive thickness is less than 2mm, debonding failure occurred, while FRP delamination failure occurred for thicker adhesive layers. The behaviour of the three adhesives was initially linear behaviour, and then became slightly non-linear and they suddenly failed by rupture. However, a bilinear bond-slip model can approximate these experimental curves closely. The proposed bilinear model has three key points as a definition of the curve; the origin (0, 0); the peak shear stress point ($\delta 1$, τf); and the ultimate point (δf, 0). The area below the curve is the interfacial fracture energy (Gf), as shown in Figure 2.12.

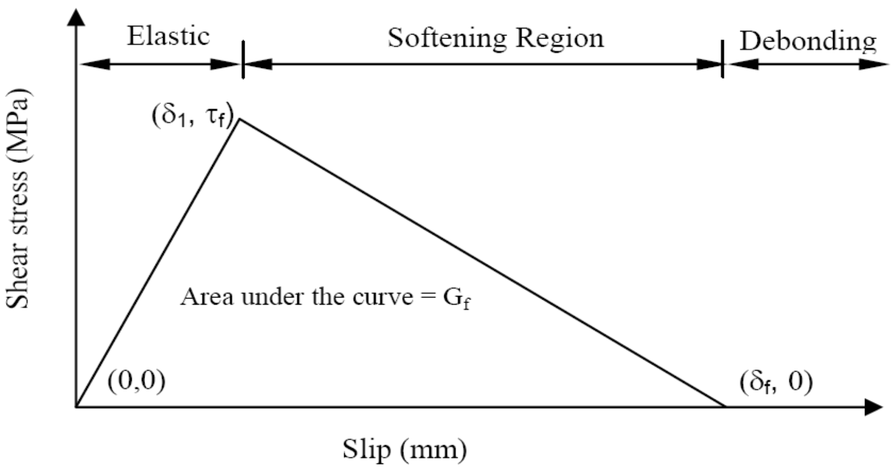

Figure 2.12: Shear stress vs. slip (Xia and Teng, 2005)

The peak and ultimate coordinate points were derived from the experimental results. When the adhesive has a high modulus of elasticity, the load-displacement curve shows a higher initial slope, and vice versa.

Continuing the previous research, another set CFRP-steel of double strap joints were tested using a Baldwin universal testing machine with a maximum capacity of 500 kN by Fawzia et al. (2010). The aim of this research was to study the bond-slip models of CFRP sheets bonded to steel plates within double strap joints. Foil strain gauges (VMMCEA-13–240UZ-120) were utilized to monitor the strain distribution along the bond line. Different parameters were used in this testing program to investigate their effect on joint behaviour and the bond slip model. The parameters used in this research were: two types of CFRP (normal modulus and high modulus), three types of adhesives (Araldite 420, MBrace saturant and Sikadur 30), two thicknesses of CFRP layers (3 and 5 plies), and different bond lengths (80–250 mm). The researchers investigated the bond slip of specimens with different adhesives, and the results showed that specimens with Araldite and MBrace had the same initial slip (the slip at maximum shear strength) of 0.05mm, whereas it was 0.04mm for specimens with Sikadur adhesive, as shown in Table 2.3 below:

Table 2.3: Material properties for three different adhesives (Fawzia et al., 2010).

Adhesive type	Shear stress (MPa)	Initial slip (mm)	Maximum slip (mm)
Araldite 420	30	0.05	0.12
MBrace saturant	23	0.05	0.12
Sikadur 30	22	0.04	0.1

In addition, the thickness of adhesive layer had a large effect on the bond slip model, the bond slip increasing as the adhesive thickness increased. The bond slip model observed from this research was a modification of the bond slip model proposed by Xia and Teng (2005) .

Colombi and Poggi (2006b) studied the strengthening of bolted joints using adhesively-bonded CFRP laminates in three groups of specimens. The first group included three types of specimens: two specimens with continuous steel plates, and the third specimen included a 20mm diameter hole with double-sided CFRP laminate. The second group included strengthening a gap of two steel plates with CFRP. The third group was a bolted joint between CFRP laminate and steel plate. The CFRP used in this test was Sika Carbodur M614, the adhesive was Sikadur 30, and the specimens were tested under static tensile load. The results showed a slight difference between the yield load of the specimens without strengthening, and that of the reinforced specimens. For specimens with a 20mm hole the stress distribution along the CFRP is shown in Figure 2.13.

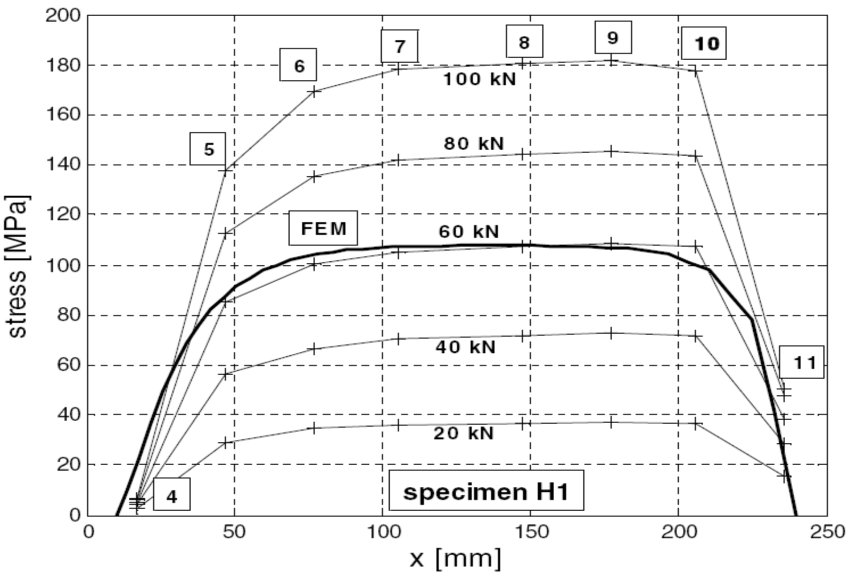

Figure 2.13: Distribution of stress with load variations along the CFRP (Colombi and Poggi, 2006b)

For the double-lap specimens, the strain gauge near the applied load and far from the joint showed a nonlinear curve starting from 35 KN. This was attributed to the non-linearity behaviour of Sikadur 30 at high load levels near the ends of the CFRP layer, while the other strain gauges near the joint showed a linear stress-strain curve response. In the bolted joints (see Figure 2.14), Sikadur 330 and Sikadur 30 adhesives were used. The results for specimens with Sikadur 330 showed that the response was almost linear up to 84.1 kN without debonding failure of the joint. When local composite failure occurred, the load increased to around 117 kN, identical to the yield load of the steel plate. Then, debonding occurred. However, the results of specimens with Sikadur 30 showed a different behaviour of the load displacement curve. With this adhesive, composite failure and FRP debonding occurred at the same previous load level.

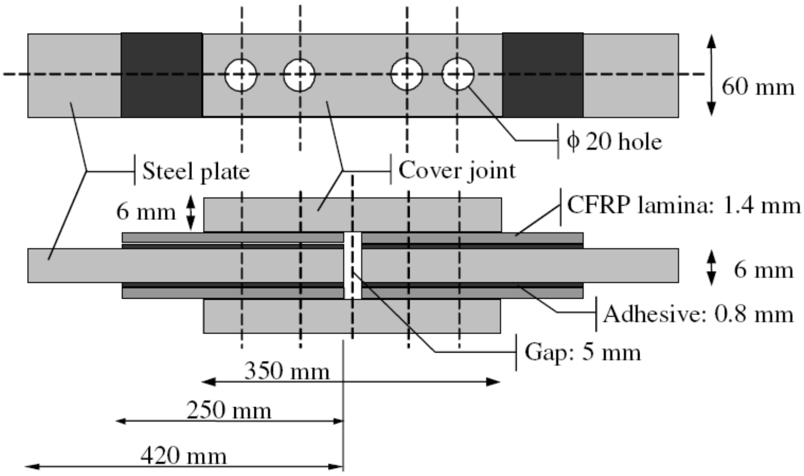

Figure 2.14 Schematic sketch of strengthening of bolted joint (Colombi and Poggi, 2006b).

Fawzia et al. (2006) studied the bond characteristics of CFRP-steel double strap joints using CFRP sheets. Normal modulus CFRP CF130 was used with a thickness of 0.176mm per layer. Three CFRP layers strengthened the joints using Araldite 420. Four specimens of CFRP-steel double strap joints were tested under axial tensile load at a loading rate of 2mm/min. The effective bond length was consistent with that reported in Jiao and Zhao (2004). Strain gauges were used to measure the strain distribution along the bond length, and the results showed that as the applied load increased, the strain at the first and second gauges increased significantly. The strain readings after the third gauge were very small and became almost zero at a distance of 75 mm from the loaded edge. In terms of load versus bond length, the curve showed linear increment for bond lengths less than the effective bond length and then it kept steady beyond bond length equal to 75mm, this bond length is the effective bond length as shown in Figure 2.15

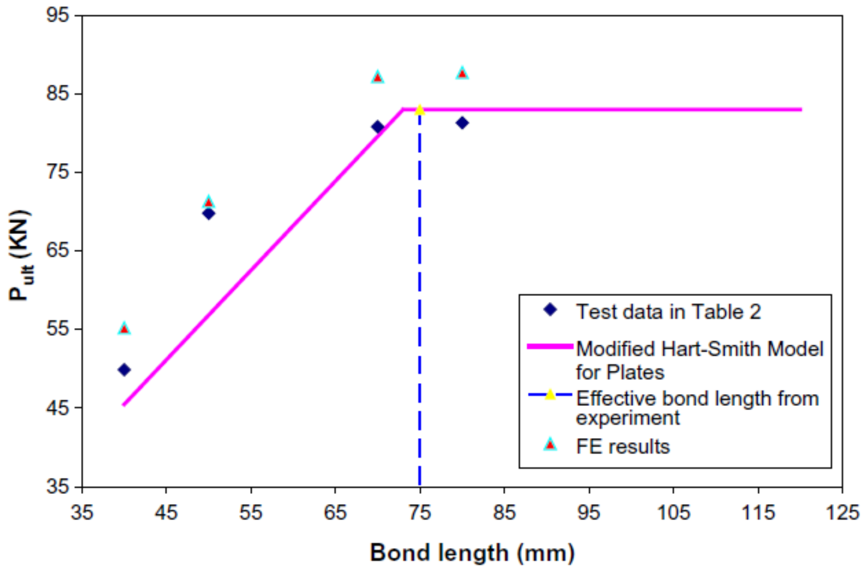

Figure 2.15: Bond force vs. bond length (Fawzia et al., 2006a).

Another study investigated the bond properties between CFRP and steel for different lap joints. Dawood and Rizkalla (2007) prepared six double-lap shear specimens to find a suitable method of bonding high modulus CFRP to steel beams. The most suitable method was decided according to the reduction in bond stress concentration, which usually occurs near the ends of the laminate. The bond configurations are shown in Figure 2.16. The results of the double-lap shear specimens showed that all specimens failed by sudden debonding of the CFRP laminate, with some adhesive remaining on the steel plate. In addition, the specimen with reverse tapers at the end of the laminate and at the middle of the joint (T2) showed an 80% increase in load capacity of the bonded joint compared with the specimens with square ends and T1. The clamped specimens showed additional 80% increase compared with T2. The same load enhancement was found for CFRP-strengthened steel beams with rounded or tapered ends and tested under bending.

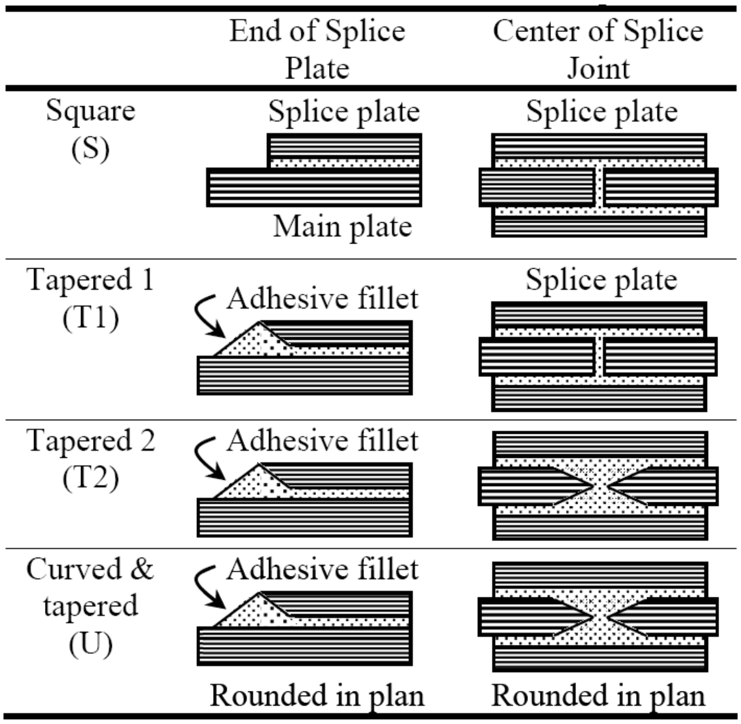

Figure 2.16: Adhesive bonding details (Dawood and Rizkalla, 2007)

The bond failure for three types of joints of steel to CFRP (double-lap joint, single-lap joint and T-peel joint) as shown in Figure 2.17 was studied by Chiew et al. (2011).

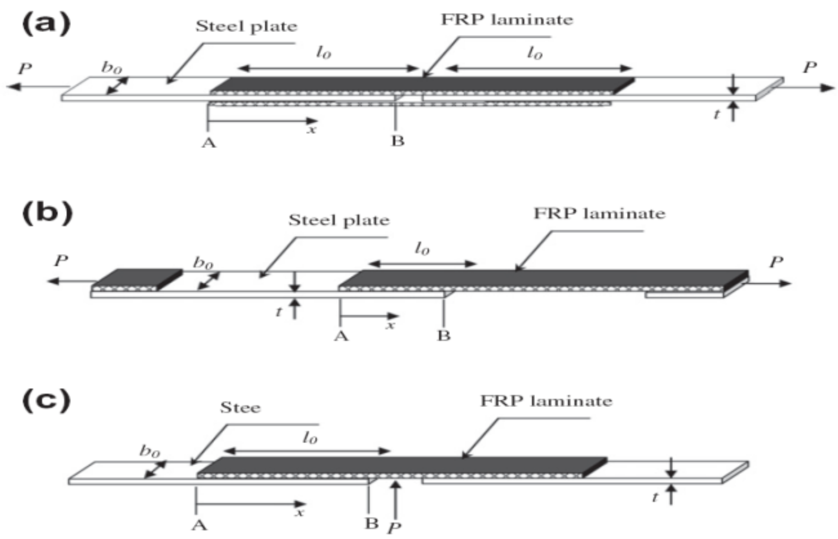

Figure 2.17: Schematic of (a) double-lap joint, (b) single-lap joint and (c) T-peel joint (Chiew et al., 2011)

CFRP laminate with a tensile strength of 2492 MPa was used and two-part saturant epoxy was used to bond the joint between CFRP and steel, the tensile strength of epoxy being 15.5 MPa. The joints were tested under axial tension load using an Instron 5500 universal electro-mechanical testing system. For joints with the same bond length, the failure loads were directly proportional to the bond width, and a lower increase in bond strength was observed for specimens with larger bond length. Figure 2.18 shows the relation between unit bond strength and unit bond length.

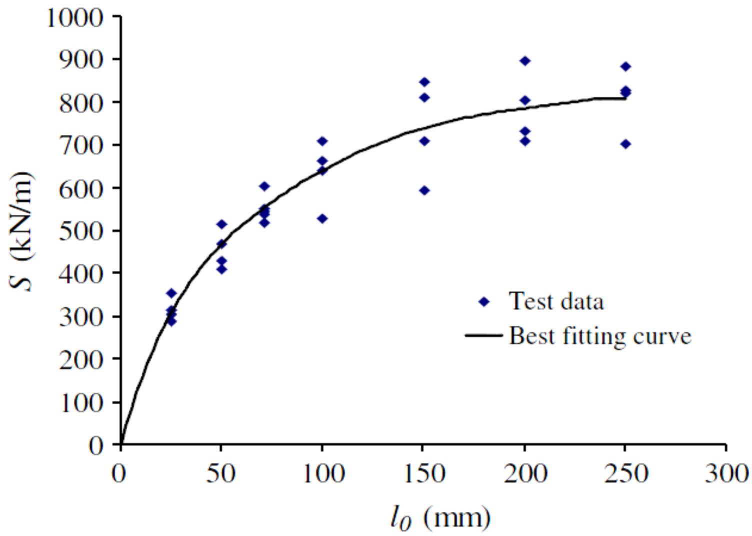

Figure 2.18: Unit bond strength vs. unit bond length for CFRP-steel double lap joints (Chiew et al., 2011)

All specimens showed adhesive failure, and all failures occurred at the adhesive–steel interface. This failure phenomenon occurred because the bond in adhesive joints is the weakest part. High shear with low tensile stress, high shear with high tensile stress and low shear with high tensile stress were the results shown by the double-lap joint, single-lap joint and T-peel joint respectively.

Another series of CFRP-steel double strap joints tests was carried out by Wu et al. (2012) , who studied the bond characteristics of double-strap joints between steel and ultra-high CFRP laminate (MBrace 460/1500). The elastic modulus of this type of CFRP is 460 GPa and the normal tensile strength is 1500 MPa. Two types of adhesives were used (Araldite 420 and Sikadur) to bond CFRP laminates to the steel surface. The specimens were tested under static tension load to investigate the failure criteria, effective bond length and bond stress of the joint. The failure mechanism for joints with Sikadur adhesive was cohesive failure, while two failure modes were observed for specimens with Araldite 420: delamination and CFRP rupture, as shown in Figures 2.19 and 2.20.

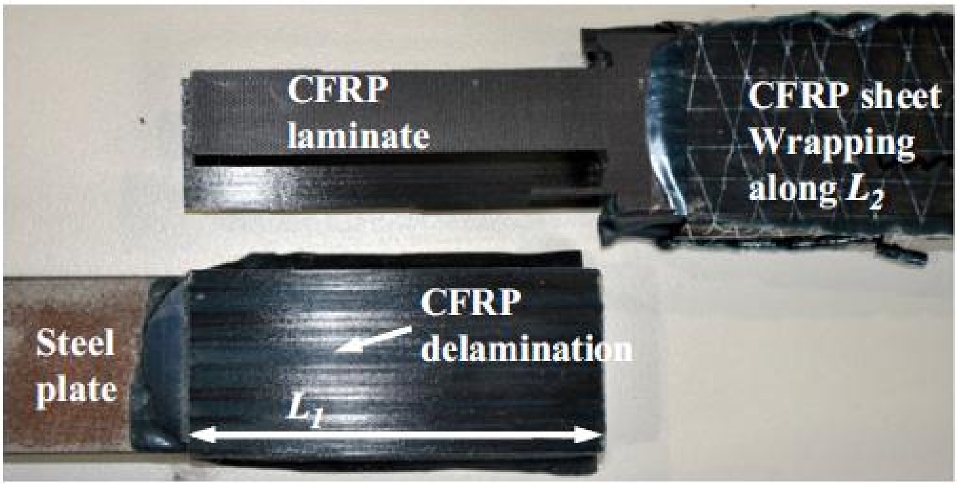

Figure 2.19: CFRP delamination for specimens with Araldite 420 and bond length 100mm (Wu et al., 2012b)

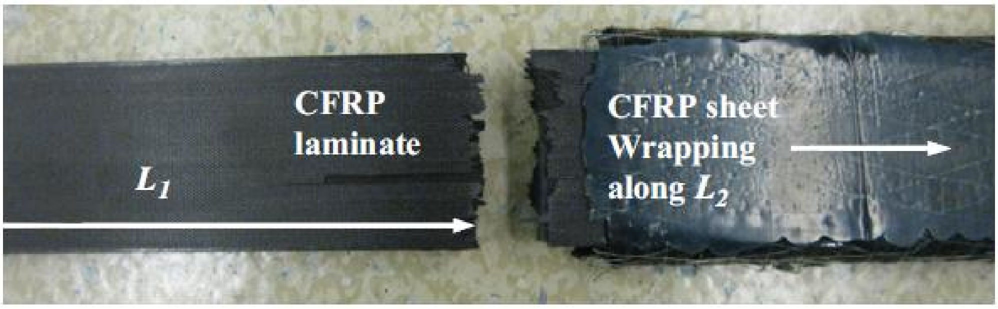

Figure 2.20: CFRP rupture for specimens with Araldite 420 and bond length 250mm (Wu et al., 2012b).

The bond stress increased with the increase of bond length up to the effective bond length, which was 110 mm for Araldite and 85 mm for Sikadur specimens. The strain generally decreased at distances far from the joint, however, the shear strength was enhanced with load level increment, and decreased from the joint to the free end of the CFRP laminate.

As shown above, significant research effort has focussed on the strengthening of steel structures using FRP under different types of static load, but less research has focussed on the effect of dynamic load on the bond between CFRP and steel. The effect of static and impact tensile loads on the bond properties of CFRP sheet-bonded steel plate joints was studied by Al-Zubaidy et al. (2012b) . Normal CFRP sheet was used to bond steel joints with one and three layers, and Araldite 420 adhesive was used to bond the CFRP to the steel. Four series of specimens were tested under quasi-static load (2mm/min) and impact load with a loading rate of 3.35m/sec, and a specimen schematic view is shown in Figure 2.21. The bond strength of the impact load with a speed of 3.35m/sec is higher than that in static load; the ratio of dynamic to static bond strength for both one and three layers of CFRP sheet was calculated, and this ratio was found to be more than 2.0 when the bond length was beyond the effective bond length. The effective bond length was not affected by the high load rate, the effective bond length under static load being about 30mm for one layer of CFRP, and 50mm for three layers of CFRP in the static test, which was the same as the loads for the impact tests. In terms of the failure mode, for 1 layer of CFRP and bond length less than the effective bond length, debonding between CFRP and adhesive occurred in the static test and CFRP delamination in the impact test. When the bond length exceeded the effective bond length of 30mm, CFRP rupture occurred in the static test, whereas CFRP rupture and CFRP delamination occurred in the impact test. For specimens with three layers of CFRP, the failure mode was a combination of debonding of CFRP and adhesive and CFRP delamination for bond lengths less than the effective bond length (50mm).

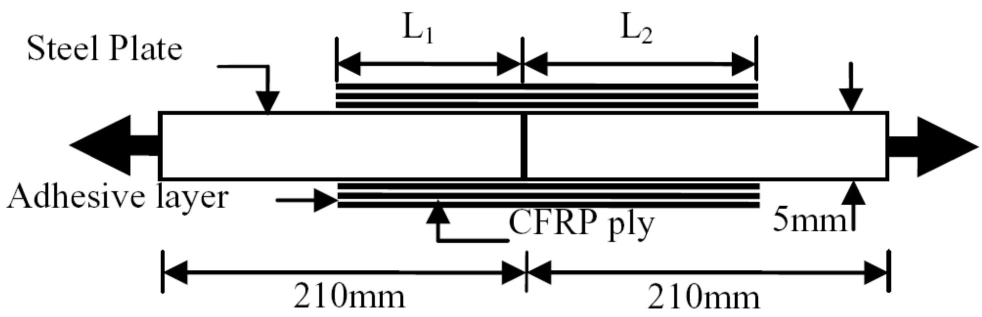

Figure 2.21: Schematic view of CFRP-steel double-strap joint (Al-Zubaidy et al., 2012b).

Al-Zubaidy et al. (2012a) continued their study of the bond characteristics of double-strap joints between normal modulus CFRP and steel plate under impact loads, conducting more tests on these joints using MBrace saturant epoxy adhesive to bond the CFRP sheet to the steel surface. A number of specimens were tested under static and dynamic tensile loads to investigate the effect of impact load on joints with different load rates. For the static tests, the load rate was 2mm/min and for the impact test the load rates were 3.35, 4.43 and 5m/s. The results showed improvement in joint strength for both types of specimens (one and three layers of CFRP) under impact speed (3.35m/s), while for load rates of 4.43 and 5m/s the bond strength started to slightly decrease. The effective bond length for the static test was 30mm for one layer of CFRP and 50mm for three layers of CFRP. However, the effective bond length for the dynamic test remained the same for one layer but there was a slight difference with three layers of CFRP (60mm). The authors attributed this to the low dynamic shear strength of MBrace saturant adhesive. For the static tests and for one layer of CFRP, the failure mode was steel and adhesive interface failure. However, there were different failure modes for the dynamic load. When the bond length was less than the effective bond length, the failure modes were as follows:

- Load rate of 3.35m/s: combination of steel and adhesive interface failure and CFRP and adhesive interface failure.
- Load rate of 4.43 and 5m/s: combination of steel and adhesive interface failure and cohesive failure (adhesive layer failure).

Regarding the three layers of CFRP, the failure mode for the static test was steel and adhesive interface failure for bond lengths less than the effective bond length, while it became a combination of steel and adhesive interface failure and cohesive failure when the bond length exceeded the effective bond length. However, for the dynamic tests there were slight changes in failure modes. In these tests, steel and adhesive interface failure combined with CFRP and adhesive interface failure could be defined as the dominant failure mode, and this failure occurred when the bond length was equal to or shorter than the effective bond length at a loading rate of 3.35 m/s. When speeds of loading were increased to 4.43 m/s and 5 m/s, the failure modes were a combination of steel-adhesive interface failure and CFRP-adhesive interface failure for bond lengths less than or exceeding the effective bond length. Figure 2.22 shows the failure modes of 3 plies of CFRP for load rates of 2mm/min, 3.35, 4.43 and 5m/sec respectively with different bond lengths.

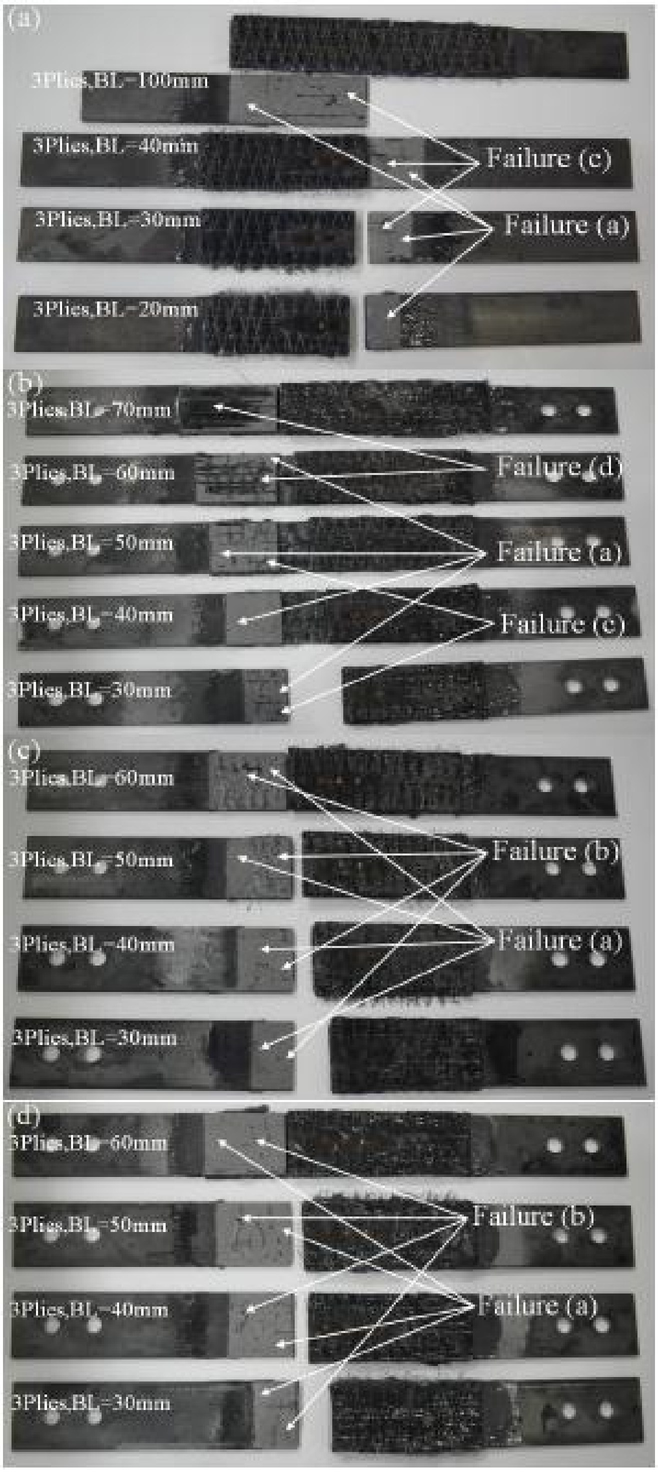

Figure 2.22: Failure modes of steel-CFRP double-strap joints with three CFRP layers (a) 3.34×10^{-5} m/s, (b) 3.35 m/s, (c) 4.43 m/s, (d) 5 m/s. (Al-Zubaidy et al., 2012a)

Failure (a) is steel and adhesive interface failure, (b) is cohesive failure, (c) is CFRP and adhesive interface failure, (d) is CFRP delamination, as explained in Zhao and Zhang (2007). The effect of impact load on strain distribution for one and three CFRP layers and at all loading rates decreased away from the joints, while a linear strain distribution was found for joints with one CFRP ply, and a nonlinear behaviour was observed for joints with three CFRP plies.

2.6 NUMERICAL INVESTIGATIONS

A three-dimensional non-linear finite element analysis was used by Fawzia et al. (2006) to simulate tensile load on CFRP-steel joints. The analytical load-carrying capacity and the strain distribution were found to be close to the experimental results. The coefficient of variation of the failure load for the experimental and analytical results was 0.033, which means there was good agreement between them. The strain results obtained from the finite element analysis along the CFRP was close to the strain gauge results from the experimental test.

Haghani (2010) used a three-dimensional linear finite element analysis to model CFRP-steel joints. Two adhesive types were modelled to bond CFRP to steel beams, Sikadur330 and Sto BPE Lim 567. The results showed that the transverse properties of the composite laminate do not significantly affect the strain distribution along the adhesive layer. The numerical results showed that there was a steel-adhesive interface failure mode for the specimens.

Fawzia et al. (2010) used three-dimensional non-linear finite element analysis to model the tensile testing of steel to CFRP joints with a brick (solid) element using the Strand7 software. The same three types of adhesive (Araldite 420, MBrace saturant and Sikadur 30) used in the experimental tests were simulated to bond the CFRP sheet to steel plate. The research also showed the analysis of adhesive mechanical properties which were tested experimentally, and the results for shear stress and bond slip for each type of adhesive specimen are shown in Figures 2.23-2.25 below:

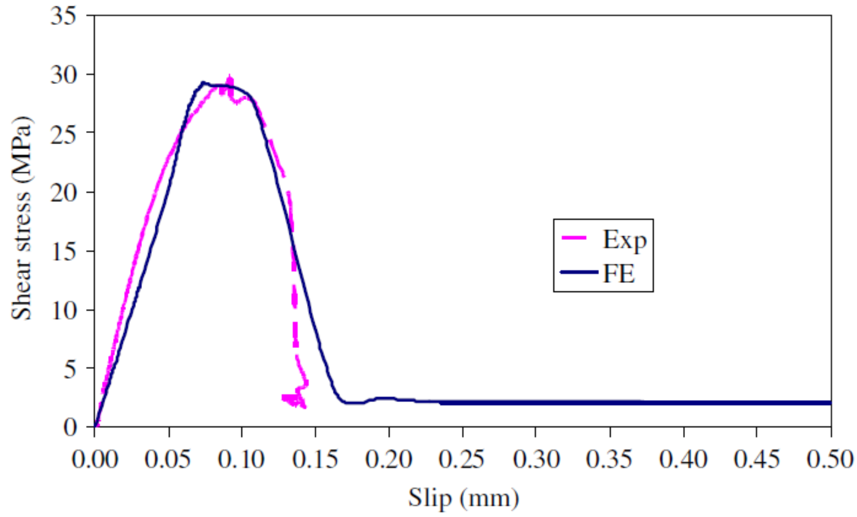

Figure 2.23 Shear stress vs. slip for Araldite 420 (Fawzia et al., 2010)

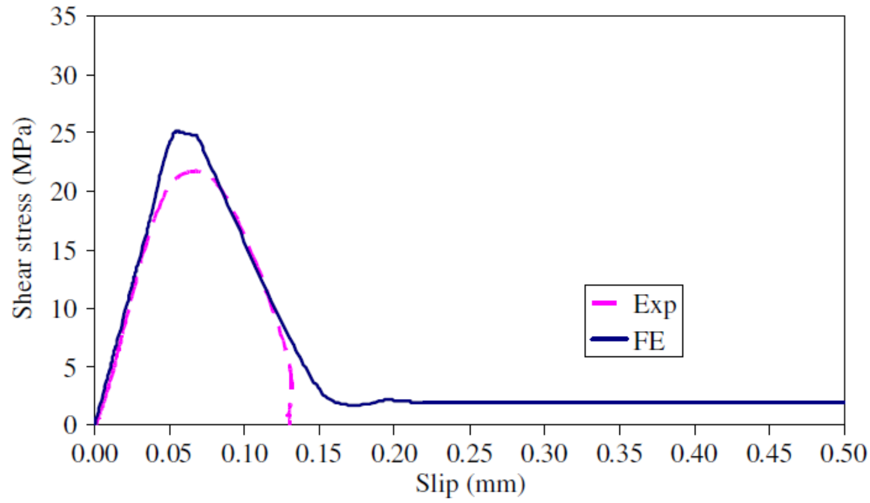

Figure 2.24: Shear stress vs. slip for MBrace (Fawzia et al., 2010)

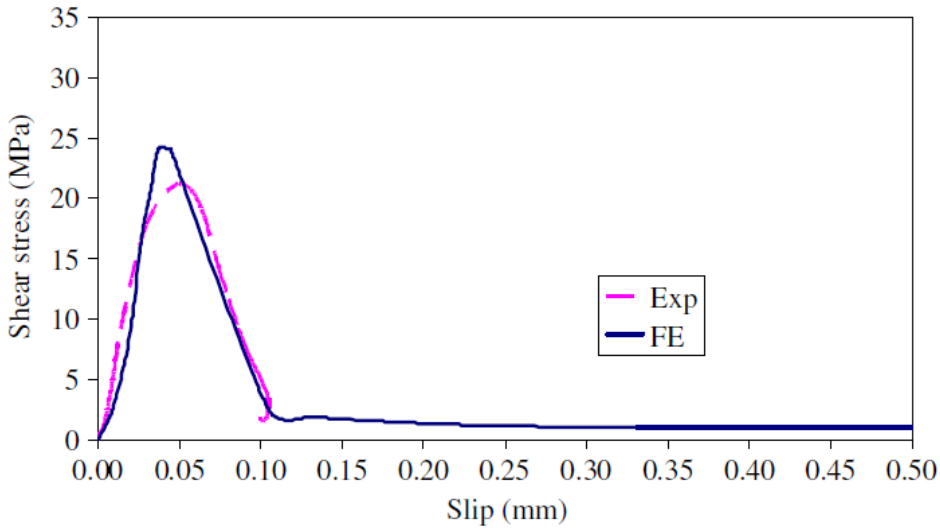

Figure 2.25: Shear stress vs. slip for Sikadur 30 (Fawzia et al., 2010)

These researchers showed that the bond slip in models is not affected by the bond length. Even if the bond length is larger than the effective bond length, the sunset joint movement and shear strength are not affected by the ultimate strain values of the different adhesives, but the maximum slip is higher for the specimens with higher strain values for their adhesive.

Kadhim (2012) studied the effect of different bond lengths of CFRP laminate-strengthened steel continuous beams. This study used three-dimensional analysis to simulate a three-point test in the ANSYS program. Two types of elements were used to simulate the materials: brick and shell. The CFRP laminate was attached to the sagging and hogging region of the beam. The results showed that the ultimate strength of the beam was increased up to 73% when the laminate lengths at the sagging and hogging regions were equal to 40% and 60% of the span length respectively.

Two-dimensional nonlinear finite element analysis was used by Wu et al. (2012) to simulate a double-strap joint of steel and CFRP using a cohesive element for the adhesive layer, while a bilinear plane strain quadrilateral element was used for the CFRP and steel layers. The results showed that for specimens with bond lengths below the effective bond length, failure started from the joint and propagated to the other end, and the failure load increased with the increase of bond length. However, for specimens with bond lengths more than the effective bond length, the failure load remained unchanged. The failure mode was within the adhesive layer for Sikadur adhesive specimens; however, it was CFRP delamination and CFRP rupture for Araldite adhesive specimens, depending on the bond length. A comparison of the experimental slip results and those from FE analysis in different locations is shown in Figure 2.26. The softening zone is clear in finite element modelling, while it is not clear in the experimental curve because of the breakage of the strain gauges after failure.

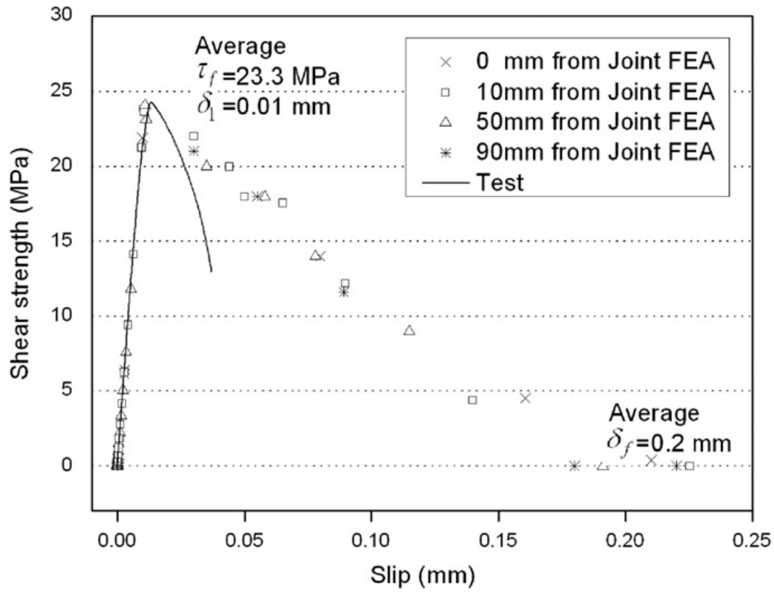

Figure 2.26: Finite element and experimental results of shear strength vs. slip (Wu et al., 2012b)

To numerically investigate the flexural behaviour of the bond between CFRP and steel beams, which was experimentally tested by Dawood and Rizkalla (2007) , a three-dimensional non-linear finite element analysis was implemented by Seleem et al. (2010). One type of element was used (brick element) to simulate steel, adhesive and CFRP. The results of the numerical simulation were consistent with the experimental results for failure load and stiffness, and this agreement was observed for both specimens with a square splice and tapered plate with adhesive fillet. Figure 2.27 shows the details of the beam.

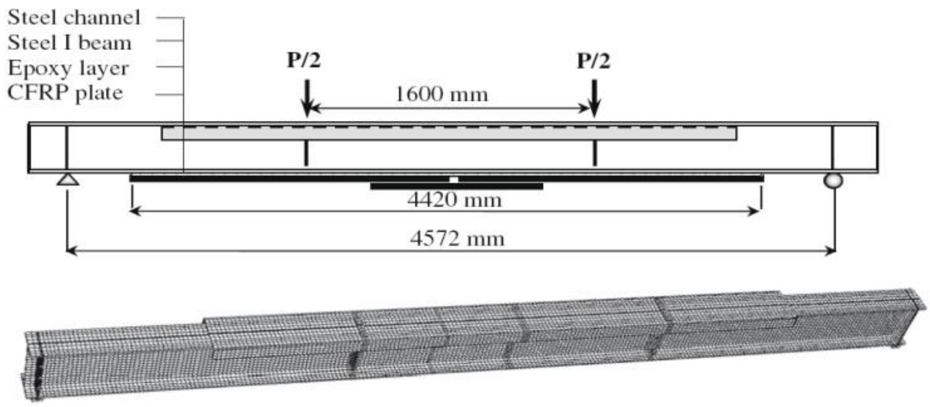

Figure 2.27: Beam tested by Dawood and Rizkalla (2007) and its simulation by Seleem et al. (2010).

Seleem et al. (2010) continued the finite element modelling to simulate another type of beam strengthened with CFRP with additional splice plates near the supports. The splice plates were attached near the supports to investigate their ability to prevent intermediate debonding. This test was experimentally carried out by Schnerch and Rizkalla (2008), as shown in Figure 2.28.

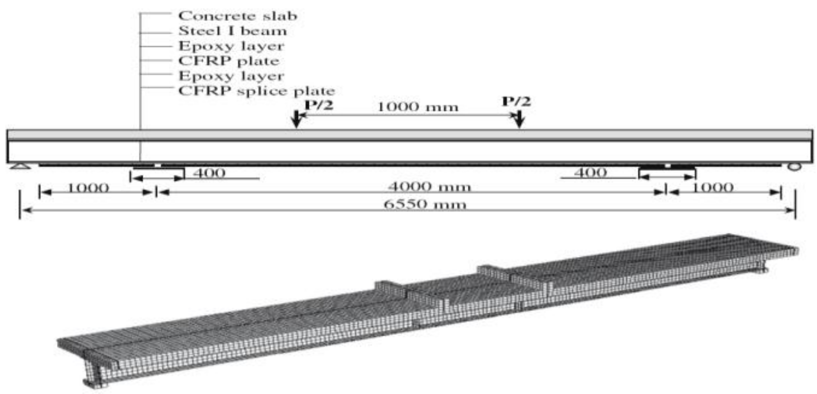

Figure 2.28: Beam tested by Schnerch and Rizkalla (2008) and its simulation by Seleem et al. (2010).

The results showed that intermediate CFRP delamination was prevented when splice plates were attached near the supports. The authors continued modelling beams with different CFRP bond lengths. When the bond length was increased from 2000 to 3500mm, the results showed no change in the failure load when the CFRP bond length was more than 3000mm, while it decreased when the CFRP bond length decreased.

A series of simulations of CFRP-bonded steel boxes subjected to blast loads was carried out by (Pereira et al., 2011). The researchers simulated three different crack orientations in steel boxes strengthened with CFRP sheets using the finite element software LSDYANA; a pressure-time triangle curve was used to represent the blast loading. As the first step in modelling, a simple steel box without cracks was simulated to obtain good geometric calibration and material modelling. The deflection results for both FE analysis and experimental tests showed a correlation of 2%, which the researchers considered to be acceptable. The second step in this simulation was modelling steel boxes with cracks facing the blast load. Three different crack orientations were studied in this research ($0^{\circ}, 45^{\circ}, 90^{\circ}$), as shown in figure 2.29.

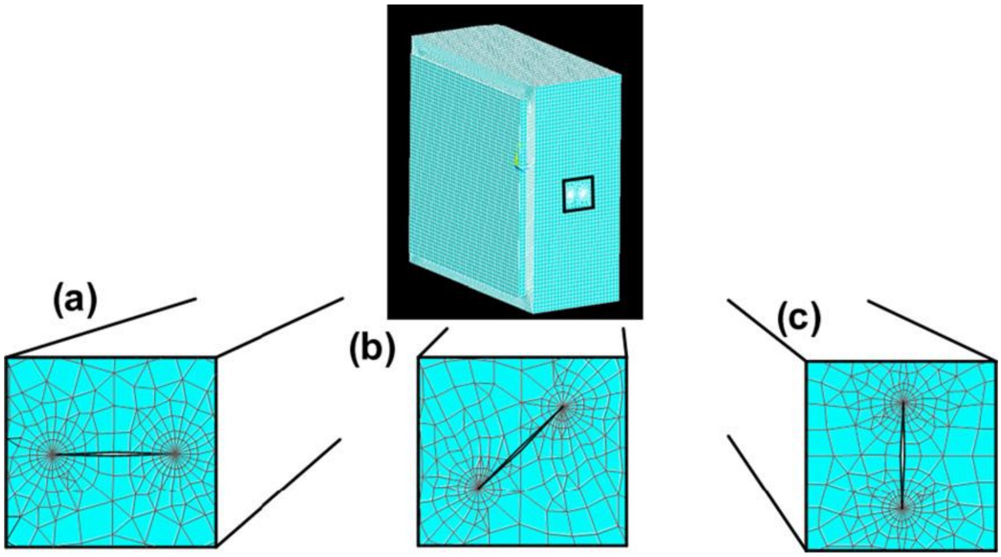

Figure 2.29: Simulation of different crack orientations (Pereira et al., 2011)

The results showed that there was no significant difference in deformation for these three cracked boxes. However, the results showed an increase of 39% in deformation between the cracked boxes and the uncracked box. The final step was modelling the cracked boxes strengthened with CFRP and finding the enhancement in load- carrying capacity of the steel boxes. The CFRP had an elastic modulus of 138 GPa.

The CFRP fabrics were attached to the cracked area, and nodes impacting the surface were utilized to model the contact between FRP and steel with a 0.3 friction coefficient to avoid any lateral movement. The results showed that the CFRP thickness has no significant influence on residual deformation; in addition, there is no significant influence on residual deformation when changing fibre orientation. The effect of CFRP size shows some effect on the deformation results, as the larger the CFRP size, the lower the deformation produced. Figure 2.30 shows a comparison of time-displacement curves for the three steel boxes (reference, cracked and repaired).

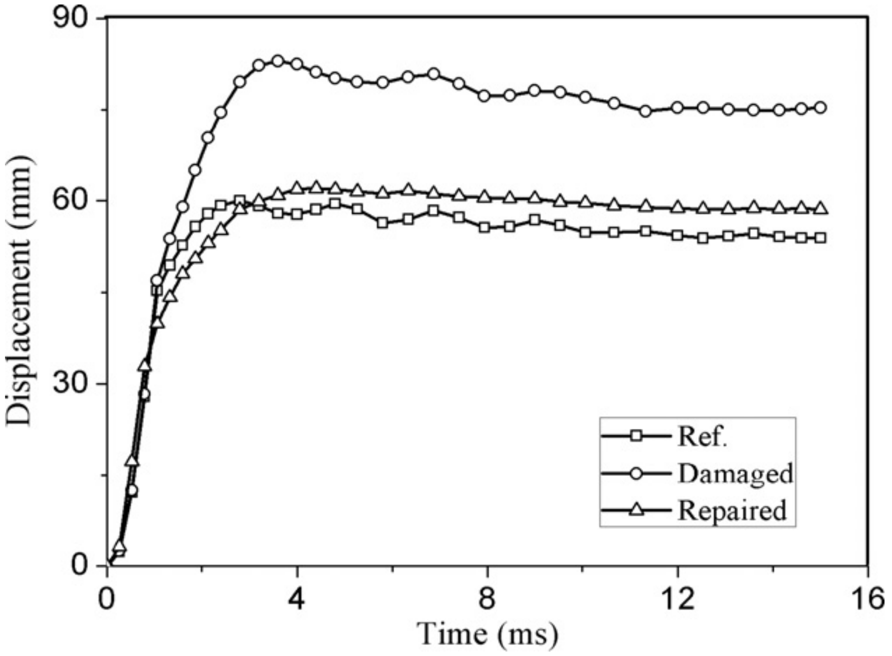

Figure 2.30: Displacement comparison of the three types of steel boxes (Pereira et al., 2011)

Yu et al. (2011) simulated a four-point load on a steel beam strengthened by CFRP at the bottom tension flange. Excellent agreement was observed for the load–deflection and the strain–deflection relationships for both FE analysis and experimental results. Three-dimensional finite element analysis was implemented using the commercial ABAQUS software. This research also showed the normal stress and shear stress propagation along the bond length. The results showed negligible stress propagation through the cohesive layer thickness (see Figure 2.31).

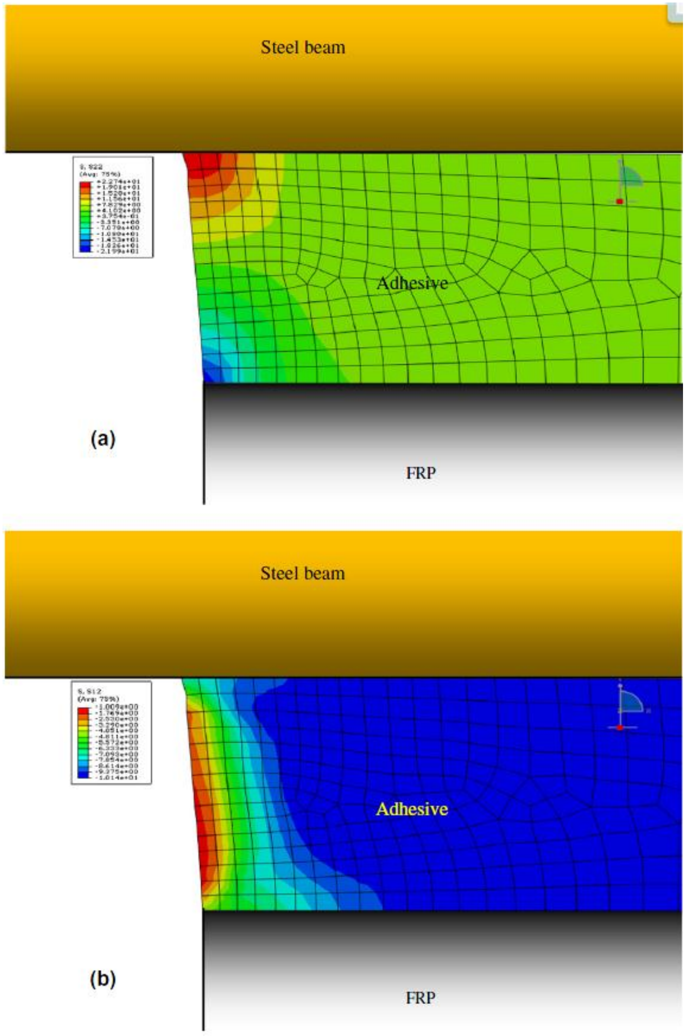

Figure 2.31: Stress distribution through adhesive thickness (a) normal stress, (b) shear stress. (Yu et al., 2011)

Al-Zubaidy et al. (2013) simulated their experiments originally conducted in 2012b and 2011 (Al-Zubaidy et al., 2012a-b; Al-Zubaidy et al., 2011a) using non-linear finite element analysis using ABAQUS software. Static and dynamic tests were simulated using ABAQUS/implicit and ABAQUS/explicit codes respectively. The steel, adhesive and CFRP were modelled as a 3-D stress element, a cohesive element and a continuum shell element, respectively.

Due to the similarity of the specimens, only one eighth of the full-scale specimen was simulated by applying symmetric boundary conditions to all nodes belonging to the YZ, XY and XZ Cartesian planes (see Figure 2.30). The results of this analysis showed that there is a good agreement between experimental and analytical analysis for the maximum load capacity, effective bond length, failure mode and strain distribution along the bond length of the joints.

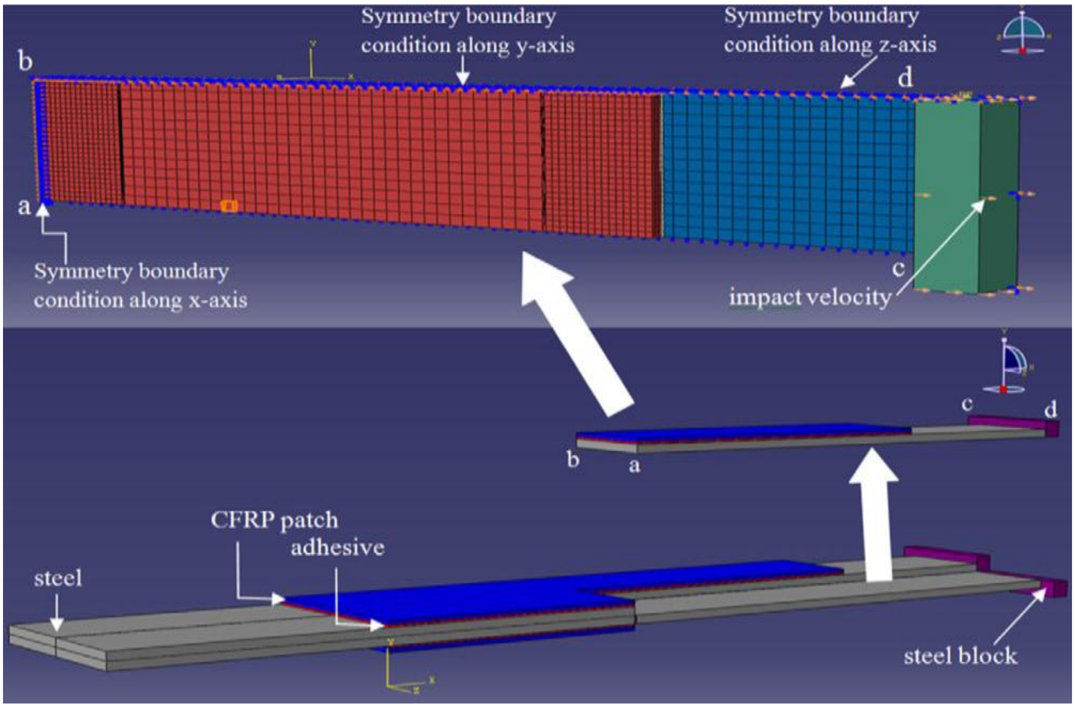

Figure 2.32: CFRP-steel models under dynamic loads (Al-Zubaidy et al., 2013)

Although the manufacturer's specifications give the properties of the materials under static load, some researchers have studied the properties of composite materials, FRP and adhesive under dynamic load. The mechanical behaviour of normal modulus CFRP under impact loads was studied by Al-Zubaidy and Zhao et al. (2011). In this research, coupons of unidirectional normal modulus CFRP and Araldite 420 epoxy were tested under tensile impact load, and the coupons were prepared in accordance with ASTM 3039\D and 3039M-07. A number of CFR and adhesive coupons were prepared and tested under impact loads. Three strain rates were utilized (54.2, 67.2 and 87.4 s-1) to find the actual tensile strength, modulus of elasticity and strain value at failure. The tensile strength of CFRP was increased by 20% to 40% compared to low strain rates, and the modulus of elasticity and ultimate failure strain were also increased by 20%. However, a massive increase in the adhesive tensile stress and elastic modulus under the high strain rates, this increment was up to 220% and 100% respectively (Al-Zubaidy and Zhao et al. 2011).

2.7 GENETINC PROGRAMMING IN COMPOSITES MATERIALS

Genetic programming (GP) is an automated method based on algorithm methodology used to find a relationship among variables in sets of data. This relationship can be expressed as equation or expression tree. Koza (1992) proposed the genetic programming as a derivation from the traditional genetic algorithm but with more complexity. Cevik et al. (2010) reported an overview on using the genetic programming and the way to finalise the analysis and generate the equation.

Recently, a number of studies have focused on prediction models for many engineering problems using genetic programming (Gandomi et al., 2011; Pala, 2008; Schafer and Peköz, 1998; Cevik, 2007; Pérez et al., 2010; Nazari et al., 2015; Sato et al., 1997; Kalfat et al., 2016; Coello et al., 1997). However, lower number of studies focused on the CFRP strengthening structures.

The prediction of structural strengthening models associated with CFRPs needs an accurate method of modelling. Gandomi et al., (2010) predicted a new formula for the compressive strength of concrete cylinders confined by CFRP, two sets of input data were used, the first set of data included the diameter of cylinder, unconfined concrete strength, tensile strength of CFRP strips and thickness of CFRP. The second set includes unconfined concrete strength and ultimate confinement pressure. All these data were adopted from a series of experimental tests and then analysed using genetic programming.

Pérez et al. (2010) presented an improvement of the EC-2 shear strength of reinforced concrete beam without web reinforcement using genetic programming. The model has specially modified the effect of the shear design parameters on the shear strength, these parameters were related to the concrete cross section, amount of flexural reinforcement and the bending-moment-shear-force interaction. The input data were obtained from the literature, the data were obtained from 1200 experimental tests on concrete beams.

Kara (2011) predicted a new formulation to evaluate the shear strength of non-web reinforced concrete beam strengthened with FRP. The GP model has the most accurate prediction than all other models. The study has also focused on evaluating the influence of the shear design parameters on the shear capacity of the concrete beam strengthened with FRP. The GP model outcome is an expression tree which can obtain the equation from it as shown in Figure 2.33.

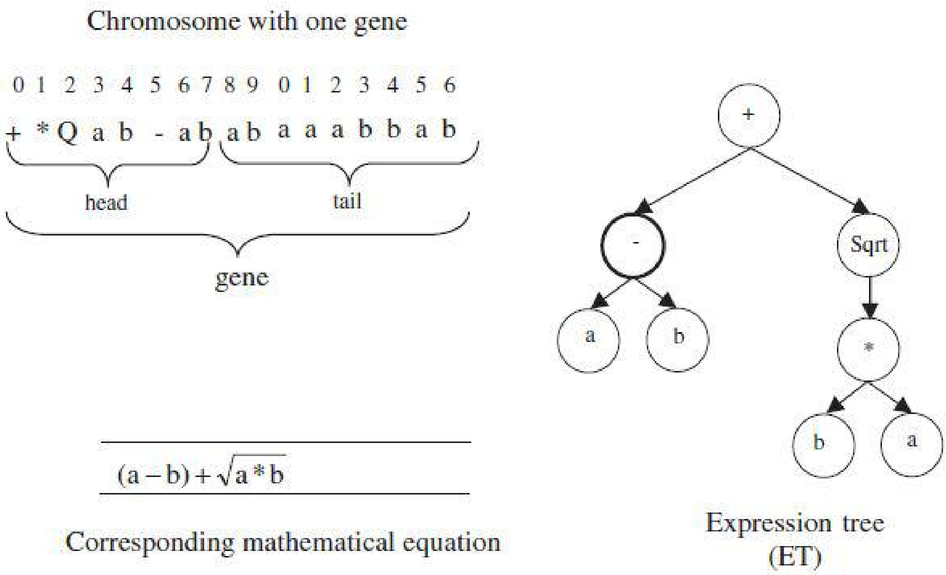

Figure 2.33: Expression tree with the corresponding chromosomes and equation (Kara, 2011).

2.8 SUMMARY

This chapter has reviewed studies of different applications of CFRP-bonded steel structures carried out by different researchers. As the bond between CFRP and steel members is the key to understanding the bond behaviour, this summary focusses on research that investigated the bond properties with various parameters, such as surface preparation methods, CFRP dimensions, adhesive thickness and bond area. The chapter also reviewed the effect of the material properties on the bond behaviour, including CFRP modulus, adhesive shear strength and type of CFRP (sheet, laminate, rods, etc.).

This literature review reported both experimental and numerical studies of the bond between CFRP and steel under quasi-static loading, with different load applications such as flexural bending, tension and compression. Although steel structures are normally subjected to both static and dynamic loadings, there has been very limited research on the effect of dynamic loadings on the bond between CFRP and steel, possibly because dynamic testing needs high-speed data acquisition and accurate load cell readings to capture data in milliseconds. Machines capable of running experimental dynamic tests are not widely available, resulting in far fewer studies on the bond behaviour between CFRP and steel under dynamic loading than static loading. No experimental and analytical research was shown to study the effect of high loading rates on the bond between CFRP laminates and steel plates. Therefore, the present research studies the dynamic behaviour of CFRP laminate-bonded steel members forming double strap joints. Different loading rates, different CFRP sections and material properties are used to find their effect on the bond. Both experimental and analytical studies are included in this research project. Four loading rates are studied in this research, starting from quasi-static loading at 2mm/min to high loading rates of 201×10^3, 258×10^3 and 300×10^3 mm/min. Three types of CFRP laminates are used (low, normal and ultra-high modulus CFRP), and different CFRP sections are used.

The above review also showed that the genetic programming models were only focused on the reinforced concrete elements or reinforced concrete elements strengthened with FRP. According to our knowledge, no research has been focussed on the design equations of FRP strengthened steel structures. A GP model is proposed in this research to predict the bond strength of CFRP-steel double strap joint under static and dynamic loadings.

CHAPTER THREE EXPERIMENTAL INVESTIGATION OF CFRP BONDED STEEL PLATES UNDER STATIC LOADS

3.1 INTRODUCTION

The use of carbon fibre reinforced polymers (CFRPs) in structural engineering has grown in the last few decades. CFRP is attractive to structural engineers due to its unique properties, including its high strength compared to its light weight, good resistance to corrosion, ease of installation due to its light weight; it also has the ability to adhere to different structural sections. Different types of CFRP are available (CFRP sheets, laminates, rods etc.); all these CFRP types can be used in the strengthening of concrete and metallic structures for different applications. As many steel structures are deteriorating due to ageing or changes in their use, they need to be strengthened to resist new applied loads. One of these loads is static tensile loading, which usually acts on steel bridges and buildings. The main issue with CFRP strengthening is the bond; adhesive layer has the major contribution to sustain the applied load. In this chapter, the bond characteristics between CFRP laminate and steel members under quasi-static loading are investigated experimentally in a series of double strap specimens. Low modulus CFRP (CFK150/2000), normal modulus CFRP (CFK 200/2000) and ultra-high modulus CFRP (MBrace laminate 460/1500) were used in this testing program. Araldite 420 epoxy was used to bond the CFRP to steel members. The outcomes focussed on maximum failure strength, strain distribution along bond length, failure mode and effective bond length.

3.2 STUDY OBJECTIVE

Recently, composite materials, especially adhesive-bonded fibres, have been used widely in civil engineering applications such as buildings, bridges and other structures. Many studies have focused on the bond characteristics between steel members and CFRP laminates, and these studies included testing and analysing these composite structural elements with different types of loads. In this chapter, the bond characteristics between steel and CFRP laminate in double strap joints under quasi-static loading are examined. After obtaining the quasi-static results, the effect of high velocity on the same specimens is discussed in detail in the next chapter. Three types of CFRP, low modulus, , normal modulus and ultra-high modulus were used in this comprehensive testing program. The main results are the ultimate bond strength, strain distribution along the bond, failure criteria, and effective bond length. This chapter also reports on the effect of CFRP properties on the results.

3.3 MATERIAL PROPERTIES

The materials that formed the CFRP-steel double strap joints were mild steel, Araldite 420 epoxy, low modulus CFRP laminate CFK 150/2000, normal modulus CFRP laminate CFK 200/2000 and ultra-high modulus CFRP laminate MBrace 460/1500. To evaluate the ability and degree of strengthening of the CFRP-to-steel joints, all materials forming the CFRP-steel double strap joints underwent mechanical property assessment. Although the mechanical properties of these materials were provided by the manufacturers, the actual mechanical properties might differ from those claimed by the manufacturers. Some studies have shown that the actual properties of these materials differ from those claimed by the manufacturers (Schnerch, 2005; Fawzia et al., 2007). It is also common to test all the materials before undertaking major testing to ensure that the mechanical properties of the materials are correct or close to the provided technical sheets. In this research, the properties of materials that formed the composite joint were examined by testing these materials under static tensile load. The main findings obtained from testing these materials were tensile strength, elastic modulus and ultimate strain. The results were then compared with the manufacturer's claims. This chapter describes the testing procedure of these materials and provides a comparison of the actual properties and those claimed by the manufacturers.

3.3.1 Carbon fibre reinforced polymers (CFRPs)

This project focusses on the bond characteristics between steel and CFRP laminate under different parameters. One of the main parameters used in this research is the CFRP type. CFRP is an advanced composite material that combines two components, matrix (adhesive) and fibres. When these two components combine together, they provide performance superior to their individual performance. Reinforced concrete is a good example to explain the idea of composite materials. Reinforced concrete is a composite material that has excellent compressive properties, and cement mortar is also a composite material which is used for bonding the structural elements. Each component of the concrete or the mortar cannot behave in the same way as it does in the composite material. For CFRPs, when the two parts (matrix and fibre) are mixed together, the outcome material has excellent properties in terms of weight, strength and resistance to different types of loadings. Three types of CFRP laminates were used in this research in order to study the bond behaviour of each type with steel members under different parameters. A number of CFRP coupons were prepared in accordance with ASTM3039-08 and tested under quasi-static loading. The same coupon dimensions were used, with the same preparation method and curing time for all types of CFRP. The CFRPs used in this project were supplied by S&P and MBrace. Both S&P and MBrace are common types of CFRP used for strengthening and repairing steel, masonry and concrete structures. The main properties that attract structural engineers to use CFRPs in repair and/or construction are:

- High tensile strength compared to steel,
- Light weight resulting in low density,
- Light weight makes the cost of transportation low,
- Good resistance to chemical exposure,
- Ease of installation eliminating the requirement of lifting,
- Good resistance to impact loading,
- Good resistance to humidity and low temperatures.

3.3.1.1 Coupon preparation

As mentioned above, all types of CFRP had the same preparation method. The low and normal modulus CFRP laminates were provided in rolls 20mm wide, which were cut to certain lengths, and the ultra-high modulus CFRP was provided in a roll 50mm wide, which was cut to certain length, then cut longitudinally to 20mm wide. Careful attention was taken to make them a constant width along the length. Figure 3.1 shows a schematic view of the CFRP coupons.

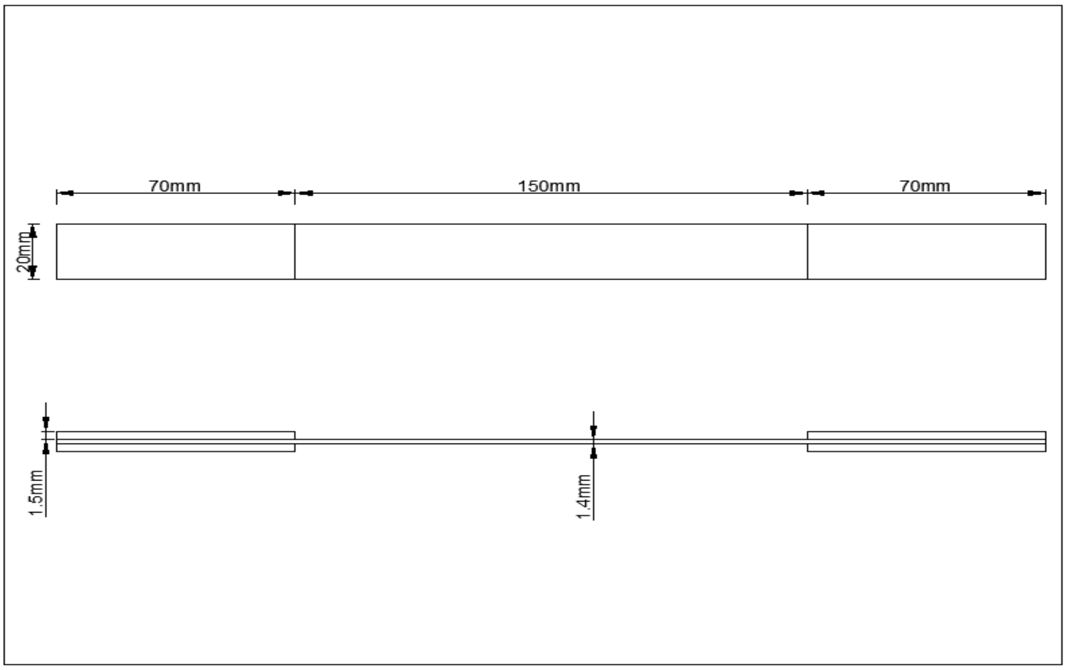

Figure 3.1: Schematic view of CFRP coupons tested under static loading (NOT TO SCALE)

To minimise the stress concentration at the two ends of the CFRP coupons, steel tabs were bonded at both ends, and the tabs can also transfer uniform stress along the coupons (Shokrieh and Omidi, 2009). The steel tabs were sandblasted to remove any grease or oil, and then they were cleaned with acetone to remove all dust and to enable good chemical bonding. All CFRP coupons were cured for more than 7 days at 25° C., as recommended by the manufacturer's instructions for Araldite 420 adhesive. Five coupons were prepared for each CFRP type.

The main results from testing CFRP were the tensile strength, ultimate strain at failure and modulus of elasticity. To measure the ultimate strain on CFRPs, two methods were used: the conventional method, by which foil strain gauges were attached on the centre of CFRP coupons; the second method was by using image correlation photogrammetry with a correlated solution camera (VIC-3D). The image correlation photogrammetry is a digital technique that measure the changes in 2D or 3D images. It often used to measure the displacement, engineering strain, engineering stress etc. According to the manufacturer's manual for the camera (VIC-3D), all CFRP coupons were painted with white paint along one side, and then each specimen was painted with black dots using a fine marker; each dot on the coupon represents one foil strain gauge. The other side of the CFRP coupon had one foil strain gauge mounted at the coupon's centre. A comparison of ultimate strain for the two readings was made. The camera captured the strain that developed on the coupons during loading (see Figure 3.2).

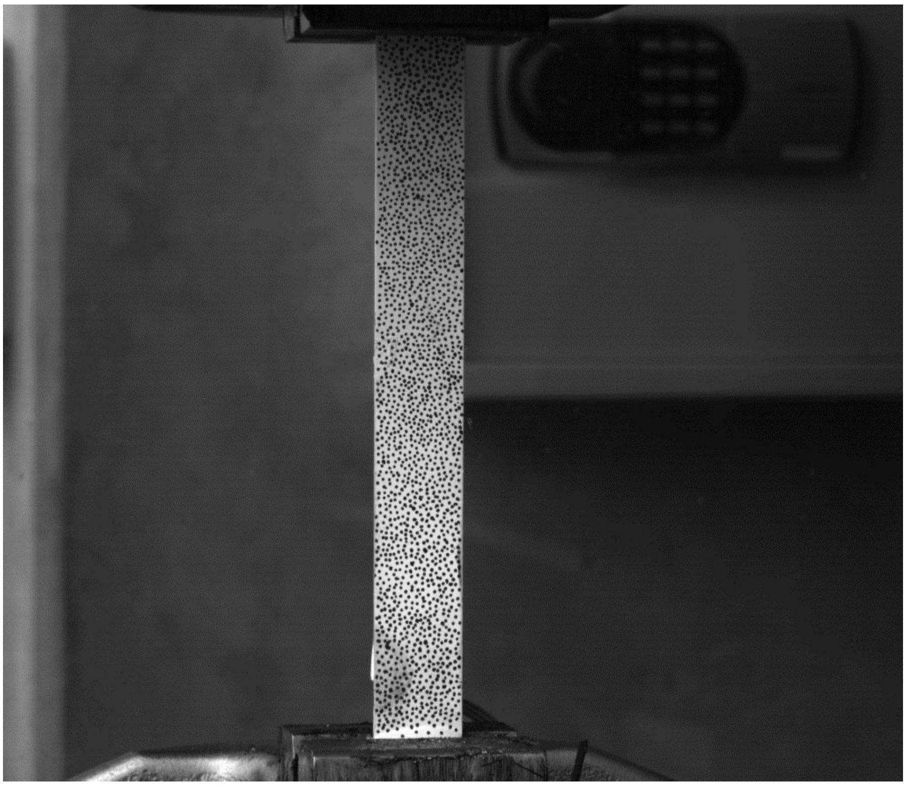

Figure 3.2: CFRP coupon painted with black dots and ready for test.

3.3.1.2 Manufacturer properties

Three types of CFRP laminates were used in this project in order to study the bond characteristics between CFRP laminate and steel members. The three types of CFRP were low modulus CFRP laminate (CFK 150/2000), normal modulus CFRP laminate (CFK 200/2000) and ultra-high modulus CFRP laminate (MBrace 460/1500). The manufacturers' properties of these CFRPs were provided by S&P and MBrace. S&P was the provider of the low and normal CFRP modulus, and MBrace was the provider of ultra-high modulus CFRP. Tables 3.1-3.3 show the tensile mechanical properties of low, normal and ultra-high modulus CFRP used in this project.

Table 3.1: Mechanical properties of low modulus CFRP laminate CFK 150/2000 specified by the manufacturer S & P

List of specifications	Low modulus 150/2000
Fibre modulus (GPa)	165
Thickness (mm)	1.4
Tensile stress (MPa)	>2800
Density (g/cm^3)	1.6
Ultimate elongation%	>1.6

Table 3.2 Mechanical properties of normal modulus CFRP laminate CFK 150/2000 specified by the manufacturer S&P

List of specifications	Normal modulus 200/2000
Fibre modulus (GPa)	205
Thickness (mm)	1.4
Tensile stress (MPa)	>2800
Density (g/cm^3)	1.6
Ultimate elongation%	>1.35

Table 3.3: Mechanical properties of ultra-high modulus CFRP laminate MBrace 460/1500 specified by the manufacturer

List of specifications	Ultra-high modulus 460/1500
Fibre modulus (GPa)	460
Thickness (mm)	1.2
Tensile stress (MPa)	1500
Density (g/cm^3)	1.82
Ultimate elongation%	0.3%

As the the tables above indicate, the CFK CFRPs have lower modulus of elasticity and higher tensile strength than the MBrace CFRP laminate. The tensile strength of low and normal CFRP laminates is 2800 MPa at a maximum elongation of 1.6% and 1.35% respectively, whereas the maximum tensile strength of the ultra-high modulus CFRP is 1500 at an elongation of 0.3%. These properties indicate that ultra-high modulus CFRP is stiffer than the other two, which means it will show less deformation under tensile loading.

3.3.1.3 Measured properties

It is common for the actual properties to differ a little from the manufacturers' properties, due to the fact that the manufacturers provide the design properties or the minimum mechanical properties of the composite materials. A number of CFRP coupon tests were conducted to obtain the actual mechanical properties of the three different CFRPs, and results were obtained for tensile strength, ultimate strain and modulus of elasticity. An MTS 250 machine was used to test these coupons under a loading rate of 2mm/min.

Low modulus CFRP laminate

In this study, low modulus CFRP laminate coupons were prepared according to ASTM3039-08 to investigate the tensile properties under quasi-static loading. The measured tensile strength, ultimate strain and modulus of elasticity were: 2854 MPa, 1.79% and 159.4 GPa respectively. Table 3.4 shows the results for all coupons.

Table 3.4: Coupon test results for low modulus CFRP laminate

Specimen label	Tensile stress (MPa)	Ultimate strain (VIC-3D)	Modulus of elasticity (GPa)
S1	2757	0.0181	152.3
S2	2890	0.0178	162.4
S3	2931	0.0177	165.6
S4	2872	0.0179	160.4
S5	2820	0.018	156.7
Average	2854	0.0179	159.4

Normal modulus CFRP laminate

Five coupons of normal modulus CFRP were prepared and tested under a loading rate of 2mm/min. The tensile properties of normal modulus CFK 200/2000 were 2861 MPa ultimate tensile strength, 1.41% ultimate strain and 203 GPa elastic modulus.

Table 3.5: Coupon test results for normal modulus CFRP laminate

Specimen label	Tensile stress (MPa)	Ultimate strain (VIC-3D)	Modulus of elasticity (GPa)
S1	2872	0.0142	202.3
S2	2831	0.0139	203.7
S3	2954	0.0148	199.6
S4	2820	0.014	201.4
S5	2830	0.0136	208.1
Average	2861	0.0141	203

Ultra-high modulus CFRP laminate

MBrace laminate 450/1500 with a thickness of 1.2mm was used in this research. The tests focussed on tensile strength, ultimate strain and tensile modulus of elasticity. The actual tensile strength, ultimate strain and modulus of elasticity were 1602.4 MPa, 0.35% and 457.2 GPa, respectively.

Table 3.6: Coupon test results for ultra-high modulus CFRP laminate

Specimen label	Tensile stress (MPa)	Ultimate strain (VIC-3D)	Modulus of elasticity (GPa)
S1	1598	0.0033	484.2
S2	1610	0.0036	447.2
S3	1599	0.0034	470.3
S4	1593	0.0037	436.4
S5	1612	0.0036	447.8
Average	1602.4	0.0035	457.8

From the results above, the stress strain curves for low, normal and ultra-high modulus CFRP were plotted (see Figure 3.3). The figure shows that the low and normal modulus CFRP curves are steeper than that for ultra-high modulus CFRP, which indicates that the higher modulus CFRP has greater stiffness. The stress is almost the same for low and normal modulus CFRPs, whereas it is much lower for ultra-high modulus CFRP.

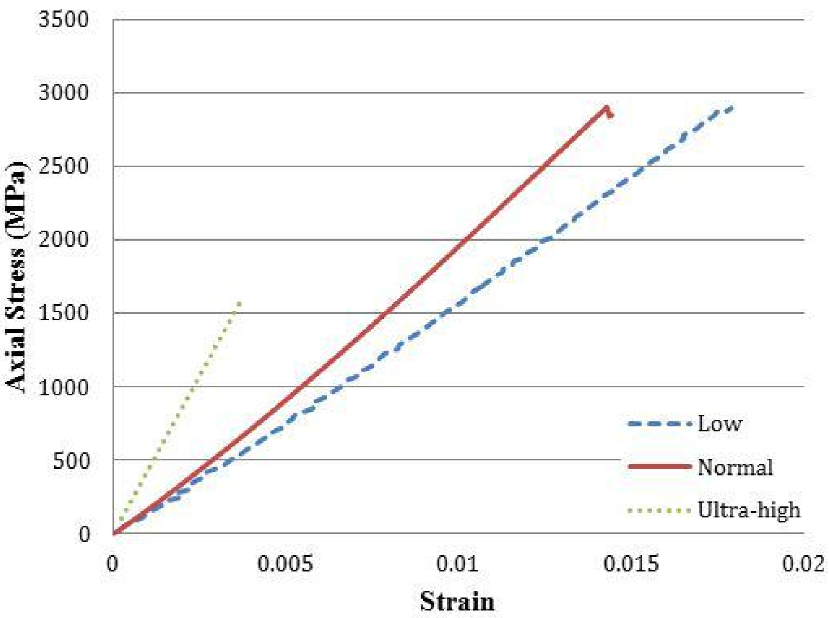

Figure 3.3: Stress-strain curves for the three different CFRPs under quasi-static loading.

3.3.1.4 Failure mode

A similar failure mode was observed for all CFRP types, with sudden failure followed by failure propagation. During the tests, the image correlation photogrammetry technique (VIC-3D) captured images. Figure 4.4 shows the failure propagation for the CFRP laminates tested under quasi-static loading with a loading rate of 2mm/min. The sudden failure of CFRP laminates indicates that CFRP is brittle material, and it shows no yielding or necking before failure.

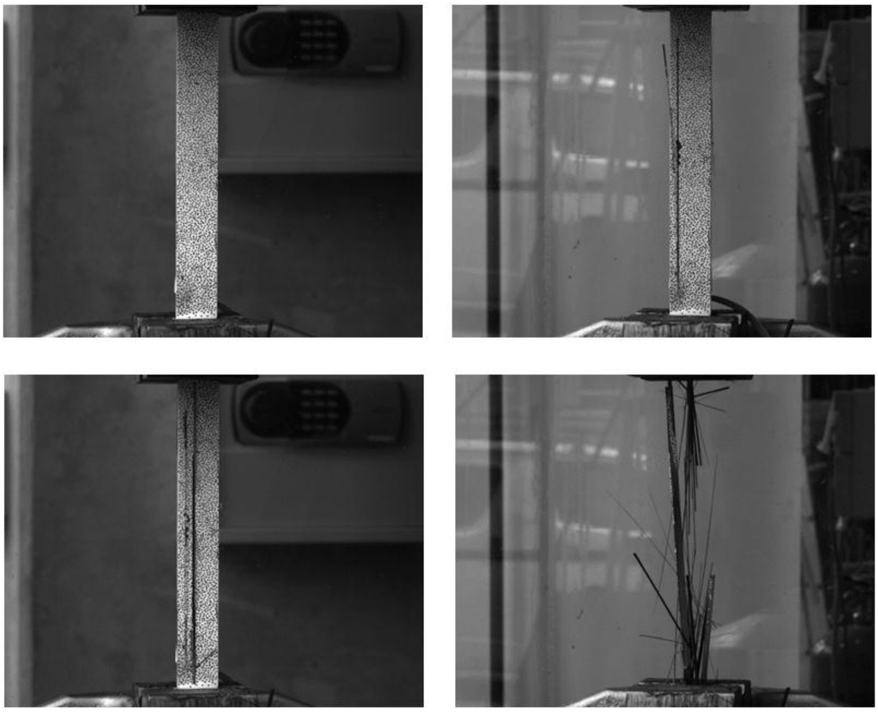

Figure 3.4: CFRP laminate failure stages

3.3.2 Araldite 420 adhesive

As mentioned in Chapter Two, Araldite 420 epoxy has been found to be the most appropriate adhesive for CFRP application to steel structures. It is important to study the mechanical properties of Araldite 420, because the adhesive layer transfers the load from the structural element to the CFRP. Therefore, knowledge of the tensile properties of the adhesive layer is the key to understanding the behaviour of CFRP-steel double strap joints under different parameters.

Araldite 420 epoxy is a two-part epoxy and a flexible and tough material. It is suitable for a wide variety of metal and fibre-reinforced composite bonding applications. It has high shear strength even at temperatures up to 70° C. The curing time is 7 days at 25° C and the working time with this epoxy is up to 45 minutes. The manufacturer-provided results for ultimate tensile strength, ultimate strain and modulus of elasticity are 32.0 MPa, 0.04 and 1900 MPa respectively.

The actual properties of Araldite 420 were investigated by (Fawzia, 2008; Al-Zubaidy et al., 2011a) under static loading. Both groups of researchers prepared the epoxy coupons according to ASTM: D638. A schematic view of the epoxy coupons is shown in Figure 3.5.

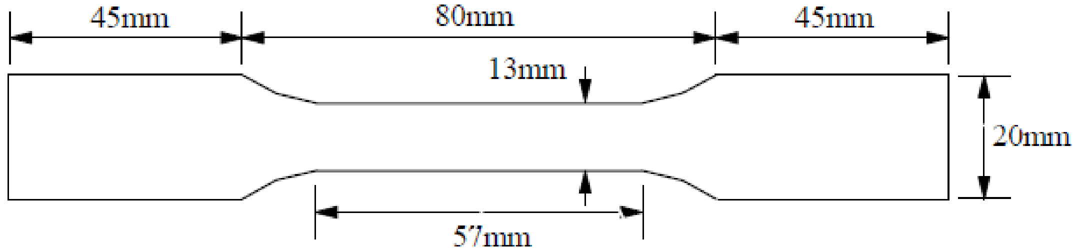

Figure 3.5: Schematic view of adhesive coupon (Fawzia, 2008)

The actual mechanical properties of the Araldite 420 epoxy are shown in Table 3.7. The tensile strength was found to be 28.6 MPa, which differs a little from the manufacturer's figure (32 MPa). The measured ultimate strain was also lower than that provided by the manufacturer.

Table 3.7: Araldite 420 mechanical properties (Fawzia, 2008)

Specimen label	Tensile strength (MPa)	Ultimate strain	Elastic modulus (MPa)	Poisson's ratio
AR1	29.9	0.020	1940	0.35
AR2	30.1	0.020	2095	0.4
AR3	28.6	0.027	1787	0.34
AR4	27.5	0.022	1916	0.38
AR5	27.0	0.029	1767	0.34
Average	28.6	0.024	1901	0.36

3.3.3 Steel plate

As this research focuses on the bond properties between steel and CFRP laminate, mild steel plates of grade A36 were used to produce the double strap joint, and the mechanical properties were investigated in this study under quasi-static loadings. Steel coupons were prepared in accordance with Australian Standards AS 1391-2007. The measured stress-strain curve is shown in Figure 3.6, and the yield and ultimate stresses were 361 MPa and 525 MPa respectively.

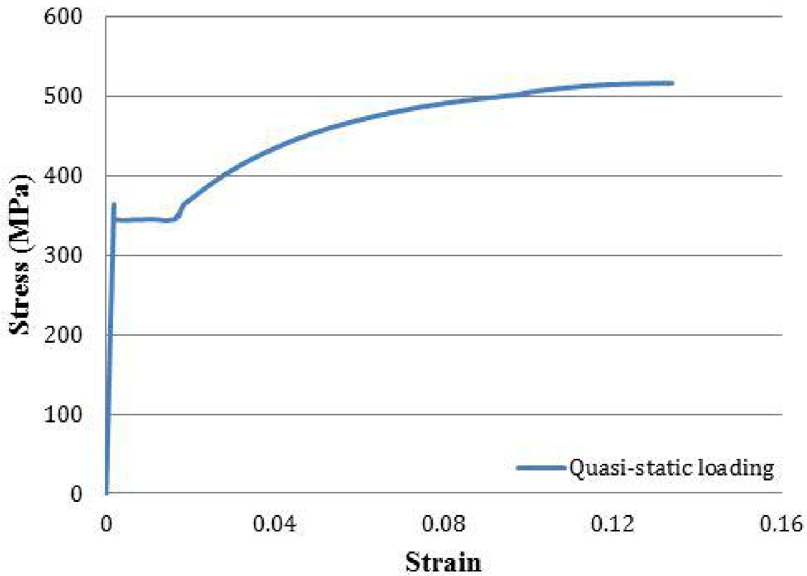

Figure 3.6: Actual stress-strain curve for steel plate under quasi-static loading

3.4 EXPERIMENTAL INVESTIGATION OF THE BOND BETWEEN CFRP AND STEEL

A number of researchers have studied the bond between CFRP and concrete or steel structural elements with different parameters (Haghani, 2010; André et al., 2012; Gamage et al., 2006; Nguyen et al., 2013; Nguyen et al., 2012; Wang and Wang, 2015; Challita et al., 2011; Barros et al., 2007; Hosseini and Mostofinejad, 2013; Cruz and Barros, 2004; Kalfat and Al-Mahaidi, 2010; Benzarti et al., 2011; Sayed Ahmad et al., 2011; Silva et al., 2013; Zhang et al., 2013; Al-Zubaidy et al., 2012a-a; Fawzia et al., 2006b; Wu et al., 2012b). The present research reports an investigation of the bond characteristics between CFRP laminate and steel plates in double strap joints. A series of double strap joint shear tests was conducted by loading the joints under quasi-static tension load. Different CFRP types were used (low modulus CFRP laminate CFK 150/2000, normal modulus CFRP laminate CFK 200/2000 and ultra-high modulus CFRP laminate MBrace 460/1500) to investigate the effect of CFRP modulus on the bond between steel and CFRP laminate. In addition, different CFRP sections were used to study the effect of CFRP section properties on the bond behaviour. CFRP laminates were attached to two steel plates bonded together using Araldite 420 epoxy (see Figure 3.7). All specimens were loaded under quasi-static tension load with a load rate of 2mm/min.

Figure 3.7: Araldite 420 Two parts A and B

3.4.1 EQUIPMENT PREPARATION AND SAFETY PROTECTION

Prior starting the specimen preparation, the apparatus was cleaned and dried to ensure it was free of any contaminants. Masks and gloves were used while preparing and applying the adhesive, due to its toxicity. The environmental conditions such as temperature, humidity and dew point were taken into account at the time of CFRP application.

3.4.2 SPECIMEN PREPARATION

This chapter presents the effect of quasi-static loading on the bond between steel and CFRP laminate. Three types of CFRP modulus were used in this testing program. Two different CFRP sections were used to study the effect of specimen size on the bond behaviour. Mild steel of grade A36, Araldite 420 adhesive, low modulus CFRP, normal modulus CFRP and ultra-high modulus CFRP were used to configure the different CFRP-steel double strap joints. The joints were manufactured by cutting the steel plate into pieces 200mm long and glueing two steel plates on their cross-sections using Araldite 420 epoxy. The two steel members were guided by an equal length steel section to keep them aligned during fastening to avoid eccentricity when loading (see Figure 3.8). The joints were then cured for 24 hours to set the adhesive.

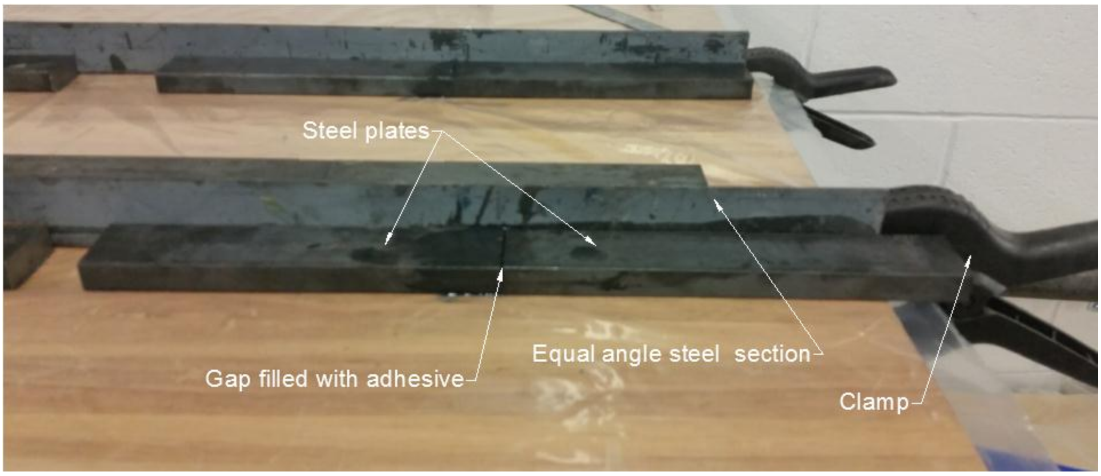

Figure 3.8: Bonding two steel plates using Araldite 420

After the adhesive set, the surfaces of the jointed steel plates were sandblasted along the bond area to remove dust, paint, oil and any other suspended materials, and to ensure a good chemical contact between the epoxy and steel along the bond area (see Figure 3.9).

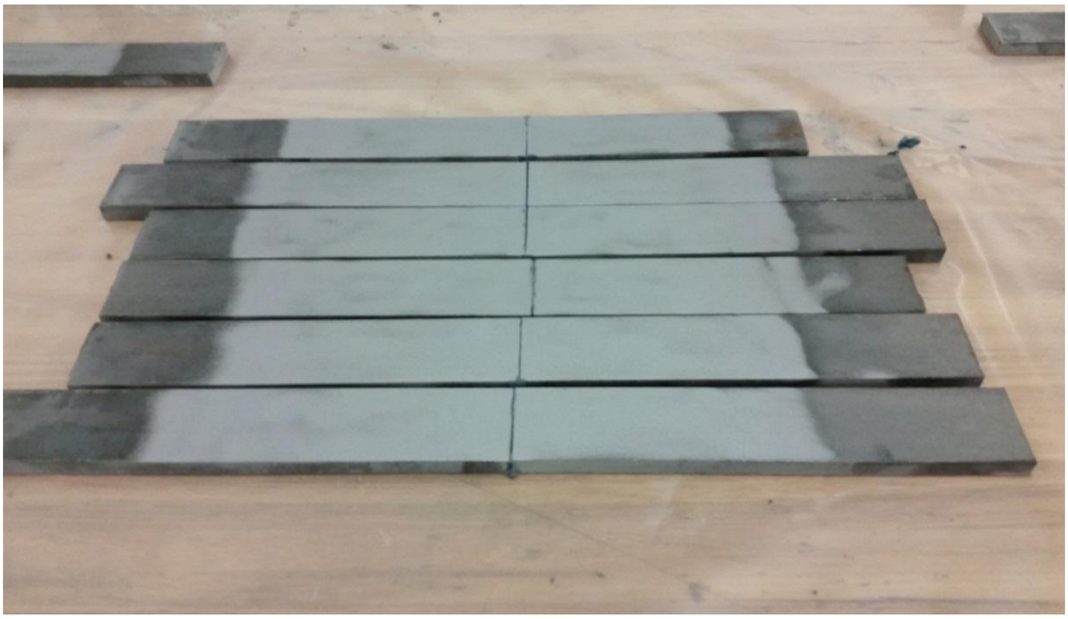

Figure 3.9: Sandblasted steel plates

The sandblasted surface was then cleaned with acetone before adhesive application to provide a chemically active surface. The adhesive layer was added after drying the steel surface according to the manufacturer's requirements. As Araldite 420 has two parts, the mixing percentages and procedures were carried out according to the manufacturer's specifications. The CFRP laminate was cut into the required lengths and wiped with acetone to ensure they were free of any dust. Since the ultra-high CFRP laminate was provided in a roll 50mm wide, special attention was taken while cutting this laminate in two directions (longitudinally to obtain the 20mm width and transversely to obtain the required bond length). Careful attention was given to ensure uniform width. The CFRP laminates were then attached to the sandblasted steel surface using the Araldite 420 epoxy. The adhesive was uniformly applied to the bond area with an approximately triangular cross-section to help the epoxy to be distributed uniformly along the bond area.

Finally, CFRP laminates were attached to the joints immediately after adding the adhesive layer to ensure that the resin was still workable. Uniform squeezing was applied when attaching the CFRP laminate to expel the air bubbles, and a steel plate supported by two washers at the ends was used for squeezing to ensure uniform adhesive thickness along the bond length. The specimens were then cured for 24 hours prior to preparing the other sides to ensure no slippage or damage occurred. The same preparation procedure was used for the other side of the specimens. As shown in Figure 3.10, the bond length from one side of the joint (L_1) was smaller than L_2 to ensure that the failure happened in the shorter side (L_1). The specimens were cured for more than 7 days, according to the manufacturer's recommendation for the adhesive.
In this study, three CFRP types (low, normal and ultra-high modulus) and two CFRP sections (10×1.4mm and 20×1.4mm) were used to study their effect on the ultimate joint capacity, the strain distribution along the bond, the failure mode and the effective bond length.

It was initially decided to use steel plates 20mm wide and 10mm thick, but after running the test, the steel yielded. Therefore, the section of steel was changed to 40mm wide and 10mm thick to ensure failure occurred within the joint.

As the width of CFRP in the two series was less than that in steel, attention was taken while attaching the laminate to ensure it was mounted along the centreline of the steel plate to provides a clear axial tension load on each specimen.
A schematic of the double strap specimen is shown in Figure 3.10 below:

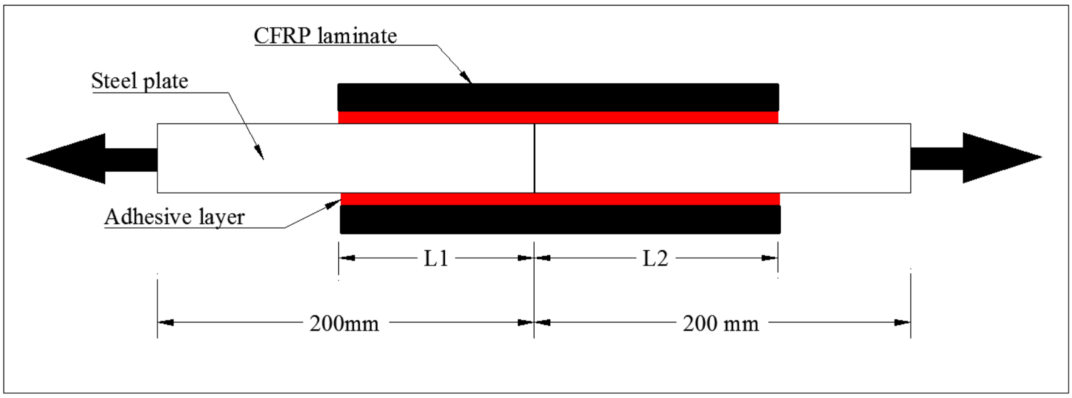

Figure 3.10: Schematic view of double strap specimen (Not to scale)

3.4.3 TEST PROCEDURE

In this research, an MTS testing machine (see Figure 3.11) with a maximum capacity of 250kN in tension with hydraulic grips was used to test the double-strap joint specimens under static tensile loads, with a loading rate of 2mm/min.

Figure 3.11: MTS testing machine with 250KN capacity

As mentioned earlier, three types of specimens were used in the static testing, with different CFRP cross-sectional areas and different moduli of elasticity. A total of 165 specimens with CFRP-steel double strap joints using Araldite 420 epoxy were tested to determine the ultimate load-carrying capacity, the effective bond length (the bond length beyond which the load stays constant), the failure modes and the strain distribution with different parameters. These 165 specimens included 66 specimens with low modulus CFRP and a cross-sectional area of 10×1.4mm, 33 specimens with low modulus CFRP and a cross-sectional area of 20×1.4mm, 33 specimens with normal modulus CFRP and a cross-sectional area of 20×1.4mm, and 33 specimens with ultra-high modulus CFRP and a cross-sectional area of 20×1.4mm. As one of the areas of interest was the strain distribution along the bond area, two methods of capturing strain were used; the conventional foil strain gauge technique and image correlation photogrammetry using the correlated solution camera VIC-3D. The foil strain gauges were attached on the centre of each joint on one side and the photogrammetry camera captured the strain along the bond area of the specimens. All specimens were painted in white along the bond area, and then each specimen was painted with black dots using a fine marker, as recommended in the manual for the VIC-3D correlated solution camera (see Figure 3.12). Each dot on the specimen represents one foil strain gauge; the camera captured the strain that developed on the double strap joint during the loading. A number of photographs were taken using the same VIC-3D correlated solution camera with high resolution to monitor the propagation of failure, as shown in Figure 3.13.

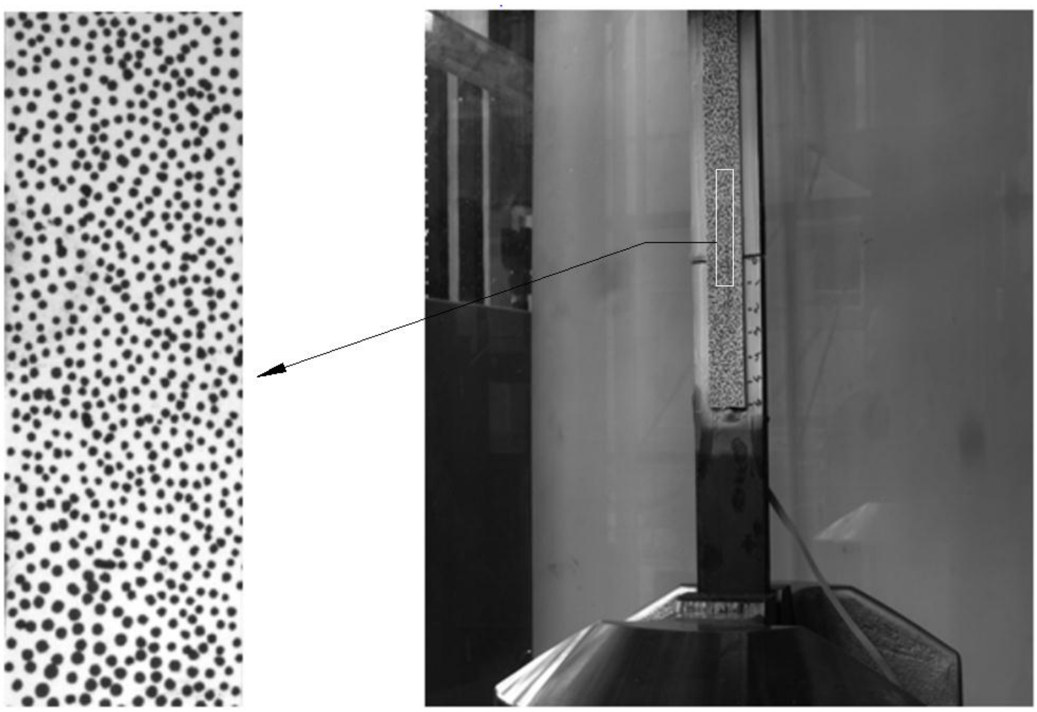

Figure 3.12: CFRP-steel double strap joint under test

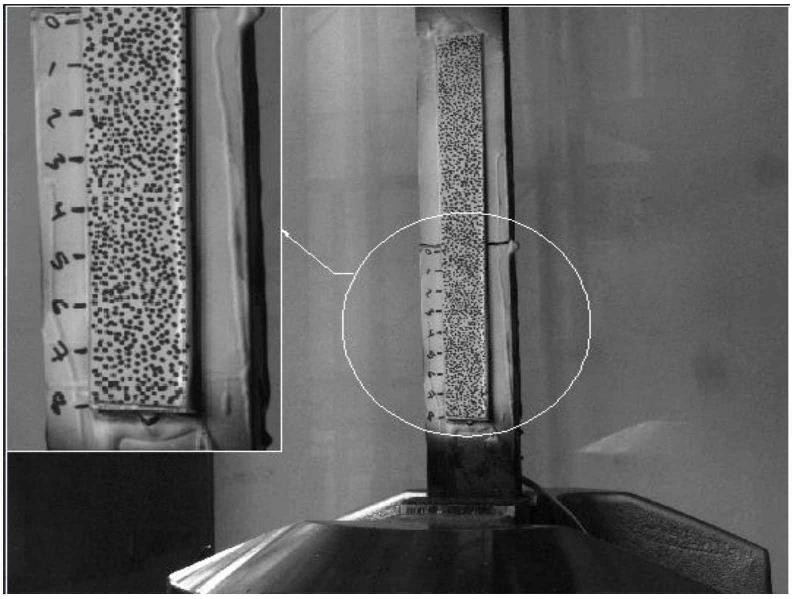

Figure 3.13: CFRP-steel double strap specimen at failure

3.4.4 Experimental Program

Four different series of CFRP-steel double strap joints were tested in the quasi-static testing; the differences in these scenarios relate to CFRP modulus and cross- sectional area. All specimens were tested under quasi-static tension load with a load rate of 2mm/min. Table 3.8 presents a summary of the testing program and the number of specimens tested under quasi-static loadings.

Table 3.8: Parameters of the quasi-static testing program

Series number	Series 1	Series 2	Series 3	Series 4
Steel cross-section (mm)	40×10	40×10	40×10	40×10
CFRP cross-section (mm)	20×1.4	10×1.4	20×1.4	20×1.2
CFRP type	Low modulus	Low modulus	Normal modulus	Ultra-high modulus
Adhesive thickness (mm)	0.5	0.5	0.5	0.5
Curing time (days)	> 7	> 7	> 7	>7
Number of specimens	33	66	33	33

The adhesive layer was calculated using the following equation:

$T_t = t_{st} + 2t_f + 2t_a$ Equation 3.1

where:

T_t: Total specimen thickness.

t_{st}: Thickness of steel plate.

t_f: Thickness of CFRP.

t_a: Adhesive thickness.

The total specimen thickness was measured using a digital Vernier. The total thickness is the average of three readings of specimen thickness.

3.5 EXPERIMENTAL RESULTS

In this research, four sets of results were obtained from the four different series tested under tensile quasi-static loading: ultimate joint capacity, strain distribution along the bond length, failure mode and effective bond length.

3.5.1 Ultimate Bond Strength

In this research, all CFRP-steel double strap joint specimens were subjected to quasi-static loadings with a load rate of 2mm/min. Different bond lengths were used to give different joint capacities, and the joint strengths were investigated with different parameters: type of CFRP (low, normal and ultra-high modulus), and CFRP section (1.4×20mm, 1.4×10mm and 1.2×20mm).

In this part of the research program, 165 CFRP-steel double strap joint specimens were tested under tensile quasi-static loading with a load rate of 2mm/min. As mentioned earlier, these 165 joints included 33, 66, 33 and 33 CFRP-steel double strap joint specimens for series 1, 2, 3 and 4 respectively. All these series had the same preparation procedure and bond lengths; the bond length of one side of the joints (L_1) was shorter than the other side (L_2) to ensure that failure occurred in the shorter side (L_1). The bond length L_1 was varied from 30mm to 130mm; each specimen with different bond length had different bond strength. Tables 3.9-3.12 show the results of bond strength for each specimen in each series,. Each bond strength value is the average value of three tested specimens. For all series, the results show that the joint strength increases as the bond length increases. The results from Tables 3.9 and 3.11 for specimens with low modulus CFRP and normal modulus CFRP respectively, the bond strength values are close to each other, which indicates that changing from low modulus CFRP to normal modulus CFRP in CFRP-steel double strap joints, the ultimate joint strengths remain steady.

Table 3.10, which shows the results for series two (specimens with small section of low modulus CFRP), indicates that the bond strength fluctuates among the same bond length specimens, and this fluctuation prevents determination of the exact bond strength for all specimens. However, the bond strength values of specimens with ultra-high modulus CFRP differ from those for the other types of CFRP (low and normal modulus), with the results showing different behaviour in terms of load increment for each bond length, as shown in Table 3.12.

Table 3.9: Test results of low CFRP-steel double strap joints with 20mm wide CFRP

Specimen label	L_1	L_2	$L_2 - L_1$	Maximum load capacity (kN)	
				S1 S2 S3	Ave
LS1-30	30	100	70	41 40.9 41.1	41.0
LS1-40	40	100	60	49.2 52.5 50.5	50.7
LS1-50	50	100	50	62.2 58.8 59	60.0
LS1-60	60	100	40	67.6 70.5 69.1	69.1
LS1-70	70	110	40	75 77.8 76.8	76.5
LS1-80	80	120	40	86.4 87.4 86.7	86.8
LS1-90	90	130	40	96.8 90.6 93.5	93.6
LS1-100	100	140	40	105 96 100	100.3
LS1-110	110	150	40	106 109.9 108	108.0
LS1-120	120	160	40	107.1 112 107	108.7
LS1-130	130	170	40	108.5 109.3 109.5	109.1

The letter L stands for low CFRP modulus, S for specimen.

Number 1 stands for the first series which had 20mm wide CFRP,

Numbers 30-130 indicate the shorter bond length (L_1) in mm.

Table 3.10 shows the test results for specimens with low modulus CFRP and 10mm wide CFRP. The aim of studying the influence of CFRP width on the bond properties is to have some knowledge about the minimum CFRP width can be used in structural rehabilitations. The reason for testing 6 specimens for each bond length was to obtain a steady bond strength for specimens with the same bond length. The results show that the maximum load capacity of a joint varies within the same bond length, i.e. different results were obtained for same bond length, as shown in Table 3.10. Since there is inconsistency in the maximum joint strength for each bond length, it is hard to obtain the values for the effective bond length and maximum bond strength. In the previous series, in which CFRP laminate had a cross-sectional area of 20×1.4mm, the joint capacity increased with the increment of the bond length, but in this series the values of the joint capacity fluctuated with the increment of the bond length (L_1). The larger bond lengths cause greater degrees of fluctuation. The author attributes this variation in load to the sensitivity of the joint; this sensitivity is due to the small width of the CFRP laminate (10mm), which can cause eccentricity during the test due to any slight movement of the laminate before the adhesive sets. In addition, the larger bond length causes higher sensitivity, as the chance of CFRP movement is higher.

Table 3.10: Test results of low CFRP-steel double strap joints with 10mm wide CFRP

Specimen label	(L1)	(L2)	(L2-L1)	Maximum load capacity (kN)						
				S1	S2	S3	S4	S5	S6	Ave
LS2-30	30	100	70	15.6	19	15.2	14	13.2	16.1	15.52
LS2-40	40	100	60	23.5	21.2	18	20.4	20.8	18.7	20.43
LS2-50	50	100	50	27.8	24.2	23.1	24.9	28	26.2	25.70
LS2-60	60	100	40	29.3	27	26.4	31	24.1	28	27.63
LS2-70	70	110	40	40.9	25.6	28.4	33.2	30.1	37.5	32.62
LS2-80	80	120	40	34	33.8	30	26.7	31.1	27	30.43
LS2-90	90	130	40	24	24.5	40.7	31.7	35.8	29.9	31.10
LS2-100	100	140	40	34.9	36	30.4	35.8	38.2	25.6	33.48
LS2-110	110	150	40	30.3	33.3	35	37.6	39.5	34	34.95
LS2-120	120	160	40	29.7	31.5	26	30.3	34.8	39.5	31.97
LS2-130	130	170	40	35.3	37.4	39.7	32.1	28.5	37.2	35.03

The letter L stands for low modulus CFRP, S for specimen

Number 2 stands for the second series, which had 10mm wide CFRP

Numbers 30-130 indicate the shorter bond length (L1) in mm

Table 3.11 shows the test results for joints with normal modulus CFRP and 20mm wide CFRP. Some researchers have used two types of CFRP modulus to show the effect of CFRP modulus on the bond characteristics between steel and CFRP (Wu et al., 2012b; Fawzia et al., 2007; Schnerch and Rizkalla, 2008). In the present test program no effect was shown between the two types of specimens, due to the fact that the failure was steel-adhesive debonding, and all force was resisted by the adhesive layer. The results show no major differences between low and normal modulus CFRP in terms of ultimate joint capacity and failure mode.

Table 3.11: Test results of double strap joint under static tensile load (Series Three)

Specimen label	L1	L2	L2 –L1	Maximum load capacity (kN) S1 S2 S3	Maximum load capacity (kN) Ave
NS-30	30	100	70	39.4 43.6 42.9	41.9
NS-40	40	100	60	50.8 53.4 50.9	51.7
NS-50	50	100	50	64.2 56.8 61	60.7
NS-60	60	100	40	69 72.5 68.1	69.9
NS-70	70	110	40	77 75.7 72.3	75
NS-80	80	120	40	87.3 87.7 87.2	87.4
NS-90	90	130	40	94.9 92.2 95.5	94.2
NS-100	100	140	40	106.1 96.2 101.7	101.3
NS-110	110	150	40	107 108.8 109.2	108.3
NS-120	120	160	40	111.2 107.6 106.7	108.5
NS-130	130	170	40	107.4 110.5 109.7	109.2

The letter N stands for normal modulus CFRP; S for specimen,

Numbers 30-130 indicate the shorter bond length (L_1) in mm

Table 3.12: Test results of ultra-high modulus CFRP-steel double strap joints with 20mm wide CFRP

Specimen label	L_1	L_2	$L_2 - L_1$	Maximum load capacity (kN)	
				S_1 S_2 S_3	Ave P_{EX}
UHS-30	30	100	70	30.4 32.9 31.7	31.76
UHS-40	40	100	60	42.9 43.5 43.57	43.3
UHS-50	50	100	50	54.7 56.7 52.1	54.4
UHS-60	60	100	40	66.2 62.5 63.7	64.1
UHS-70	70	110	40	72 73 74.6	73.2
UHS-80	80	120	40	73 72.9 73.4	73.1
UHS-90	90	130	40	73.2 73.4 72.3	73.0
UHS-100	100	140	40	73.5 73.6 72.4	73.2
UHS-110	110	150	40	72.8 73.6 73.7	73.4
UHS-120	120	160	40	72.9 73.8 73.1	73.3
UHS-130	130	170	40	72.1 73.6 73.9	73.2

The letters UH stand for ultra-high modulus CFRP, S for specimens

Numbers 30-130 indicate the shorter bond length (L_1) in mm

The maximum joint capacity for specimens with low and normal modulus CFRP were about 110kN for a bond length of 110mm, whereas 73kN was the maximum bond strength for joints with ultra-high modulus CFRP for a bond length of 70mm. There are two possible reasons for the decrease in bond strength for joints with ultra-high modulus CFRP compared to specimens with low and normal modulus CFRP. The tensile strength and ultimate strain of the ultra-high modulus CFRP are lower than those for the low and normal modulus CFRP. In addition, the thickness of ultra-high modulus CFRP is smaller than that of the other CFRPs used, which decreases the axial stress of CFRP.

3.5.2 Effective bond length

The effective bond length is the second result that was obtained from the quasi-static experimental tests of CFRP-steel double strap joints. The effective bond length can be defined as the bond length beyond which no further increment occurs in the joint capacity. The effective bond length was theoretically observed by Hart-Smith (1973) , and his model used elastic-plastic adhesive rather than pure elastic or non-linear behaviour. The failure mechanism was totally dependent on the maximum shear strain of the adhesive at the location of highest strain or stress values. A number of researchers have studied this concept experimentally for different types of CFRP and sections (Fawzia et al., 2006b; Liu et al.; Al-Zubaidy et al., 2012a-a; Nguyen et al., 2011). For the current project, the effective bond length was varied depending on the CFRP properties. For specimens with low and normal modulus CFRP, the effective bond length was found to be 110mm, whereas it was found to be 70mm for specimens with ultra-high modulus CFRP. Figure 3.14 shows the plots of joint capacities in kN versus the bond length for all joint types.

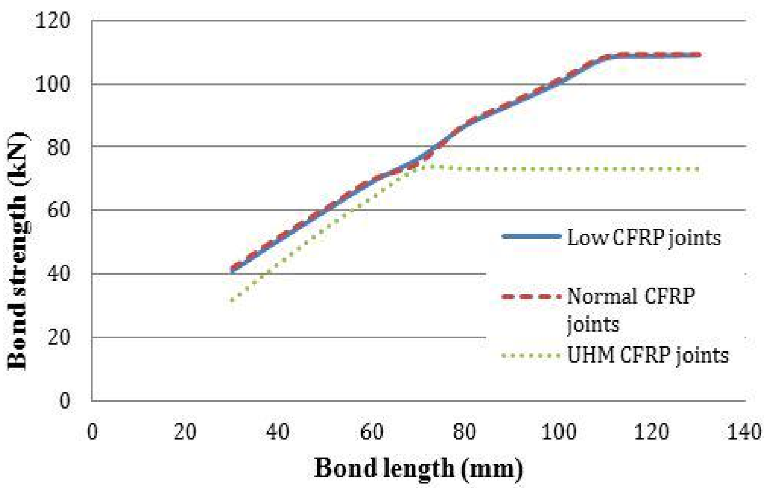

Figure 3.14: Bond strength vs. bond length for all joint types

The current results for low modulus CFRP joints were compared with those of previous studies. Xia and Teng (2005) used low modulus CFRP laminates in double strap joints and loaded them under quasi-static loading. The only difference in the parameters is the

CFRP width, which is 20mm for the current test and 50mm in their study. Different effective bond lengths were found in both tests. Xia and Teng (2005) found that the effective bond length was 140mm for low modulus CFRP-steel joints with 50mm wide CFRP; however, the current test showed 110mm as the effective bond length for the same joint with 20mm wide CFRP. Figure 3.15 shows the comparison between the current tests and the tests carried by (Xia and Teng, 2005). The plot shows the average bond strength per unit width versus the bond length. The effective bond length can be obtained when the turning point exists on the graph. Figure 3.16 shows the bond strength and bond length relation for joints with normal modulus CFRP, and changing from low modulus to normal modulus has no effect on the effective bond length, the effective bond length being 110mm for both joints.

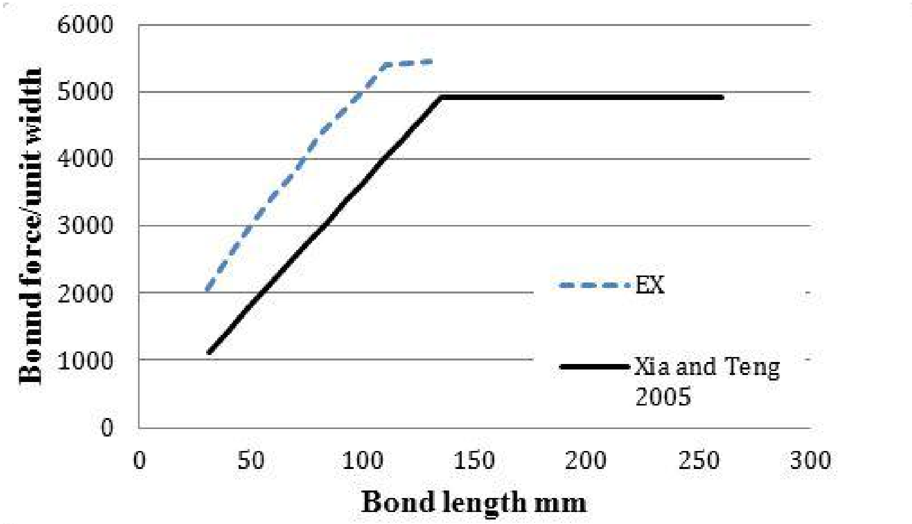

Figure 3.15: Ultimate joint strength per unit width vs. bond length for low modulus CFRP-steel double strap joints

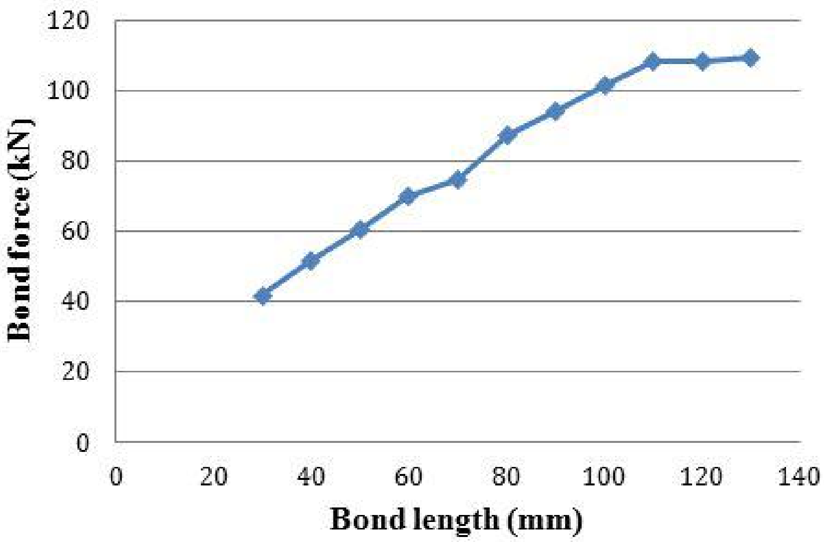

Figure 3.16: Ultimate joint strength vs. bond length for normal modulus CFRP-steel double strap joints

with ultra-high modulus CFRP modulus. A significant decrease in effective bond length was observed from these test results compared to the previous two joints. The effective bond length dropped to 70mm. This drop can be explained by the ultimate strain value of the joints with ultra-high CFRP modulus, as the smaller strain causes less stretch in joints, which results in earlier failure.

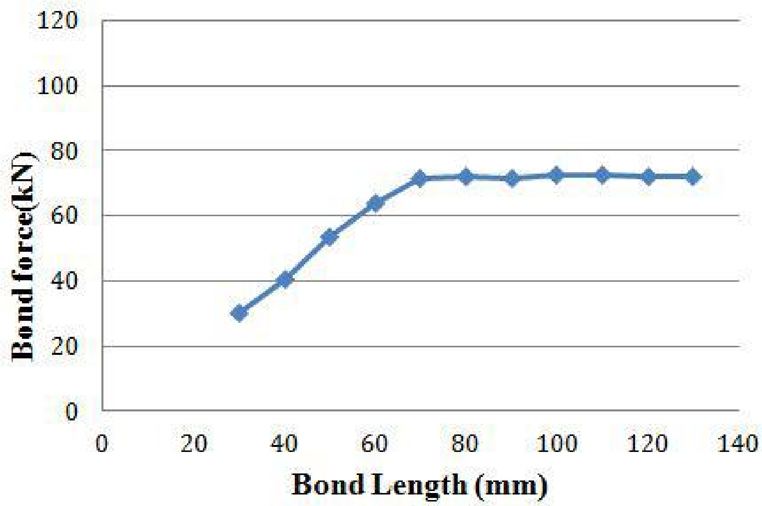

Figure 3.17: Ultimate joint strength per unit width vs. bond length for ultra-high modulus CFRP-steel joints

The results in the above figures are the average capacity of three specimens for each bond length. From the above comparison for low CFRP joints tests, it is obvious that the effective bond length is affected by the CFRP width; the smaller the CFRP width, the shorter the effective bond length, and vice versa.

3.5.3 Failure modes

One of the most important outcomes of the current test program is the failure pattern of the CFRP-steel double strap specimens, which provides greater understanding of load transfer and the material that resists more in composite joints. Zhao and Zhang (2007) summarized the six expected failure modes for adhesively-bonded joints between steel and CFRP. These six failure modes are shown in Figure 3.17.

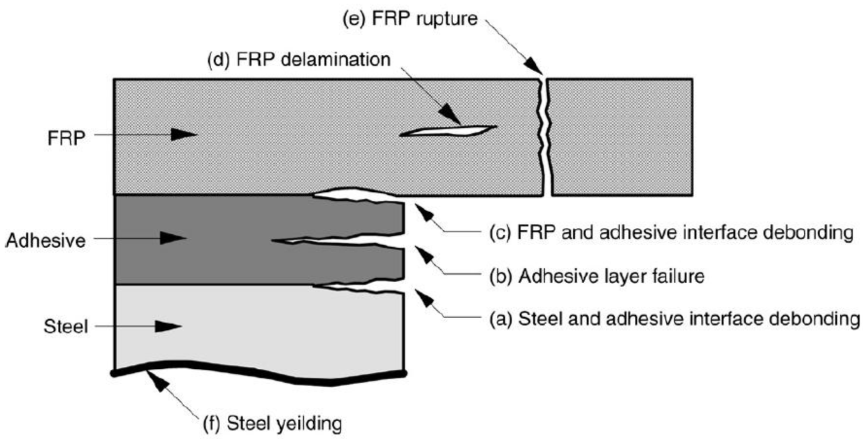

Figure 3.18: Possible failure modes of FRP-steel adhesively bonded joints (Zhao and Zhang, 2007)

The six failure modes in the figure above can be defined as follows: (a) steel and cohesive layer interface failure, (b) cohesive layer failure, (c) FRP and adhesive debonding failure, (d) CFRP delamination, (e) CFRP rupture and (f) steel yielding failure. Depending on these proposed failure modes, there are some differences in failure mechanisms in the four different series. In the current testing program, some differences in failure mechanisms in the four different series were detected. For series one, which had low modulus CFRP and 20mm wide CFRP, the failure mode was found to be mixed between steel-adhesive debonding (a) and adhesive layer failure (b) for bond lengths below the effective bond length. As shown in Figure 3.18, the failure mode is different when the bond length reaches close to and beyond the effective bond length and becomes completely steel-adhesive debonding, as shown in Figure 3.19. This change in failure mode at this range of bond lengths gives an indication of the range of effective bond length, which is another way to prove the effective bond length in addition to maximum failure capacity. The above failures indicate that static tension load is mainly sustained by the adhesive layer. This failure also occurs in adhesively-bonded joints with CFRP, as claimed by (Jiao and Zhao, 2004; Xia and Teng, 2005).

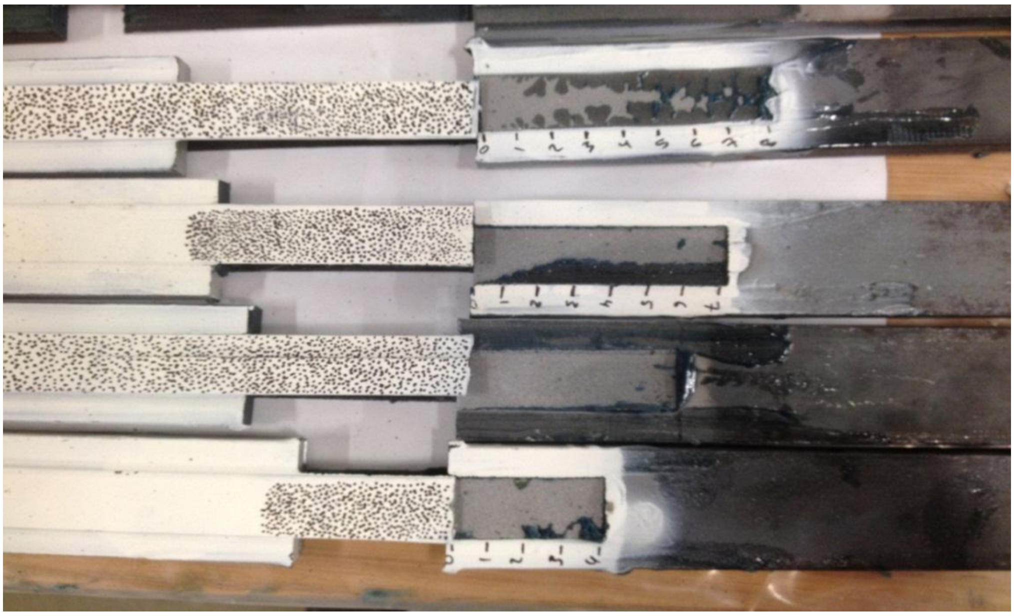

Figure 3.19: Failure modes for specimens with low modulus CFRP and bond lengths less than the effective bond length

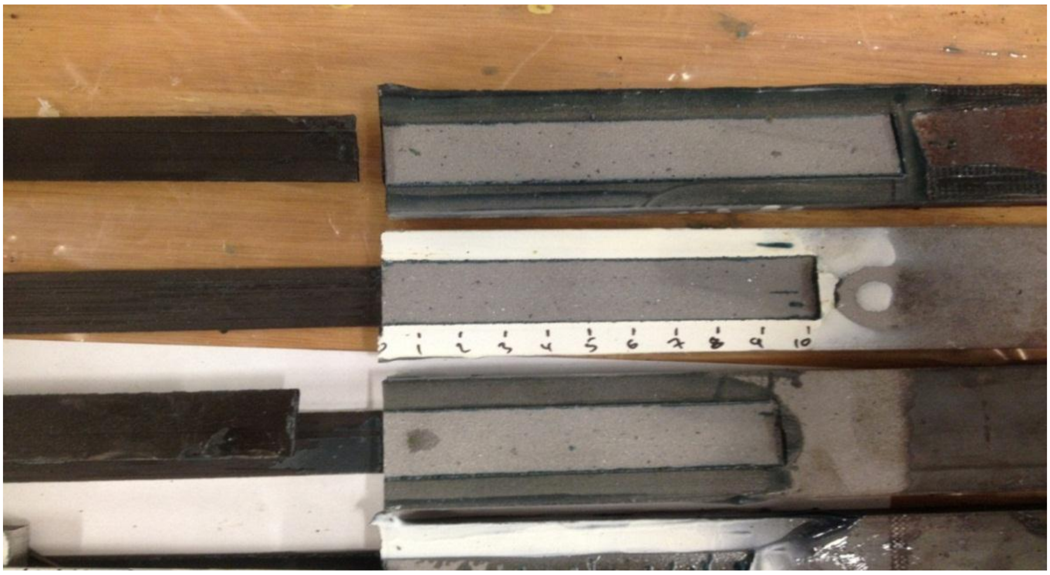

Figure 3.20: Failure modes for specimens with low modulus CFRP and bond lengths close to the effective bond length

The failure mode in the next series, which had 10mm wide CFRP and low modulus CFRP was FRP delamination (d) for all bond lengths, as shown in Figure 3.20.

Figure 3.21: FRP delamination for specimens with low modulus CFRP 10mm wide

This failure mode could not be assumed to be the actual failure mode of these specimens, due to fluctuations in results, as shown in Table 3.10. This fluctuation was due to the sensitivity of the small width CFRP-steel double strap joints to any slight movement. As the bond strength and the effective bond length could not be obtained, the failure mode of this series was assumed to be unrealistic and to have some errors.

For specimens in series three, which had normal modulus CFRP modulus and 20mm wide CFRP, the failure mode for all bond lengths was steel and adhesive debonding (Failure mode a). The failure mode of this series of tests is shown in Figures 3.21 and 3.22.

Figure 3.22: Failure mode for specimens with normal modulus CFRP.

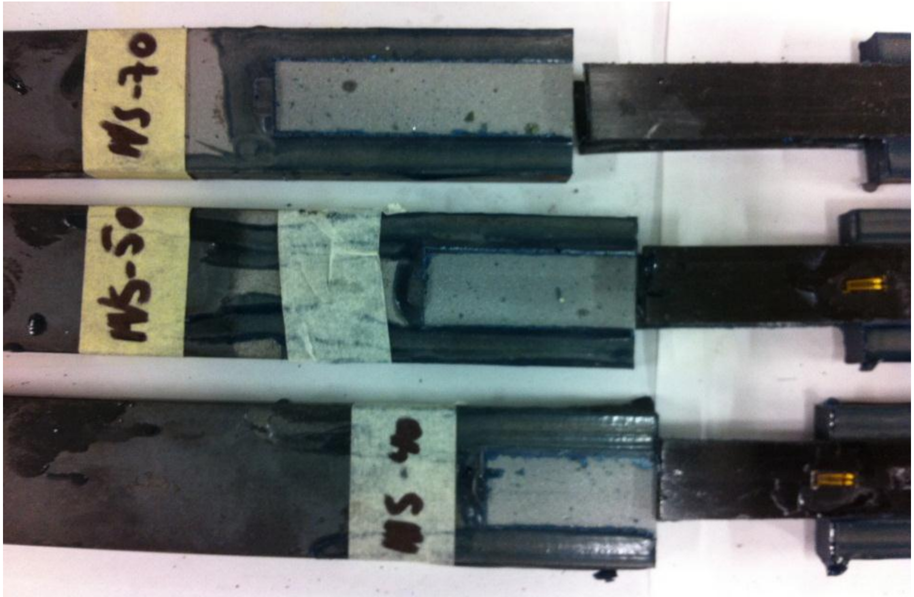

Figure 3.23: Failure mode for specimens with normal modulus CFRP.

The failure mode of the current series of test indicates that the adhesive layer completely sustains the quasi-static tension force.

The specimens with ultra-high modulus CFRP 20mm wide had a completely different mode of failure compared to the previous sets of specimens. The failure mechanism of the ultra-high modulus CFRP-steel joints under quasi-static load was shown to be CFRP delamination for specimens with bond lengths less than the effective bond length, and CFRP rupture for specimens with bond lengths equal to and beyond the effective bond length. Figures 3.23 and 3.24 show the failure modes for this set of specimens, the failure modes in this set of joints indicate that the tensile loading is mainly resisted by the CFRP itself within the CFRP-steel double strap joints. The change in failure mode at bond lengths equal to the effective bond length is another proof of the effective bond length rather than the ultimate load capacity.

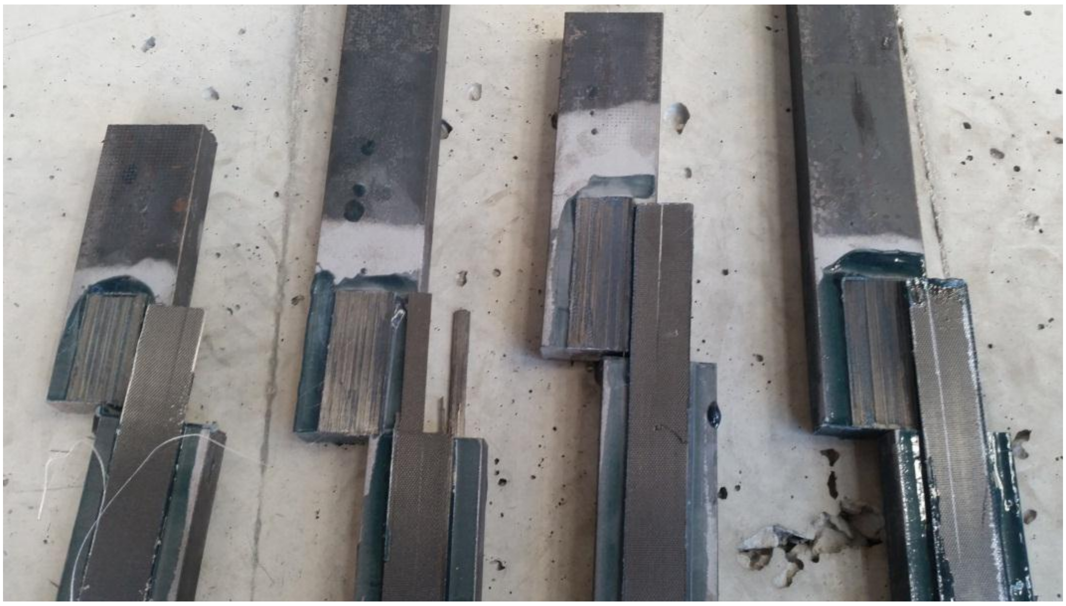

Figure 3.24: FRP delamination for ultra-high modulus CFRP-steel joints with bond lengths less than the effective bond length

Figure 3.25: FRP rupture for ultra-high modulus CFRP-steel joints with bond lengths beyond the effective bond length

The CFRP/steel double strap joints are subjected to tension load which causes direct shear force among the joint layers. For this, the shear stress was included in the discussion. In order to study the impact of failure mode on the bond stress of the specimens along the bond line, the current results of normal modulus CFRP specimens were compared with those of Al-Zubaidy et al. (2011b) , who used CFRP sheets. Figure 3.25 shows the average bond stress versus bond length for their tests and the current results. Evidently, the laminates in the current tests have higher bond strengths for the same bond lengths. This is attributed to the type of failure modes observed in the two systems. Laminate CFRP specimens exhibited steel-adhesive debonding, while the failure mode observed in the sheet CFRP tests was delamination within the CFRP sheet.

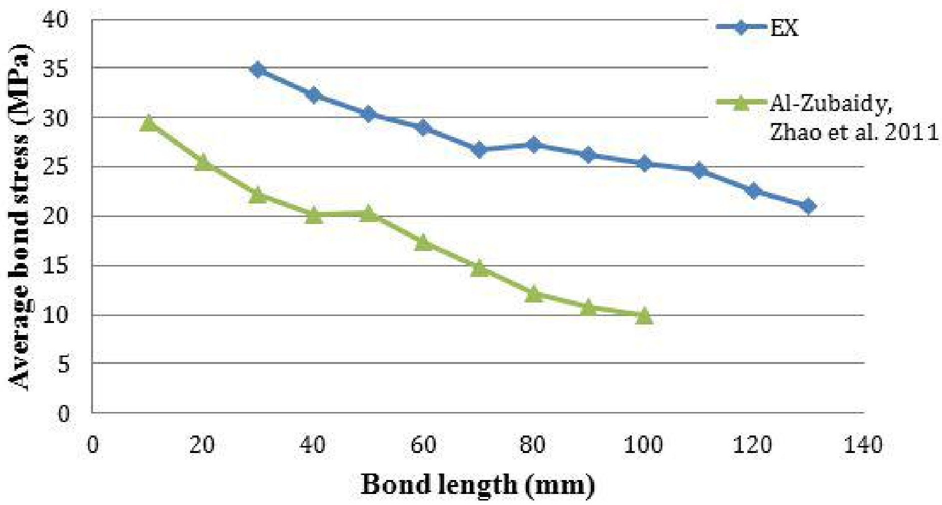

Figure 3.26: Average shear stress vs. bond length for normal modulus CFRP-steel double strap joints.

Table 3.13 below summarises all the failure mechanisms for the different CFRP-steel double strap joints, including low modulus CFRP-steel double strap joints with 20mm wide CFRP, normal modulus CFRP-steel double strap joints with 20mm wide CFRP, and ultra-high modulus CFRP-steel double strap joints with 20mm wide CFRP.

Table 3.13: Summary of the failure modes of the three different CFRP-steel double strap joints

Joint with:	Loading rate 2mm/min	
	Below EBL	Beyond EBL
Low modulus CFRP	a & b	a
Normal modulus CFRP	a	a
Ultra-high modulus CFRP	b & d	e

EBL = effective bond length.

Failures a, b, d and e are steel-adhesive debonding, adhesive failure, FRP delamination and FRP rupture respectively, as explained in Figure 3.17.

3.5.4 Strain distribution along the bond length

The strain distribution along the bond length of CFRP-steel double strap joints was also studied in this research, based on two methods of capturing strain: image correlation photogrammetry for capturing strain at any point along the bond using the correlated solution camera VIC-3D, and foil strain gauges to capture the strain at the centre of joints only. The results of these two methods were compared and the results are plotted in Figure 3.26. The figure shows that the strain gauge reading at the joint is very close to that captured by the image correlation photogrammetry technique; the same results were achieved for all specimens. As the readings of strain values from the strain gauges and image correlation photogrammetry technique matched, all ultimate and distributed strain readings have been obtained from the correlated solution camera, as it gives the strain at different locations along the CFRP laminate within the double-strap joint specimen. The strain was obtained at each 10mm from the joint; measurements were sketched on specimens before the test, as shown in Figure 3.27.

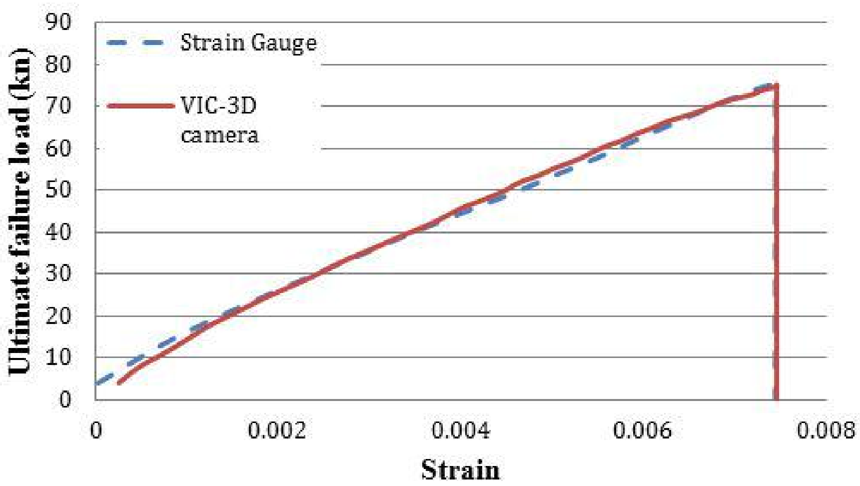

Figure 3.27: Ultimate joint strength vs. strain for the two methods of capturing strain.

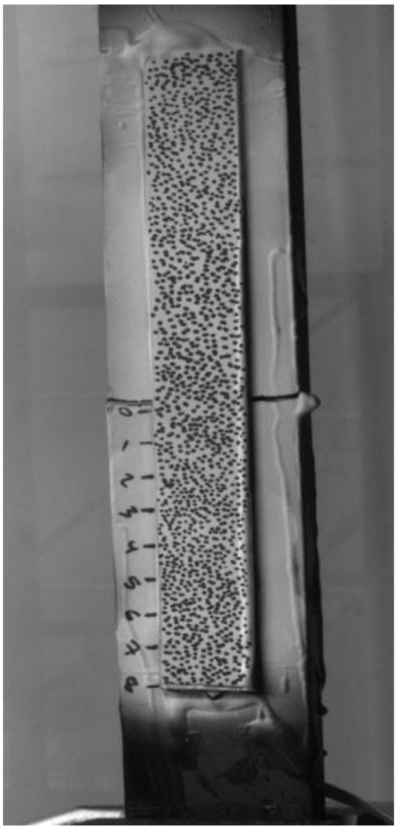

Figure 3.28: Specimen with distance measurements.

In the case of strain distribution along the bond length between low modulus CFRP and steel plate, the results show that maximum strain occurs at the joint, and then it decreases linearly away from the joint. The strain values at the far end of the joint and for all load levels are close to each other, as shown in Figure 3.28. The same curve trend was obtained from specimens with normal modulus CFRP, but with a little difference in strain values, as shown in Figure 3.29. The load level can be defined as the ratio of the applied load to the maximum failure load obtained from the test results.

The strain distribution along the bond between ultra-high modulus CFRP-steel double strap joints is shown in Figure 3.30. The trend of strain distribution is similar to that of the other two joints; the maximum strain is shown at the joint and it decreases away from it. A significant decrease in the ultimate strain value for joints with ultra-high modulus CFRP was observed compared to those with low and normal modulus CFRP. A comparison of ultimate stress against ultimate strain for the two types of CFRP in CFRP-steel double-strap specimens is shown in Figure 3.31.

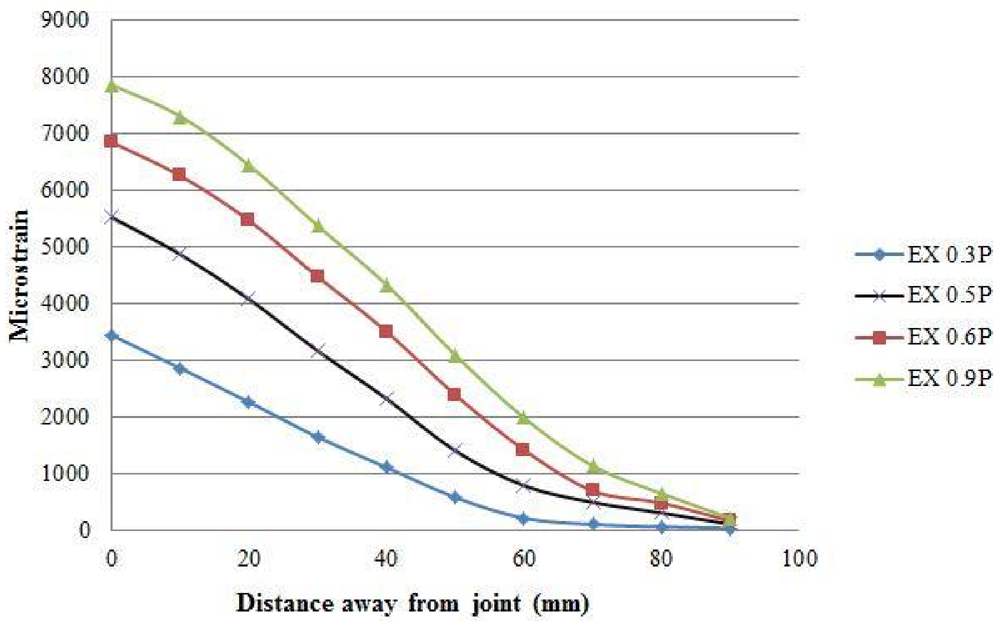

Figure 3.29: Strain distribution for specimen with low modulus CFRP.

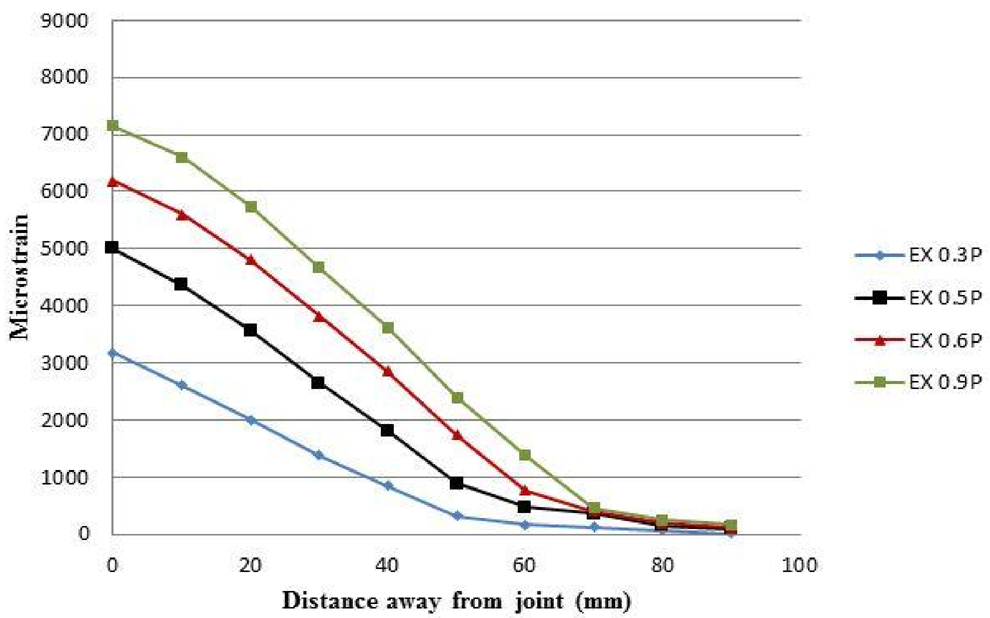

Figure 3.30: Strain distribution for specimens with normal modulus CFRP.

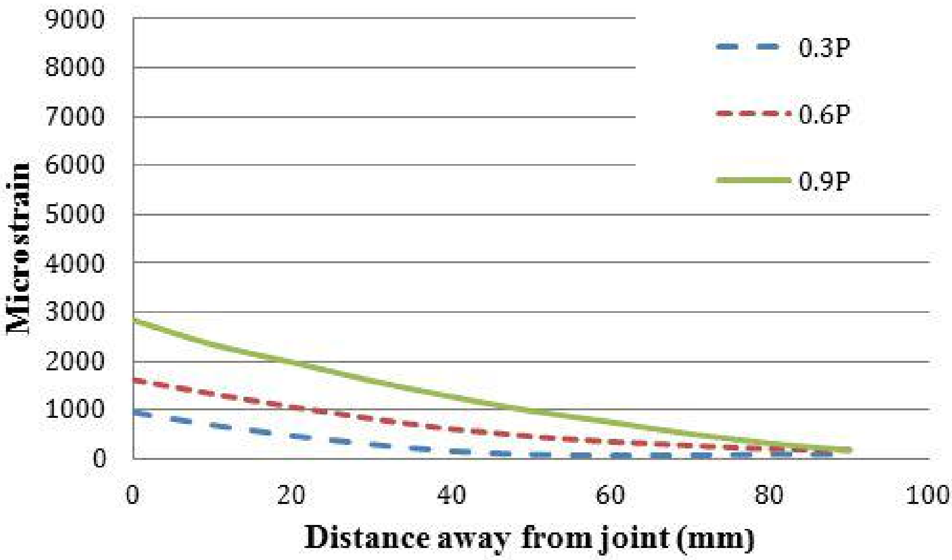

Figure 3.31: Strain distribution along the bond of UHM CFRP-steel double strap joints.

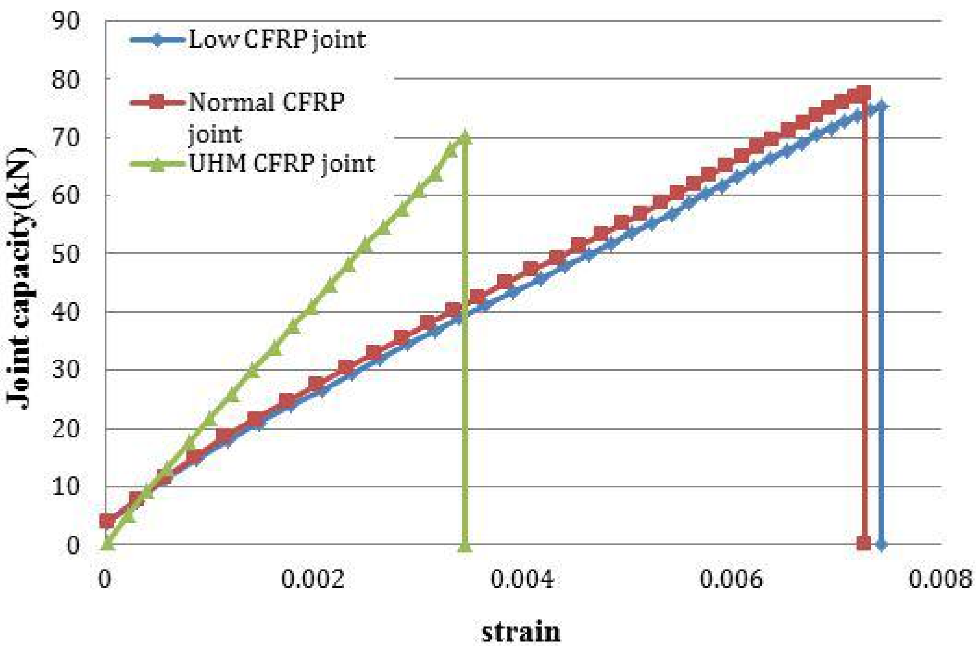

Figure 3.32: Load vs. strain for the three CFRP-double strap joints.

3.6 CONCLUSION

A number of CFRP-steel double strap specimens were loaded under tension force with a load rate of 2mm/min, using an MTS machine with a maximum capacity of 250 kN. The aim of this research was to investigate the bond characteristics between CFRP laminate and steel members. Three types of CFRPs were used in this research, low modulus CFRP (165 GPa), normal modulus CFRP (205 GPa) and ultra-high modulus

CFRP (460 GPa). Araldite 420 epoxy was used to bond the CFRP laminate to steel joints. Two different CFRP sections were used (20× 1.4mm and 10×1.4mm) in order to investigate the effect of CFRP section on the bond characteristics between CFRP and steel in the double strap joints. Bond strength, strain distribution along the bond, effective bond length and failure mode were tested in this program. Two methods of capturing strain were used: image correlation photogrammetry and foil strain gauges. The following observations can be made:

- The actual material properties of low, normal and ultra-high modulus CFRP Araldite 420 epoxy and steel plate were found to be close to the manufacturers' claimed properties.
- Using small-sized CFRP laminate with a width of 10mm does not give accurate results, as the adhesive size is small and its capacity to resist the load is very sensitive to any movement
- For 20mm wide CFRP, changing from low to normal modulus CFRP has no effect on the effective bond length, which is found to be 110mm for both types of CFRP in the double-strap joint specimens. In contrast, a significant change in the effective bond length for specimens with ultra-high modulus CFRP was observed, and the value of the effective bond length for specimens with ultra-high modulus CFRP is 70 mm
- CFRP width has an influence on the effective bond length. For specimens with low modulus CFRP and 20mm wide CFRP, the effective bond length was 110mm, whereas it was found to be 140mm for specimens with low modulus CFRP 50mm wide. For specimens with ultra-high modulus CFRP 20mm wide, the effective bond length was 70mm, whereas it was found to be 110mm for the same joint with a 50mm bond width.
- For all types of specimens (low modulus CFRP, normal modulus CFRP and ultra-high modulus CFRP), the maximum strain was found to be at the joint and decreased away from joint, and the same strain distribution curve was found for all joints with different values.
- Changing from low to normal modulus CFRP has insignificant effects on the maximum failure strain and strain distribution, and lower strain values were observed for specimens with normal modulus CFRP compared to those with low modulus CFRP. However, a significant decrease was observed in the ultimate

strain and strain distribution along the bond length for specimens with ultra-high modulus CFRP. This decrement is due to the modulus of elasticity of CFRP, which is 450 GPa.

- Little increment in the maximum joint capacity was found when using normal modulus CFRP in the double-strap joint specimens compared to the low modulus CFRP specimens. However, a significant decrease was observed in the maximum failure capacity for specimens with ultra-high modulus CFRP, due to the low CFRP tensile strength (1500 MPa) and the thickness of 1.2mm.
- Failure modes for both specimens with low and normal modulus CFRP were quite similar; the failure mode was debonding between steel and adhesive, in addition to some adhesive failure, which occurs for both types of specimens. In contrast, different failure modes were observed for specimens with ultra-high modulus CFRP: FRP delamination for specimens with bond lengths below the effective bond length, and FRP rupture for specimens with bond lengths equal to and beyond the effective bond length.

CHAPTER FOUR EXPERIMENTAL INVESTIGATION OF THE BOND CHARACTERISTICS BETWEEN STEEL AND CFRP LAMINATE UNDER IMPACT LOADS

4.1 INTRODUCTION

Adhesively-bonded structural joints are usually subjected to dynamic loadings during their service life. Civil structures need to be monitored and investigated regularly; strengthening is sometimes needed when cracks occur due to the structure ageing, or when the use of the structure changes. Strengthening with CFRPs is a common method which has attracted structural engineers in the last decades. Conventional methods have disadvantages, as they are time-consuming, they increase the dead load of structures and they require mechanical lifting and anchoring devices for installation. CFRPs eliminate these disadvantages because they are light in weight, easy to install and have high tensile strength. The key to the strengthening is the bond between the CFRP and the structural member. The bond between steel and CFRP sheet under impact loading has been studied previously with different parameters (Pereira et al., 2011; Challita et al., 2011; Al-Zubaidy et al., 2012a-b), but the effect of impact loading on the bond between steel and CFRP laminate is not yet fully understood. This chapter is a continuation of Chapter Three, and reports on an experimental investigation of the bond characteristics between steel and CFRP laminate under impact loadings. Three types of CFRP were used to strengthen steel joints using Araldite 420 as a bonding material: low modulus CFRP (165 GPa), normal modulus CFRP (205 GPa) and ultra-high modulus CFRP (460 GPa).

4.2 STUDY OBJECTIVE

Recently, composite materials and especially adhesively-bonded fibres have been used widely in civil engineering applications such as buildings, bridges and other structures. Many studies have focused on the bond characteristics between steel members and CFRP, by testing and analysing these composite structural elements with different types of loads. Although these studies have covered different types of loading, the effect of impact loading on this bond remains little understood. It is important to study the bond properties between CFRP laminate and steel structures under impact loading, as this kind of load is common in structures, specially bridges, off-shore platforms and buildings. The aim of this study is to fill the gap in knowledge found in Chapter Two, by preparing a large number of specimens to study the bond properties of CFRP-steel double strap joints under impact tensile loading. To examine the effect of load rates on bond, specimens were subjected to various load rates (201×10^3, 258×10^3 and 300×10^3 mm/min). These loading rates represent low intensity of blast, earthquake and wave loadings or any type of sudden impact loading on structures such as car accidents and mass falls on structures. Araldite 420 epoxy was used in bonding CFRP to steel; three types of CFRP laminate (low, normal and ultra-high modulus) were used with different bond lengths from 20mm to 130mm. The experimental work included three main series of double strap joints, the first with low modulus CFRP, the second with normal modulus CFRP and the last with ultra-high modulus CFRP. Each series was tested under the three loading rates mentioned above to determine the maximum failure load, effective bond length, strain distribution along the bond and failure mode.

4.3 EXPERIMENTAL INVESTIGATION OF THE MATERIAL PROPERTIES

The materials used in this experimental program to form the CFRP-steel double strap joints were mild steel, Araldite 420 epoxy, low modulus CFRP laminate CFK 150/2000, normal modulus CFRP laminate CFK 200/2000 and ultra-high modulus CFRP laminate MBrace 460/1500. To achieve a full understanding of the bond behaviour between CFRP laminate and steel plates, the mechanical properties of the materials are required. Normally the manufacturers' technical sheets provide the mechanical properties of the materials under static loading. However, for the purposes of the present research, an investigation of the dynamic properties of the composite materials was conducted. The investigation was carried out under three different load rates to obtain the materials' properties under the same loading rates used to test the CFRP-steel double strap joints.

4.3.1 Carbon Fibre Reinforced Polymers (CFRPs)

The dynamic properties of the three types of CFRP used in this project were experimentally investigated. CFRP coupon specimens were prepared for all CFRP types in accordance with ASTM 3039-08. All CFRP types were tested under three loading rates: 201×10^3, 258×10^3 and 300×10^3 mm/min.

4.3.1.1 Coupon preparation

All types of CFRP coupons had the same preparation method. CFRP laminate rolls were cut into a number of plates; each plate was 190mm long, 20mm wide and 1.4mm thick for low and normal modulus CFRP, while the ultra-high modulus CFRP coupons had the same dimensions except that they were 1.2mm thick. Each CFRP coupon was bonded by steel tabs using Araldite 420 epoxy at its two ends to decrease the stress concentration near the grips. The steel tabs were sandblasted to remove any contaminated materials, and they were then wiped with acetone to remove any remaining dust. The CFRP coupons were cured for more than 7 days at 25° C to obtain the full capacity of adhesive, as recommended by manufacturer. A schematic view of a CFRP coupon is shown in Figure 4.1.

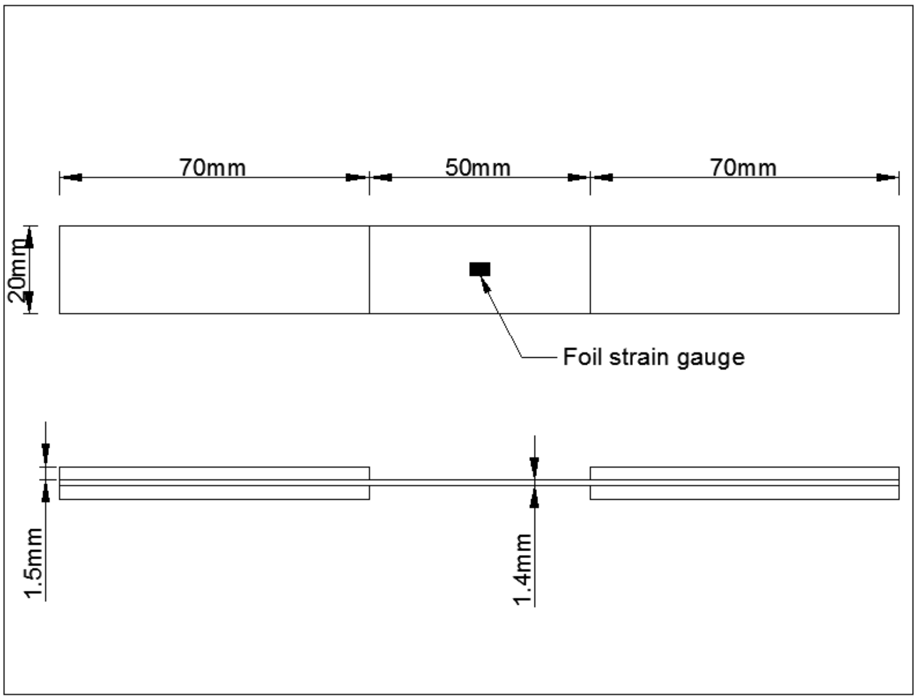

Figure 4.1: Schematic view of CFRP coupon tested under dynamic loading (NOT TO SCALE)

The mechanical properties of CFRP investigated were: ultimate tensile strength, ultimate failure strain and modulus of elasticity. To find the ultimate failure strain, a foil strain gauge was mounted at the centre of each coupon; the image correlation photogrammetry technique could not be used in this test due to the low numbers of data taken in the second (maximum of two). Five CFRP coupons were prepared and tested for each load rate. Table 4.1 shows the total number of CFRP coupons tested in this stage of the research.

Table 4.1 : Total number of CFRP coupons tested under dynamic loading

Load rate (mm/min)	201×10^3	258×10^3	300×10^3
Low modulus CFRP	5	5	5
Normal modulus CFRP	5	5	5
UHM modulus CFRP	5	5	5
Total number of coupons	45		

4.3.1.2 Measured properties

The dynamic properties of the materials used to form the double strap joints were investigated, and the tensile strength, ultimate strain and modulus of elasticity of the three types of CFRPs are reported in the following sections.

Low modulus CFRP

Low modulus CFRP was used in this research to strengthen steel joints under dynamic loading. This low modulus CFRP produced by S&P Laminates (CFK 150/2000) is a brittle material with unidirectional fibres with high tensile strength. The values of tensile strength, ultimate strain and Young's modulus under dynamic loading were 3567MPa, 0.019 and 184.5GPa, 4149.1MPa, 0.022 and 188.2 GPa, 4443.1MPa, 0.023 and 192 GPa for loading rates of 201×10^3mm/min, 258×10^3 mm/min and 300×10^3 mm/min respectively.

Normal modulus CFRP

Normal modulus CFRP was also used in CFRP-steel double-strap specimens; these specimens were tested under three loading rates. The normal modulus CFRP was provided by S&P Laminates. CFK 200/2000 is a brittle material with unidirectional fibres with high tensile strength. It has a higher modulus of elasticity (E) than S&P Laminates CFK 150/2000. The values of tensile strength, ultimate failure strain and Young's modulus under dynamic loading were 3578MPa, 0.0158 and 226.4 respectively for the loading rate of 201×10^3mm/min, 4151MPa, 0.018 and 230.6 GPa respectively for the loading rate of 258×10^3 mm/min, and 4487MPa, 0.0193 and 232.4 GPa respectively for the loading rate of 300×10^3 mm/min.

Ultra-high modulus CFRP

MBrace laminate 450/1500 with a thickness of 1.2mm was used in the CFRP-steel double strap joints tested under dynamic loading. The tensile strength, ultimate strain and modulus of elasticity were 1967MPa, 0.37% and 531.6 GPa respectively for the loading rate of 201×10^3mm/min, 2263MPa, 0.425% and 532.4 GPa respectively for the loading rate of 258×10^3 mm/min, and 2394.3 MPa, 0.45% and 532.1GPa respectively for the loading rate of 300×10^3 mm/min.

4.3.2 Araldite 420

Araldite 420 epoxy has two parts, A and B. It has non-linear stress-strain behaviour. As mentioned in Chapter Two, this epoxy has high shear strength. The tensile properties of the adhesive layer under dynamic loading are the key to understanding the behaviour of CFRP-steel double strap joints under different loading rates.

The actual properties of Araldite 420 under the three loading rates of 201×10^3mm/min, 258×10^3 mm/min and 300×10^3 mm/min were investigated by Al-Zubaidy, (2012). Adhesive coupons were prepared in accordance with ASTM: D638-01. Figure 4.2 shows an schematic view of an epoxy coupon specimen. The adhesive coupon specimens were cured for more than 7 days to obtain the full adhesive capacity, as specified in the manufacturer's instruction for use.

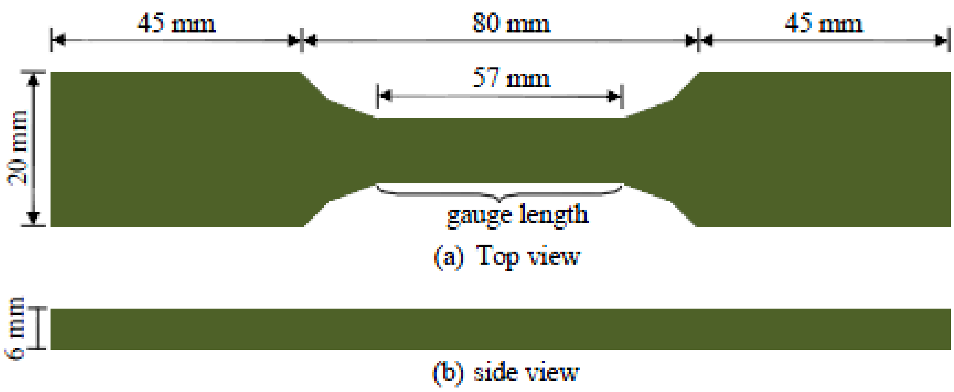

Figure 4.2: Dimensions of adhesive coupon for dynamic testing (Al-Zubaidy, 2012)

The measured tensile strength, ultimate strain and modulus of elasticity of this epoxy under different loading rates were: 93.25 MPa and 2874.93 MPa, 96.06 MPa and 2997.7 MPa, 99.42 MPa and 3102 MPa for loading rates of 201×10^3mm/min, 258×10^3 mm/min and 300×10^3 mm/min respectively. All the above results were experimentally investigated by Al-Zubaidy, (2012). The stress strain curves of Araldite 420 epoxy were plotted under the three loading rates, and the results are shown in Figure 4.3.

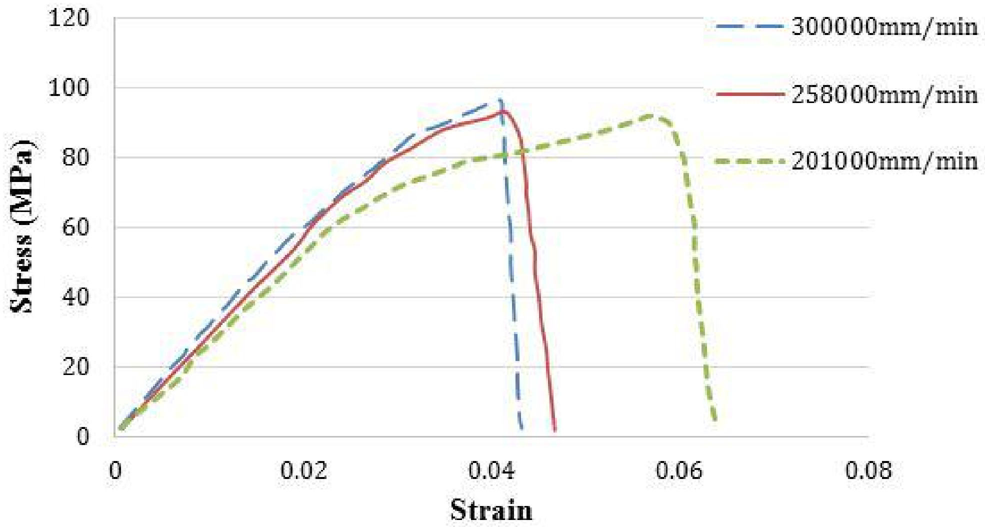

Figure 4.3: Stress-strain curve for Araldite 420 under different loading rates (Al-Zubaidy, 2012) (Re-plotted).

4.3.3. Steel plate

Mild steel plates with a thickness of 16mm were utilised in this testing program to avoid steel yielding failure. A number of steel dog-bone specimens were prepared in accordance with Australian Standard AS 1391-07. The dynamic properties of steel were investigated under three loading rates: 201×10^3mm/min, 258×10^3mm/min and 300×10^3 mm/min. The mechanical properties of mild steel under dynamic loading were different to those under quasi-static loading. The examined dynamic properties were yield stress, ultimate tensile strength and modulus of elasticity. The measured properties were: 628.4 MPa, 770.8 MPa and 246.6 GPa, 691 MPa, 826.9 MPa and 232.4 GPa, 740.2 MPa, 866.6 MPa and 217.1 GPa respectively for loading rates of 201×10^3mm/min, 258×10^3 mm/min and 300×10^3 mm/min respectively. Figure 4.4 shows the stress-strain curves under the three dynamic loading rates.

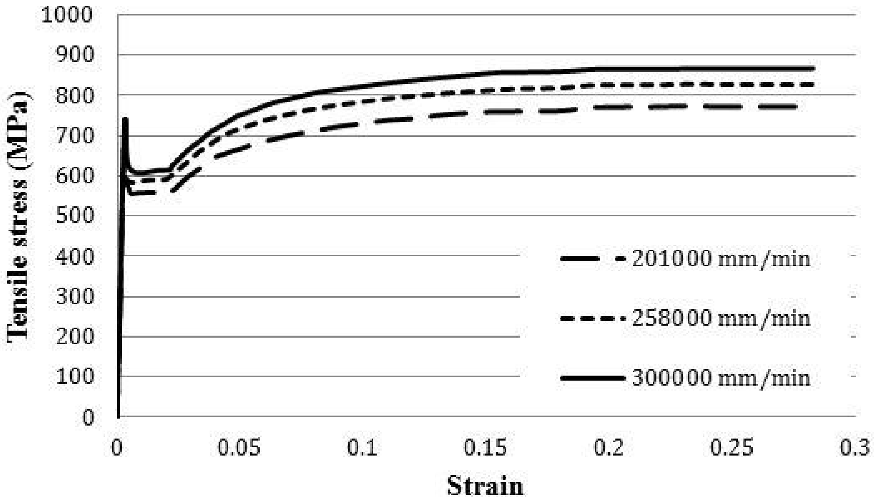

Figure 4.4: Stress-strain curves of mild steel under different dynamic loading rates

4.4 EXPERIMENTAL INVESTIGATION OF THE BOND BETWEEN CFRP AND STEEL

As mentioned previously, this chapter reports on the effect of high loading rates on the bond behaviour between CFRP laminates and steel. In order to have a full understanding of the effect of high loading rates on this bond, three different types of CFRP were used (low modulus CFRP laminate CFK 150/2000, normal modulus CFRP laminate CFK 200/2000 and ultra-high modulus CFRP laminate MBrace 460/1500). The three loading rates used in this test were 201×10^3, $258\times10^3$and 300×10^3 mm/min.

A total of 198 CFRP-steel double strap joints were prepared and tested under the different loading rates. As this comprehensive experimental program focussed on finding the bond properties between CFRP laminate and steel in double strap joints, the main properties examined in this test were the maximum joint capacity, failure mode, effective bond length and strain distribution along the bond. Three groups of tests were conducted; each group had three types of CFRP: low, normal and ultra-high modulus. The difference among these groups was the loading rate. For the first group, a loading rate of 201×10^3 mm/min was applied to the three types of joints. For the second group, a loading rate of 258×10^3 mm/min was applied to all types of CFRP-steel double strap joints. For the last group, a load rate of 300×10^3 mm/min was applied to all types of joints. The quasi-static results explained in Chapter Three are considered to be the reference data for comparison with the results in this chapter. The aim of this test was to measure the degree of enhancement under impact tension load compared to the quasi-static tension load. Each specimen was tested three times, and the average results were adopted. All specimens with the different parameters had the same preparation and material properties except the CFRP modulus. The bond length for the first two groups varied from 40mm to 110mm, and from 20mm to 90mm for the third group of joints. Table 4.2 shows the total number of tests in this program.

Table 4.2: Total number of specimens tested under dynamic loading

CFRP Modulus	Low modulus CFRP joints			Normal modulus CFRP joints			UHM modulus CFRP joints		
Load Rate (mm/min)	201×10^3	258×10^3	300×10^3	201×10^3	258×10^3	300×10^3	201×10^3	258×10^3	300×10^3
No. of spec	24	24	24	24	24	24	27	-	27
Total	72			72			54		

4.4.1 Brief description of the impact drop mass machine

Although structures are usually subjected to both static and dynamic loading, the experimental research in the past has focussed mainly on static tests, and less research uses dynamic testing due to the complexity of running the dynamic tests. Testing structural members under impact loading has some difficulties due to the very fast speed of the impact test; the high speed of impact loading requires some specific apparatus, which should be compatible with fast data acquisition to capture the impact data within very short period. Although there are some new brands of testing machines with very specific and precision data analysis, they are expensive, and their high cost leads to limitations in their availability. As mentioned in the literature review, a number of techniques are used to run impact tests on composite materials, such as the Charpy pendulum, falling weight, hydraulic machines and overpressure charge (Pereira et al., 2011; Barré et al., 1996; Fernie and Warrior, 2002). Therefore, a drop mass machine was utilized to produce the different impact loading rates on CFRP-steel joints, in order to investigate the effect of high loading rates on the bond characteristics between steel and CFRP laminates.

A drop mass machine was design by Holzer (1978) in order to investigate the dynamic compressive properties of mild steel. A modification of this machine was carried out by Grzebieta (1990) to increase the machine's capacity and ensure it could break the cylinders tested in his project. In 2012 the drop-mass rig was modified to carry tension force by Al-Zubaidy (2012) (see Figure 4.5). The principle of the newly-designed rig depends on the gravity equation. An adjustable cross head for heights up to 3 meters is needed to obtain the required velocity, and the three meter height is divided into equal distances of 0.3m by welding crossbar step supports along both sides of the frame, to enable different velocities to be obtained. The fabricated rig is connected to a TDAS PRO high-speed data acquisition system at a sample rate up to 300 kHz, as shown in Figure 4.6.

Figure 4.5: Drop-mass testing machine

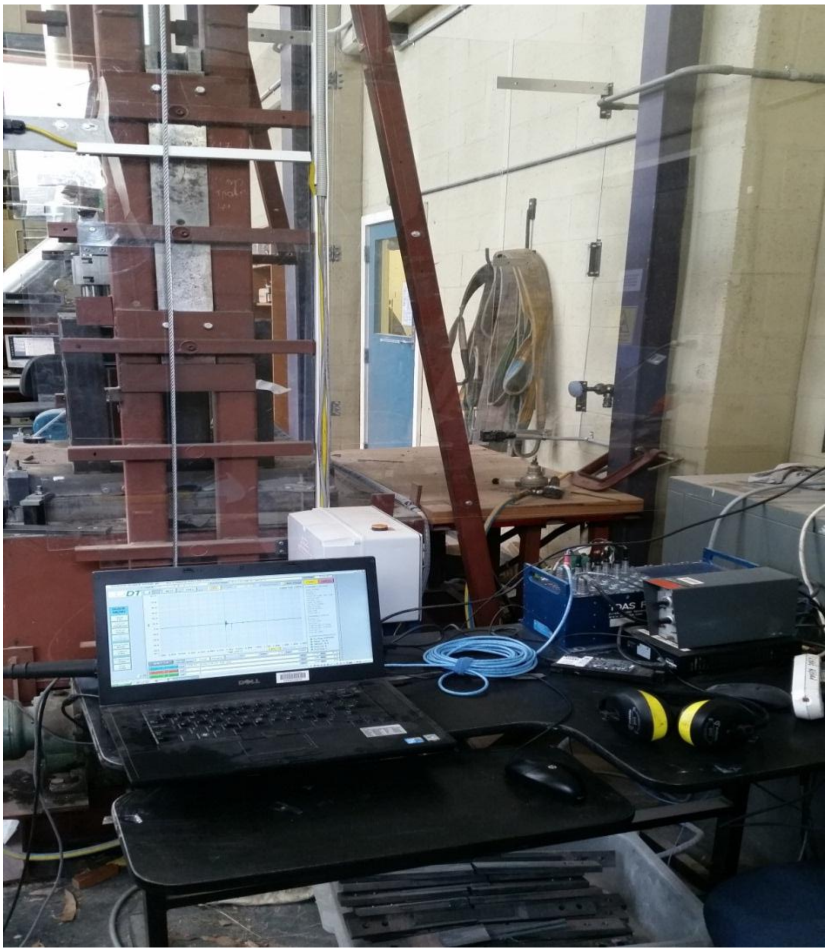

Figure 4.6: Data acquisition system

4.4.2 Specimen preparation

In this testing program, all specimens had the same material properties and dimensions with the exception of the CFRP modulus in order to investigate the dynamic properties of different types of joints. The specimen preparation was achieved by bonding two steel plates (200mm long, 16mm thick and 40mm wide) together using Araldite 420. It is very important to keep the alignment of the two steel plates straight to have a clear tension force while loading specimens, and the alignment of the two steel plates is controlled by fastening them behind a fixed steel member with an L-section, as shown in Figure 4.7.

Figure 4.7: Bonding two steel plates using Araldite 420

The surface of the jointed steel plates was sandblasted to remove oil, paint and grease along the bond length. The surface was then cleaned with acetone to remove all remaining dust and chemically to achieve a good bond between steel and CFRP. As Araldite 420 has two parts, A and B, the mixing procedure was carried out according to the manufacturer's specifications. CFRP laminates were cut into different lengths and wiped with acetone to ensure they were free of dust. The adhesive layer was then applied along the required bond length with an approximately triangular cross-section, to help the epoxy to be distributed uniformly along the bond area. Finally, CFRP laminate was attached to the joints immediately after adding the adhesive layer to ensure that the resin was still workable. Uniform squeezing was applied after CFRP attachment to expel the air bubbles by pushing the laminate with a steel plate supported on two washers at the ends of steel plate. This step was necessary to ensure a uniform adhesive thickness along the bond length. Specimens were then cured for 24 hours prior to preparing the other side. The same preparation procedure was applied to the other side of the specimens. The CFRP dimensions were 20mm wide, 1.4mm thick and different bond lengths (30-130 for low and normal modulus CFRP-steel double strap joints and 20-90mm for ultra-high modulus CFRP-steel double strap joints). The specimens were cured for 7-10 days to achieve the maximum capacity of the epoxy, as recommended by the manufacturer. A schematic view of a double-strap specimen is shown in Figure 4.8.

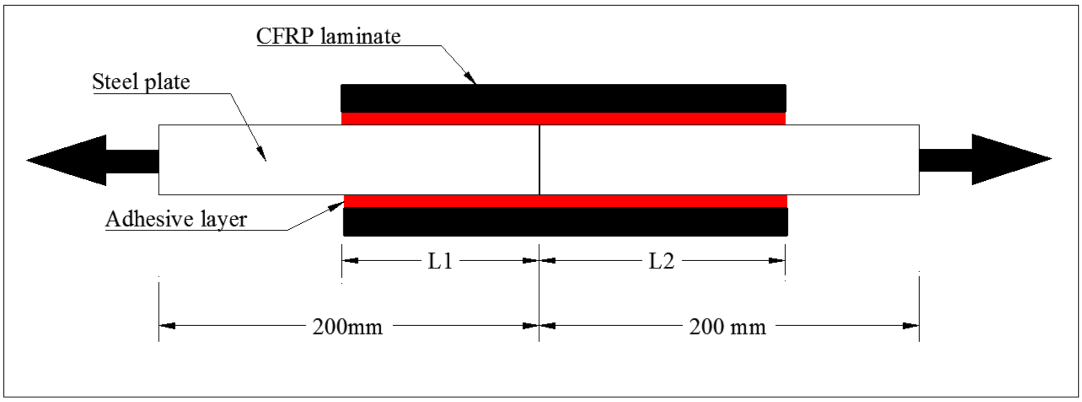

Figure 4.8: Schematic view of double-strap specimen (NOT TO SCALE)

The bond length on one side of the joint (L_1) was shorter than (L_2) to ensure failure occurred in the shorter side (L_1).

4.5 TEST SET-UP

A number of methods are used to run the impact tension tests; one of these methods is the drop-mass method. A drop-mass machine was used in this program to test the CFRP-steel double strap joints. This machine was changed from an impact compression rig to an impact tension rig by manufacturing a mass rig (Figure 4.9 and 4.10) at Monash University for some impact tension load tests (Al-Zubaidy et al., 2012a-b).

Figure 4.9: The manufactured impact tension rig.

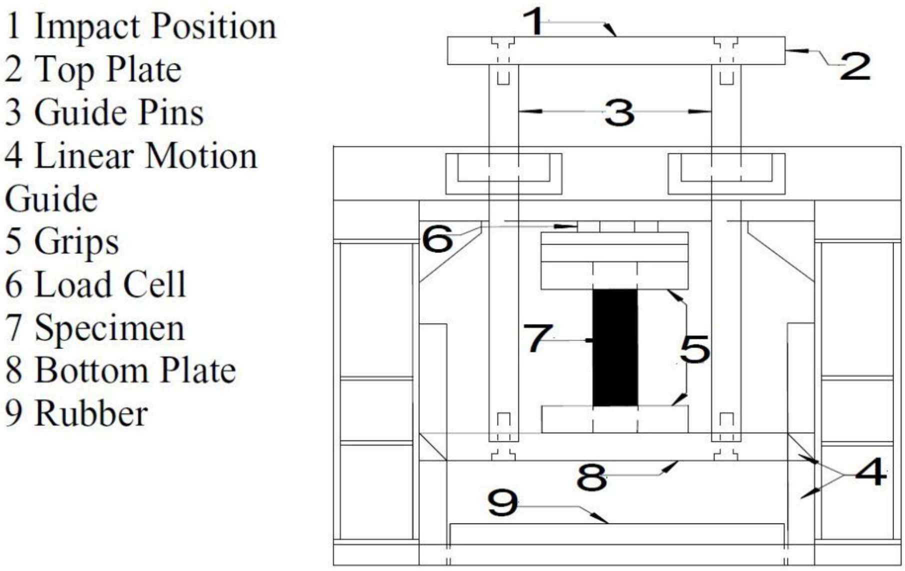

Figure 4.10: Schematic view of the fabricated tensile impact rig (Al-Zubaidy et al., 2011b)

The load cell was mounted above the top fixed grips to reduce the dummy noise in the exported data, as recommended by Fernie and Warrior (2002). In this test, the basic formula for velocity was used, which is:

$$\nu = \sqrt{2gh} \qquad \text{Equation 4-1}$$

where:

ν = velocity in (m/sec)

g = gravity (m/sec^2)

h = he height of dropping mass (m), so changing the drop-mass height results in different applied velocities.

A mass of 300Kg was dropped on the specimens from different heights (0.575, 0.975 and 1.275 m). These heights generate velocities of 201×10^3, 258×10^3 and 300×10^3 mm/min respectively according to the equation above. To calculate the applied strain rates, it is necessary to measure the adhesive thickness, and this was measured using a digital measuring tool. The thickness was found to be 0.5mm using the calculations below:

$$T_t = t_{st} + 2t_f + 2t_a \qquad \text{Equation 4.2}$$

where:

T_t: Total specimen thickness.

t_{st}: Thickness of steel plate.

t_f: Thickness of CFRP.

t_a: Adhesive thickness.

If the thicknesses of steel and CFRP laminate are known, the adhesive thickness can be found by deducting the thicknesses of steel and CFRP layers from the total thickness. The shear strain rate can be evaluated using the formula below, which was developed by Takiguchi, Izumi et al. (2004):

$$\dot{\gamma} = \dot{\nu}/t_a$$

where:

γ = shear strain rate

ν = velocity

t_a = adhesive thickness

As a result, depending on the three velocities (201×10^3, 258×10^3 and 300×10^3 mm/min) the shear strain rates are $6700s^{-1}$, $8600s^{-1}$ and $10000s^{-1}$ respectively.

To monitor the longitudinal tensile strain distribution along the CFRP-steel bond length, a number of foil strain gauges were mounted along the bond length of each double-strap specimen. These strain gauges were attached on the centreline of the CFRP laminate at a constant distance of 2mm between each gauge, starting from the mid-joint and along the shorter side (L_1). The collection of data from the load cell and strain gauges was at a sample rate of 150 kHz.

Load-time curves for the two different CFRP-steel double strap joint specimens with the different loading rates (201×10^3, 258×10^3 and 300×10^3 mm/min) are shown in Figures 4.11 and 4.12.

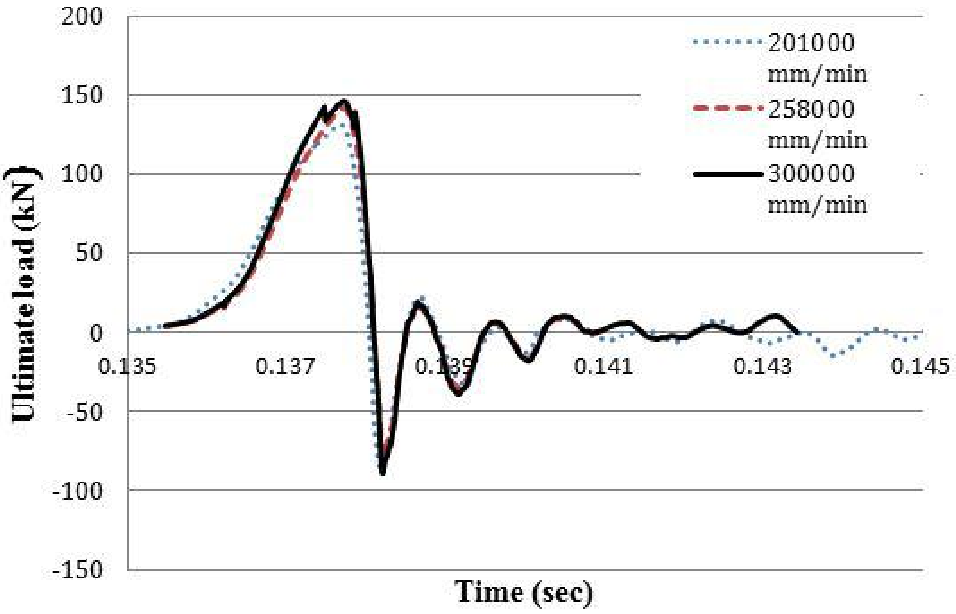

Figure 4.11: Load-time curve for the low modulus CFRP-steel double strap specimen

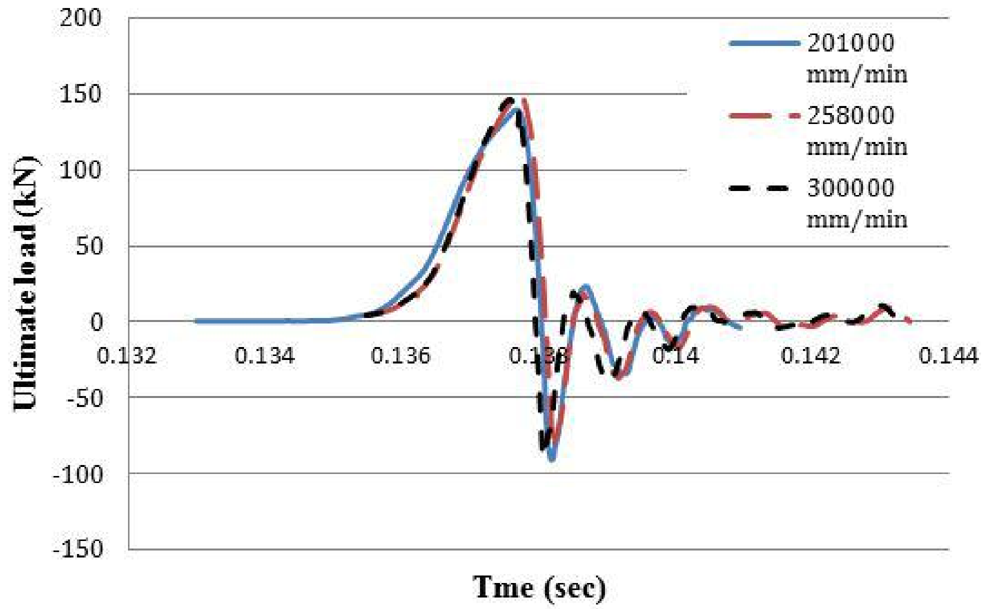

Figure 4.12: Load-time curve for the normal modulus CFRP-steel double strap specimen

Strain gauges were mounted on the top of CFRPs at distances of 20mm starting from the joints to the shorter end (L_1). This strain gauge arrangement gives full strain distribution data along the bond length. A specimen and strain gauge locations are shown in Figure 4.13 below.

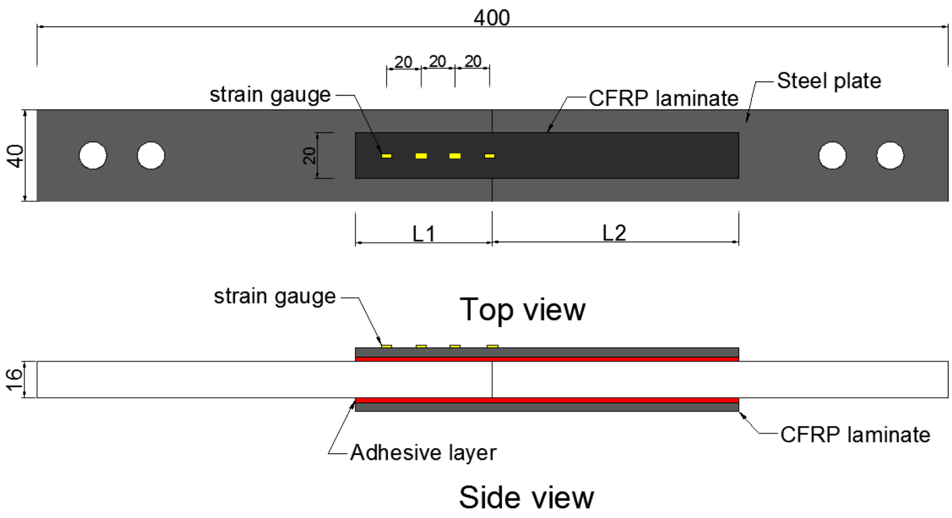

Figure 4.13: Schematic view of strain gauge locations along CFRP-steel specimen.

Figure 4.14 shows CFRP-steel double strap joint inside the impact tension rig of the drop-mass machine and ready for the test. A number of strain gauges were attached as per the schematic drawing.

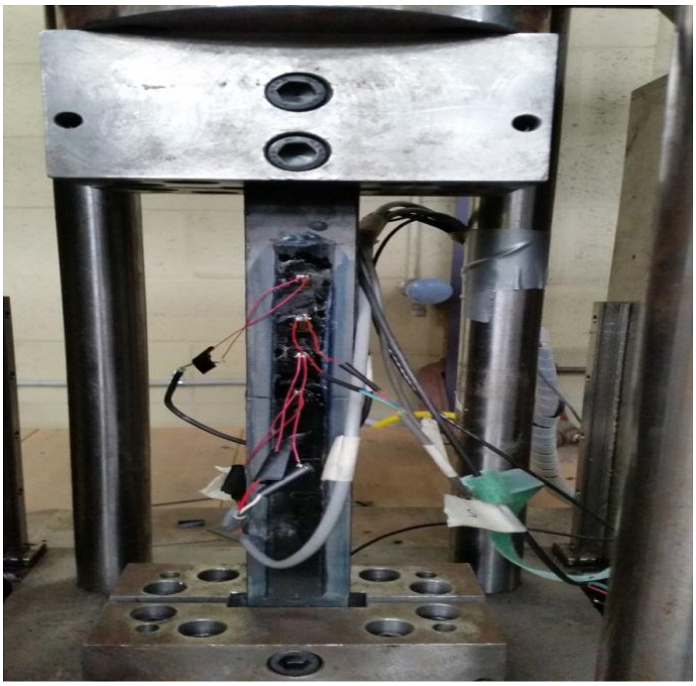

Figure 4.14: Specimen inside the drop-mass rig and connected to strain gauges

4.6 RESULTS AND DISCUSSION

All CFRP-steel double strap joints were tested under the three loading rates. To investigate the bond properties between steel and CFRP laminates, four different results were obtained: maximum tensile joint strength, effective bond length, strain distribution along the bond and the failure mode. All these results were then compared with the results obtained from quasi-static testing (Chapter Three) to evaluate the degree of enhancement under dynamic loading.

4.6.1: Ultimate joint strength

Three types of CFRP-steel double strap joint specimens were tested under impact loading with different loading rates (201×10^3, 258×10^3 and 300×10^3 mm/min). Each group had different modulus CFRP (low, normal and ultra-high), and each group was tested under the three loading rates. All specimens had the same preparation and curing time, and the results of specimens with low and normal modulus CFRP tested under the loading rate of 201×10^3mm/min are summarised in Table 4.3. The specimen labels that begin with L mean specimens with low modulus CFRP, specimens that begin with N mean specimens with normal modulus CFRP and the number following L or N represents the bond length. L_1 and L_2 are the lengths starting from the joint to the far ends at each side of the joint, as shown in Figure 4.13; L_2 is constant for all specimens and longer than L_1 to ensure that failure occurred within the shorter side. F_3 and F_4 are the ultimate joint capacities for the specimens with low and normal modulus CFRP respectively. Each joint was tested three times, and the average of these readings was considered to be the actual bond force in kN. Tables 4.3-4.7 show that the bond strength increases as the bond length increases, then it tends to be constant at a certain bond length, defined as the effective bond length. Table 4.4 shows all details of the dynamic results of low and normal modulus CFRP-steel double strap specimens with a loading rate of 258×10^3 mm/min. F_5 and F_6 represent the ultimate bond force for each bond length and for low and normal modulus CFRP respectively. Table 4.5 shows the last loading speed of 300×10^3 mm/min. The results for both types of CFRP-steel double strap joints show an insignificant increase in loading capacities compared to the specimens tested under the load rate of 258×10^3 mm/min. However, significant joint capacity enhancement is shown compared to the loading rate of 201×10^3 mm/min. F_7 and F_8 in Table 4.5 represent the ultimate bond force for each bond length for low and normal modulus CFRP respectively.

Table 4.3: Dynamic results for load rate of 201×103 mm/min

Label for F_3	Label for F_4	L_1 (mm)	L_2 (mm)	F_3 (kN)	Ave F_3 (kN)	F_4 (kN)	F_4 (kN)
LS-40	NS-40	40	100	84.6 86.1 85.2	85.3	88.1 89 92.1	89.7
LS-50	NS-50	50	100	100 102.7 98.3	100.3	102.6 105.3 97.4	101.7
LS-60	NS-60	60	100	109.5 104.7 105.8	106.6	106.4 109.1 109.6	108.4
LS-70	NS-70	70	110	110.1 115.9 115.7	113.9	116.6 118.2 110.3	115.0
LS-80	NS-80	80	120	122 121.8 117.2	120.3	125.4 121.9 121.4	122.9
LS-90	NS-90	90	130	131.1 130.3 132	131.1	130.1 128.1 131.9	130
LS-100	NS-100	100	140	131.5 131 128.4	130.3	132.9 132.1 130.2	131.7
LS-110	NS-110	110	150	132.9 130.0 130.8	131.2	130.4 129.9 132.8	131

F_3: The ultimate bond strength for low modulus CFRP

F_4: The ultimate bond strength for normal modulus CFRP

Table 4.4: Dynamic results for load rate of 258×10^3 mm/min

Label for F_5	Label for F_6	L_1 (mm)	L_2 (mm)	F_5 (kN)	Ave F_5 (kN)	F_6 (kN)	Ave F_6 (kN)
LS-40	NS-40	40	100	104 105.4 98.4	102.6	103.3 106.7 106.3	105.4
LS-50	NS-50	50	100	117.0 116.3 115.1	116.1	118.3 119 115.5	117.6
LS-60	NS-60	60	100	123.8 124.6 122.4	123.6	125.1 124.5 126.4	125.3
LS-70	NS-70	70	110	135.7 132.6 133.1	133.8	130.4 133.1 131.4	131.6
LS-80	NS-80	80	120	142.0 138.8 137.8	139.5	139.1 136.1 141	138.7
LS-90	NS-90	90	130	145.9 147.1 145.9	146.3	146.1 145.1 145.9	145.7
LS-100	NS-100	100	140	147.0 147.7 146.1	146.9	147.5 143.9 148.5	146.6
LS-110	NS-110	110	150	147.1 147.6 146.5	147.1	147.6 142.5 148.6	146.2

F_5: The ultimate bond strength for low modulus CFRP

F_6: The ultimate bond strength for normal modulus CFRP

Table 4.5: Dynamic results for load rate of 300×10^3 mm/min

Label for F_7	Label for F_8	L_1 (mm)	L_2 (mm)	F_7 (kN)	Ave F_7 (kN)	F_8 (kN)	Ave F_8 (kN)
LS-40	NS-40	40	100	101.9 105.4 103.4	103.6	105.9 104.9 106.5	105.8
LS-50	NS-50	50	100	117.6 119.7 120.6	119.3	119.1 123.5 120.7	121.1
LS-60	NS-60	60	100	126.4 129.1 128.9	128.1	130.6 128.1 131.1	129.9
LS-70	NS-70	70	110	132 137.6 137.3	135.6	133.7 136.9 138.4	136.3
LS-80	NS-80	80	120	139.9 143.2 140.9	141.3	142.4 140.1 143.6	142
LS-90	NS-90	90	130	148.2 146.6 145.9	146.9	147.9 148.6 148.2	148.2
LS-100	NS-100	100	140	141.5 149.6 148.3	146.4	146.6 148.1 148.2	147.6
LS-110	NS-110	110	150	146.6 143.6 148.5	146.2	148.3 149.1 146.9	148.1

F_7: The ultimate bond strength for low modulus CFRP

F_8: The ultimate bond strength for normal modulus CFRP

Joints with ultra-high modulus CFRP were tested under two loading rates: 201×10^3, and 300×10^3 mm/min. The results show a decrease in bond strength compared to the other two types of joints. The reason for this decrease is that the tensile strength is lower for ultra-high modulus CFRP compared to low and normal modulus CFRP. However, a significant increase in bond force is shown compared to the quasi- static test results, which are discussed in the next section.

Tables 4.6 and 4.7 show the test results of ultra-high modulus CFRP-steel double strap joints.

Table 4.6: Dynamic results for ultra-high modulus CFRP-steel joints with load rate of 201×10^3 mm/min

Specimen label F_9	L1 (mm)	L2 (mm)	F_9	Ave F_9
UHMS-20	20	100	35.6 33.5 37.4	35.5
UHMS-30	30	100	44.3 44.2 47.5	45.3
UHMS-40	40	100	46.1 44.6 45.7	45.5
UHMS-50	50	100	45.6 45.1 44.6	45.1
UHMS-60	60	100	47.1 44 45.9	45.7
UHMS-70	70	110	46.2 46.4 44.8	45.8
UHMS-80	80	120	46.5 45.1 43.5	45
UHMS-90	90	130	46.1 46.4 45.5	46
UHMS-100	100	140	45.9 44.4 46.5	45.6

F_9 : The ultimate bond strength for ultra-high modulus CFRP

Table 4.7: Dynamic results for UHM CFRP-steel double strap joints under load rate of 300×10^3 mm/min

Specimen label F_{10}	L_1 (mm)	L_2 (mm)	F_{10}	Ave F_{10}
UHMS-20	20	100	45.1 42.6 44.9	44.2
UHMS-30	30	100	56.4 55.4 57.8	56.5
UHMS-40	40	100	57.4 55.5 56.4	56.4
UHMS-50	50	100	56.3 56.1 56.8	56.4
UHMS-60	60	100	57.4 56.8 56.6	56.9
UHMS-70	70	110	56.3 55.3 58.9	56.8
UHMS-80	80	120	56.1 56.7 56.4	56.4
UHMS-90	90	130	56.1 56.8 56.7	56.5
UHMS-100	100	140	57.2 56.1 58.1	57.1

F_{10} : The ultimate bond strength for ultra-high modulus CFRP

The same behaviour in bond strength increment observed for specimens with low and normal modulus CFRP was shown for specimens with ultra-high modulus CFRP, the bond strength increasing as the bond length increases. In the above two tables, the letters UHM in specimen labels mean ultra-high modulus and S means specimen, and the following numbers 20-100 are the bond length.

As Tables 4.3-4.7 show, the ultimate joint strengths of CFRP-steel double-strap specimens with normal modulus CFRP are very close to those of specimens with low modulus CFRP, whereas they are lower for joints with ultra-high modulus CFRP. The steady state of bond strength of low and normal modulus CFRP-steel joints illustrates that the adhesive makes the most contribution in carrying the load, and it reaches its maximum capacity until it fails. The results also show that there is a good enhancement in joint capacity when changing from a loading rate 201×10^3 mm/min to 258×10^3 and 300×10^3 mm/min, and an insignificant increase is observed in joint capacities between the last two loading rates (258×10^3 and 300×10^3 mm/min). The increase in joint enhancement for the three groups of specimens can be attributed to the high shear and tensile strengths of the adhesive under high loading rates (Al-Zubaidy et al., 2011a).

4.6.2: Comparison with static results (Chapter Three)

To highlight the effect of impact loading on the bond strength of CFRP-steel double-strap joint specimens, and to find the capacity enhancement in the different types of joints with low, normal and ultra-high modulus CFRP, a comparison is made in this chapter. Tables 4.8, 4.9 and 4.10 show the bond strength results of both quasi-static loading and the three dynamic loadings.

Table 4.8: Comparison of bond strength between two load rates: 2mm/min and 201×10^3 mm/min

Specimen label	L_1	L_2	Low modulus CFRP joints		Normal modulus CFRP joints		F_3/F_1	F_4/F_2
			F_1	F_3	F_2	F_4		
S3-30	30	100	41.0	--	41.9	--	--	--
S3-40	40	100	50.7	85.3	51.7	89.7	1.68	1.74
S3-50	50	100	60.0	100.3	60.7	101.7	1.67	1.68
S3-60	60	100	69.1	106.6	69.8	108.4	1.54	1.55
S3-70	70	110	76.5	113.9	75	115.0	1.49	1.53
S3-80	80	120	86.8	120.3	87.4	122.9	1.39	1.41
S3-90	90	130	93.6	131.1	94.2	130	1.40	1.38
S3-100	100	140	100.3	130.3	101.3	131.7	1.30	1.30
S3-110	110	150	108.0	131.2	108.3	131	1.21	1.21
S3-120	120	160	108.7	--	108.5	--	--	--
S3-130	130	170	109.1	--	109.2	--	--	--

F_1, F_2: maximum load capacity for specimens with low and normal modulus CFRP respectively under quasi-static loading with velocity of 2mm/min

F_3, F_4: maximum load capacity for specimens with low and normal modulus CFRP respectively under dynamic loading with velocity of 201×10^3mm/min

Table 4.9: Comparison of bond strength between two load rates: 2.0 and 258×10^3 mm/min

Specimen label	L_1	L_2	Low modulus CFRP joints		Normal modulus CFRP joints		F_5/F_1	F_6/F_2
			F_1	F_5	F_2	F_6		
S3-30	30	100	41.0	--	41.9	--	--	--
S3-40	40	100	50.7	102.6	51.7	105.4	2.02	2.04
S3-50	50	100	60.0	116.1	60.7	117.6	1.94	1.94
S3-60	60	100	69.1	123.6	69.8	125.3	1.79	1.80
S3-70	70	110	76.5	133.8	75	131.6	1.75	1.75
S3-80	80	120	86.8	139.5	87.4	138.7	1.61	1.59
S3-90	90	130	93.6	146.3	94.2	145.7	1.56	1.55
S3-100	100	140	100.3	146.9	101.3	146.6	1.46	1.45
S3-110	110	150	108.0	147.1	108.3	146.2	1.36	1.35
S3-120	120	160	108.7	--	108.5	--	--	--
S3-130	130	170	109.1	--	109.2	--	--	--

F1, F2: maximum load capacity for specimens with low and normal modulus CFRP respectively under quasi-static loading with velocity of 2mm/min

F5, F6: maximum load capacity for specimens with low and normal modulus CFRP respectively under dynamic loading with velocity of 258×10^3mm/min

Table 4.10: comparison of bond strength between two load rates: 2mm/min and 300×10^3 mm/min

Specimen label	L_1	L_2	Low modulus CFRP joints		Normal modulus CFRP joints		F_7/F_1	F_6/F_2
			F_1	F_7	F_2	F_8		
S3-30	30	100	41.0	--	41.9	--	--	--
S3-40	40	100	50.7	103.6	51.7	105.8	2.04	2.05
S3-50	50	100	60.0	119.3	60.7	121.1	1.99	2.00
S3-60	60	100	69.1	128.1	69.8	129.9	1.85	1.86
S3-70	70	110	76.5	135.6	75	136.3	1.77	1.82
S3-80	80	120	86.8	141.3	87.4	142	1.63	1.62
S3-90	90	130	93.6	146.9	94.2	148.2	1.57	1.57
S3-100	100	140	100.3	146.4	101.3	147.6	1.46	1.46
S3-110	110	150	108.0	146.2	108.3	148.1	1.35	1.37
S3-120	120	160	108.7	--	108.5	--	--	--
S3-130	130	170	109.1	--	109.2	--	--	--

F1, F2: maximum load capacity for specimens with low and normal modulus CFRP respectively under quasi-static loading with velocity of 2mm/min,

F7, F8: maximum load capacity for specimens with low and normal modulus CFRP respectively under dynamic loading with velocity of 300×10^3mm/min.

Table 4.11: Comparison of bond strength for ultra-high modulus CFRP joints under static and dynamic loadings

Specimen label	L_1	L_2	HF_1	F_9	F_{10}	F_9/HF_1	$F10/HF_1$
UHMS-20	20	100	-	35.5	44.2	-	-
UHMS-30	30	100	31.7	45.3	56.5	1.43	1.78
UHMS-40	40	100	43.3	45.5	56.4	1.05	1.30
UHMS-50	50	100	54.4	45.1	56.4	0.83	1.04
UHMS-60	60	100	64.1	45.7	56.9	0.71	0.89
UHMS-70	70	110	73.2	45.8	56.8	0.63	0.78
UHMS-80	80	120	73.1	45	56.4	0.62	0.77
UHMS-90	90	130	73	46	56.5	0.63	0.77
UHMS-100	100	140	73.2	45.6	57.1	0.62	0.78

HF_1: ultimate joint strength of ultra-high modulus CFRP-steel double strap joints under loading rate 2mm/min.

F_9, F_{10}: maximum load capacity for specimens with ultra-high modulus CFRP under loading rates of 201×10^3 and 300×10^3mm/min.

As shown in the tables above, the bond strength of the double strap joint specimens increases up to 100% when increasing the loading rate from quasi-static loading at 2mm/min to high loading rates. This significant increase in bond strength can be attributed to the fact that the shear strength of the Araldite 420 adhesive is higher under high loading rates than static loadings. The bond enhancement is shown to be high for small bond lengths and lower for longer bond lengths; the same trend of enhancement was observed by Al-Zubaidy et al. (2012b) when CFRP sheet was used to build the double strap specimens. For specimens with ultra-high modulus CFRP, the bond strength enhancement is lower than that in low and normal modulus CFRP. Inspection of the mode of failure of specimens with ultra-high modulus CFRP under static and dynamic loading, revealed that all specimens failed within the FRP laminate. This indicates that since the quasi-static and dynamic tension loads for specimens with ultra-high modulus CFRP were completely sustained by the laminate, the ratios of F_9/HF_1 and F_{10}/HF_1 in Table 4.11 are completely dependent on the mechanical properties of ultra-high modulus CFRP under static and dynamic loadings.

4.6.3 Effective bond length

Essentially, the principle of the effective bond length in the FRP composite joints was proposed by Hart-Smith (1973) . This model used elastic-plastic adhesive rather than pure elastic or non-linear behaviour, and the failure mechanism was totally dependent on the maximum shear strain of the adhesive at the location of highest strain or stress values. The influence of high loading rates on the effective bond length was studied in the present research; the ultimate joint strength versus bond length curves of all types of CFRP-steel double strap joints (low, normal and ultra-high modulus CFRP) were plotted, and the results are shown in Figures 4.15-4.17. The figures show that the ultimate joint strength increases approximately linearly with bond length increment, and then at a certain bond length (known as the effective bond length) the joint strength reaches a maximum value. Beyond this bond length, further increasing the bond length has virtually no effect on joint strength or produces only minor improvement. According to this behaviour of load versus bond length, the effective bond length was shown to be 90mm for both low and normal modulus CFRP under the three loading rates (201×10^3 mm/min, 258×10^3 mm/min, 300×10^3 mm/min). However, for joints with ultra-high modulus CFRP the effective bond length decreased to 30mm. This decrease can be attributed to the lower ultimate strain value of ultra-high modulus CFRP compared to that of low and normal modulus CFRP under dynamic loading. The effective bond length for specimens with normal modulus CFRP sheet tested by Al-Zubaidy (2012) was found to be 40mm under high load rates. However, the effective bond length was also studied by Al-Zubaidy (2012) for specimens tested under different loading rates, and CFRP sheet was used in the double strap joints. The effect of static and fatigue loading on the effective bond length was also studied by (Liu et al., 2005b; Wu et al., 2012b). Different effective bond lengths were observed due to the different parameters used.

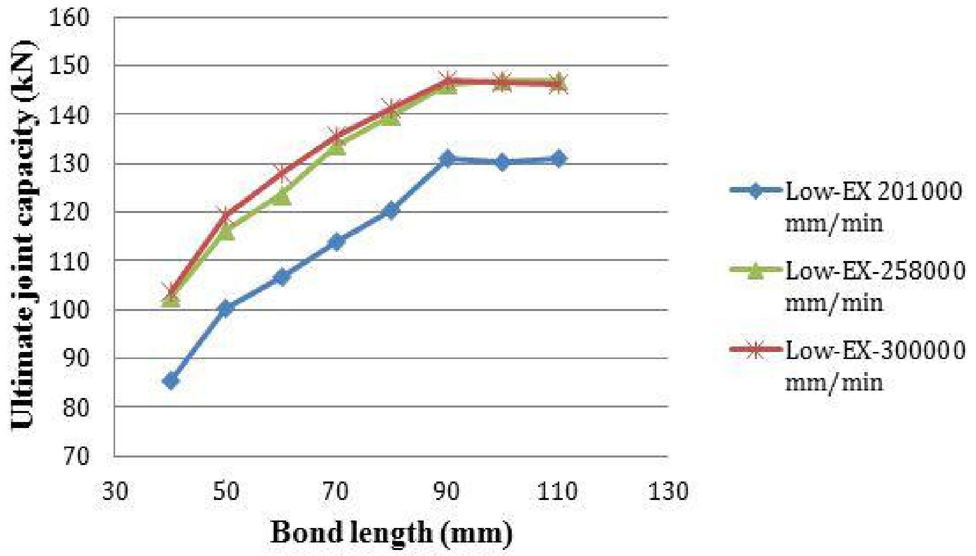

Figure 4.15: Joint strength vs. bond length for low modulus CFRP-steel joints under different impact loads

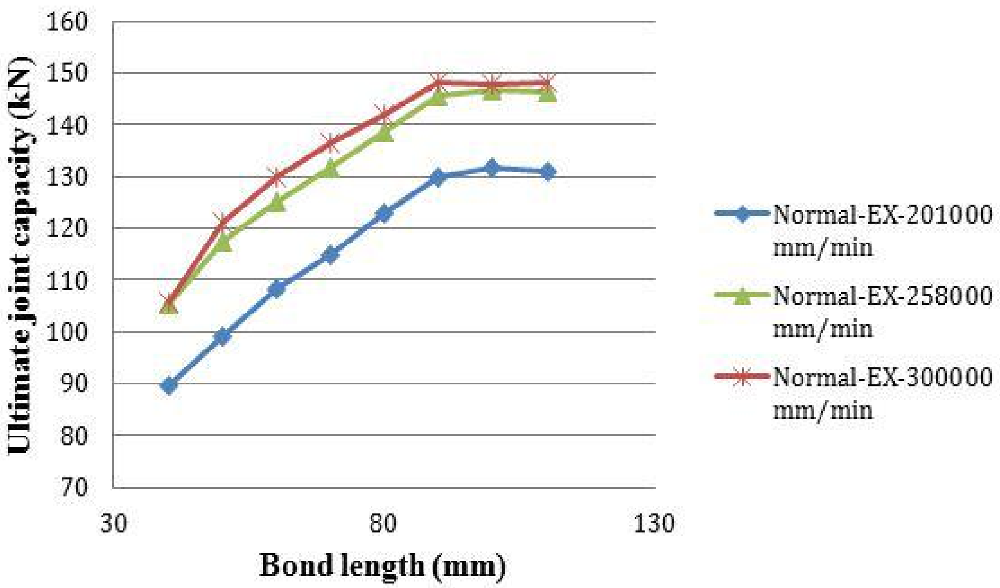

Figure 4.16: Joint strength vs. bond length for normal modulus CFRP-steel joints under different impact loads.

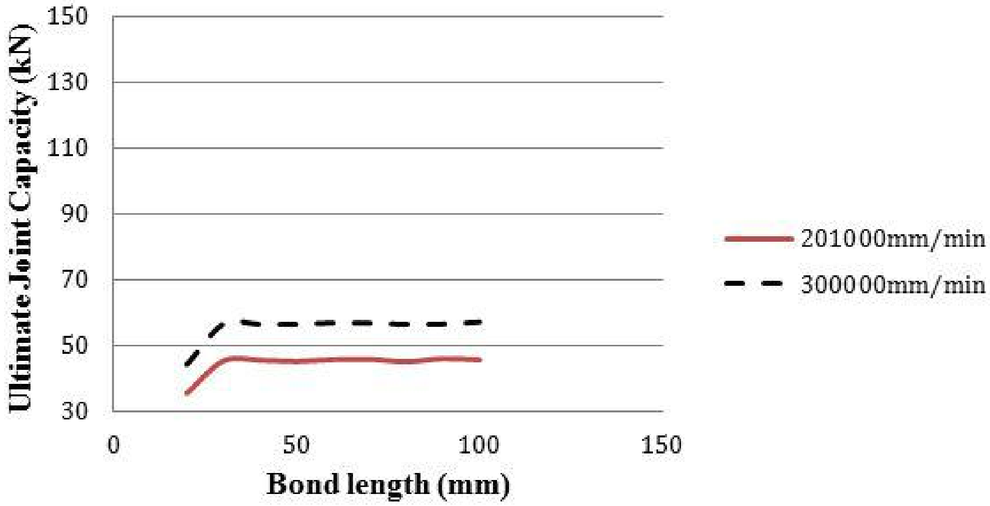

Figure 4.17: Joint strength vs. bond length for ultra-high modulus CFRP-steel joints under different impact loads

4.6.4 Comparison with static results (Chapter Three)

To evaluate the effect of high load rates on the effective bond length of the CFRP-steel double strap joint specimens, a comparison of the static and dynamic results was carried out. Figures 4.18 and 4.19 show the plots of ultimate joint strength versus the bond length for low and normal modulus CFRP-steel double strap joints respectively, and for all loading rates starting from quasi-static loading 2mm/min to the high loading rates 201×10^3, 258×10^3 and 300×10^3mm/min. The results show a significant effect on the joint enhancement and the effective bond length value. The effective bond length for specimens with low and normal modulus CFRP in quasi-static loading was 110mm, whereas it was 90mm for all impact load rates. Moreover, these results of dynamic tests are consistent with the experimental tests carried out by Al-Zubaidy et al. (2012b) , who found the same trend of load versus bond length curve as in the present experimental tests, and the effective bond length is lower for specimens tested under dynamic loading than those tested under quasi-static loading. The effect of high load rate on the effective bond length of ultra-high modulus CFRP-steel double strap joints is also studied, Figure 4.20 shows the ultimate joint strength versus the bond length of these joints. A significant decrease in the effective bond length can be observed, the effective bond length for specimens tested under quasi-static loading being 70mm, while it was 30mm for all impact loading rates. The reduction of effective bond length values under dynamic loads and for all types of joints is mainly due to the high shear strength of the adhesive under high loading rates.

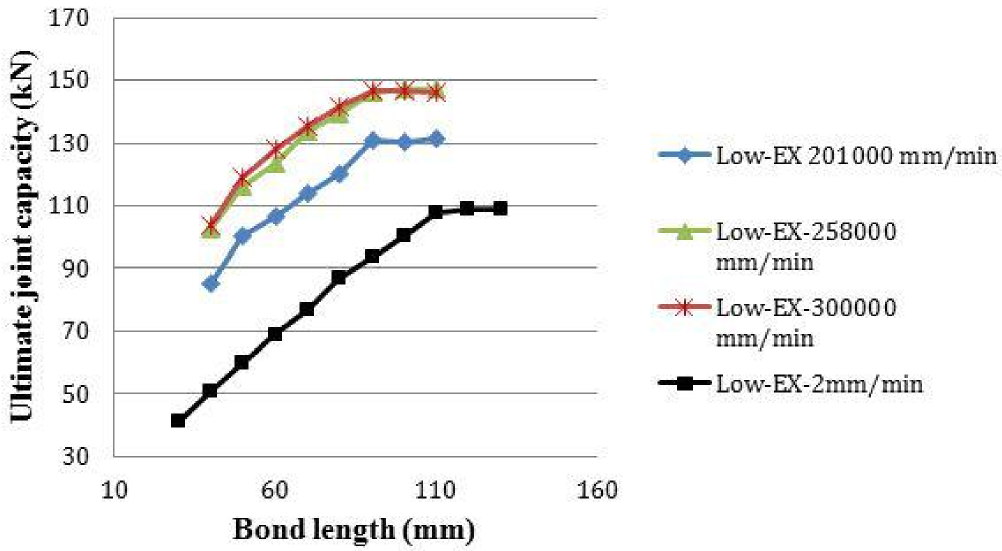

Figure 4.18: Ultimate bond strength vs. bond length for low modulus CFRP-steel joints for all loading rates (static and dynamic)

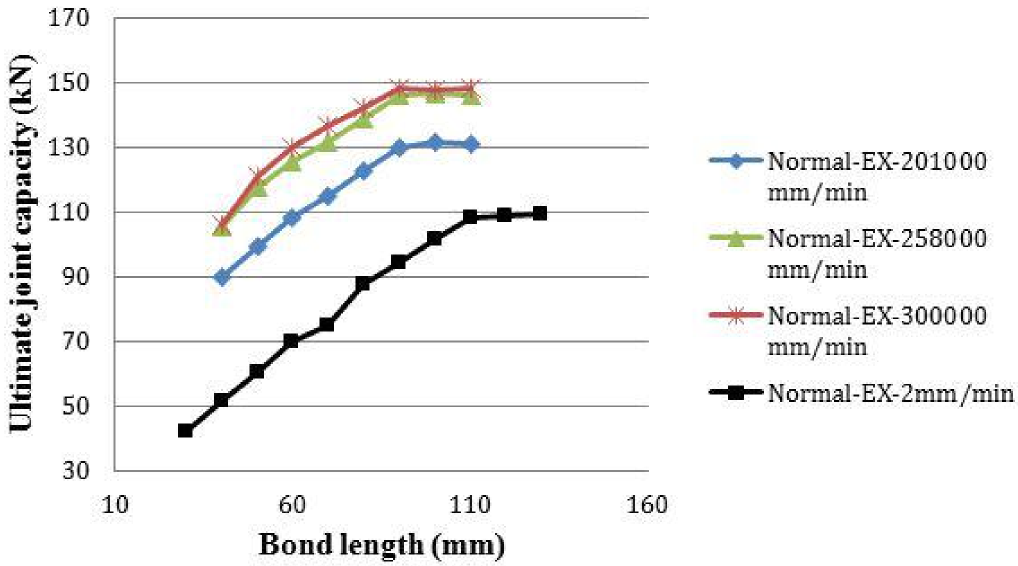

Figure 4.19: Ultimate bond strength vs. bond length for normal modulus CFRP-steel joints for all loading rates (static and dynamic)

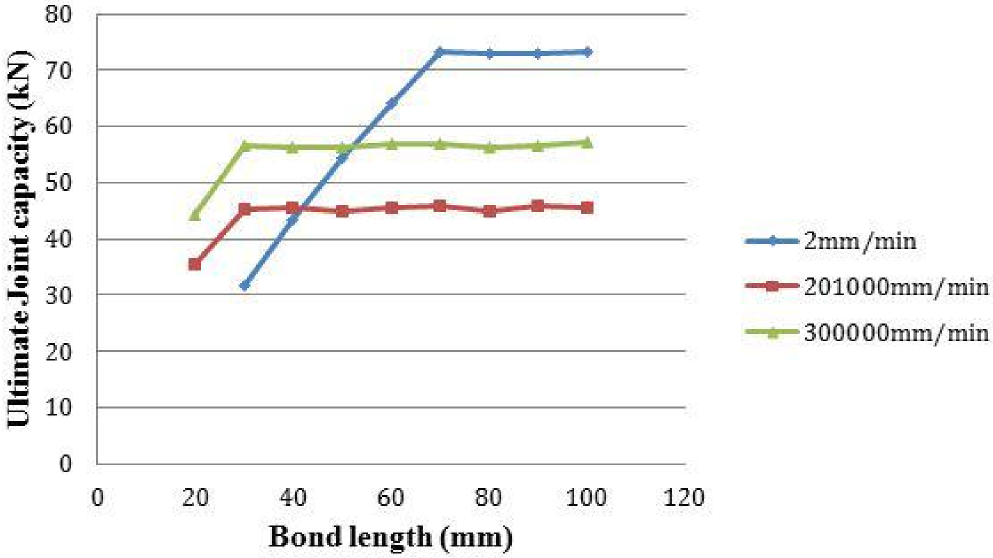

Figure 4.20: Ultimate bond strength vs. bond length for ultra-high modulus CFRP-steel joints for all loading rates (static and dynamic)

4.6.5 Effect of high velocity on the strain distribution along the bond length

Based on the strain gauge readings, the strain distribution along the bond length was investigated at specific points along the bond area; the distance between strain gauges was 20mm, starting from the joint to the far end of the short length L_1 as shown in Figures 4.13 and 4.14.

The strain distribution curves along the bond of the different CFRP-steel joints had the same trend. Figures 4.21-4.23 show the strain distributions along the low modulus CFRP-steel joints for three different load levels and 30%, 60% and 90% of the ultimate joint strength. Load level can be defined as the ratio of the applied load to the ultimate load achieved. The results show a maximum strain value occurs at the centre of the joint, and then it starts to decrease away from the joint for all load levels and all loading rates. For specimens with normal modulus CFRP, Figures 4.24-4.26 show the trend of strain distribution along the bond length of the specimens at different load levels. At distances close to the far end of the joint, the strain values are constant for the three different load levels, i.e. there is less difference in strain values at the far end points compared to at points close to the centre of the joint. The strain values of normal modulus CFRP specimens showed an insignificant decrease, due to the smaller ultimate strain for normal modulus CFRP compared to low modulus CFRP under dynamic loading. For joints with ultra-high modulus CFRP, a significant decrease in strain values is observed compared to the low and normal modulus CFRP joints (see Figures 4.27 and 4.28). The decrease in ultimate strain for these joints is attributed to the very low ultimate strain of ultra-high modulus CFRP compared to the low and normal modulus CFRP under static and dynamic loading.

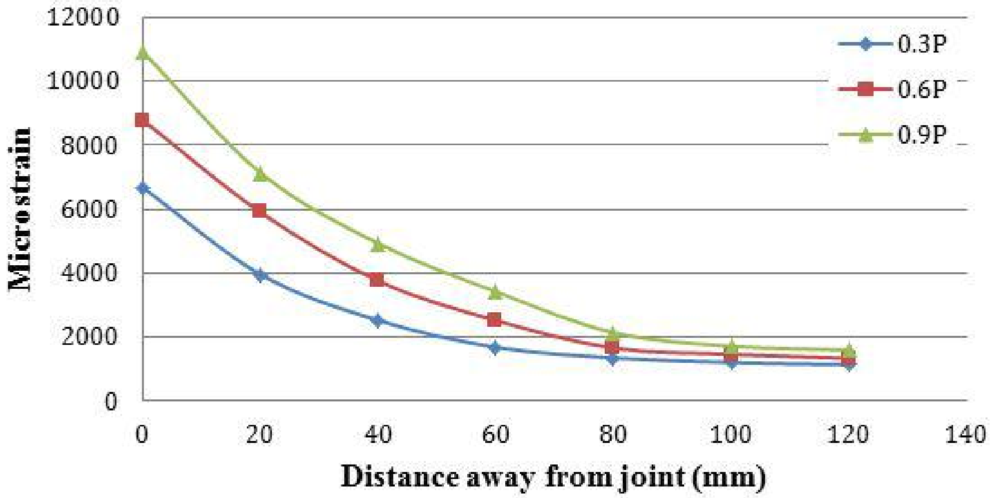

Figure 4.21: Strain distribution along the bond length for low modulus CFRP-steel joints under loading rate of 201×10^3 mm/min

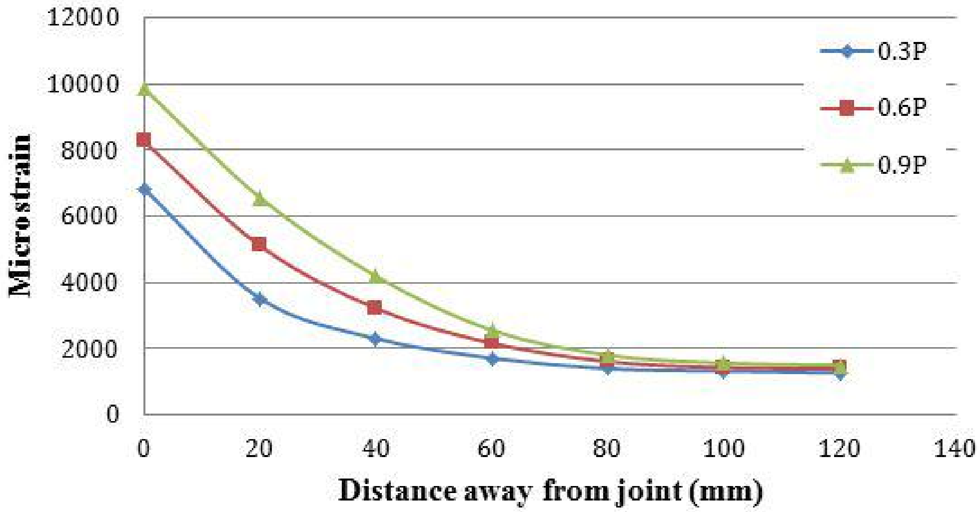

Figure 4.22: Strain distribution along the bond length for low modulus CFRP-steel joints under loading rate of 258×10^3 mm/min

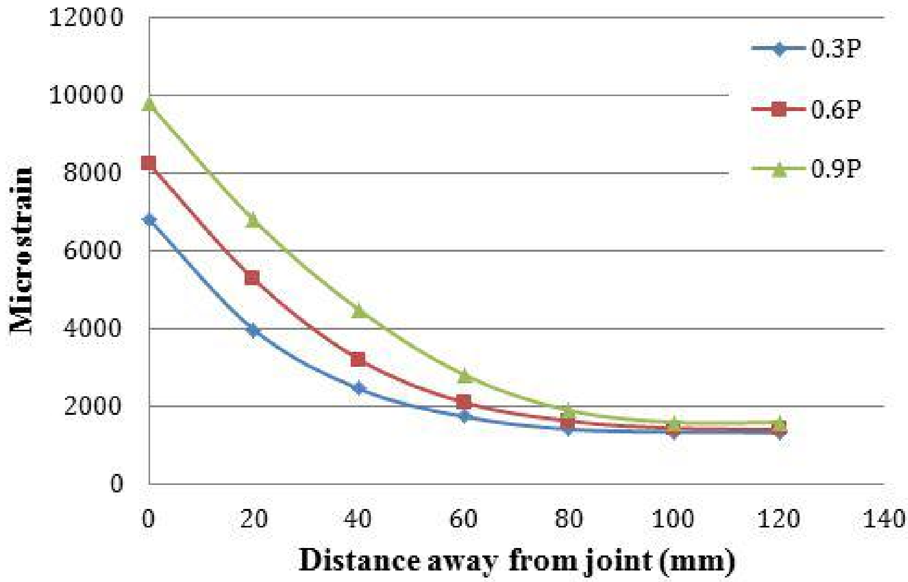

Figure 4.23: Strain distribution along the bond length for low modulus CFRP-steel joints under loading rate of 300×10^3 mm/min

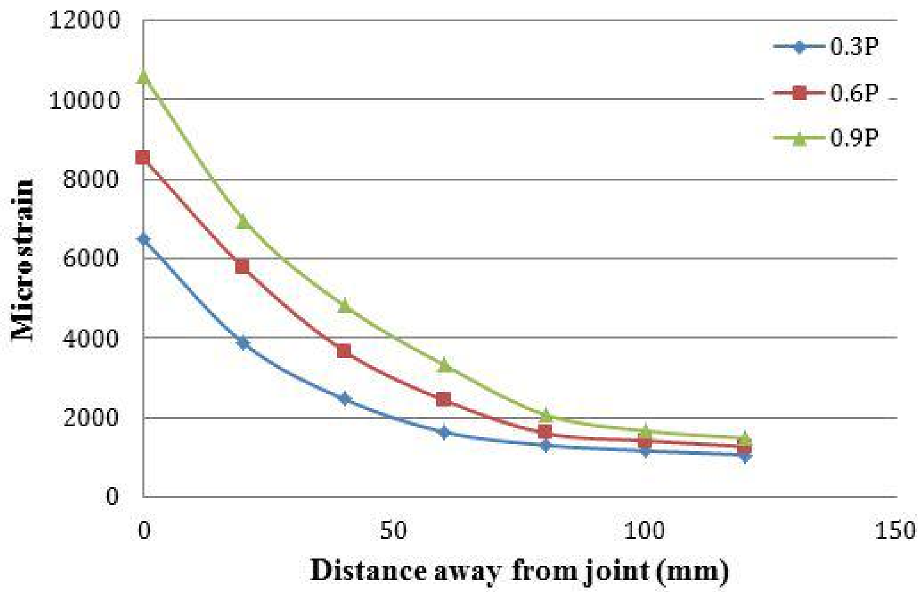

Figure 4.24: Strain distribution along the bond length for normal modulus CFRP-steel joints under loading rate of 201×10^3 mm/min

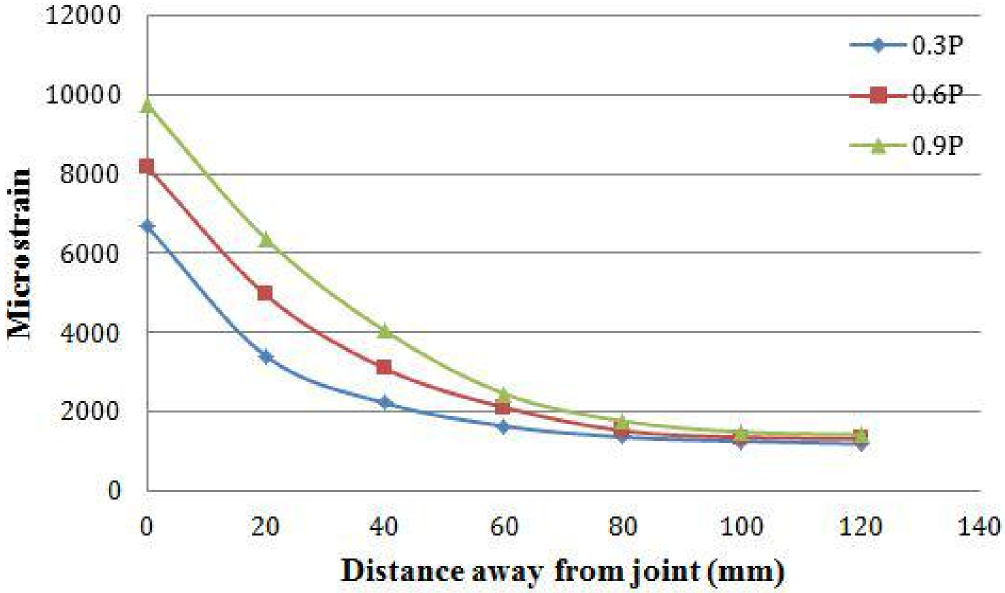

Figure 4.25: Strain distribution along the bond length for normal modulus CFRP-steel joints under loading rate of 258×10^3 mm/min

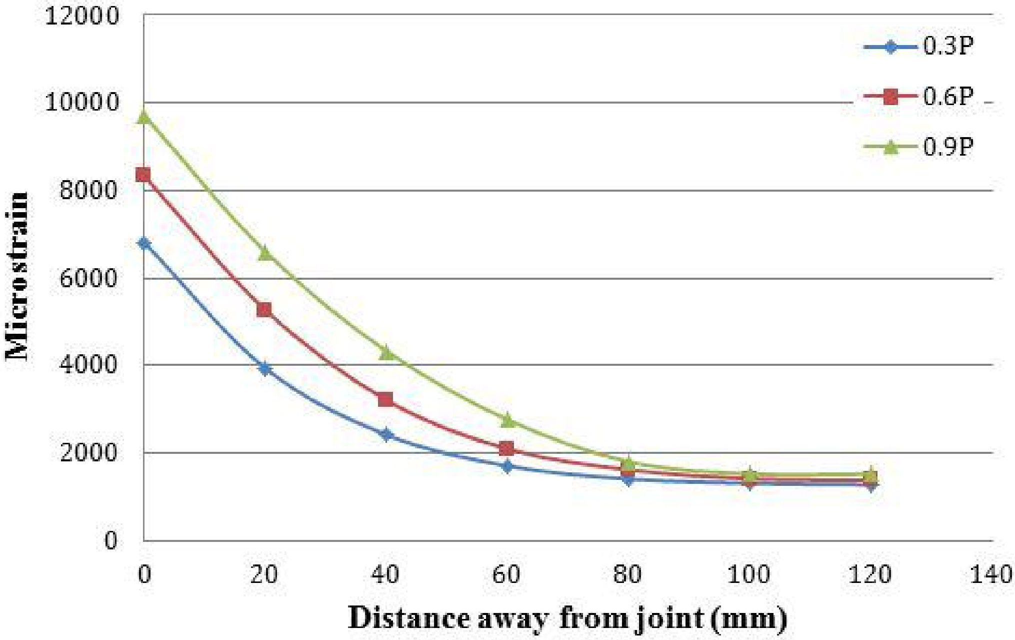

Figure 4.26: Strain distribution along the bond length for normal modulus CFRP-steel joints under loading rate of 300×10^3 mm/min

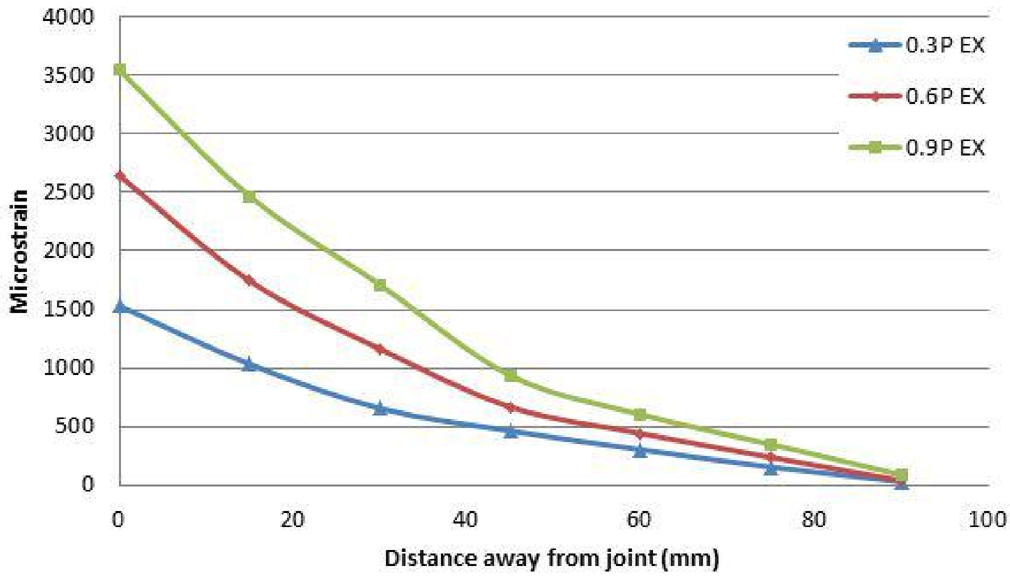

Figure 4.27: Strain distribution along the bond length for ultra-high modulus CFRP-steel joints under loading rate of 201×10^3 mm/min

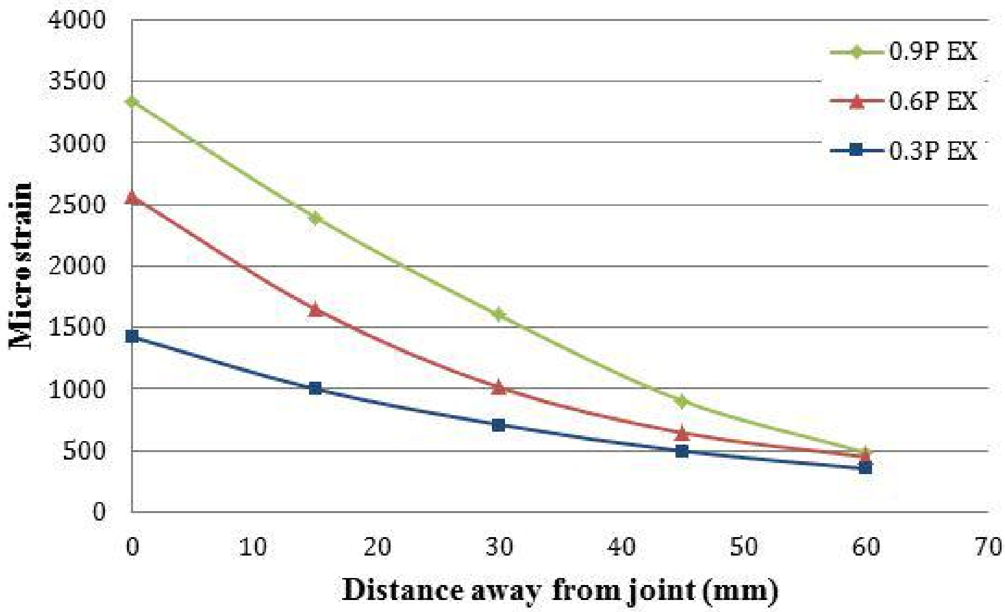

Figure 4.28: Strain distribution along the bond length for ultra-high modulus CFRP-steel joints under loading rate of 300×10^3 mm\min

4.6.6 Comparison with static test (Chapter Three)

The strain distribution along the bond length of CFRP-steel double-strap specimens under impact loadings was different to those tested under quasi-static loading. The maximum strain values versus different bond lengths plots showed less non-linearity under quasi-static loading than those under dynamic loadings. The same trend was shown for all loading rates, with a maximum strain at the joint and then it decreases far away from the joint. The maximum strain values under dynamic loadings were higher than those under static loading, due to the fact that the ultimate strain values of the three types of CFRP are lower in static than in dynamic loadings. Figures 4.29 and 4.30 show the strain distribution of the same joint tested under static and dynamic loading.

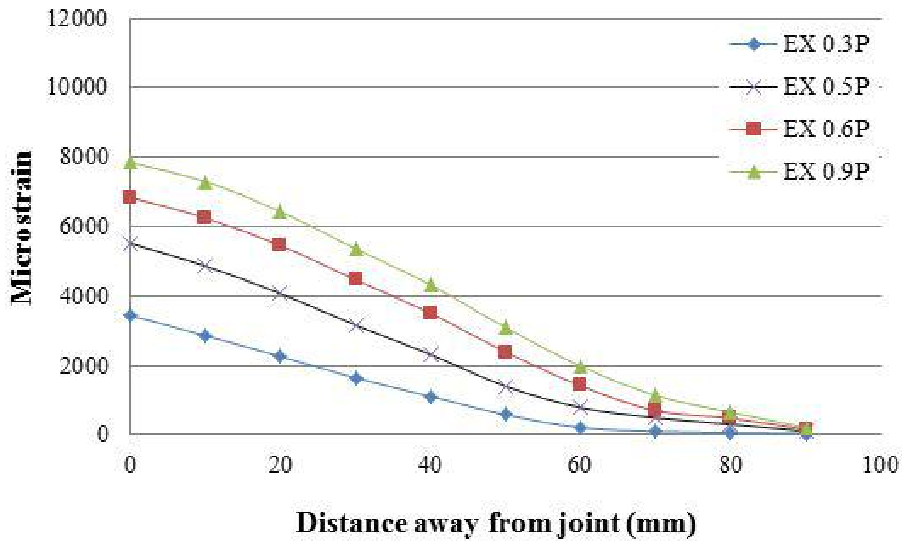

Figure 4.29: Strain distribution along the bond length for low modulus CFRP joints under loading rate of 2 mm/min

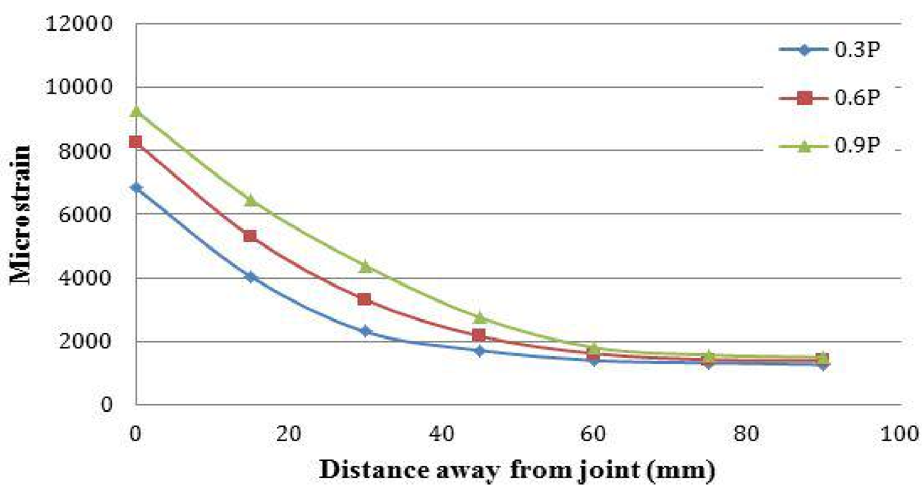

Figure 4.30: Strain distribution along the bond length for low modulus CFRP joints under loading rate of 300×10^3 mm/min

Generally, the maximum strain values for specimens tested under the loading rate of 201×10^{3} mm/min are less than those tested under loading rates of 258×10^{3} and 300×10^{3} mm/min. The general behaviour of all strain distribution plots is non-linear and the slope starts to shift away from the joint. Strain values differ from one load level to another, showing low strain values at low load levels which increase as the load increases and reaches its ultimate level.

4.6.7 Effect of high velocity on the failure mode

Studying the failure modes of the CFRP-steel double strap joints gives more understanding of the contribution of the CFRP layers contribution to carrying the loads. In this research, the failure modes were classified according to the six failure modes proposed by Zhao and Zhang (2007) for the CFRP-steel adhesive joints. These failure modes are (a) steel and adhesive interface debonding, (b) adhesive layer failure, (c) CFRP and adhesive interface debonding, (d) CFRP delamination, (e) CFRP rupture and (f) steel yielding. Figure 5.31 shows a schematic view of these failure modes.

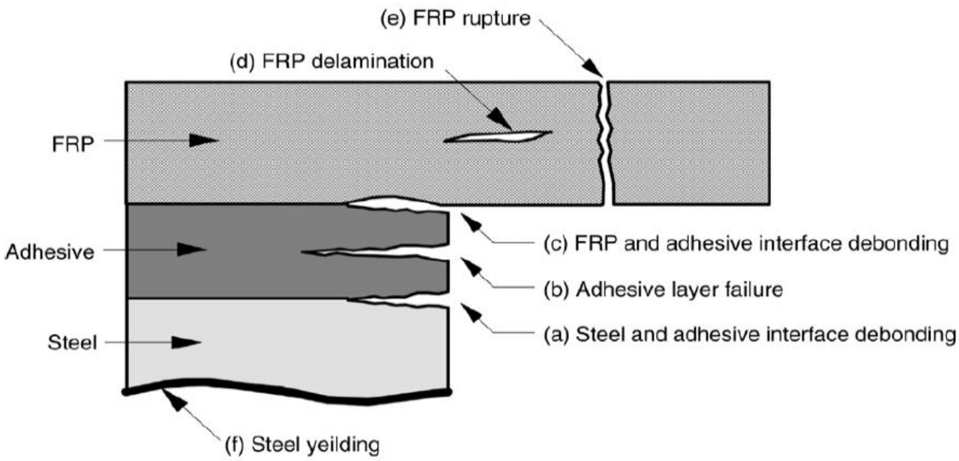

Figure 4.31: Suggested failure modes for CFRP-steel double-strap joints (Zhao and Zhang, 2007)

The failure modes of the current tests were different from one joint to another. The failure mode of low modulus CFRP-steel double strap joints tested under loading rates of 201×10^{3} and 258×10^{3} mm/min was mixed between (a) steel and adhesive interface debonding and (b) adhesive layer failure occurred as shown in Figures 4.32 and 4.33. However, for the same joints tested under a loading rate of 300×10^{3} mm/min, the failure mode was a mixture of (a) steel and adhesive interface debonding, (b) adhesive layer failure, and (d) FRP delamination for all bond lengths, as shown in Figure 4.34. For joints with normal modulus CFRP, the failure mode was constant for all dynamic loading rates and all bond lengths, being a mixture of (a) steel and adhesive interface debonding, (b) adhesive layer failure and (d) FRP delamination for all bond lengths, as shown in Figures 4.35 and 4.36.

Figure 4.32: Failure mode for specimens with low modulus CFRP under load rate of 201×10^3 mm/min

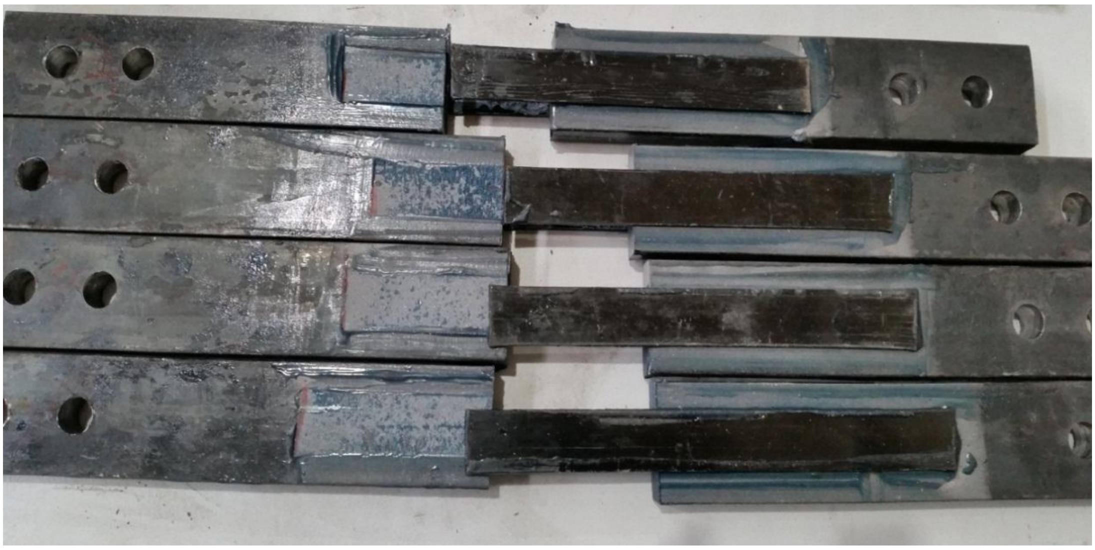

Figure 4.33: Failure mode for specimens with low modulus CFRP under load rate of 258×10^3 mm/min

Figure 4.34: Failure mode for specimens with low modulus CFRP under load rate of 300×10^3 mm/min.

Figure 4.35: Failure mode of normal modulus CFRP under load rates of 201×10^3 and 258×10^3 mm/min

Figure 4.36: Failure mode for specimens with normal modulus CFRP under load rate of 300×10^3 mm/min.

For joints with ultra-high modulus CFRP tested under load rates of 201×10^3 mm/min and 300×10^3 mm/min, the failure mode was mixed between (b) adhesive layer failure and (d) FRP delamination for all loading rates, as shown in Figures 4.37 and 4.38.

Figure 4.37: Failure mode for specimens with ultra-high modulus CFRP under load rate of 201×10^3 mm/min.

Figure 4.38: Failure mode for specimens with ultra-high modulus CFRP under load rate of 300×10^3 mm/min

5.6.8 Comparison with static test results (Chapter Three)

There were some differences in failure modes between quasi-static and impact tests for the CFRP-steel double strap joints. The main reason for these changes is that the material properties under static loading are different to those under dynamic loading. The mode of failure for specimens tested under quasi-static loading was mostly debonding between steel and adhesive for low and normal modulus CFRP joints, whereas the general failure patterns for the same joints tested under dynamic loading were mixed between adhesive failure and FRP failure. This change in failure mode indicates the high shear strength of epoxy under dynamic tension loads, which allows CFRP to sustain more load until both adhesive and CFRP fail together. The same attribution applies for joints with ultra-high modulus CFRP, where the failure mode was FRP rupture for joints tested under static loading and FRP delamination under dynamic loading. The explanation for this change in failure mode is that the ultimate strain of ultra-high modulus CFRP is smaller under static load than dynamic loading. This difference in ultimate strain affects the deformation of adhesive under static load, resulting in less deformation in the adhesive, leading to FRP rupture. More deformation occurs in the adhesive in the joints tested under dynamic loading, which causes FRP delamination (i.e. the adhesive makes some contribution to carrying the load).

To summarise the failure modes of all joints tested in this comprehensive experimental program, Table 4.12 shows the failure modes of all joints tested under all loading rates (2mm/min, 201×10^3, 258×10^3 and 300×10^3mm/min)

Table 4.12: Failure modes for all joint types tested under all loading rates

CFRP modulus used	2mm/min		201×10^3mm/min		258×10^3mm/min		300×10^3mm/min	
	<EBL	>EBL	< EBL	>EBL	< EBL	>EBL	< EBL	>EBL
Low	a & b	a	a & b	a & b	a & b	a & b	a,b & d	a,b & d
Normal	a	a	a,b & d	a,b & d	a, b & d	a,b & d	a,b & d	a,b & d
UHM	b & d	e	b & d	b & d	b & d	b & d	b & d	b & d

<EBL: Below the effective bond length,

>EBL: Beyond the effective bond length.

Failure modes a, b, d and e are steel and adhesive interface debonding, adhesive layer failure, CFRP delamination and CFRP rupture respectively, as shown in Figure 4.31.

4.7 CONCLUSION

A comprehensive experimental testing program was conducted to investigate the bond characteristics between CFRP laminates and steel plates under dynamic load. A series of CFRP-steel double strap joint specimens were prepared and tested under impact tension force with three loading rates, 201×10^3, 258×10^3 and 300×10^3mm/min. A drop-mass machine with a maximum capacity of 200kN in tension was used in the tests. Three types of CFRPs (low modulus (165 GPa), normal modulus (205 GPa) and ultra-high modulus (460 GPa)) were used in this research. Araldite 420 epoxy was used to bond the CFRP laminate to steel joints, and bond strength, strain distribution along the bond area, effective bond length and failure mode were determined. The following conclusions can be drawn:

- The actual material properties of CFRPs and Araldite 420 epoxy under dynamic loadings are higher than those under static loading,

- The ultimate bond strength of the joints tested under dynamic loadings increases by up to 100% compared to the ultimate strength tested under quasi-static loadings,
- The higher the load rate, the higher the ultimate bond strength for all types of joints. However, an insubstantial increase in the bond strength occurs beyond the loading rate of 258×10^3 mm/min, due to the marginal increase in the materials' strength beyond this loading rate.
- The effective bond lengths for specimens tested under dynamic loading are smaller than for specimens tested under quasi-static loading
- The effective bond length is the same for the same joint tested under the three different loading rates,
- There is a significant decrease in the effective bond length for joints with ultra-high modulus CFRP compared to the joints with low and normal modulus CFRP tested under dynamic loading. This explains the effect of the ultimate strain of CFRP laminate on the effective bond length.
- The same effective bond length is observed for low and normal modulus CFRP-steel double strap joints tested under the three different loading rates, because there is little difference in the ultimate strain between the two CFRPs.
- There is less non-linearity of the strain distribution curves for quasi-static loadings than dynamic loadings.
- The ultimate strain of the CFRP-steel double strap joints under dynamic loadings is higher than that under quasi-static loadings.
- Insubstantial changes occur in the ultimate strain values for all types of joints under the last two impact loading rates, 258×10^3 and 300×10^3mm/min
- The failure modes for joints tested under dynamic loading are completely different from those tested under quasi-static loading. Most failures in static testing were debonding for low and normal modulus CFRP, whereas FRP failure was observed in the specimens tested under dynamic loading.
- For joints with ultra-high modulus CFRP the failure mode in static testing was FRP delamination for joints below the effective bond length, and FRP rupture for joints beyond the effective bond length. In contrast, the failure mode was FRP delamination for all bond lengths for specimens tested under impact load.

CHAPTER FIVE NON-LINEAR FINITE ELEMENT ANALYSIS OF CFRP- BONDED STEEL PLATES

5.1 INTRODUCTION

Finite element analysis (FEA) provides safe design and economic products, as experimental tests have challenges related to cost, time consumption, accuracy etc. In addition, FEA can be used to analyse the cause of failure during load-carrying. Almost all fields of engineering, including mechanical engineering, civil engineering, and electrical engineering use FEA for those reasons. However, real experiments are still important for specific load applications or special geometry. Chapters Three and Four showed the experimental effect of static and dynamic loading on CFRP-steel double strap joints. In this chapter, CFRP-steel double strap joints are simulated using non-linear FEA.

Non-linear FEA was used in this research to simulate the static and dynamic behaviour of double strap joints of CFRP laminate bonded to steel plate using Araldite 420 epoxy. Three types of joints with low, normal and ultra-high modulus CFRP were simulated, each type of CFRP being bonded to steel members and tested under quasi- static and dynamic loadings. The load rate for static testing was 2mm/min and three different loading rates were used for the dynamic loading, 201×10^{3}, 258×10^{3} and 300×10^{3}mm/min. Four parameters were numerically predicted and compared with those in the experiments reported in Chapters three and four. The four parameters are: effective bond length, maximum failure load, failure mode, and strain distribution along the bond. Details of specimen simulation are also included in this chapter, which reports the results of two main investigations. The first investigation is of the static and dynamic tensile properties of the materials which formed CFRP-steel joints, which are CFRP, adhesive and steel. The second investigation is of the bond properties between steel and CFRP under static and dynamic loadings. These simulations were carried out using the commercially available non-linear FEA software ABAQUS 6.13.

5.2 FINITE ELEMENT MODELLING

The numerical simulation can be modelled as two-dimensional or three-dimensional modelling, depending on the project or specimen size. 2-D and 3-D modelling each have advantages and disadvantages. 2-D modelling does not require a powerful computer while modelling and running the analysis, and it is simple as the geometry is drawn in X and Y directions only. The disadvantage of using 2-D modelling is that the results obtained are not very accurate compared to those produced by 3-D modelling. 3-D modelling provides precise results and modes of failure but with some difficulties in modelling, related to the properties of the computer used and the time required. A powerful computer was provided for this research to build the double strap joints using the appropriate software. In this research, 3-D modelling was used to simulate the quasi-static and dynamic loadings with different loading rates. The small-scale size of the specimens and the existence of a powerful computer were good reasons to simulate the experimental tests using 3-D finite element modelling. Moreover, the choice of 3-D modelling in this research was necessary to enable good comparisons between the actual test results and the FE analysis by obtaining accurate results in terms of failure modes, strain distribution, ultimate bond strength and effective bond length. ABAQUS 6.13 software was used to numerically investigate the effect of high load rates on the bond characteristics between CFRP laminates and steel plates in double strap joints. ABAQUS/implicit and ABAQUS/explicit were used to simulate quasi-static and dynamic loadings respectively. ABAQUS/implicit offers an extensive elements library and can be used for general analysis (linear and non-linear analysis). It has a very good capability to contact the composite material's layers. ABAQUS/implicit uses a stiffness-based solution technique that is unconditionally stable; moreover, it needs a large disk space due to the large number of iterations. ABAQUS/explicit applies both linear and non-linear analysis procedures, and offers large numbers and types of elements that are suited to explicit analysis. ABAQUS/explicit can solve the most complex contacts; it has two algorithms for modelling contacts: general and contact pairs. General contact allows contact between a number of regions to a single interface, while the contact pairs algorithm provides contact between two surfaces. ABAQUS/explicit uses an explicit integration solution technique which is conditionally stable, and much smaller disk space is required when using ABAQUS/explicit compared to ABAQUS/implicit. The most important difference between the two products is that ABAQUS/implicit is more efficient for analysing smooth non-linear problems, whereas ABAQUS/explicit is the best choice for solving problems with a wave propagation analysis. All the above information about ABAQUS/implicit and ABAQUS/explicit is from the ABAQUS manual (ABAQUS, 2013).

5.2.1 FE mesh and geometry

Finite element analysis requires the use of a sufficient mesh size in modelling structures to ensure accurate results for quasi-static and dynamic modelling, as a coarse mesh causes inaccurate results (ABAQUS, 2013). The finer mesh density gives more accurate analysis, but further mesh refinement might cause a negligible change in the solution. In this case the mesh is said to converge. For the current research, two models were simulated, one with coarse mesh and the other one with fine mesh, both models were typical in geometry and material properties, and similar bond behaviour was obtained. Therefore a mesh size of 0.5 mm was selected for both CFRP and adhesive layers.

Due to the symmetry of specimen geometry in X, Y and Z directions, and to take advantage of the positive features of FEA, only one eighth of the full-scale specimen was modelled. Symmetric boundary conditions were applied to all nodes in other Cartesian planes (YZ, XZ and XY). The full-scale specimens were two steel plates each 200mm long, 40mm wide and 10mm thick, with different CFRP lengths starting from 30 to 130, different CFRP widths (10 and 20mm), and CFRP thicknesses of 1.2 and 1.4 mm. The thickness of the adhesive was 0.5mm for all specimens, and was measured before the experiments using the following calculation:

$$T_t = t_{st} + 2t_f + 2t_a \qquad \text{Equation 5.1}$$

where,

T_t: Total specimen thickness.
t_{st}: Thickness of steel plate.
t_f: Thickness of CFRP.
t_a: Adhesive thickness.

In adhesively-bonded composite joints, the loads transfer from the inner substance (steel) to the outer substance (CFRP laminate) through the adhesive layer. For this reason, the adhesive layer had a finer mesh than that in steel. Figure 5.1 shows the simulation of one eighth of a full-scale specimen for bond length of 100mm of CFRP laminate. The figure also shows the symmetry boundary conditions applied along the YZ, XZ and XY Cartesian planes of the specimen.

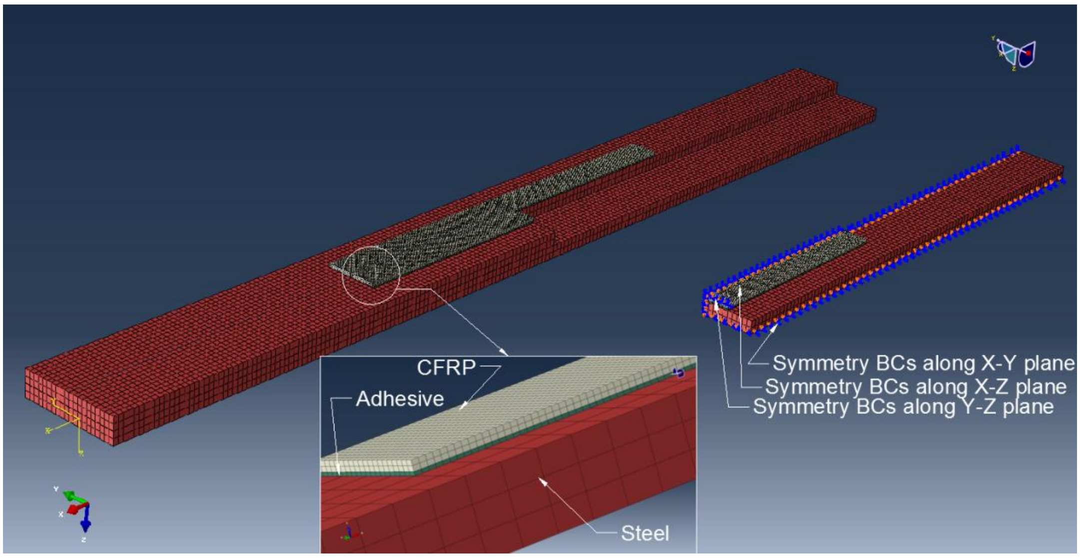

Figure 5.1: 3-D model of full-size CFRP-steel double strap joint.

Figure 5.2 shows the joint components (steel, adhesive and CFRP). The mesh size of the CFRP was selected as the same as the mesh size of the adhesive, to ensure accurate results were obtained, especially at areas near the joint and to enable good understanding of the strain distribution at small intervals along the bond length.

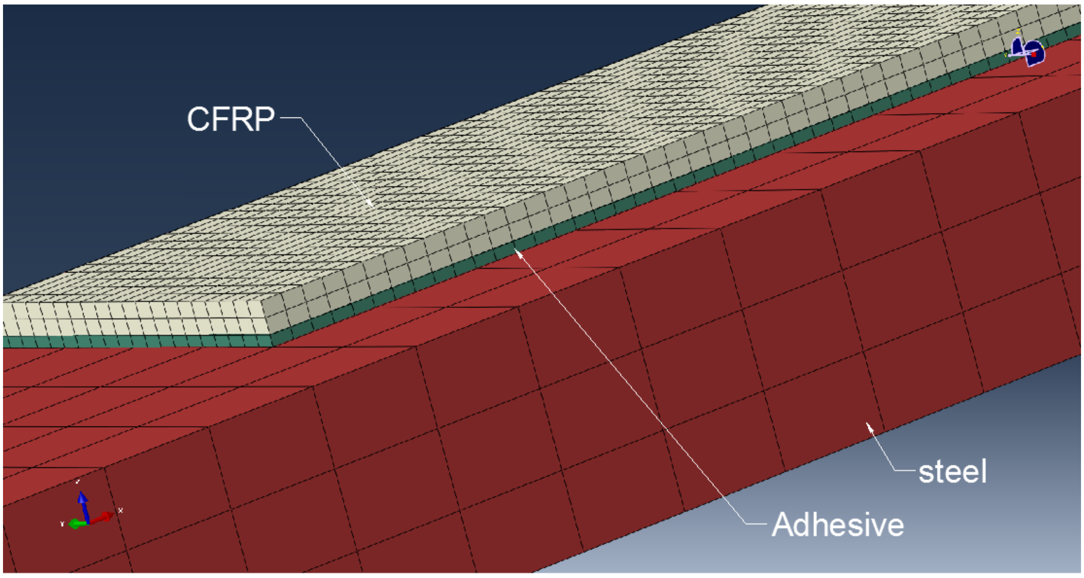

Figure 5.2: CFRP-steel double strap joint showing the three layers (steel, adhesive and CFRP)

5.2.2 Details of modelling double strap joints under quasi-static loading

A total of 44 CFRP-steel double strap joints were modelled in this research using Abaqus/implicit, to numerically investigate the effect of CFRP properties on the bond characteristics between CFRP laminate and steel plates in double strap joints. The simulation was conducted with four groups of modelling, depending on the experimental tests described in Chapter Three. The first group of simulations modelled CFRP-steel double strap joints with low modulus CFRP and 20mm CFRP width, the second group modelled double strap joints with normal modulus CFRP and 20 mm CFRP width, the third group modelled double strap joints with low modulus CFRP and 10mm CFRP width, and the last group modelled CFRP-steel double strap joint specimens with ultra-high modulus CFRP and 20mm CFRP width. 11 models for each group were simulated with different bond lengths starting from 30mm to 130mm. Three different materials were defined in the simulations, which were the three layers forming the CFRP-steel double strap joints. These materials were steel, adhesive and CFRP laminate. The geometry of each material was defined in accordance with the symmetry boundary conditions along X, Y and Z Cartesian, and the three parts (steel, adhesive and CFRP) were first defined in terms of their dimensions and then material properties were defined and assigned to the related parts. After defining all these material and section properties, the CFRP-steel double strap joints were assembled. Then, contact between the layers' surfaces was applied to transfer load from the outer substance to the inner substance. The adhesive layer was tied with steel on one side and with CFRP on the other side. This tie constraint prevents parts from sliding out and ensures the load transfers from one part to another (ABAQUS, 2013). By default, ABAQUS/implicit uses the master-slave contact algorithm, which means the nodes on the slave surface should not be penetrated by the other surface (the master). To prevent this happening, restrictions should be placed on the master surface. For this reason, master-slave surfaces were carefully chosen by following the rule recommended in the ABAQUS 2013 manual that the slave surface has finer meshing than the master surface. To match the experiments, displacement was applied as a boundary condition at one end of the steel plate.

5.2.3 Details of modelling double strap joints under dynamic loading

A total of 72 CFRP-steel double strap joint models were simulated using ABAQUS/explicit, in order to numerically investigate the effect of high loading rates on the bond between CFRP laminate and steel under impact tension load. Three groups of joints were simulated, each group having a different type of CFRP in the double strap joints, and each group was simulated under three different load rates. Table 5.1 shows the details of the total number of joints for each group.

Table 5.1: Summary of total number of CFRP-steel double strap joint models

CFRP Modulus	low CFRP			normal CFRP			UHM CFRP		
Load rate (mm/min)	201×10^3	258×10^3	300×10^3	201×10^3	258×10^3	300×10^3	201×10^3	258×10^3	300×10^3
No. of models	8	8	8	8	8	8	8	8	8
Total no. of models	24			24			24		

Eight models were built up for each load rate, different bond lengths were used for each set of models, and the bond length was varied from 30mm to 130mm to enable full understanding of the numerical behaviour of CFRP-steel double strap joints under different loading rates.

The results were then compared to those from the experimental tests at the same three loading rates (201×10^3, 258×10^3 and 300×10^3 mm/min). The dynamic modelling showed the addition of a steel block, this block represents the actual grips which are fixed to the movable part of the impact rig. These grips were fixed on the movable part of the impact rig. This steel block was used to apply impact loading with different loading rates on the specimens. To restrict the movement of the steel block to be in one direction, another tie constraint was added between the steel block and steel surface of the double strap joint to avoid sliding steel block, and to transfer the applied velocity from the steel block to the CFRP-steel double strap joint. The same symmetry boundary conditions were applied along X, Y and Z Cartesian, as shown in Figure 5.3.

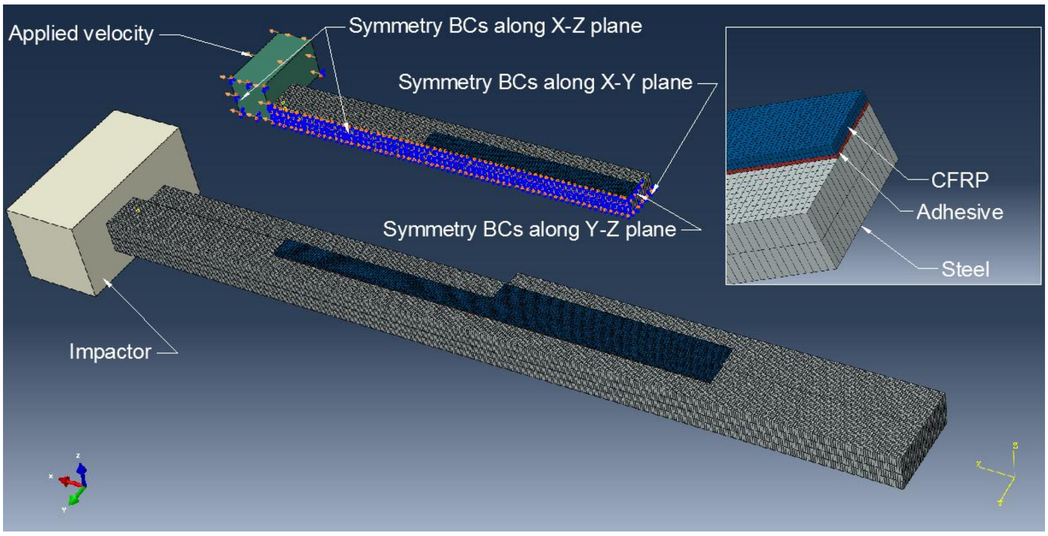

Figure 5.3: Full model of CFRP-steel double strap joint under dynamic loading with the boundary conditions.

5.3 ELEMENT SELECTION

The FE software ABAQUS has different types of elements defined in its elements library CFRP-steel double strap joints are composite materials containing three different layers (steel, adhesive and CFRP laminate), and these three materials were modelled with three different elements. An 8-node linear brick, reduced integration, hourglass control C3D8R element was used to model the steel plate, an 8-node 3-D cohesive element COH3D8 was used to model the adhesive layer, while the CFRP laminate was modelled using an 8-node quadrilateral in-plane general-purpose continuum shell, reduced integration with hourglass control, finite membrane strains element (SC8R). ABAQUS can simulate more accurately a model's through-thickness response using the continuum shell elements. Continuum shell elements allow a fully 3-D model which is more attractive than the brick elements in terms of computations because they have the ability to capture shear stress through thickness without using one element per layer (Falzon et al., 1999). The continuum shell elements are based on shell theory and have the same appearance as 3-D continuum solids, but have similar kinematic and constitutive behaviour to conventional shell elements.

5.4 COMPOSITE FAILURE AND DEGRADATION MODEL OF CFRP LAMINATE

Damage to composite materials used in strengthening structures must be investigated in FE analysis, as the failure in CFRP-steel adhesively-bonded joints usually occurs within the composite material, either in the CFRP or in the bonding material (adhesive). Cohesive failure, adhesive debonding and FRP delamination are the three common failure modes that might occur in CFRP-steel joints. ABAQUS software provides a range of failure models for different types of materials in its built-in library. ABAQUS can predict the onset and propagation of failure for elastic-brittle materials with anisotropic behaviour. One of the required properties to use this model is that the material has linear-elastic response; CFRP has this response, as mentioned in Chapter Three. Since damage in CFRP is initiated without significant plasticity deformation, plasticity can be ignored when modelling this material.

ABAQUS assumes the fibres in fibre-reinforced polymers to be parallel to one direction, as shown in Figure 5.4.

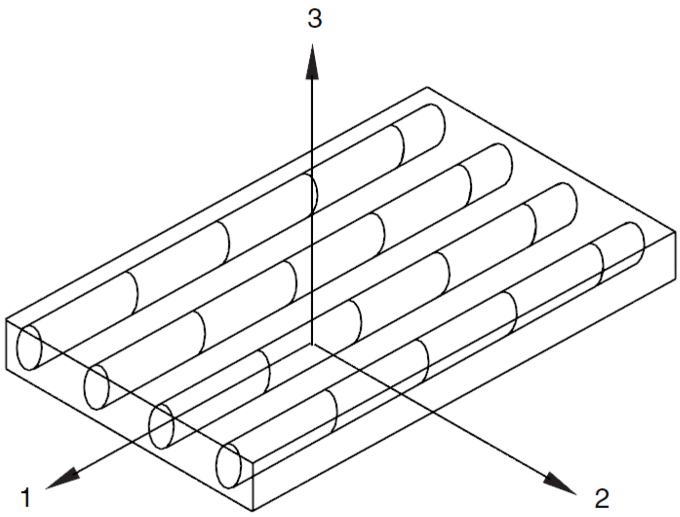

Figure 5.4: Fibres in fibre-reinforced unidirectional lamina as assumed in ABAQUS 2013

The investigation of the failure initiation and propagation was achieved by using the damage model which employs Hashin's failure criteria (Hashin and Rotem, 1973) and depending on the continuum failure mechanism which is based on (Hashin and Rotem, 1973; Matzenmiller et al., 1995; Camanho and Dávila, 2002) . In ABAQUS 6.13 four failure modes are defined for fibre-reinforced materials as follows:

* Fibre ruptures in tension,

* Fibre buckling and kinking in compression,

* Matrix cracking under transverse tension and shearing,

* Matrix crushing under transverse compression and shearing.

5.4.1 CFRP damage initiation

Damage initiation means the start of degradation in a material. Hashin's theory (Hashin and Rotem, 1973) is used in ABAQUS's damage initiation criteria for fibre reinforced composites, and this theory is utilised in both ABAQUS/explicit and ABAQUS/implicit. Four damage initiation mechanisms are to be satisfied in these damage criteria: fibre tension, fibre compression, matrix tension and matrix compression. The formulas for these damage modes are as follows (ABAQUS, 2013):

Fibre rupture in tension $(\hat{\sigma}_{11} \geq 0)$

$$F_f^t = \left(\frac{\hat{\sigma}_{11}}{X^T}\right)^2 + \alpha\left(\frac{\bar{\tau}_{11}}{S^L}\right)^2 \qquad \text{Equation 5.2}$$

Fibre compression $(\hat{\sigma}_{11} < 0)$

$$F_f^c = \left(\frac{\hat{\sigma}_{11}}{X^C}\right)^2 \qquad \text{Equation 5.3}$$

Matrix tension $(\hat{\sigma}_{22} \geq 0)$

$$F_m^t = \left(\frac{\hat{\sigma}_{22}}{Y^T}\right)^2 + \left(\frac{\bar{\tau}_{12}}{S^L}\right)^2 \qquad \text{Equation 5.4}$$

Matrix compression $(\hat{\sigma}_{22} < 0)$

$$F_m^c = \left(\frac{\hat{\sigma}_{22}}{2S^T}\right)^2 + \left[\left(\frac{Y^C}{2S^T}\right)^2 - 1\right]\frac{\hat{\sigma}_{22}}{Y^C} + \left(\frac{\bar{\tau}_{12}}{S^L}\right)^2 \qquad \text{Equation 5.5}$$

where,

X^T: Longitudinal tensile strength of fibre,

X^C: Longitudinal compression strength of fibre,

Y^T: Transverse tensile strength of fibre,

Y^C: Transverse compression strength of fibre,

S^L: Longitudinal shear strength of fibre,

S^T: Transverse shear strength of fibre, A: is a coefficient that determines the contribution of the shear stress to the fibre tensile initiation criterion,

$\hat{\sigma}_{11}, \hat{\sigma}_{22}$ and $\hat{\tau}_{11}$: the components of the effective stress tensor, $\hat{\sigma}$ which is used to calculate the initiation criteria, $\hat{\sigma}$ can be calculated from:

$$\hat{\sigma} = M\,\sigma \qquad \text{Equation 5.6}$$

where, σ is the true stress, and M is the damage operator:

$$M = \begin{bmatrix} \frac{1}{(1-d_f)} & 0 & 0 \\ 0 & \frac{1}{(1-d_m)} & 0 \\ 0 & 0 & \frac{1}{(1-d_s)} \end{bmatrix} \qquad \text{Equation 5.7}$$

where,

d_f: The internal variable that characterizes the fibre

d_m: The internal variable that characterizes the matrix

d_s: The internal variable that characterizes shear damage

These three variables can be derived from the damage variables d_f^t, d_f^c, d_m^t and d_m^c

Corresponding to the four model equations (fibre rupture in tension ($\hat{\sigma}_{11} \geq 0$), fibre compression ($\hat{\sigma}_{11} < 0$), matrix tension ($\hat{\sigma}_{22} \geq 0$), matrix compression ($\hat{\sigma}_{22} < 0$)) discussed previously, they are as follows:

$$d_f = \begin{cases} d_f^t, & \text{if } \hat{\sigma}_{11} \geq 0 \\ d_f^c, & \text{if } \hat{\sigma}_{11} < 0 \end{cases} \qquad \text{Equation 5.8}$$

$$d_m = \begin{cases} d_m^t, & \text{if } \hat{\sigma}_{22} \geq 0 \\ d_m^c, & \text{if } \hat{\sigma}_{22} < 0 \end{cases} \qquad \text{Equation 5.9}$$

$$d_s = 1-(1-d_f^t)(1-d_f^c)(1-d_m^t)(1-d_m^c) \qquad \text{Equation 5.10}$$

Before any damage initiation and evolution, the damage operator M is equal to the defined matrix, so $\hat{\sigma} = \sigma$ (ABAQUS, 2013). The damage operator becomes more complex once damage initiation and propagation occur. Each damage initiation mode (fibre tension, fibre compression, matrix tension and matrix compression) has an associated output variable. The damage initiation criteria must be used with the continuum shell element used to model the CFRP laminate to be able to show the accurate failure mode from the model. ABAQUS/explicit and ABAQUS/implicit have some additional output variables related to damage initiation at a material spot in the fibre reinforced composite damage model. These variables are as follows:

DMICRT: All damage initiation criteria components,

HSNFTCRT: The ultimate estimation of the tensile initiation standard which occurred during the analysis of the fibre

HSNFCCRT: The ultimate estimation of the compressive initiation standard which occurred during the analysis of the fibre

HSNMTCRT: The ultimate estimation of the tensile initiation standard which occurred during the analysis of the matrix

HSNMCCRT: The ultimate estimation of the compressive initiation standard which occurred during the analysis of the matrix.

The above parameters indicate whether an initiation criterion in a failure mode is adequate or not. For the above variables, a value of less than 1.0 means that the criterion is not satisfied, and a value of 1.0 or higher indicates that the damage criterion is satisfied.

5.4.2 CFRP damage evolution

One of the advantages of using ABAQUS software is that it models the damage evolution which occurs after CFRP damage initiation, the damage initiation models the damage sunset in fibre reinforced composites, while the damage evolution models the failure propagation along the elements. The damage evolution in ABAQUS assumes that failure is described by the propagation of the material stiffness degradation, followed by material failure. It requires linearly elastic behaviour for the undamaged material. The damage evolution model also considers the four different failure modes (fibre tension, fibre compression, matrix tension and matrix compression) and uses the four damage variables to describe the damage for each failure mode. In addition, Hashin and Rotem, (1973) damage initiation must be combined with the damage evolution model. This failure model is based on energy dissipation during the analysis of the damage model. After failure occurs, the damage initiation model can show what happened during the failure, including the removal of elements from the mesh. Before the failure sunset, the material response is considered to be linearly elastic with the stiffness matrix of a plane stress orthotropic material. The response of the material can be calculated from:

$$\sigma = C_d\, \varepsilon, \qquad \text{Equation 5.11}$$

where, ε is the material strain and C_d is the damage elasticity matrix which equals:

$$C_d = \frac{1}{D}\begin{bmatrix} (1-d_f)\,E_1 & (1-d_f)(1-d_m)\nu_{21}\,E_1 & 0 \\ (1-d_f)(1-d_m)\nu_{12}\,E_2 & (1-d_m)\,E_2 & 0 \\ 0 & 0 & (1-d_s)\,GD \end{bmatrix} \qquad \text{Equation 5.12}$$

where,

$D = 1 - (1 - d_f)(1 - d_m)\nu_{12}\nu_{21}$

d_f: The current state of fibre damage,

d_m: The current state of matrix damage,

d_s: The current state of shear damage,

E_1: Modulus of elasticity in the fibre direction for CFRP laminate,

E_2: Modulus of elasticity in the matrix direction for CFRP laminate,

G: The shear modulus for the CFRP laminate,

ν_{12} and ν_{21} are Poisson's ratios, and

$\hat{\sigma}_{11}$ and $\hat{\sigma}_{22}$: the components of effective stress tensor

To reduce mesh dependency during material softening, ABAQUS adds a characteristic length L^C into the formula, and uses the constitutive law as a stress-displacement relation. The failure mode variable will behave like the stress-displacement relationship after damage initiation occurs. Figure 5.5 shows the stress-displacement curve, and the positive part represents the linearly elastic behaviour of the material before cracking initiation.

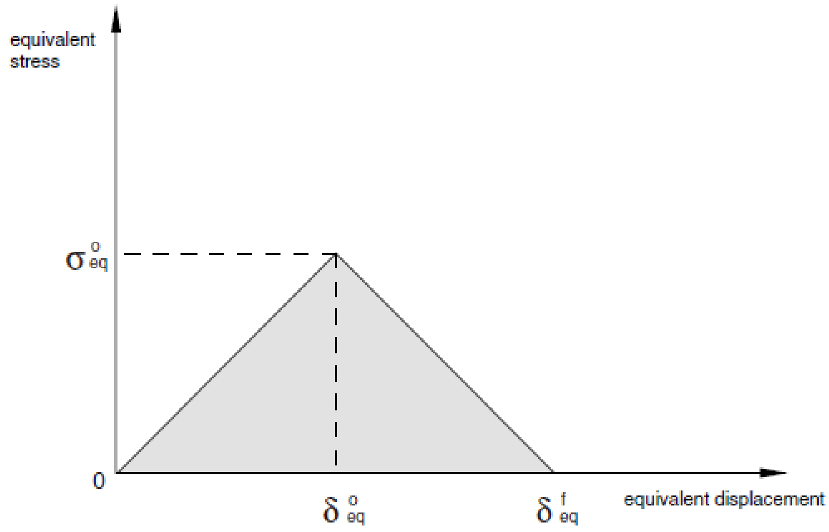

Figure 5.5: Linearly elastic evolution (ABAQUS, 2013)

The negative part in the curve above reflects the behaviour after damage initiation. After damage initiation (when $\delta_{eq} \geq \delta^{0}_{eq}$), the failure variable of a specific mode is given by the following equation:

$$d = \frac{\delta^{f}_{eq}(\delta_{eq} - \delta^{0}_{eq})}{\delta_{eq}(\delta^{f}_{eq} - \delta^{0}_{eq})} \qquad \text{Equation 5.13}$$

where,

δ^{0}_{eq}: The initial equivalent displacement at which the initiation criterion for that mode is achieved,

δ^{f}_{eq}: The displacement at which the material is completely damaged in this failure mode.

The characteristic length L^{C} is totally based on the element geometry and formulation, and is measured as the length of the line across an element for a first order element and it is half of the same typical length for a second order element.

Figure 5.6 shows the damage variable as a function of equivalent displacement.

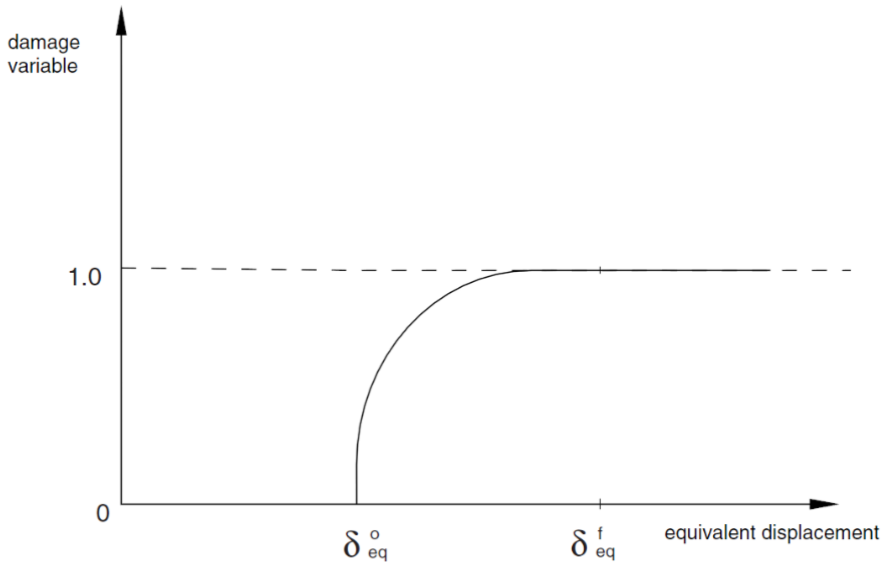

Figure 5.6: Damage parameter as a function of equivalent displacement (ABAQUS, 2013)

Equivalent displacement and stress for each of the failure modes mentioned above are defined as:

Fibre rupture in tension $(\hat{\sigma}_{11} \geq 0)$

$$\delta_{eq}^{ft} = L^C \sqrt{\langle\varepsilon_{11}\rangle^2 + (\varepsilon \propto_{12}^2} \qquad \text{Equation 5.14}$$

$$\delta_{eq}^{ft} = \frac{\langle\sigma_{11}\rangle\langle\varepsilon_{11}\rangle + \tau\propto_{12}\varepsilon_{12}}{\delta_{eq}^{f}/L^C} \qquad \text{Equation 5.15}$$

Fibre compression $(\hat{\sigma}_{11} < 0)$

$$\delta_{eq}^{ft} = L^C \langle-\varepsilon_{11}\rangle \qquad \text{Equation 5.16}$$

$$\delta_{eq}^{fc} = \frac{\langle-\sigma_{11}\rangle\langle-\varepsilon_{11}\rangle}{\delta_{eq}^{fc}/L^C} \qquad \text{Equation 5.17}$$

Matrix tension $(\hat{\sigma}_{22} \geq 0)$

$$\delta_{eq}^{mt} = L^C \sqrt{\langle\varepsilon_{22}\rangle^2 + \varepsilon_{12}^2} \qquad \text{Equation 5.18}$$

$$\sigma_{eq}^{mt} = \frac{\langle\sigma_{22}\rangle\langle\varepsilon_{22}\rangle + \tau_{12}\varepsilon_{12}}{\delta_{eq}^{mt}/L^C} \qquad \text{Equation 5.19}$$

Matrix compression $(\hat{\sigma}_{22} < 0)$

$$\delta_{eq}^{mc} = L^{C}\sqrt{\langle -\varepsilon_{22}\rangle^{2} + \varepsilon_{12}^{2}}$$ Equation 5.20

$$\sigma_{eq}^{mc} = \frac{\langle -\sigma_{22}\rangle\langle -\varepsilon_{22}\rangle + \tau_{12}\varepsilon_{12}}{\delta_{eq}^{mc}/L^{C}}$$ Equation 5.21

where,

L^{c}: is the characteristic length which is based on the element geometry and formulation.

$\langle\ \rangle$: This symbol represents the Macaulay bracket operator.

5.5 ADHESIVE FAILURE AND DEGRADATION MODEL

The adhesive layer is the most important layer in CFRP-steel double strap joints, as it transfers loads from steel to CFRP under different types of loadings. Choosing an appropriate element to model the adhesive layer is very important and the key to obtaining accurate results. ABAQUS offers a special typical element known as a cohesive element. A cohesive element is suitable for modelling adhesive, bonded interfaces, gaskets and rock fractures (ABAQUS, 2013). The mechanical behaviour of these elements depends on the application and assumptions about the deformation and stress states that are related to each application. This classification is based on a continuum description of the material, a traction-separation description of the interface or a uniaxial stress state appropriate for modelling gaskets and/or laterally unconstrained adhesive patches. ABAQUS defines adhesive joints as those where two materials are connected together by a glue, as shown in Figure 5.7.

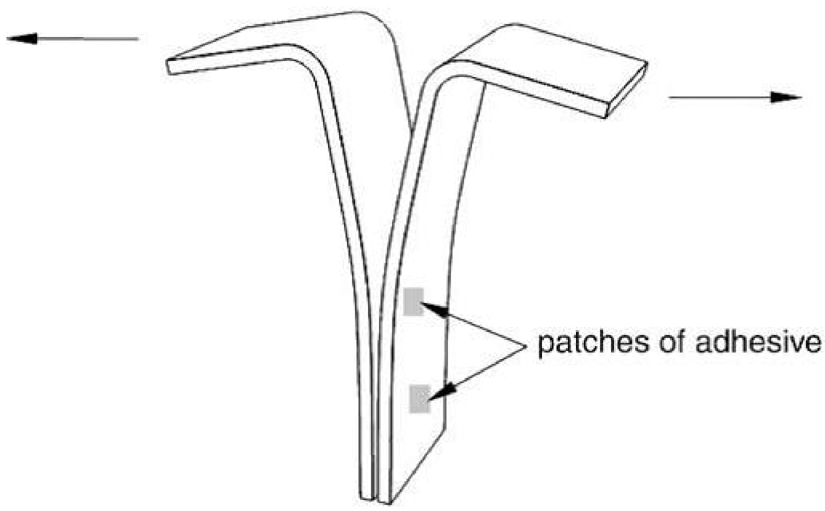

Figure 5.7: Definition scheme of the adhesive joint in ABAQUS (ABAQUS, 2013).

Using the cohesive element with a continuum-based model should correspond to finite adhesive thickness, which is the same property as that measured in the experimental program.

Damage initiation and evolution for the cohesive zone can be modelled by utilising cohesive elements. In the definition of this type of element it is restricted to modelling one layer of an element through its thickness; otherwise the results might be unreliable. The cohesive element models the initial loading, damage onset, and damage evolution leading to final failure.

Three different methods can be used to simulate the cohesive element: traction-separation-based modelling, continuum-based modelling, and gaskets or laterally unconstrained adhesive patches. The traction-separation response is primarily specified for bonded interfaces where the cohesive layer is very thin, and the thickness of the adhesive layer is generally smaller than that of the other materials that form adhesively-bonded joints. As these properties match CFRP-steel double strap joints well, traction-separation-based modelling was used to model the adhesive layer in the current project. Generally, cohesive elements are utilized to model the adhesive layer in CFRP-steel double strap joints by using the traction-separation function as a constitutive response of a cohesive element. The traction-separation law:

- Can be used model delamination at the cohesive layer,
- Allows definition of the other properties of the material such as fracture energy as a function of the ratio of normal to shear deformation at the interface,
- Assumes a linear elastic response prior to damage, as shown in Figure 5.8
- Allows multiple failure modes.

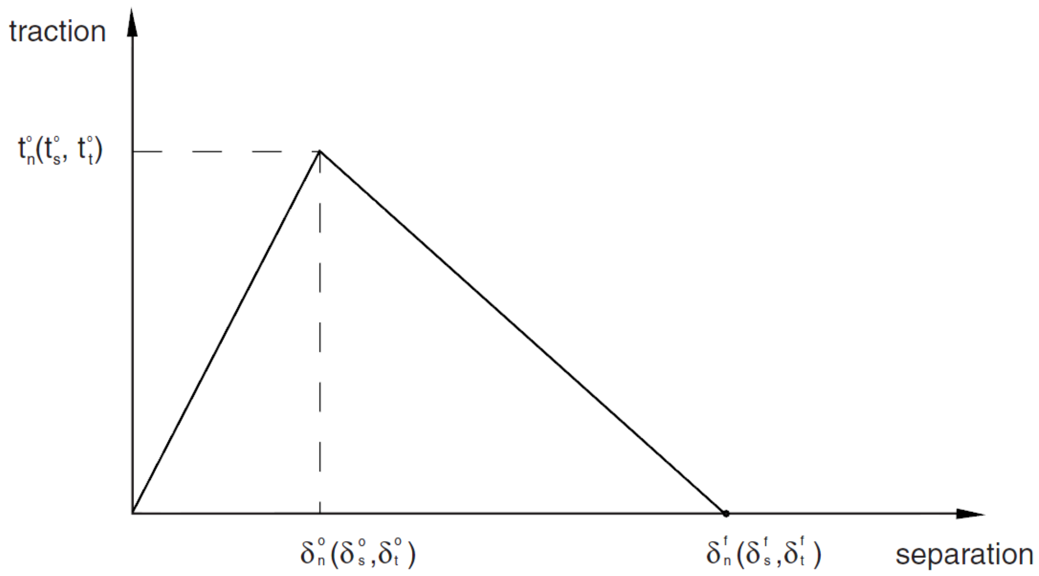

Figure 5.8: Typical traction-separation curve (ABAQUS, 2013).

According to the figure above, the cohesive behaviour is linearly elastic at the first part of the curve and when damage occurs, the elastic behaviour is described in terms of an elastic constitutive matrix that relates the nominal stresses to the nominal strains through the interface. The nominal stresses are defined as the force components divided by the area at each related point, while the nominal strains are defined as the separation divided by the thickness at each related point. The nominal traction stress vector (t) consists of three components, of which t_n, t_s are in 2-D problems, and t_t is in 3-D problems. These three components correspond to separations δ_n, δ_s and δ_t respectively. The nominal strains are defined as

$$\varepsilon_n = \frac{\delta_n}{T_o} \qquad \text{Equation 5.22}$$

$$\varepsilon_s = \frac{\delta_s}{T_o} \qquad \text{Equation 5.23}$$

$$\varepsilon_t = \frac{\delta_t}{T_o} \qquad \text{Equation 5.24}$$

where, T_o is the original thickness of the cohesive element.

The elastic behaviour can be written as:

$$t = \begin{Bmatrix} t_n \\ t_s \\ t_t \end{Bmatrix} = \begin{bmatrix} k_{nn} & k_{ns} & k_{nt} \\ k_{ns} & k_{ss} & k_{st} \\ k_{nt} & k_{st} & k_{tt} \end{bmatrix} \begin{Bmatrix} \varepsilon_s \\ \varepsilon_n \\ \varepsilon_t \end{Bmatrix} = [k]\,\varepsilon \qquad \text{Equation 5.25}$$

This elasticity matrix provides fully coupled behaviour among all components of the traction and separation vectors.

5.5.1 Adhesive damage initiation

The damage initiation and progression at the cohesive layer can be modelled with cohesive elements using both ABAQUS/implicit and ABAQUS/explicit. The process of failure starts when stresses or strains satisfy certain damage initiation criteria. ABAQUS has different damage initiation criteria under traction separation law. These are:

- Maximum nominal stress criterion

  Initiation in damage starts when the ultimate nominal stress ratio meets a value of one. It can be expressed as:

$$\mathrm{Max}\left\{\frac{\langle t_n\rangle}{t_n^{\circ}} \quad \frac{t_s}{t_s^{\circ}} \quad \frac{t_t}{t_t^{\circ}}\right\} = 1 \qquad \text{Equation 5.26}$$

  where, t_n, t_s, t_t are the stresses in the adhesive layer in three directions (normal, first and second shear direction respectively).

  t_n°, t_s°, t_t° are the maximum values of stresses of the adhesive layer in three directions (normal, first and second shear direction, respectively).

- Maximum nominal strain criterion

  Initiation in damage starts when the ultimate nominal strain ratio meets a value of one. It can be expressed as:

$$\mathrm{Max}\left\{\frac{\langle \varepsilon_n\rangle}{\varepsilon_n^{\circ}} \quad \frac{\varepsilon_s}{\varepsilon_s^{\circ}} \quad \frac{\varepsilon_t}{\varepsilon_t^{\circ}}\right\} = 1 \qquad \text{Equation 5.27}$$

  ε_n, ε_s, ε_t are the values of strains in the adhesive layer in three directions (normal, first and second shear direction respectively).

  ε_n°, ε_s°, ε_t° are the maximum values of nominal strain in the adhesive layer in three directions (normal, first and second shear direction respectively).

- Quadratic stress criterion

  Initiation in damage starts when a quadratic interaction function involving the nominal stress ratios meets a value of one. It can be expressed as:

$$\left\{\frac{\langle t_n \rangle}{t_n^{\circ}}\right\}^2 + \left\{\frac{t_s}{t_s^{\circ}}\right\}^2 + \left\{\frac{t_t}{t_t^{\circ}}\right\}^2 = 1 \qquad \text{Equation 5.28}$$

- Quadratic strain criterion

Initiation in damage starts when a quadratic interaction function involving the nominal strain ratios meets a value of one. It can be expressed as:

$$\left\{\frac{\langle \varepsilon_n \rangle}{\varepsilon_n^{\circ}}\right\}^2 + \left\{\frac{\varepsilon_s}{\varepsilon_s^{\circ}}\right\}^2 + \left\{\frac{\varepsilon_t}{\varepsilon_t^{\circ}}\right\}^2 = 1 \qquad \text{Equation 5.29}$$

5.5.2 Adhesive damage evolution

Damage evolution occurs after the damage initiation of the adhesive layer, and the cohesive material stiffness starts to decrease according to the damage evolution law, which describes the rate at which the material stiffness is degraded when the corresponding damage initiation criterion is met. The degradation in the adhesive material can be calculated by the scalar damage parameter (D), which reflects the overall failure in the adhesive layer and calculates the mixed failure effect. (D) has a range from 0 which means undamaged material to 1 which means fully damaged material. The stress components of the traction-separation model are affected by damage, according to the following equation:

$$t_n = \begin{cases} (1-\mathrm{D})\bar{t}_n, & \bar{t}_n \geq 0 \\ \bar{t}_n, & \text{otherwise, (no damage to compressive stiffness)} \end{cases} \qquad \text{Equation 5.30}$$

Otherwise, no damage to compressive stiffness occurs.

$$t_s = (1 - D)\ \bar{t}_s \qquad \text{Equation 5.31}$$

$$t_t = (1 - D)\ \bar{t}_t \qquad \text{Equation 5.32}$$

where,

$\bar{t}_n$, $\bar{t}_s$ and $\bar{t}_t$ are the stress components calculated by the elastic traction-separation behaviour for the current strains without damage.

The mode mix of the deformation fields in the cohesive zone quantifies the relative properties of normal and shear deformation. ABAQUS has two measures of modes, the first based on the energies and the second based on tractions. Because the damage progression is dependent on the energy that dissipates due to the damage process, the energies method has been selected in this study, and the fracture energy is defined in the material properties with either linear or exponential softening behaviour. The mix-mode definitions based on energies are as follows:

$$m_1 = \frac{G_n}{G_T} \qquad \text{Equation 5.33}$$

$$m_2 = \frac{G_s}{G_T} \qquad \text{Equation 5.34}$$

$$m_3 = \frac{G_t}{G_T} \qquad \text{Equation 5.35}$$

Where:

G_n, G_s, G_t are the work done by the tractions and their conjugate relative displacements in the normal, first and second shear directions respectively.

G_T: is the sum of G_n, G_s and G_t

The power law fracture criterion is used to define the dependence of the fracture energy on the mix-mode.

Failure in the mix-mode conditions is generated by a power law interaction of those energies which cause failure in each mode separately. This definition is known as the power law criterion, which is given by:

$$\left\{\frac{G_n}{G_n^C}\right\}^{\alpha} + \left\{\frac{G_s}{G_s^C}\right\}^{\alpha} + \left\{\frac{G_t}{\varepsilon_t^{\circ}}\right\}^{\alpha} = 1 \qquad \text{Equation 5.36}$$

The mixed-mode fracture energy $G^C = G_n + G_s + G_t$, where G_n^C, G_s^C *and* G_t^C are the critical fracture energies required to cause failure in the normal, the first and the second shear directions, respectively.

5.6 INVESTIGATION OF THE MATERIAL PROPERTIES BY FINITE ELEMENT ANALYSIS

As shown in Chapter Three, all materials (steel, CFRP and adhesive) that formed the double strap joints were experimentally investigated in order to determine their static and dynamic mechanical properties (ultimate stress, ultimate strain and elastic modulus). Prior to numerical verification of the different types of double strap joints, it was decided to verify the material properties under both static and dynamic load rates. ABAQUS/implicit was used to investigate the mechanical properties under quasi-static loading, while ABAQUS/explicit was used to determine the materials' mechanical properties under dynamic loading. The aim of this analysis was to ensure that all materials used to form the double strap joints were modelled correctly using finite element analysis.

5.6.1 Numerical properties of CFRP laminate

Since different CFRP laminates were used in this research to build the double strap joints, the mechanical properties of low, normal and ultra-high modulus CFRP were experimentally investigated in this research. In this chapter, the mechanical properties of different CFRP moduli are numerically investigated under quasi-static and dynamic loading. The same quasi-static and dynamic loading rates as those used in the experimental program were used in FE modelling. The loading rates were 2 mm/min for quasi-static loading, and 201×10^3, 258×10^3 and 300×10^3 mm/min for dynamic loading. A total of 16 models were simulated in order to investigate the mechanical properties of all types of CFRPs (low, normal and ultra-high modulus) under the existing four loading rates. As mentioned earlier, the CFRP composite material was modelled using an 8-node quadrilateral in-plane general-purpose continuum shell, reduced integration with hourglass control, finite membrane strains element (SC8R). Only one quarter of the specimen was simulated due to the symmetry in material and geometry, and symmetry boundary conditions were applied in X and Y directions, as shown in Figures 5.9 and 5.10.

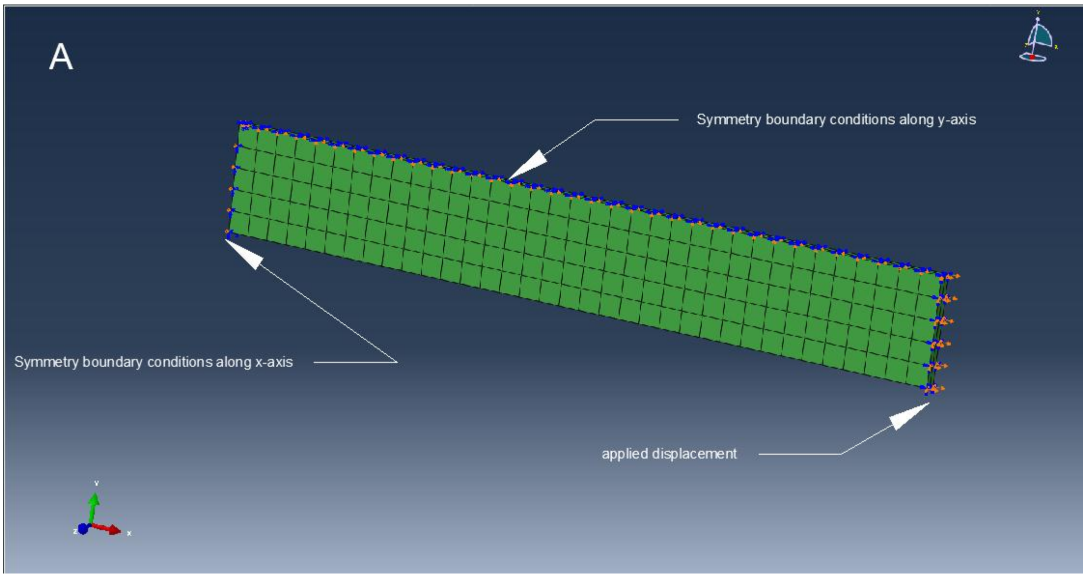

Figure 5.9: CFRP model with symmetry boundary conditions for quasi-static loading.

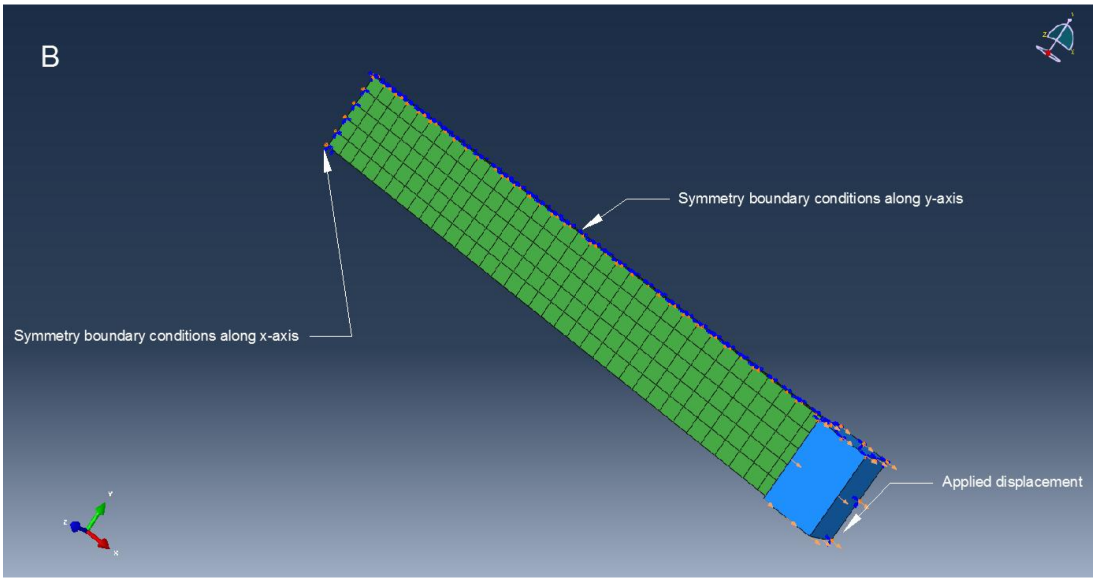

Figure 5.10: CFRP model with symmetry boundary conditions for dynamic loading.

In relation to the mechanical properties of the different CFRP laminates, the stress-strain curves are plotted in Figures 5.11 and 5.12; the figures shows comparisons of the results from the experimental tests and the numerical models.

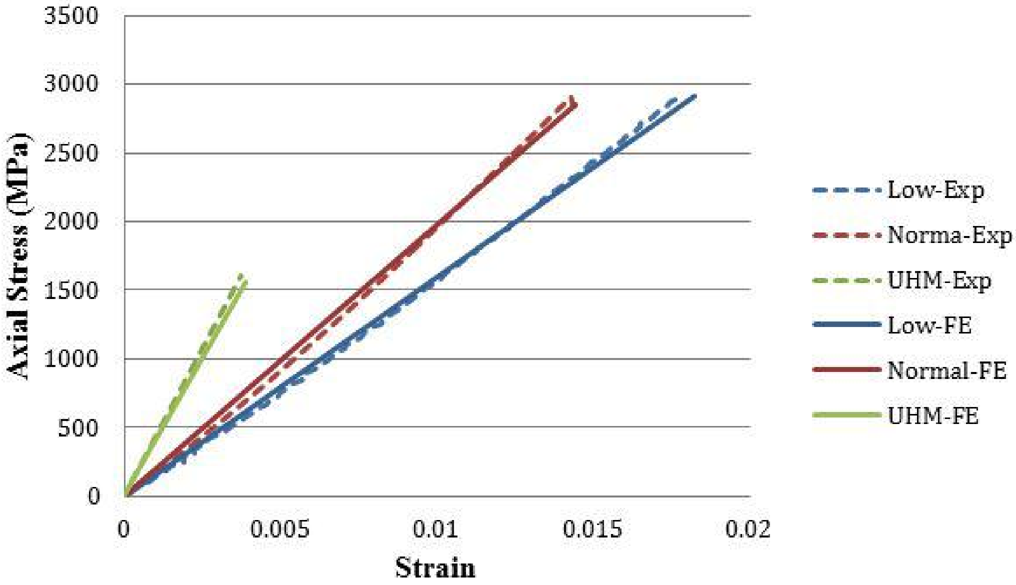

Figure 5.11: Comparison of the numerical and experimental stress-strain curves for the three different CFRPs

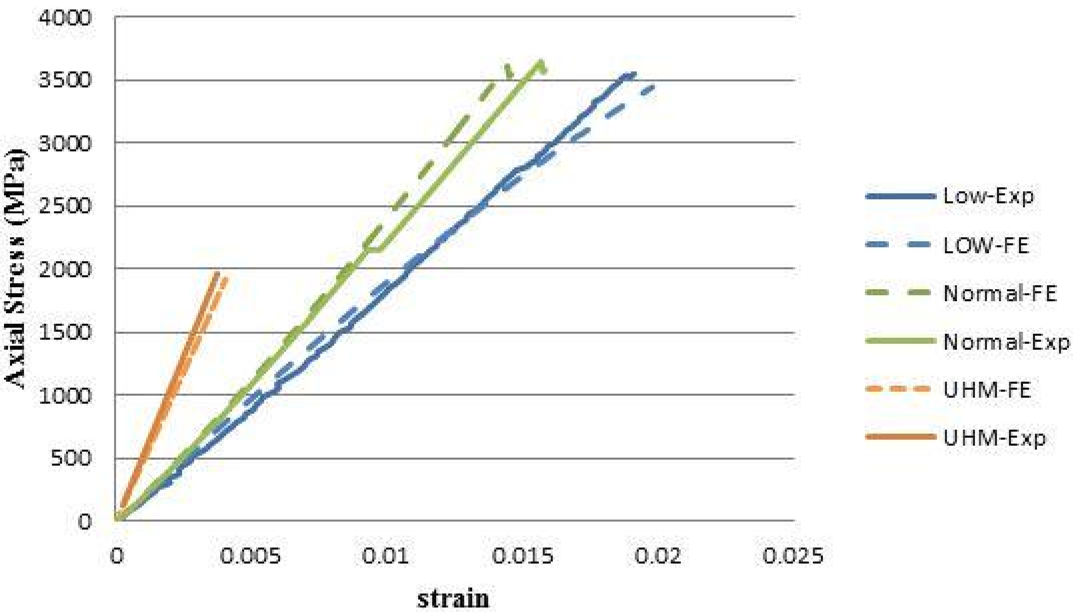

Figure 5.12: Comparison of the numerical and experimental stress-strain curves for the three different CFRPs under dynamic loading

Figure 6.13 shows the numerical failure criteria for the CFRP laminate under static and dynamic loadings. The same failure mode was observed for all types of CFRP laminates.

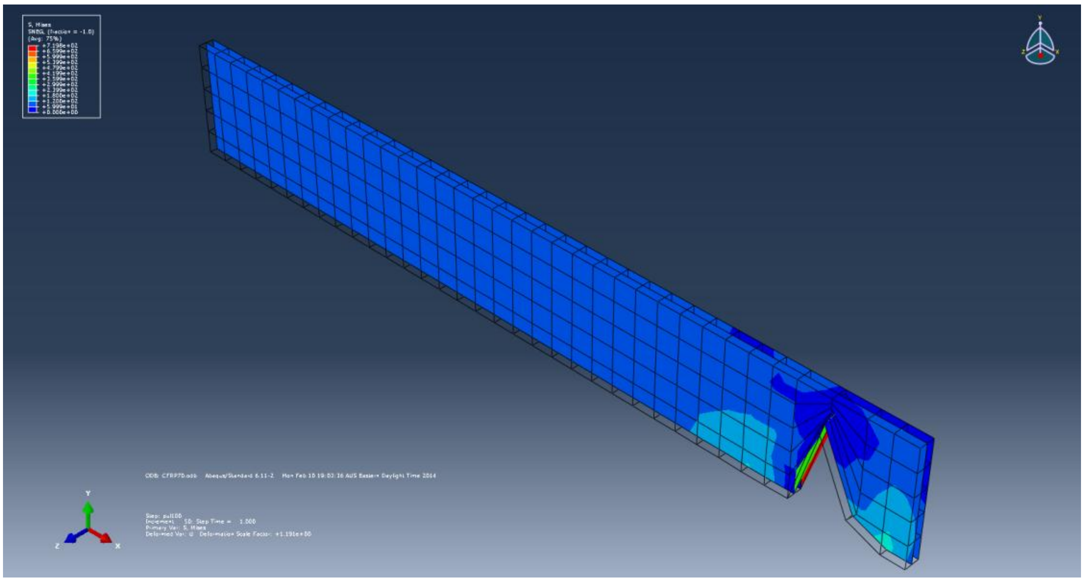

Figure 5.13: Numerical failure mode of CFRP laminates

5.6.2 Numerical properties of Araldite 420 epoxy

The Araldite 420 adhesive was also modelled using FEA, and both ABAQUS/implicit and ABAQUS\explicit were used for quasi-static and dynamic loadings respectively. As mentioned earlier, the adhesive was modelled using an 8-node 3-D cohesive element COH3D8. As the CFRP-steel double strap joints were subjected to quasi-static and dynamic tension loads, the adhesive layer was mainly subjected to shear force. Therefore, the CFRP-steel double strap joints mainly resisted the applied tension force through the adhesive. Four models were built up in ABAQUS in order to numerically investigate the shear strength of the adhesive, and the results from the numerical simulation were compared with the experimental results claimed by Al-Zubaidy (2012) . Good agreement between the numerical simulation and the experimental results was shown for all loading rates (2 mm/min for quasi-static loading, and 201×10^3, 258×10^3 and 300×10^3 mm/min for dynamic loading). Figure 5.14 shows the numerical model of a steel single lap joint, which was developed to determine the numerical properties of the adhesive.

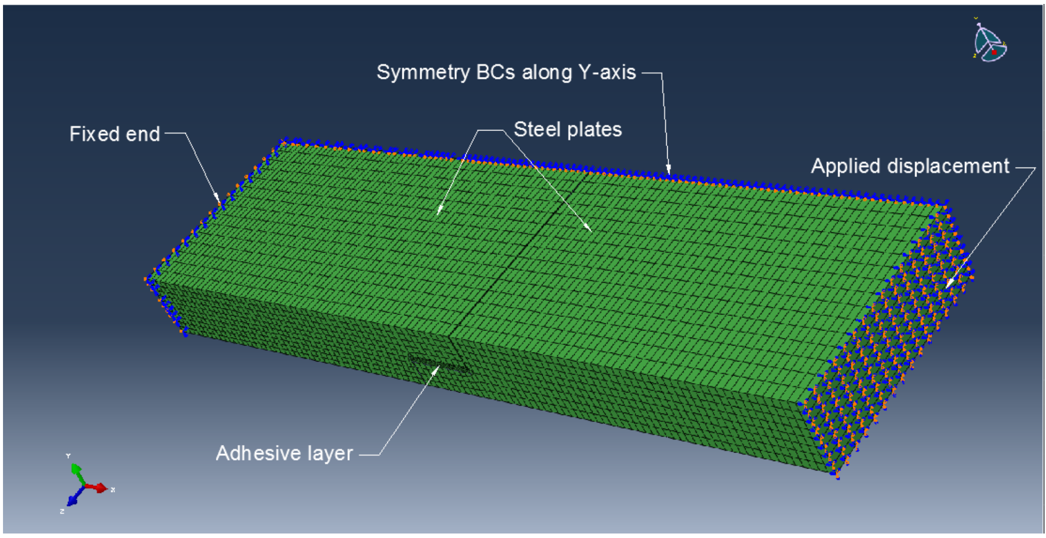

Figure 5.14: Steel single-lap modelling showing the boundary conditions.

The numerical shear strength results from the single-lap steel joints were compared with the actual adhesive properties claimed by Al-Zubaidy (2012). Figure 5.15 shows good agreement between the current numerical simulation results and the experimental tests.

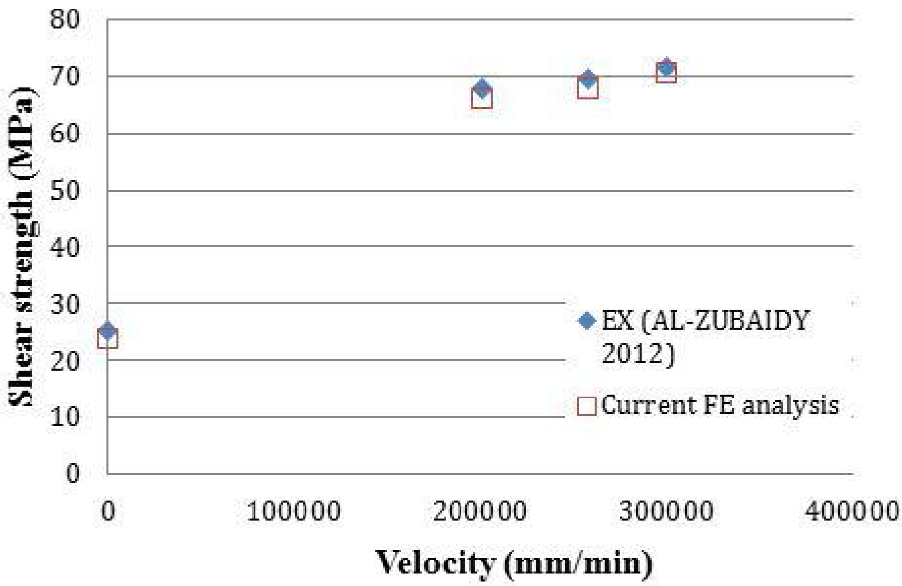

Figure 5.15: Comparison of the numerical adhesive shear strength results with the experimental results obtained by (Al-Zubaidy, 2012) (Re-Plotted)

5.6.3 Numerical properties of steel plate

The steel plates used in the CFRP-steel double strap joints were 200 mm long, 40mm wide and 16mm thick for dynamic or 10mm thick for static testing. The elastic and plastic stress and strain data were investigated experimentally (see Chapters Three and

Four) in order to obtain the actual mechanical properties, and the measured mechanical properties were used in FE modelling. One half of the steel coupon was simulated (see Figure 5.16) using an 8-node linear brick, reduced integration, hour glass control C3D8R element. Four steel coupon models were simulated in ABAQUS/implicit and ABAQUS/explicit to investigate the mechanical properties under quasi-static and three impact loadings respectively. The results of the numerical analysis were compared and plotted with those from the experimental data (see Figure 5.17). The results show excellent agreement between analytical and experimental results in term of the stress-strain curves, indicating that FE models for quasi-static and dynamic loading effectively represent the materials that formed the double strap joints.

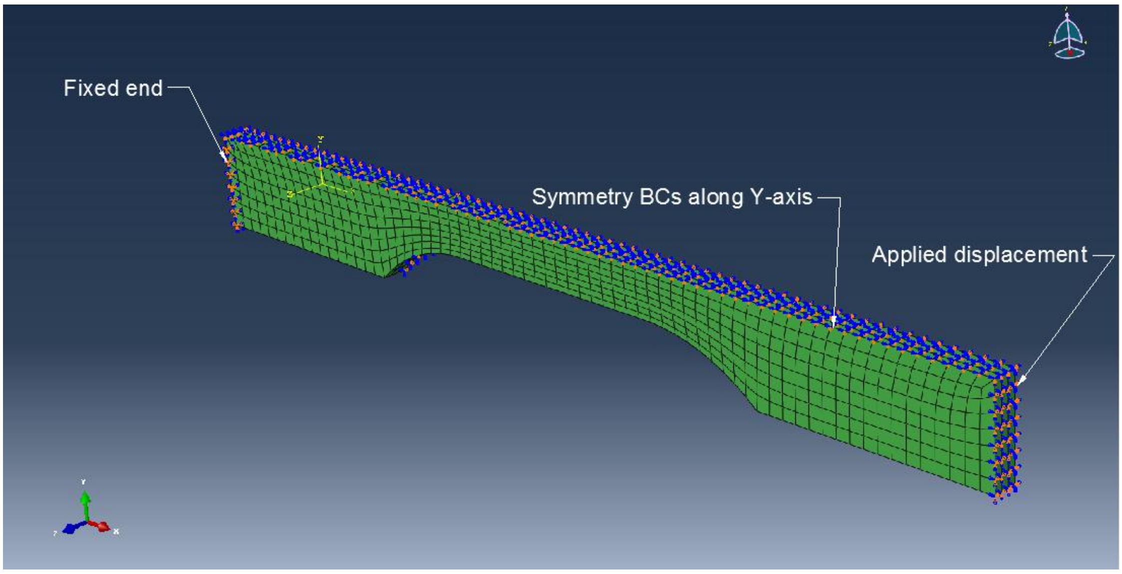

Figure 5.16: 3-D modelling of steel plate coupon.

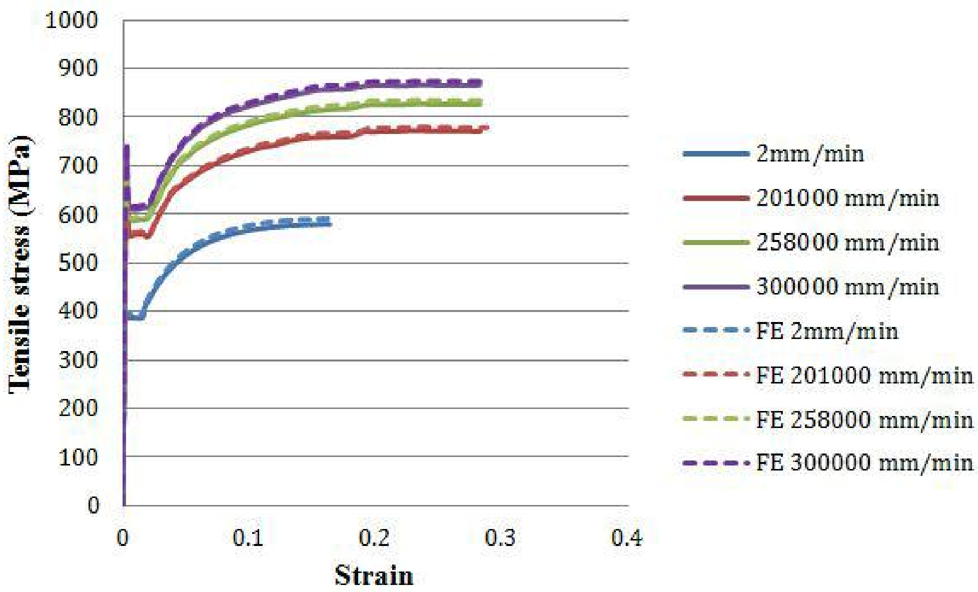

Figure 5.17: Comparison of the stress-strain curves for analytical and experimental results under four different loading rates

5.7 NUMERICAL INVESTIGATION OF CFRP-BONDED STEEL PLATES UNDER QUASI-STATIC LOADING.

To prove the efficiency of FE modelling of CFRP-steel double strap joints using ABAQUS/implicit, a total of 44 models were built in ABAQUS in order to numerically investigate the effect of CFRP modulus and CFRP section on the bond characteristics between CFRP and steel in double strap joint specimens. These models had the same geometry as the actual specimens, as explained in Chapter Three. These 44 models included 11 models of joints with low modulus CFRP and 20 mm CFRP width, 11 models of joints with low modulus CFRP and 10 mm CFRP width, 11 models of joints with normal modulus CFRP and 20 mm CFRP width, and finally 11 models of joints with ultra-high modulus CFRP and 20 mm CFRP width. Different bond lengths were used, from 30mm to 130mm. The results obtained from these models were ultimate joint strength, strain distribution along the bond, failure patterns and effective bond length. All the results were compared with the corresponding results obtained from the experimental investigation.

5.7.1: Comparison of ultimate bond strength based on numerical analysis and experimental results

As mentioned above, four different series were simulated using ABAQUS/implicit to model the CFRP-steel double strap joints under quasi-static loading. The ultimate joint capacities for both the experimental tests and the analytical models of CFRP-steel double-strap joints are summarised in Tables 5.2-5.5.The same parameters as those used in the experimental tests were used in the FE analysis with quasi-static loading (2 mm/min) and various bond lengths from 30mm to 130mm were used for all series. As shown in Table 5.3, the experimental results for specimens with low modulus CFRP and 10mm CFRP section, show inconsistency in the maximum joint strength for each bond length. However, for the FE models, a constant increase in the bond strength is shown. This difference in results can be attributed to the fact that the small bond is sensitive to any movement of the composite material, whereas this sensitivity is not considered in FE analysis.

Table 5.2: Comparison of experimental test and FEA for specimens with low modulus CFRP and 20mm wide CFRP

Specimen label	L1	L2	L2 –L1	Maximum load capacity (kN)		$\frac{P_{FE}}{P_{EX}}$
				P_{FE}	Ave P_{EX}	
S3-30	30	100	70	30.1	41.0	0.73
S3-40	40	100	60	40.1	50.7	0.79
S3-50	50	100	50	51.2	60.0	0.85
S3-60	60	100	40	59.2	69.1	0.85
S3-70	70	110	40	68.4	76.5	0.89
S3-80	80	120	40	79.2	86.8	0.91
S3-90	90	130	40	88.1	93.6	0.85
S3-100	100	140	40	94	100.3	0.93
S3-110	110	150	40	100.4	108.0	0.92
S3-120	120	160	40	100.8	108.7	0.92
S3-130	130	170	40	101.	109.1	0.92

Table 5.3: Comparison of experimental tests and FEA for specimens with low modulus CFRP and 10mm wide CFRP

Spec. label	L_1	L_2	L_2-L_1	Maximum load capacity (kN) ($\boldsymbol{P_{EX}}$)							$\boldsymbol{P_{FE}}$
				S1	S2	S3	S4	S5	S6	Ave	
S2-30	30	100	70	15.6	19	15.2	14	13.2	16.1	15.52	15.4
S2-40	40	100	60	23.5	21.2	18	20.4	20.8	18.7	20.43	20.7
S2-50	50	100	50	27.8	24.2	23.1	24.9	28	26.2	25.70	26.3
S2-60	60	100	40	29.3	27	26.4	31	24.1	28	27.63	32.1
S2-70	70	110	40	40.9	25.6	28.4	33.2	30.1	37.5	32.62	34
S2-80	80	120	40	34	33.8	30	26.7	31.1	27	30.43	39.1
S2-90	90	130	40	24	24.5	40.7	31.7	35.8	29.9	31.10	42.4
S2-100	100	140	40	34.9	36	30.4	35.8	38.2	25.6	33.48	42.8
S2-110	110	150	40	30.3	33.3	35	37.6	39.5	34	34.95	51.2
S2-120	120	160	40	29.7	31.5	26	30.3	34.8	39.5	31.97	51.6
S2-130	130	170	40	35.3	37.4	39.7	32.1	28.5	37.2	35.03	51.7

Table 5.4: Comparison of experimental test results and FEA results for specimens with normal modulus CFRP and 20mm wide CFRP

Specimen label	L_1	L_2	$L_2 - L_1$	Maximum load capacity (kN)		$\frac{P_{FE}}{P_{EX}}$
				P_{FE}	Ave P_{EX}	
NS-30	30	100	70	30.8	41.9	0.73
NS-40	40	100	60	40.1	51.7	0.77
NS-50	50	100	50	50.4	60.7	0.83
NS-60	60	100	40	59.4	69.8	0.85
NS-70	70	110	40	67.2	75	0.89
NS-80	80	120	40	80	87.4	0.91
NS-90	90	130	40	89.2	94.2	0.94
NS-100	100	140	40	96.3	101.3	0.88
NS-110	110	150	40	101.6	108.3	0.93
NS-120	120	160	40	100.8	108.5	0.92
NS-130	130	170	40	101.2	109.2	0.92

Table 5.5: Comparison of experimental test results and FEA results for specimens with ultra-high modulus CFRP and 20mm wide CFRP

Specimen label	L_1	L_2	$L_2 - L_1$	Maximum load capacity (kN)		$\frac{P_{FE}}{P_{EX}}$
				P_{FE}	Ave P_{EX}	
UHS-30	30	100	70	30.15	31.7	0.95
UHS-40	40	100	60	40.4	43.3	0.93
UHS-50	50	100	50	53.4	54.4	0.98
UHS-60	60	100	40	63.7	64.1	0.99
UHS-70	70	110	40	71.6	73.2	0.98
UHS-80	80	120	40	71.9	73.1	0.98
UHS-90	90	130	40	71.4	73.	0.98
UHS-100	100	140	40	72.6	73.2	0.99
UHS-110	110	150	40	72.4	73.4	1.67
UHS-120	120	160	40	72.1	73.3	0.98
UHS-130	130	170	40	72.3	73.2	0.99

The tables above show that the ratio of ($\frac{P_{FE}}{P_{EX}}$) has an average starting value of 0.77 for the first two bond lengths, then it starts to increase and ranges between 0.85 to 0.94 for the remaining bond lengths. This range of the ultimate joint capacity ratio is considered to be acceptable.

5.7.2 Comparison of the effective bond length values based on numerical and experimental results

The effective bond length of the CFRP-steel double-strap joints was experimentally studied with different CFRPs, and also investigated numerically in this project. Figures 5.18-5.120 illustrate comparisons between the experimental investigation and numerical modelling results for the three types of CFRP. It is obvious from both investigations that changing from low to normal modulus CFRP has no effect on the effective bond length; the effective bond length is 110mm, which is similar to the FEA results. However, a significant impact on the effective bond length is shown for specimens with ultra-high modulus CFRP. For both the numerical simulation and experimental results, the effective bond length for specimens with ultra-high modulus CFRP was found to be 70 mm (see Figure 5.20).

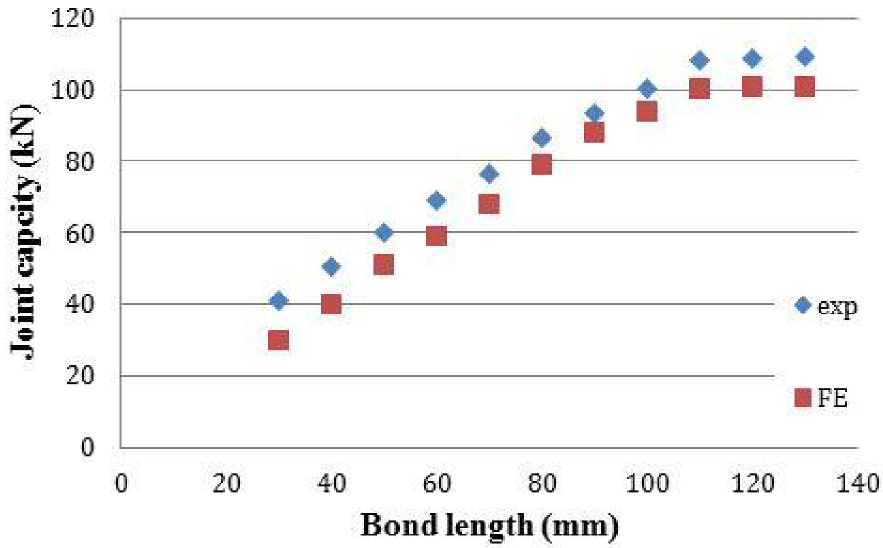

Figure 5.18: Joint capacity vs. bond length for specimens with 20 mm wide CFRP and low modulus CFRP

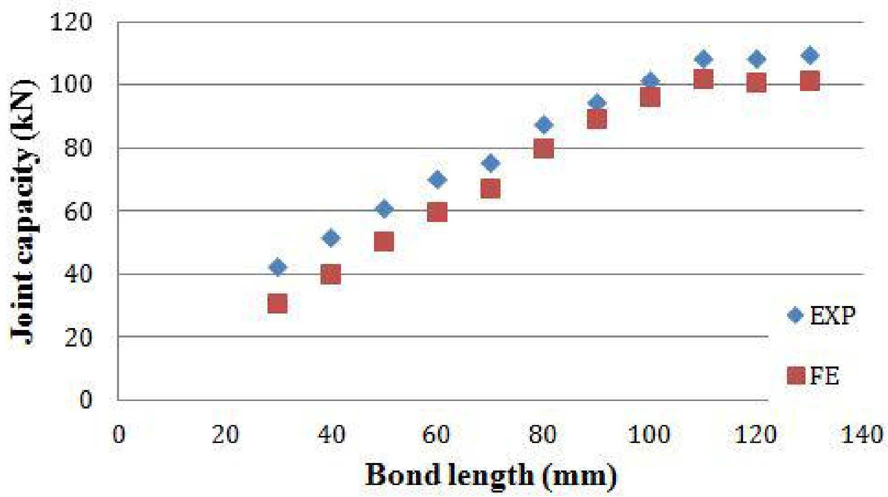

Figure 5.19: Joint capacity vs. bond length for specimens with 20 mm wide CFRP and normal modulus CFRP

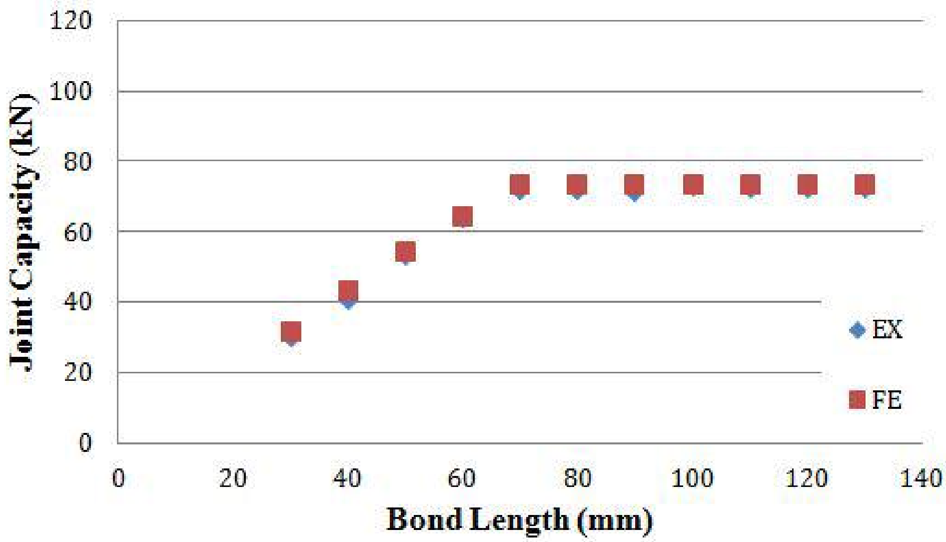

Figure 5.20: Joint capacity vs. bond length for specimens with 20mm wide CFRP and ultra-high modulus CFRP

No comparison of joints with small CFRP size was made; it is difficult to obtain experimentally the effective bond length for this type of joint, as the small size of CFRP has negative effects on the results, which show some fluctuation in the maximum joint capacity for the same bond length.

5.7.3 Comparison of numerical and experimental strain distribution along the bond

Based on the strain distribution data along the bond for both the experimental tests and the numerical simulations, and for all types of joints (with low, normal and ultra-high CFRP modulus), comparisons of strain distribution along the bond length for all joints are made at different load levels as shown in Figures 5.21-5.23. The experimental data were obtained using image correlation photogrammetry, which gives strain results at any point along the bond, and the data were taken for each 10mm distance, starting from the joint to the shorter end. In the FE simulation, the strain data were taken from locations corresponding to the experimental data locations.

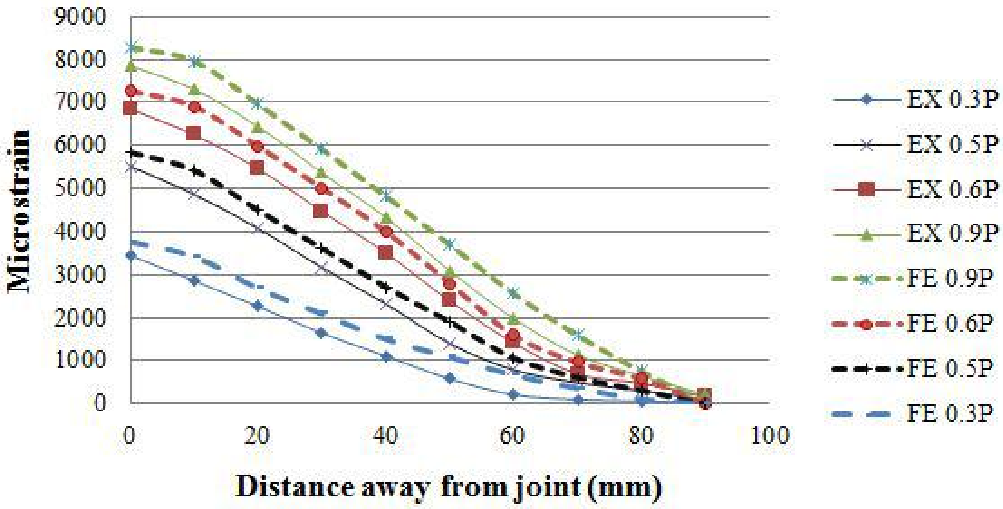

Figure 5.21: Strain distribution for specimens with low modulus CFRP.

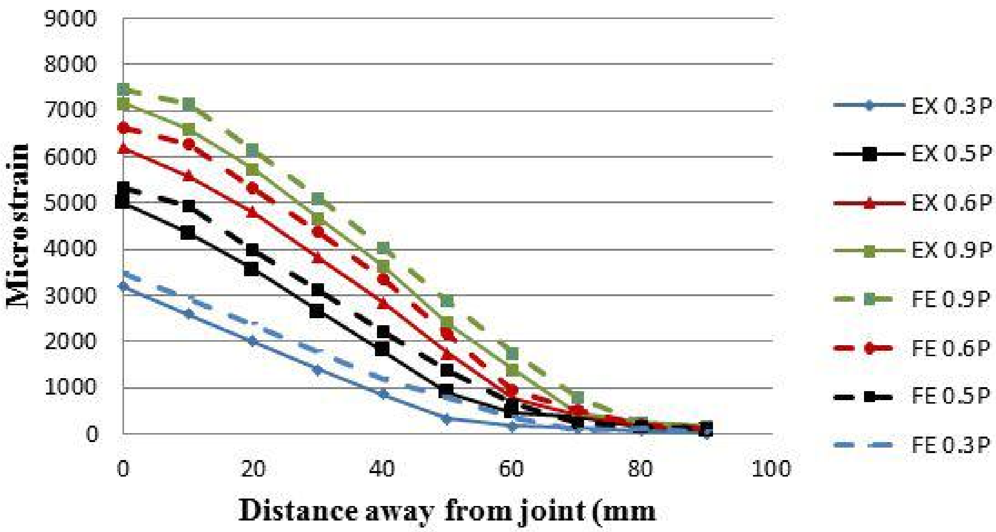

Figure 5.22: Strain distribution for specimens with normal modulus CFRP.

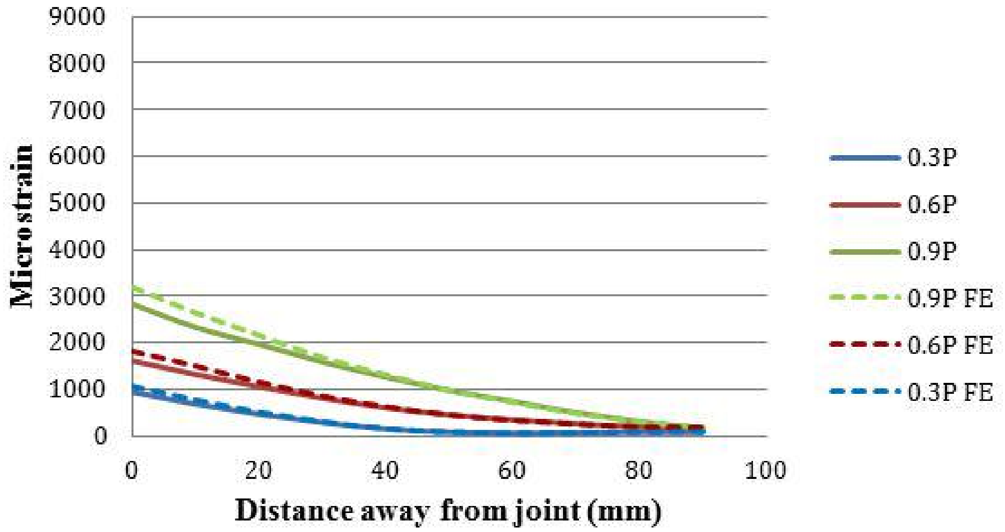

Figure 5.23: Strain distribution for specimens with ultra-high modulus CFRP.

From the figures above, it is obvious that FE models are able to simulate the strain distribution along the bond length, and good agreement in strain results is shown for the three types of joints under quasi-static loading with the loading rate of 2 mm/min. The same trend along the bond was shown for both the numerical analysis and experimental results.

5.7.4 Comparison of the numerical and experimental failure modes for CFRP-steel double strap joints

Based on the experimental failure patterns, there were some differences in failure mechanism in the four different series, as mentioned earlier in this chapter. For the current test program, the failure modes were varied for the four series, and the differences related to the CFRP properties used. For Series One, which had low modulus CFRP and 20mm wide CFRP, the failure mode was found to be mixed between steel-adhesive debonding and adhesive layer failure for bond lengths less than the effective bond length. This failure is clearly detected in FE modelling, as shown in Figure 5.24. An almost similar numerical failure mode was observed for specimens with normal modulus CFRP. For series with low modulus CFRP and 10mm CFRP width, the experimental failure mode was FRP delamination, while steel-adhesive debonding was detected in the numerical simulation, as shown in Figure 5.25. Obtaining a different failure mode from FE models for joints with low modulus CFRP and 10mm CFRP width, is further proof that the results from experimental tests are unreliable. Due to the fact that the effect of small application errors could lead to some eccentricities in the load transfer from the steel to laminates while the FE analysis assumes perfect alignments, no reliable comparisons between the experimental and FE results is possible.

For joints with low modulus CFRP and 20mm width, the failure mode is different when the bond length reaches close to the effective bond length and becomes completely steel-adhesive debonding. The outcomes from FEA for the above three series are very close to the experimental results, and de-bonding failure is very clear. However, adhesive failure is not shown clearly, as adhesive failure occurs at a certain distance from the joint.

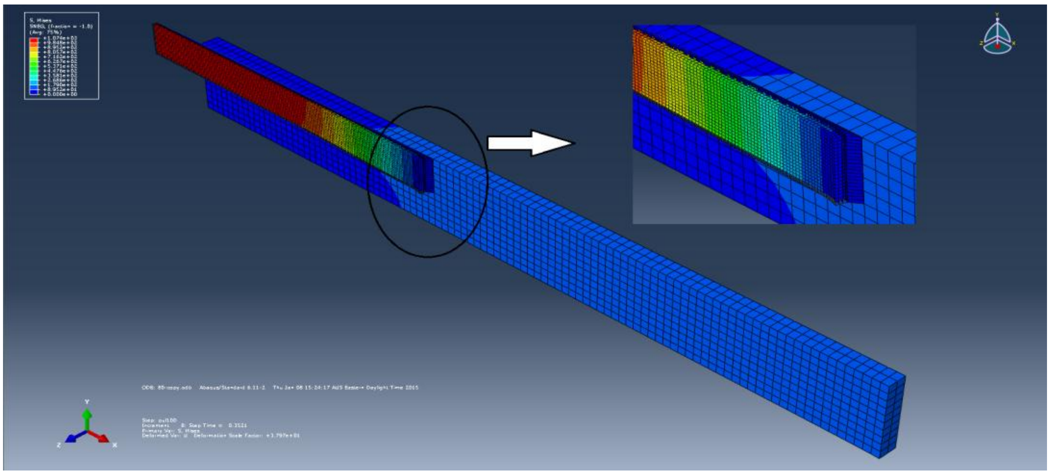

Figure 5.24: Steel-adhesive debonding of specimens with low and normal modulus CFRP and 20mm CFRP width

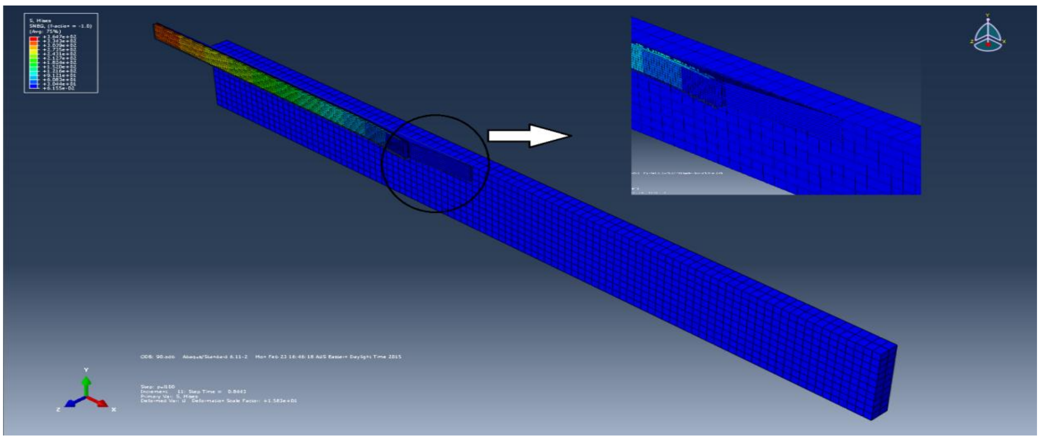

Figure 5.25: Steel-adhesive debonding of specimens with low modulus CFRP and 10mm CFRP width

For specimens with ultra-high modulus CFRP, the failure mode was completely different from that of the previous joints (Series 1, 2 and 3). The failure mode for the last series (ultra-high modulus CFRP-steel double strap joints) was shown to be FRP delamination for specimens with bond lengths below the effective bond length, and FRP rupture for specimens beyond the effective bond length. Exactly the same failure patterns were observed from FEA,. Figures 5.26 and 5.27 show the failure modes of this type of joint.

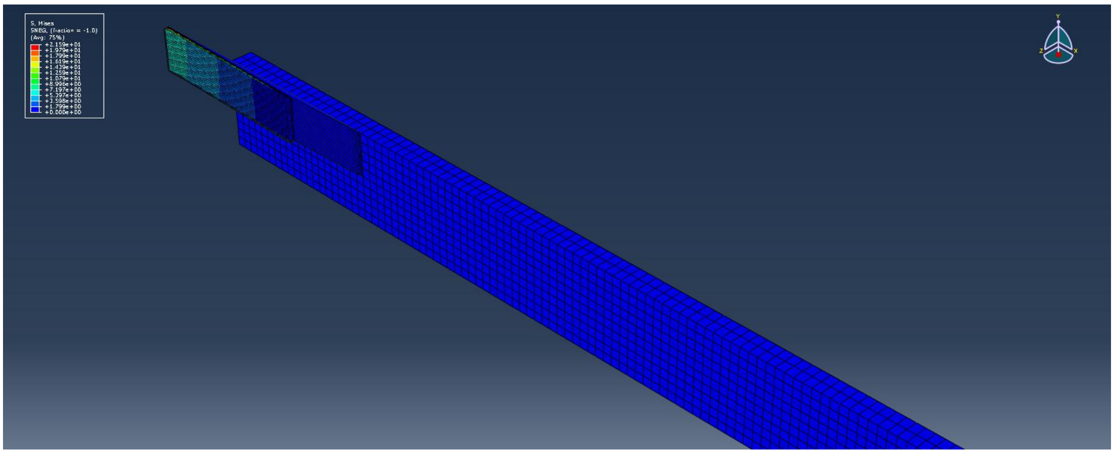

Figure 5.26: FRP delamination of specimens with ultra-high modulus CFRP and bond lengths below the effective bond length

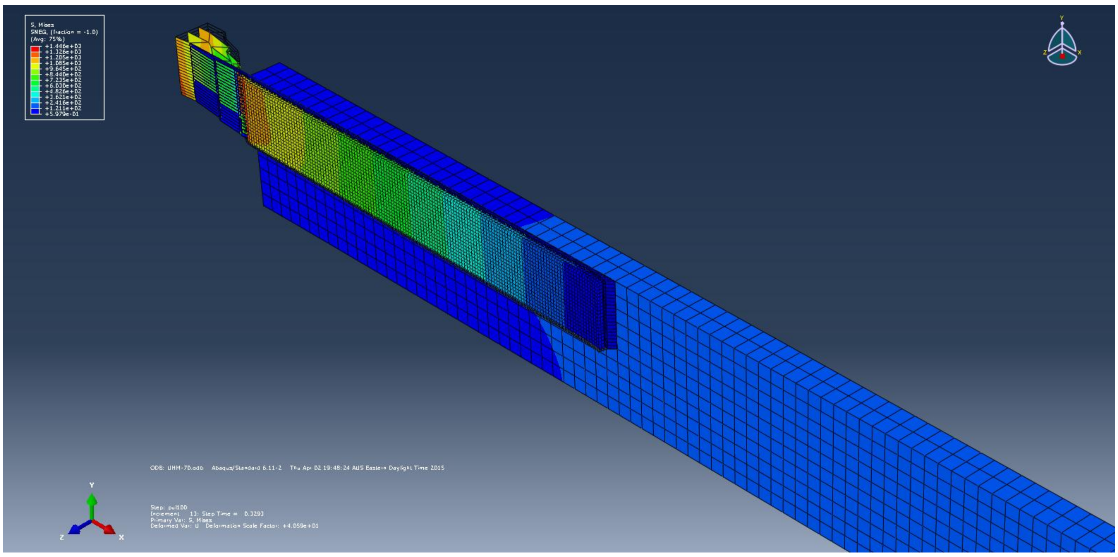

Figure 5.27: FRP rupture of specimens with ultra-high modulus CFRP and bond lengths below the effective bond length

5.8 NUMERICAL INVESTIGATION OF CFRP-BONDED STEEL PLATES UNDER IMPACT LOADING.

A total of 72 CFRP-steel double strap joint models were numerically developed using ABAQUS/explicit to investigate the effect of high loading rates on the bond characteristics between steel and different CFRP laminates. The loading rates used in this simulation were the same as those used in the experimental tests: 201×10^3, 258×10^3 and 300×10^3 mm/min. The 72 models included 24 models for each type of joint. Each set of joints was modelled under the three loading rates summarised earlier in Table 5.1, and each loading rate had 8 models of bond length ranging from 40 mm to 110mm. The results obtained from these models were the ultimate joint strength, strain distribution along the bond, failure patterns and effective bond length. All the results were compared with the corresponding results obtained from the experimental investigation.

5.8.1: Comparison of the ultimate bond strength based on numerical analysis and experimental results

All types of CFRP-steel double-strap joints were simulated in ABAQUS/explicit, in order to numerically investigate the effect of high loading rates on the bond strength between CFRP and steel. Tables 5.6 to 5.11 show comparisons of the ultimate joint capacities based on the results of the numerical investigation and experimental tests on the CFRP-steel double strap joints, with different CFRPs and different loading rates. For models with ultra-high modulus CFRP, three loading rates were used in the simulation, whereas only two loading rates were applied to specimens in the experimental investigation.

Table 5.6: Dynamic results for load rate of 201×10^3 mm/min

Specimen label for F_3	Specimen label for F_4	L_1 (mm)	L_2 (mm)	Ave $F_{3\ Ex}$	$F_{3\ FE}$	$\frac{F_{3FE}}{F_{3EX}}$	Ave $F_{4\ EX}$	$F_{4\ FE}$	$\frac{F_{4FE}}{F_{4EX}}$
LS-40	NS-40	40	100	85.3	93.3	1.09	89.7	94.5	1.05
LS-50	NS-50	50	100	100.3	105.4	1.05	101.7	106.3	1.07
LS-60	NS-60	60	100	106.6	111.6	1.05	108.4	112.3	1.04
LS-70	NS-70	70	110	113.9	119.3	1.05	115.0	121.5	1.06
LS-80	NS-80	80	120	120.3	126.1	1.05	122.9	128.3	1.04
LS-90	NS-90	90	130	131.1	134.9	1.03	130	135.1	1.04
LS-100	NS-100	100	140	130.3	134.9	1.04	131.7	135.1	1.03
LS-110	NS-110	110	150	131.2	134.9	1.03	131	135.1	1.03

F_3: The ultimate bond strength for low modulus CFRP-steel joints under load rate of 201×10^3 mm/min,
F_4: The ultimate bond strength for normal modulus CFRP-steel joints under load rate of 201×10^3 mm/min

Table 5.7: Dynamic results for load rate of 258×10^3 mm/min

Specimen label for F_5	Specimen label for F_6	L_1 (mm)	L_2 (mm)	Ave $F_{5\ EX}$	$F_{5\ FE}$	$\frac{F_{5FE}}{F_{5EX}}$	Ave $F_{6\ EX}$	$F_{6\ FE}$	$\frac{F_{6FE}}{F_{6EX}}$
LS-40	NS-40	40	100	102.6	107.1	1.04	105.4	110.1	1.04
LS-50	NS-50	50	100	116.1	119.9	1.03	117.6	123.5	1.05
LS-60	NS-60	60	100	123.6	130.4	1.05	125.3	123.4	0.98
LS-70	NS-70	70	110	133.8	137.5	1.03	131.6	138.6	1.05
LS-80	NS-80	80	120	139.5	144.4	1.03	138.7	146.3	1.05
LS-90	NS-90	90	130	146.3	149.8	1.02	145.7	150.2	1.03
LS-100	NS-100	100	140	146.9	149.8	1.02	146.6	150.3	1.02
LS-110	NS-110	110	150	147.1	149.8	1.02	146.2	150.2	1.02

F_5: The ultimate bond strength for low modulus CFRP-steel joints under load rate of 258×10^3 mm/min,
F_6: The ultimate bond strength for normal modulus CFRP-steel joints under load rate of 258×10^3 mm/min.

Table 5.8: Dynamic results for load rate of 300×10^3 mm/min.

Specimen label for F_7	Specimen label for F_8	L_1 (mm)	L_2 (mm)	Ave $F_{7\,EX}$	$F_{7\,FE}$	$\frac{F_{7FE}}{F_{7EX}}$	Ave $F_{8\,EX}$	$F_{8\,FE}$	$\frac{F_{8FE}}{F_{8EX}}$
LS-40	NS-40	40	100	103.6	109.4	1.06	105.8	111.3	1.05
LS-50	NS-50	50	100	119.3	122.1	1.02	121.1	124.2	1.03
LS-60	NS-60	60	100	128.1	131.4	1.03	129.9	133.6	1.03
LS-70	NS-70	70	110	135.6	138.7	1.02	136.3	140.1	1.03
LS-80	NS-80	80	120	141.3	145.4	1.03	142	147.3	1.04
LS-90	NS-90	90	130	146.9	151.2	1.03	148.2	152.6	1.03
LS-100	NS-100	100	140	146.4	150.9	1.03	147.6	152.5	1.03
LS-110	NS-110	110	150	146.2	151.1	1.03	148.1	152.5	1.03

F_7: The ultimate bond strength for low modulus CFRP-steel joints under load rate of 300×10^3 mm/min,

F_8: The ultimate bond strength for normal modulus CFRP-steel joints under load rate of 300×10^3 mm/min.

Table 5.9: Dynamic results for UHM CFRP-steel double strap joints under load rate of 201×10^3 mm/min

Specimen label F_9	L_1 (mm)	L_2 (mm)	Ave $F_{9\,EX}$	$F_{9\,FE}$	$\frac{F_{9FE}}{F_{9EX}}$
UHMS-20	20	100	35.5	37.7	1.06
UHMS-30	30	100	45.3	47.6	1.05
UHMS-40	40	100	45.5	47.9	1.05
UHMS-50	50	100	45.1	47.6	1.05
UHMS-60	60	100	45.7	47.6	1.04
UHMS-70	70	110	45.8	47.4	1.03
UHMS-80	80	120	45	47.6	1.05
UHMS-90	90	130	46	47.7	1.03
UHMS-100	100	140	45.6	47.7	1.04

F_9: The ultimate bond strength for ultra-high modulus CFRP-steel joints under load rate of 201×10^3 mm/min

Table 5.10: Dynamic results for UHM CFRP-steel double strap joints under load rate of 258×10^3 mm\min

Model name	L_1 (mm)	L_2 (mm)	$F_{10\,FE}$
UHMS-20	20	100	45.1
UHMS-30	30	100	57.4
UHMS-40	40	100	57.6
UHMS-50	50	100	57.5
UHMS-60	60	100	57.4
UHMS-70	70	110	57.4
UHMS-80	80	120	57.4
UHMS-90	90	130	57.5
UHMS-100	100	140	57.4

F_{10}: The ultimate bond strength for ultra-high modulus CFRP-steel joints under load rate of 258×10^3 mm/min

Table 5.11: Dynamic results for UHM CFRP-steel double strap joints under load rate of 300×10^3 mm/min

Specimen label F_4	L_1 (mm)	L_2 (mm)	Ave $F_{11\ EX}$	$F_{11\ FE}$	$\frac{F_{11FE}}{F_{11EX}}$
UHMS-20	20	100	44.2	45.9	1.03
UHMS-30	30	100	56.5	58.6	1.03
UHMS-40	40	100	56.4	58.7	1.04
UHMS-50	50	100	56.4	58.6	1.03
UHMS-60	60	100	56.9	58.6	1.02
UHMS-70	70	110	56.8	58.7	1.03
UHMS-80	80	120	56.4	58.8	1.04
UHMS-90	90	130	56.5	58.6	1.03
UHMS-100	100	140	57.1	58.6	1.02

F_{11}: The ultimate bond strength for ultra-high modulus CFRP-steel joints under load rate of 300×10^3 mm/min

As the tables above show, the ratio of ($\frac{F_{FE}}{F_{EX}}$) for all types of joint does not exceed 7%. For models with ultra-high modulus CFRP under the loading rate of 258×10^3 mm/min, the numerical bond strength results are very close to those for the loading rate of 300×10^3 mm/min, and these results match well those with low and normal modulus CFRP. Therefore, there is little difference in bond properties between the load rates of 258×10^3 mm/min and 300×10^3 mm/min.

5.8.2 Comparison of the effective bond length based on numerical and experimental results

The effective bond length of CFRP-steel double-strap joints was investigated numerically and experimentally for different types of CFRP and different load rates. The effective bond length can be defined as the bond length beyond which no further increase in joint capacity occurs. Figures 5.28-5.30 compare results of the experimental investigation and numerical modelling for the three types of CFRP. For all load rates, it is obvious from both investigations that changing from low to normal modulus CFRP has no effect on the effective bond length (similar to the behaviour noted in the quasi-static investigation). The effective bond length observed from the experimental and finite element results is 90mm. However, a significant effect on the effective bond length is shown for specimens with ultra-high modulus CFRP. Based on the numerical and experimental results, the effective bond length was found to be 30 mm (see Figure 5.30).

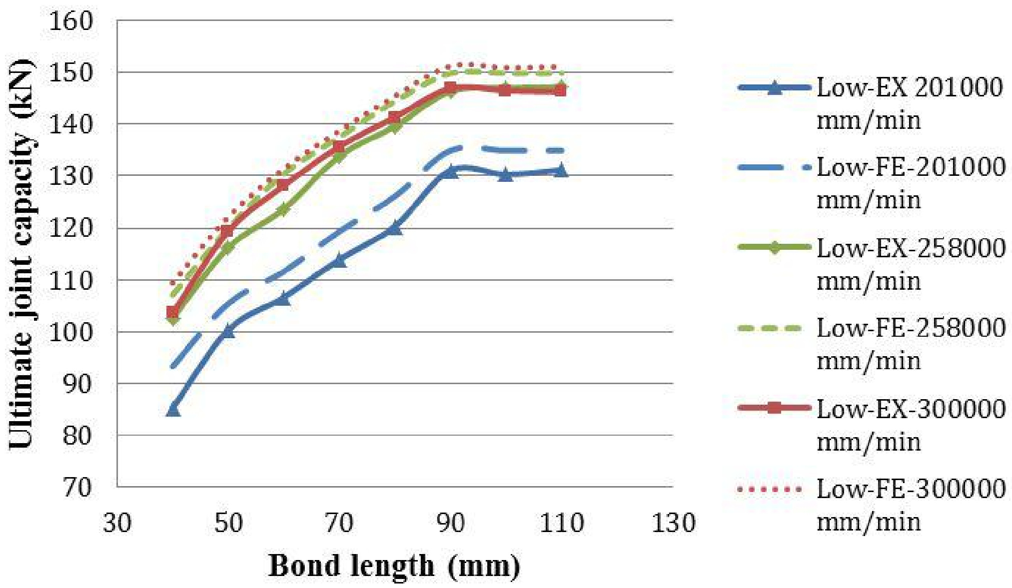

Figure 5.28: Ultimate bond strength vs. bond length for joints with low modulus CFRP under all impact loading rates

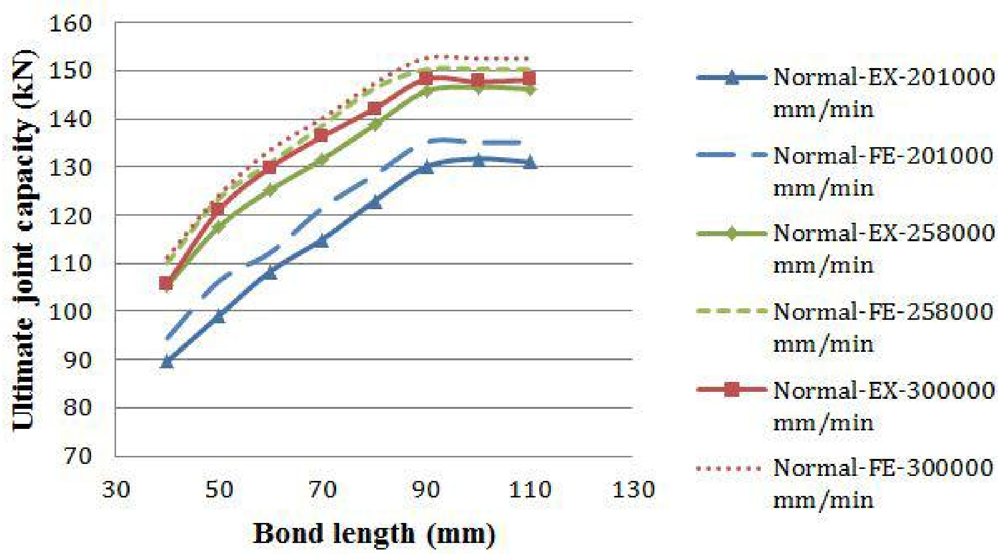

Figure 5.29: Ultimate bond strength vs. bond length for joints with normal modulus CFRP under all impact load rates

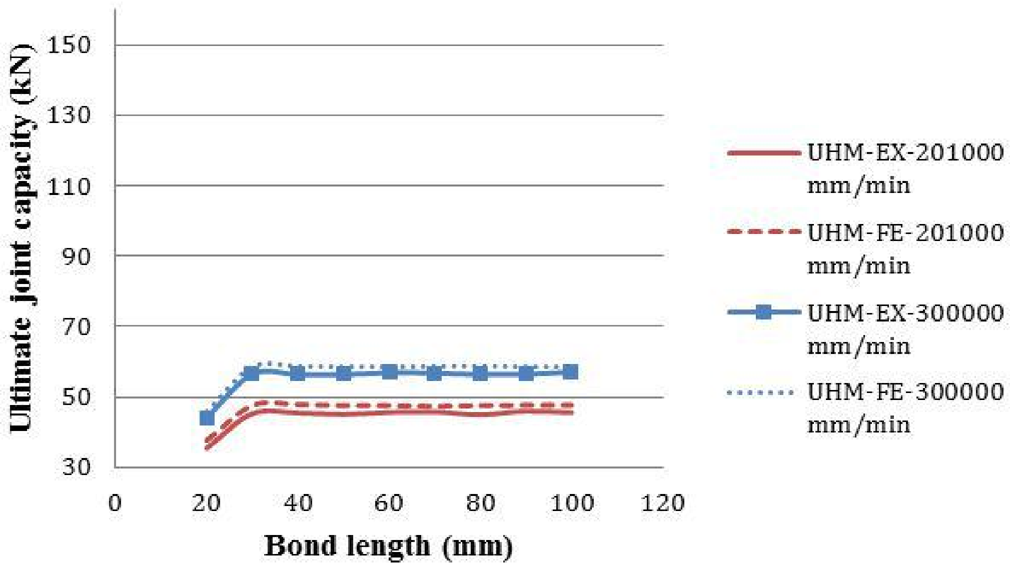

Figure 5.30: Ultimate bond strength vs. bond length for joints with ultra-high modulus CFRP under all impact load rates

From the figures above, the effective bond length and bond strength for joints with ultra-high modulus CFRP are less than those for the other two joints. This decrease in joint properties is due to the fact that the tensile strength and thickness of ultra-high modulus CFRP is lower than that in low and normal modulus CFRP. The same effective bond lengths were observed from both FEA and experimental tests.

5.8.3 Comparison of the numerical and experimental strain distribution along the bond

Based on the strain distribution data along the bond for both the experimental tests and the numerical simulations, for all types of joints (with low, normal and ultra-high modulus CFRP), comparisons were made at different load levels. Figures 5.31-5.33 compare the strain distributions along the bond for the three types of joints. The experimental data were obtained from strain gauges mounted on the top of the CFRP laminate along the bond length at a distance of 15mm between each other, starting from the joint to the shorter end. In the FE simulation, the strain data were taken from locations corresponding to the experimental data locations. Since the strain distributions along joints with low modulus CFRP were close to those with normal modulus CFRP, the figures below show the results of joints with low modulus CFRP only. The strain distributions obtained from FE analysis were in reasonable agreement with the experimental results for all loading rates.

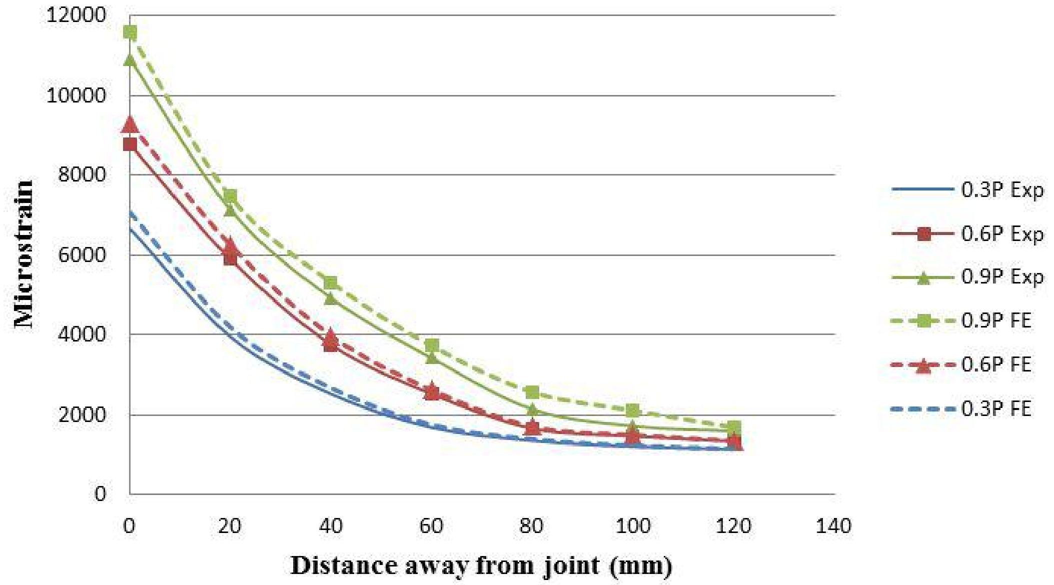

Figure 5.31: Strain distribution vs. bond length of low modulus CFRP-steel joints from experimental tests and FE models for loading rate of 201×10^3 mm/min

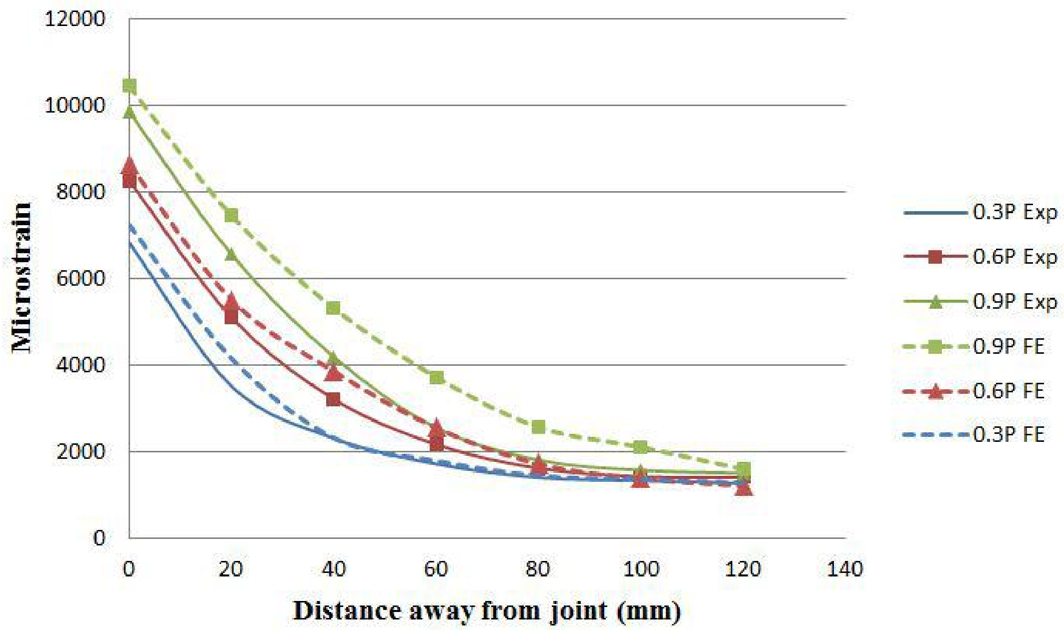

Figure 5.32: Strain distribution vs. bond length of low modulus CFRP-steel joints from experimental tests and FE models for loading rate of 258×10^3 mm/min

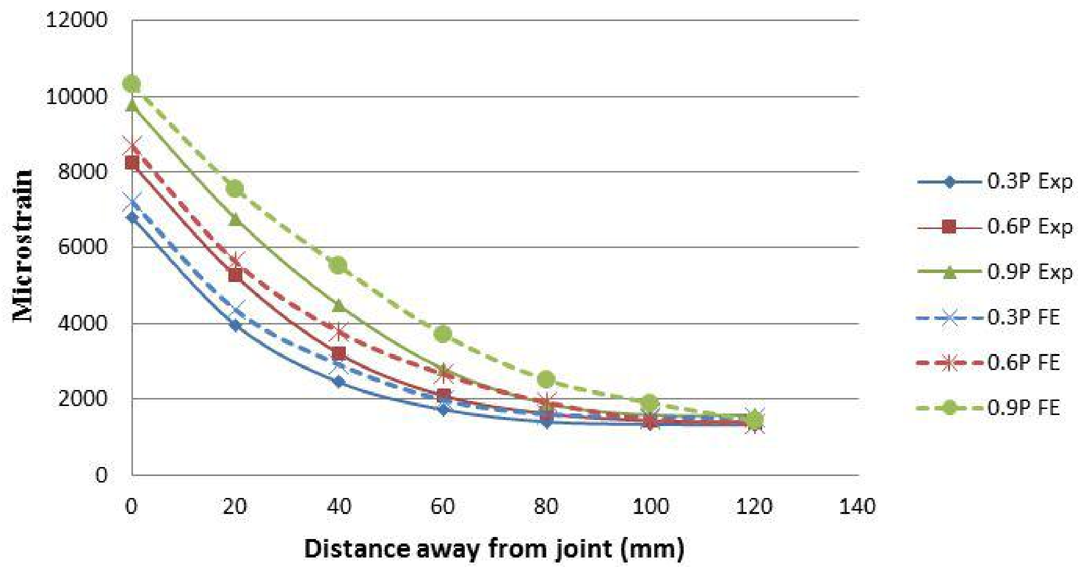

Figure 5.33: Strain distribution vs. bond length of low modulus CFRP-steel joints from experimental tests and FE models for loading rate of 300×10^3 mm/min

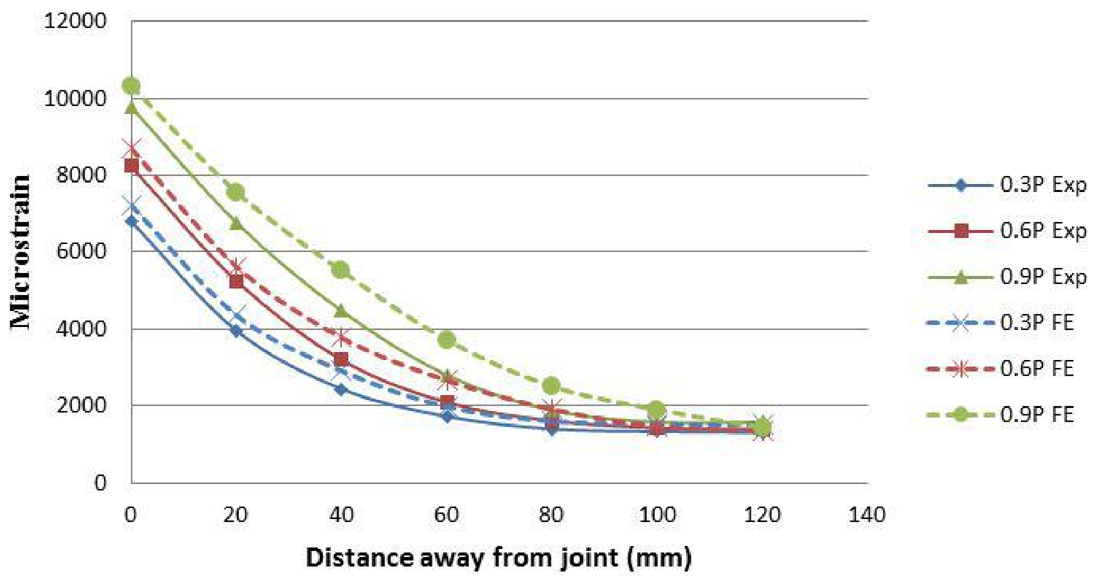

Figure 5.34: Strain distribution vs. bond length of normal modulus CFRP-steel joints from experimental tests and FE models for loading rate of 201×10^3 mm/min

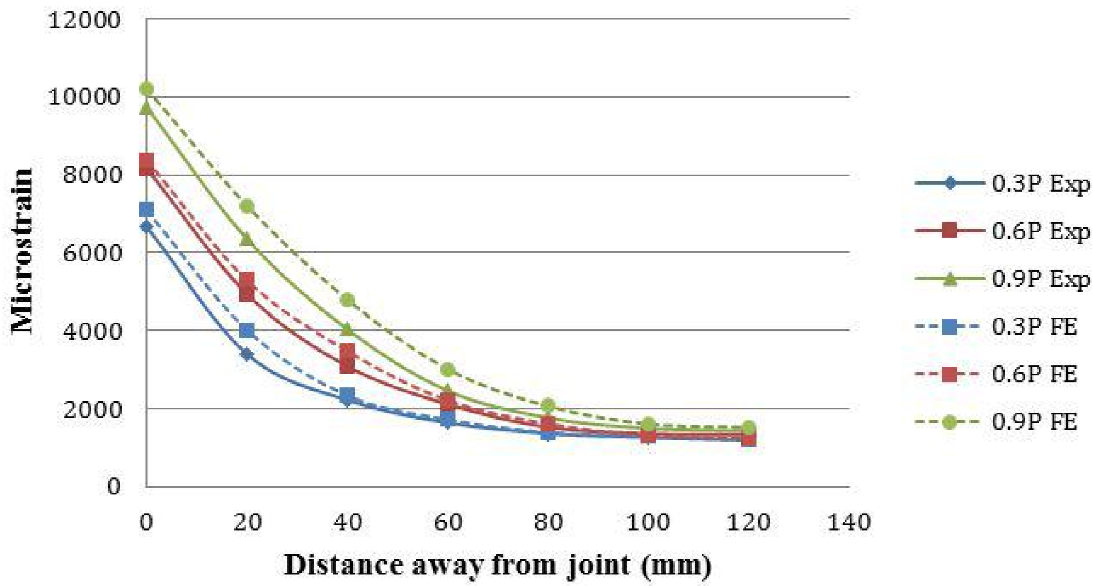

Figure 5.35: Strain distribution vs. bond length of normal modulus CFRP-steel joints from experimental tests and FE models for loading rate of 258×10^3 mm/min

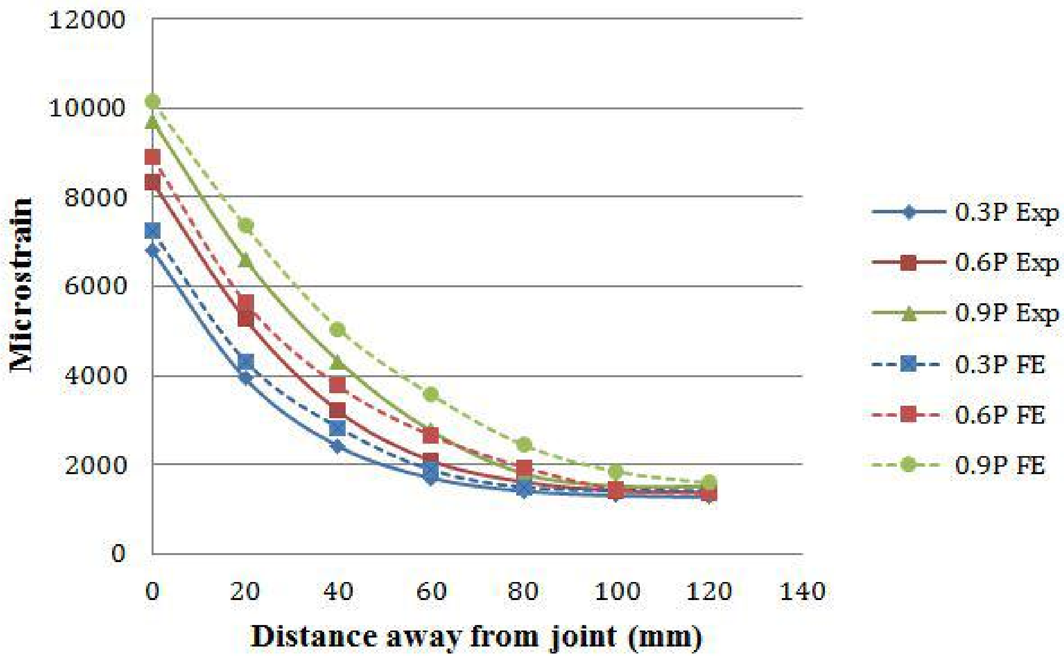

Figure 5.36: Strain distribution vs. bond length of normal modulus CFRP-steel joints from experimental tests and FE models for loading rate of 300×10^3 mm/min

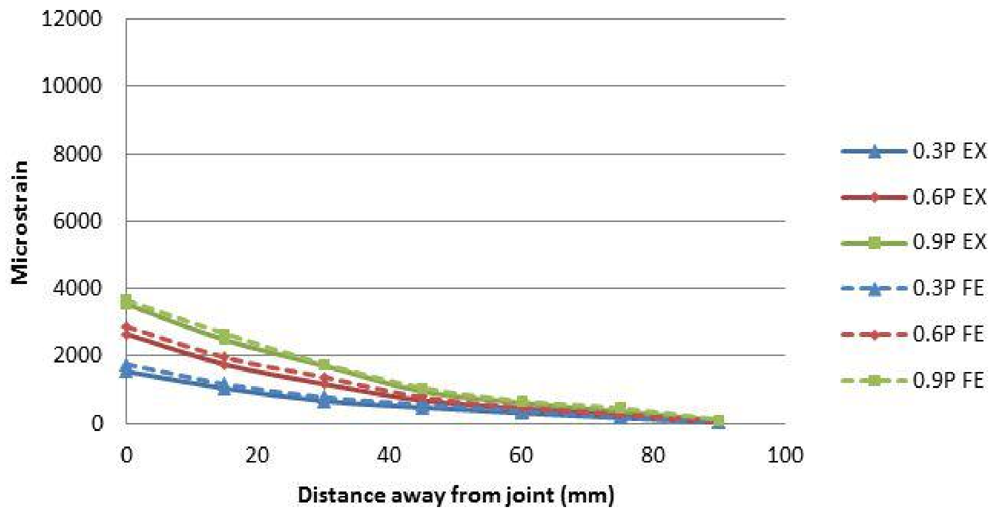

Figure 5.37: Strain distribution vs. bond length of UHM CFRP-steel joints from experimental tests and FE models for loading rate of 201×10^{3} mm\min

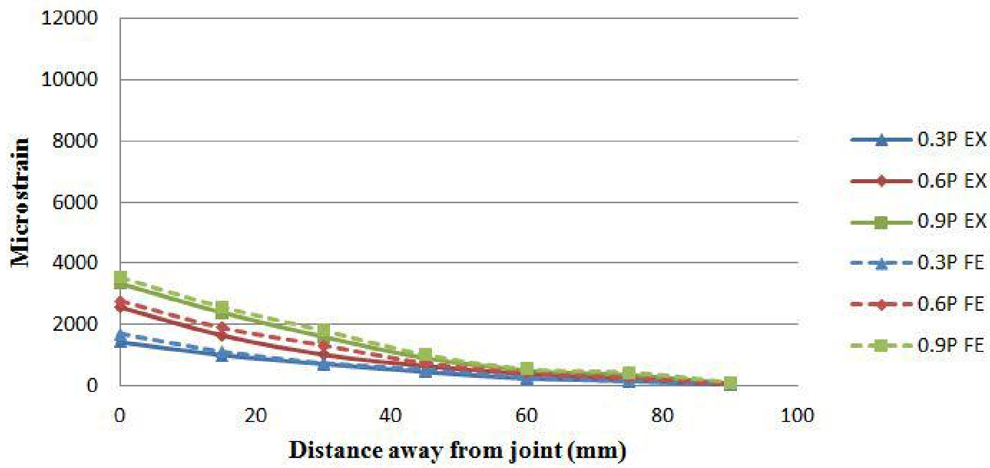

Figure 5.38: Strain distribution vs. bond length of UHM CFRP-steel joints from experimental tests and FE models for loading rate of 300×10^{3} mm/min

5.8.4 Comparison of numerical and experimental failure modes for CFRP-steel double strap joints

Based on the failure modes observed in the experimental tests, there were some changes in failure mechanism for the different joints. For joints with low modulus CFRP and loading rates of 201×10^{3} and 258×10^{3} mm/min, the failure mode was mixed between adhesive-steel debonding and adhesive layer failure. However, the same joints had different failure modes for the loading rate of 300×10^{3} mm/min, which were mixed between adhesive-steel debonding, adhesive layer failure and CFRP delamination for all bond lengths. FEA detected some of these failures under the different loading rates. The failure mode obtained from FE was debonding and some fibre delamination for models with low modulus CFRP at loading rates 201×10^3 and 258×10^3 mm/min, as shown in Figure 5.39.

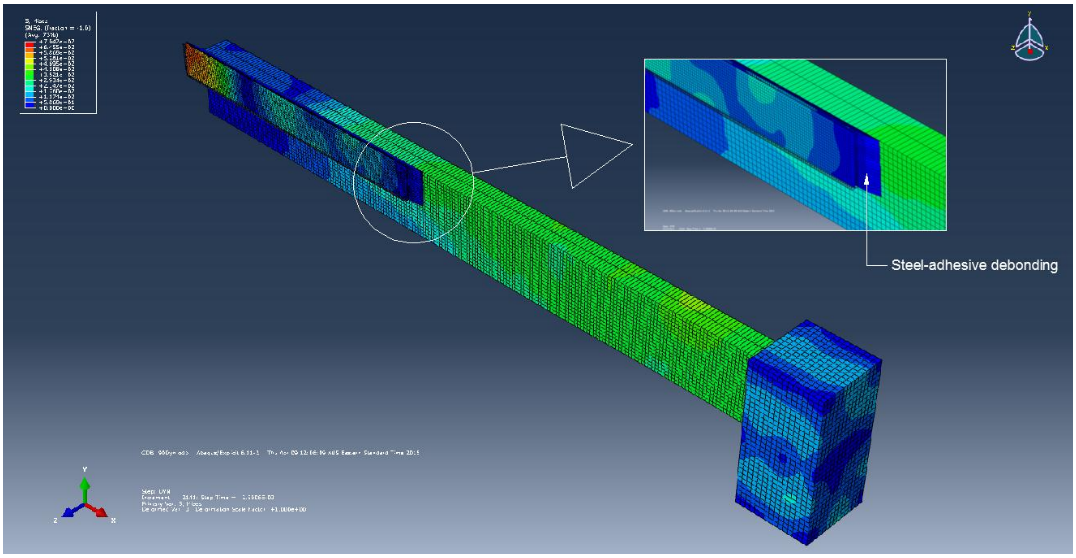

Figure 5.39: Steel-adhesive debonding of joints with low modulus CFRP at loading rates of 201×10^3 and 258×10^3 mm/min.

The failure mode observed from FEA of the same joint with the loading rate of 300×10^3 mm/min showed steel-adhesive debonding and some FRP delamination, as shown in Figure 5.40.

For models with normal modulus CFRP, the failure mode for all joints was typically the same as that shown for joints with low modulus CFRP.

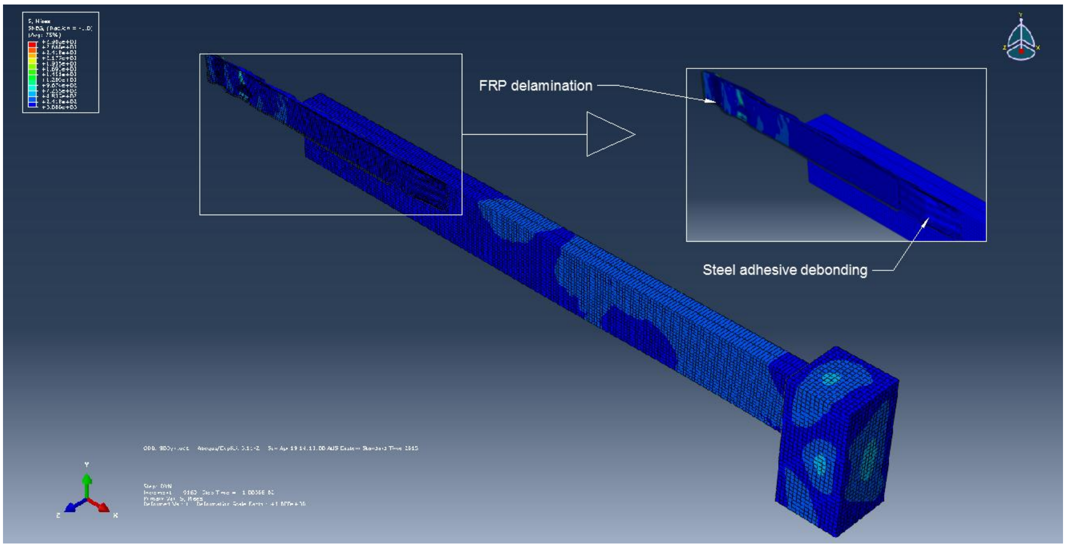

Figure 5.40: Steel-adhesive debonding and FRP delamination of joints with low modulus CFRP at loading rate of 300×10^3 mm/min.

The experimental investigation of the failure mode for joints with ultra-high modulus CFRP showed two failure modes, FRP delamination and adhesive failure, for all bond lengths and two loading rates 201×10^3 and 300×10^3mm/min. Consequently, the FE models showed very close failure patterns for the two loading rates. Figures 5.41 and 5.42 show the numerical failure modes.

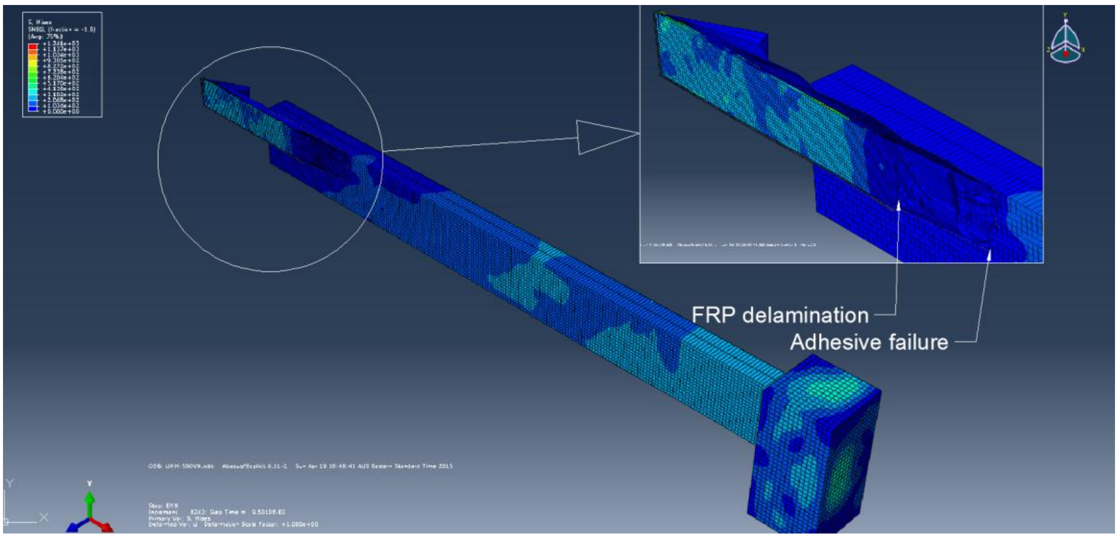

Figure 5.41: Adhesive failure and FRP delamination of joints with UHM CFRP at loading rate of 201×10^3 mm/min.

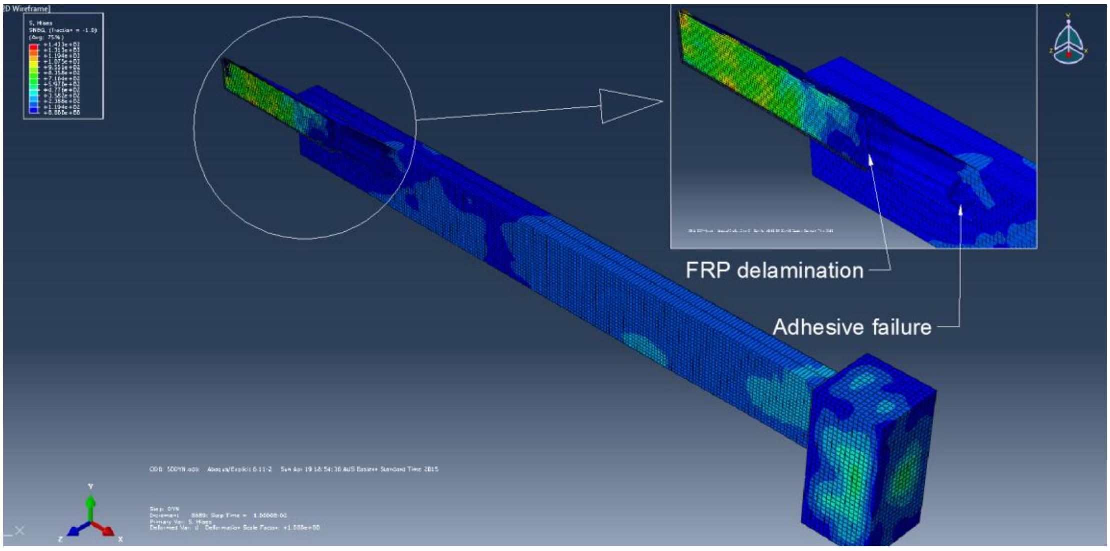

Figure 5.42: Adhesive failure and FRP delamination of joints with UHM CFRP at loading rate of 300×10^3 mm/min.

5.9 CONCLUSION

In this chapter, three-dimensional FEA was utilised to model different CFRP-steel double strap joints. Three types of CFRP were used in order to validate the ability of FEA to model these types of joints, using ABAQUS/implicit and ABAQUS/explicit for quasi-static and impact loadings respectively. All components of the double strap joint (steel, CFRP and adhesive) were simulated to numerically examine their mechanical properties. Steel was modelled as a 3-D stress element, however, CFRP was modelled using continuum shell elements and the adhesive was modelled using cohesive elements. The findings can be summarised as follows:

- FEA is able to simulate the components of CFRP-steel double strap joints under both quasi-static and dynamic loadings. The numerical analysis results of steel, CFRP and adhesive were consistent with those obtained by experimental investigation.
- ABAQUS/implicit and ABAQUS/explicit are both able to simulate CFRP-steel double strap joints under both quasi-static and dynamic loading, and for all different CFRP types. The predictions of bond strength, failure mode, effective bond length and strain distribution along the bond agreed reasonably well with those obtained from the experimental tests.

- There was good agreement on bond strength results between the numerical simulations and the experimental tests. The numerical analysis results showed slightly higher bond strengths than those from the actual tests, while for quasi-static testing the numerical simulation showed slightly lower bond strengths than those from the actual tests.
- The effective bond length was predicted very well for all types of joints, and under the different loading rates (2, 201×10^3, 258×10^3 and 300×10^3 mm/min).
- Failure modes for all types of joints were predicted well. However, some models could not show the adhesive failure because this happens in the middle of the joints, and the numerical simulations show the failure at the joints and the far ends.

The trend of strain distribution along the bond length was very close for all types of joints and under all loading rates. However, there were minor differences in strain values at the different load levels between the numerical simulation and experimental results. These differences are considered to be acceptable.

CHAPTER SIX A NEW FORMULATION OF CFRP-STEEL DOUBLE STRAP JOINTS USING GENETIC PROGRAMMING

6.1 INTRODUCTION

Genetic programming (GP) is an automated method based on algorithm methodology which is used to find a relationship among variables in sets of data. The concept of GP was originated from genetic algorithms (GAs) with more complexity, and was first proposed by Koza (1992). Cevik et al. (2010) reported an overview on the use of GP and the way to finalise the analysis and generate the equation. The architecture of the outcome model is mainly an expression tree (ET) which contains a number of chromosomes. Each chromosome has one of the input parameters and is associated with a constant variable. A number of ETs may exist for one model, and these are ETs linked together by one of the mathematical functions. An example of an EP with the corresponding features is shown in Figure 6.1.

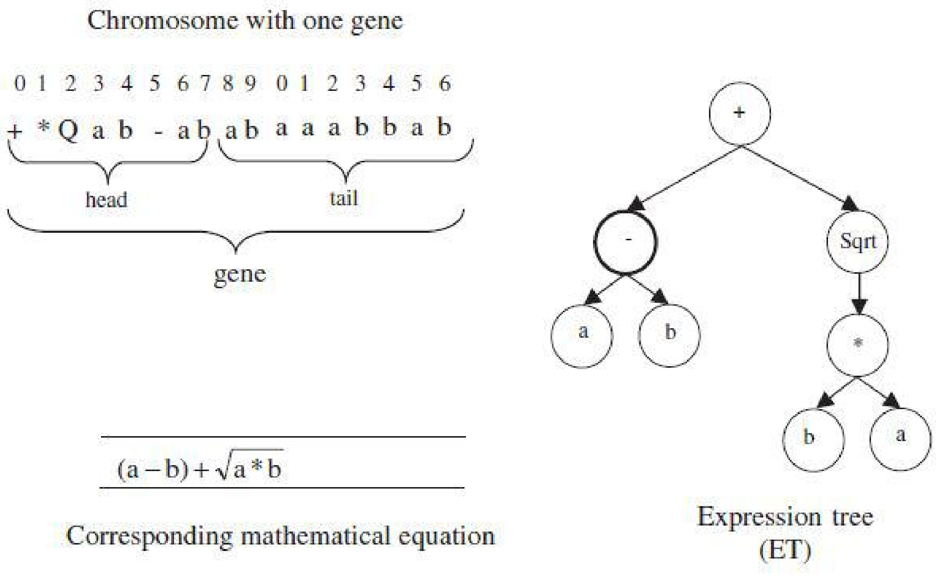

Figure 6.1: Expression tree with the corresponding chromosomes and equation (Kara, 2011).

As shown previously, a number of studies have focused on the bond characteristics between steel and CFRP using different parameters (Liu et al., 2005b; Pereira et al., 2011; Al-Mosawe et al., 2015; Liu et al., 2010; Fawzia et al., 2005; Jiao and Zhao, 2004; Fernando et al., 2009; Nguyen et al., 2013). Different parameters were used in previous research such as CFRP modulus, CFRP width, bond length, adhesive type, different environmental conditions and load rates. These parameters were used to illustrate the bond properties between CFRP and steel members. All studies have mainly focussed on evaluating the bond strength, effective bond length, strain distribution along the bond and failure mode. Although the design guidelines for FRP-strengthened concrete structures already exist, no design guidelines exist for FRP strengthening of steel structures. Therefore, more studies need to be conducted to have a full understanding of the bond behaviour between steel and CFRP with different parameters, including using CFRP laminates, high loading rates and different modulus CFRP. In order to simplify the strengthening procedure for CFRP to steel, this chapter proposes GP to generate an expression tree and equation model of the bond strength for CFRP-steel double strap joints. Bond length, CFRP modulus and loading rate are the three different parameters considered in this study to evaluate the bond strength mathematically.

GP modelling techniques for CFRP laminates bonded to steel joints do not exist yet. GP can be used to predict the properties of CFRP-steel double strap joints by providing sufficient and precise data. These data can be obtained from a large number of experimental tests or accurate numerical analysis. This chapter presents the prediction of bond strength for CFRP laminate bonded to steel joints under different parameters.

6.2 DATA COLLECTION

Three types of data sets were used in this model: training, validation and testing. The input data for these three sets were collected from previous studies on CFRP-steel double strap joints test reported in previous chapters. The input data are presented in different studies showing both experimental and numerical results. Three input parameters were used in modelling: CFRP modulus, CFRP bond length and loading rate. Three types of CFRP modulus were used: low modulus CFRP (165 GPa), normal modulus CFRP (210 GPa) and ultra-high modulus CFRP (450 GPa). The bond length was varied from 20 mm to 130 mm for each type CFRP-steel joint. However, the loading rates were 2mm/min as quasi-static loading, and a range of high loading rates was applied, from 201×10^3 mm/min to 300×10^3 mm/min. The data for three loading rates were taken from the experimental tests, these loading rates being 201×10^3, 258×10^3 and 300×10^3 mm/min. The other loading rates were chosen between the lower and higher impact load rates. The data of the other loading rates were based on FE analysis of this type of joint (Al-Mosawe et al., 2015; Al-Mosawe et al., 2015b; Al-Mosawe et al., 2015c). In total, 180 inputs were used including 153, 15 and 15 groups used for training, testing and validating the model, respectively.

6.3 GENETIC PROGRAMMING PARAMETERS

GeneXproTools 5.0 software was utilised to develop a predicted model of the ultimate bond strength of CFRP laminate-bonded steel joints. Figure 6.2 shows the ET based on the current GP modelling, and d_0, d_1 and d_2 represent CFRP bond length (L_f), load rate (v) and CFRP modulus (E_f), respectively. Basic mathematical functions were selected to produce the ET: addition, subtraction, multiplication, division, x2 and inverse. The software was able to choose the best selection of functions with best value of error. The model limitations and characteristics are shown in Table 6.1. The values of the parameters in this table are important to highlight the precision of the model's complexity. The most important parameters are the number of Sub-ETs, number of chromosomes and head size. The best way to calculate the values of these parameters was using single gene and obtaining the number of chromosomes and head size. A trial and error method was used, changing the value of the gene and monitoring the other values until an acceptable value of error was obtained. This method was used as there is currently no method available to determine the values of the parameters. The numbers of genes, chromosomes and head size used in this study were 3, 15 and 5 respectively. Figure 6.2 shows the ET obtained from the model, showing the basic functions linking the sub-ETs together. It was found that the selection of the linking function influences the precision of the results. By adopting different linking functions and monitoring the results, the multiplication function shows the most suitable function.

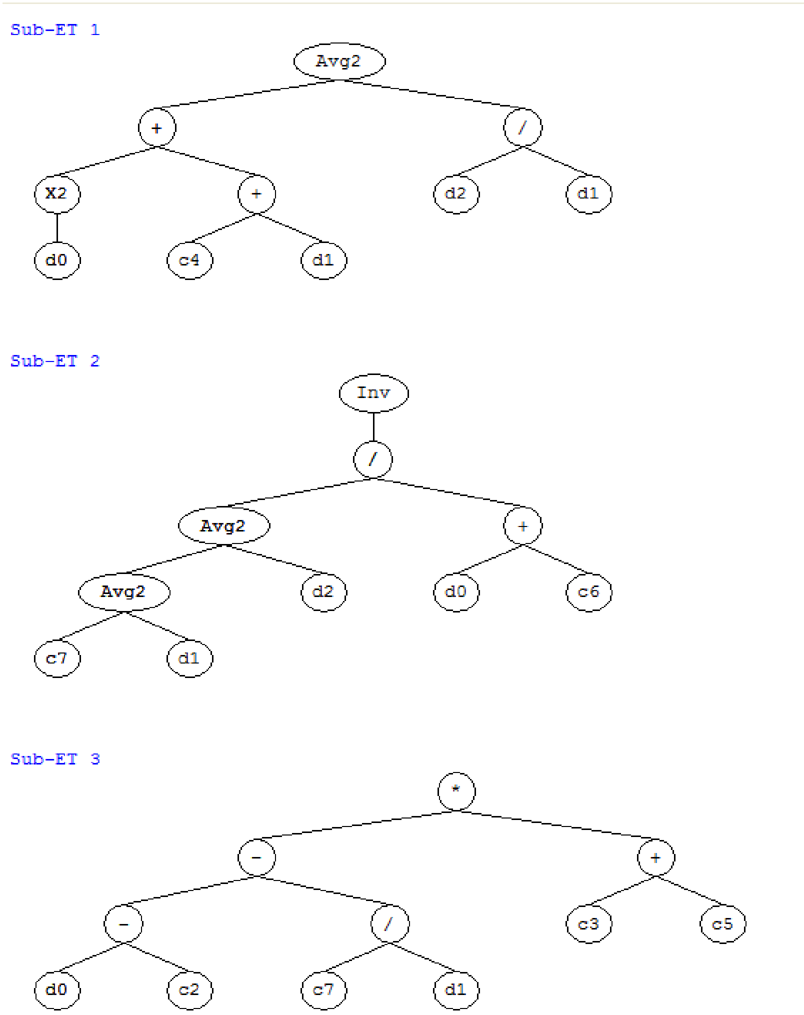

Figure 6.2: Expression tree of the GP model

Table 6.1: Parameters and characteristics of the model

Parameter	Value
Number of genes (Sub ETs)	3
Linking function	Multiplication
Number of variables used	7
Chromosomes	15
Head size	5
Lower bound	10
Upper bound	-10
Mutation	0.044
Fitness function	RRSE
Inversion	0.1
Transposition	0.1
Constants per gene	1

6.4 GENETIC PROGRAMMING RESULTS

The outcomes of the model can be presented as an equation as follows:

$$\tau = [0.5\,(d_o^2 + 26765.5 + d_1) + \frac{d_2}{d_1}] \times \frac{(d_0 - 229.4)}{0.25(-78537 + d_1) + 0.5 d_2} \times -8.37 \times [(d_0 + 24.1) + \frac{78537}{d_1}] \qquad \text{Equation 6.1}$$

where:

τ is the ultimate joint capacity in N

d_0 is the bond length in mm which can be represented as L_f,

d_1 is the load rate (mm/min) which can be represented as ν,

d_2 is the elastic modulus of CFRP (MPa) which can be represented as E_f.

The equation can be re-written in accordance with the new notations as follows:

$$\tau = [0.5\,\left(L_f^2 + 26765.5 + \nu\right) + \frac{E_f}{\nu}] \times \frac{(L_f - 229.4)}{0.25(-78537 + \nu) + 0.5 E_f} \times -8.37 \times [\left(L_f + 24.1\right) + \frac{78537}{\nu}] \qquad \text{Equation 6.2}$$

The model was validated by examining the coefficient of determination (R^2), mean absolute error (*MAE*), root mean square error (*RMSE*), relative absolute error (*RAE*) and root relative square error (*RRSE*) using the following equations (Nazari et al. 2015):

$$R^2 = 1 - \left(\frac{\sum_i (t_i - o_i)^2}{\sum_i (o_i)^2}\right) \quad \text{Equation 6.3}$$

$$MAE = \frac{1}{n}\sum_i |t_i - o_i| \quad \text{Equation 6.4}$$

$$RMSE = \sqrt{\frac{1}{n}\sum_i (t_i - o_i)^2} \quad \text{Equation 6.5}$$

$$RAE = \frac{\sum_i |t_i - o_i|}{\sum_i \left|t_i - \frac{1}{n}\sum_i t_i\right|} \quad \text{Equation 6.6}$$

$$RRSE = \sqrt{\frac{\sum_i (t_i - o_i)^2}{\sum_i \left(t_i - \frac{1}{n}\sum_i t_i\right)^2}} \quad \text{Equation 6.7}$$

Where, t_i is the target parameter, o_i is the output parameter and n is the number of datasets.

Table 6.2 shows the values of R^2, *MAE*, *RMSE*, *RAE*, *RRSE* and *MAPE* for the three types of datasets, training, testing and validating phases.

Table 6.2: R2 and errors of training, testing and validation of the model

Phase	R^2	*MAE*	*RMSE*	*RAE*	*RRSE*
Training	0.92	9681	11178	0.27	0.28
Testing	0.90	10496	11600	0.30	0.31
Validating	0.92	10496	11600	0.30	0.31

Figure 6.3 illustrates the correlation between the actual test results and the predicted results for the ultimate joint capacity of CFRP-steel double strap joints. The plot shows a large percentage of data at the region where the experimental bond strength is in the range of 50000N-60000N. The reason for the large number of data in the first region (50000N-60000N) is that the experimental joint capacity for joints with ultra-high CFRP modulus was constant at early stages of bond length, and this area is considered as the range of the model which has highest percentage of error.

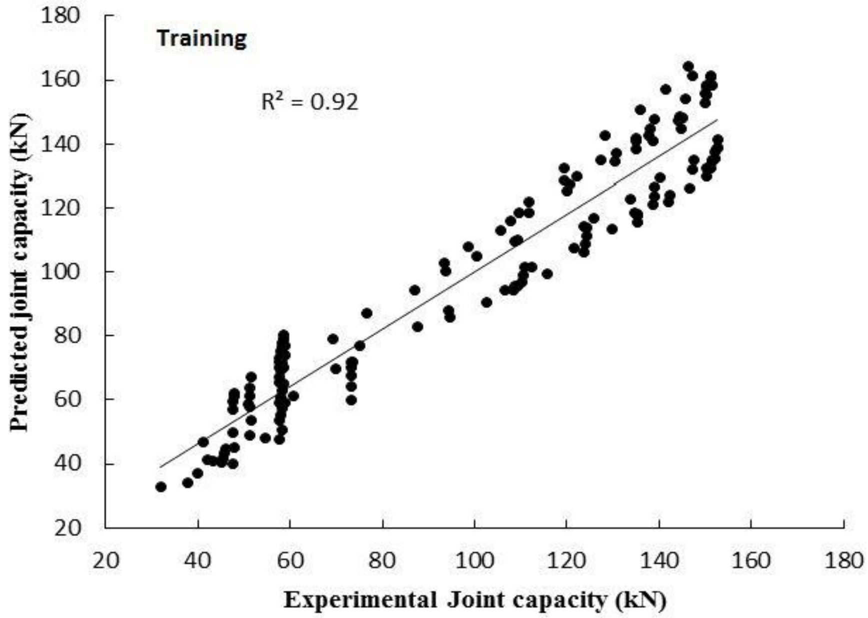
Training
R² = 0.92
Predicted joint capacity (kN)
Experimental Joint capacity (kN)
180
160
140
120
100
80
60
40
20
20
40
60
80
100
120
140
160
180

(a)

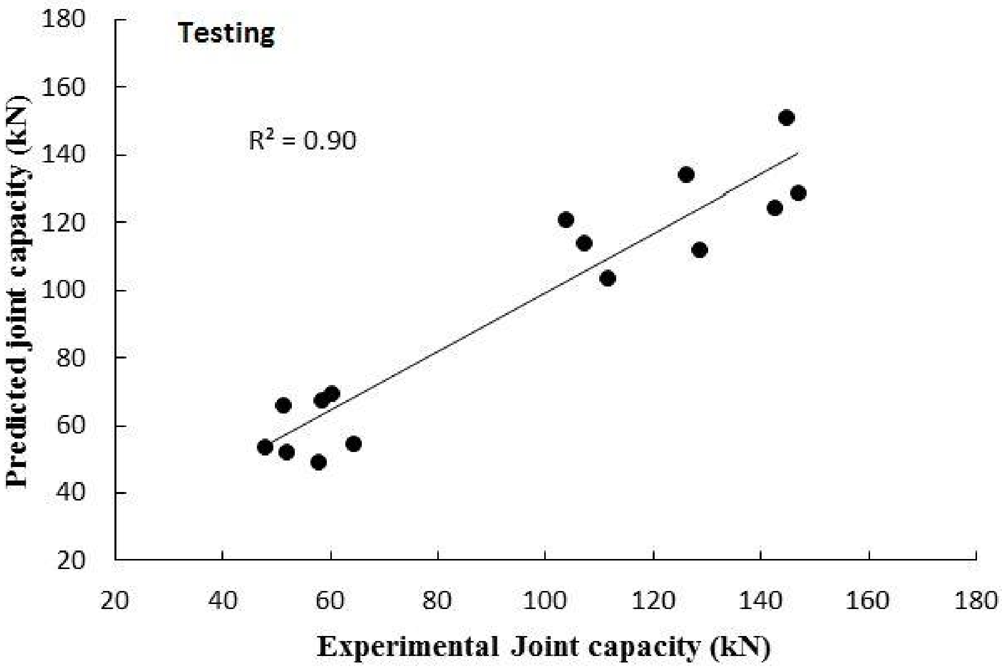
Testing
R² = 0.90
Predicted joint capacity (kN)
Experimental Joint capacity (kN)
180
160
140
120
100
80
60
40
20
20
40
60
80
100
120
140
160
180

(b)

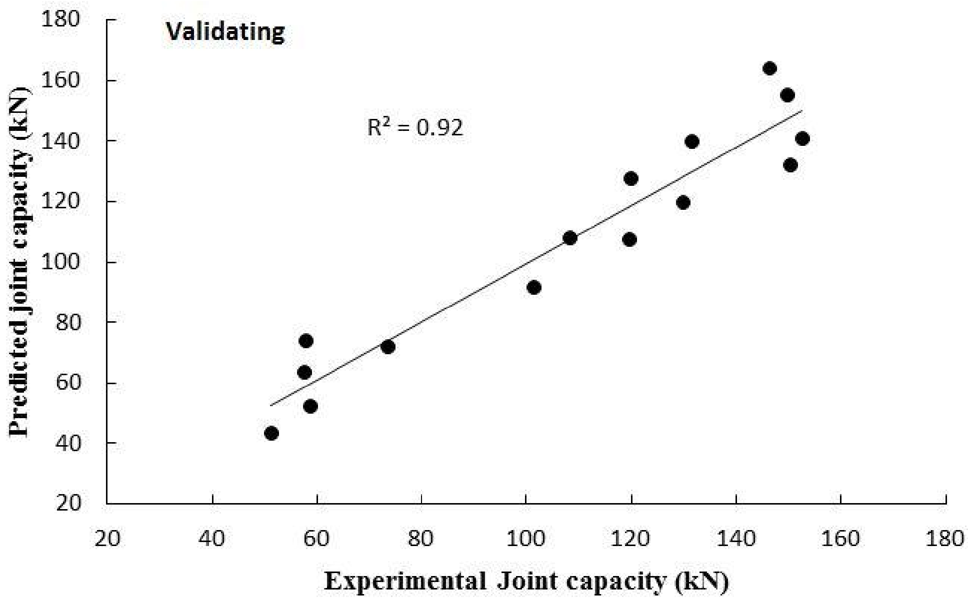

(c)

Figure 6.3 : correlation of the model (a) training, (b) testing, (c) validating

Details of the experimental inputs and experimental and predicted bond strength are shown in Tables 6.3 and 6.4 for quasi-static and dynamic loading, respectively. These data show the values of bond strength predicted by the GP model. As a number of parameters were used in this model, the tables below show the data for only two loading rates with the same CFRP modulus. The complete data sets and the predicted bond strength can be found in Appendix A.

Table 6.3: Model inputs and experimental and predicted bond strength for quasi-static loading

Sample number	d_0 mm	d_1 mm/min	d_2 GPa	Experimental bond strength (kN)	Predicted bond strength (kN)	% error
1	30	2	210	41.9	41.7	-0.40
2	40	2	210	51.7	52.2	1.00
3	50	2	210	60.7	61.6	1.46
4	60	2	210	69.8	69.9	0.11
5	70	2	210	75.0	77.1	2.66
6	80	2	210	87.4	83.1	-5.13
7	90	2	210	94.2	88.1	-6.96
8	110	2	210	108	94.4	-14.7
9	120	2	210	109	95.7	-13.3
10	130	2	210	109	95.7	-14.1
					AAE%	5.98

Table 6.4: Model inputs and experimental and predicted bond strength for dynamic loading

Sample number	d_0 mm	d_1 mm/min $\times 10^3$	d_2 GPa	Experimental bond strength (kN)	Predicted bond strength (kN)	% error
1	40	258	165	107	114	6.18
2	50	258	165	120	125	4.38
3	60	258	165	130	135	3.33
4	70	258	165	137	143	3.62
5	80	258	165	144	149	2.89
6	90	258	165	150	153	2.06
7	100	258	165	150	155	3.62
8	110	258	165	150	156	4.02
					AAE%	3.76

The average absolute error value for the whole data set (Table 6.3, Table 6.4 and Appendix A) is 10.3%, while the maximum value of error for all data is 27.3%.

Figure 6.4 shows the comparison between experimental and predicted bond strength vs. the bond length. Figure 6.4(a) shows the comparison of bond strength versus the bond length for joints loaded under quasi-static loading, while Figure 6.4(b) shows the same relation under a loading rate of 258×10^3 mm/min.

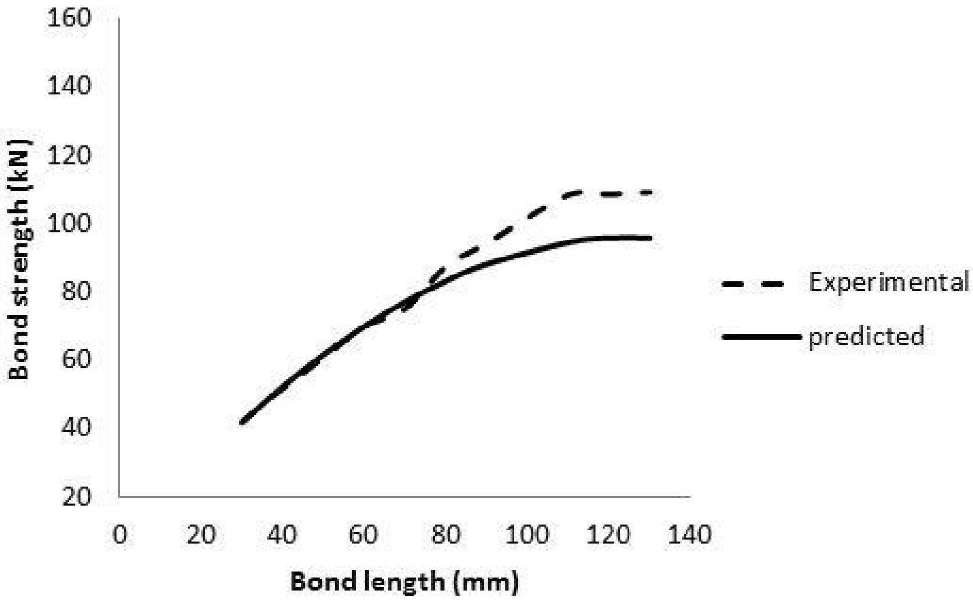

(a)

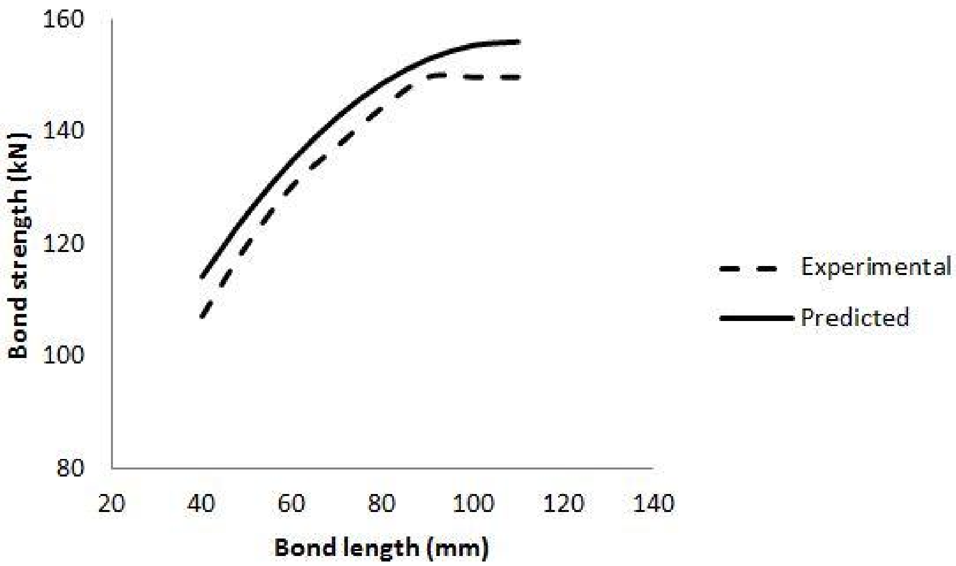

(b)

Figure 6.4 : Comparison between experimental and predicted bond strength vs. bond length (a) quasi-static loading, (b) impact load rate 258× 103 mm/min

From the above figures, it is obvious that the GP model is a good predictor of bond strength. The model also predicts the effective bond length for joints: 110mm for quasi-static loading and 90mm for dynamic loading.

6.5 CONCLUSION

This chapter has studied the assessment of a new model for evaluating the bond strength of CFRP-steel double strap joints based on a GP modelling approach. The input data were obtained from a series of experimental tests and numerical modelling. The input data has three different parameters, and each parameter has a range of values. The CFRP bond length varied from 20mm-130mm, and the loading rate range was 2 - 300×103 mm/min, while three CFRP moduli were used (low modulus 165 GPa, normal modulus 210 GPa and ultra-high modulus 450 GPa). The GP model showed good agreement with the experimental bond strength data. The average absolute error for all data is 10.3%, indicating the accuracy of GP modelling, while the maximum error for the whole dataset is 27.3%. The experimental and predicted bond strength vs. bond length curves have similar trends for all joints with the different parameters. The equation generated from the GP model is applicable for the current data ranges of loading rates, bond lengths and CFRP modulus. The current prediction is a good contribution to the development of the design guidlines of FRP-strengthened steel structures, as it can predict the maximum bond capacity of a joint.

CHAPTER SEVEN CONCLUSION AND FUTURE WORK

7.1 CONCLUDING REMARKS

The use of carbon fibre reinforced polymers (CFRPs) in structural strengthening has grown in the last few decades. CFRP is attractive to structural engineers due to its unique properties, such as its high strength compared to its light weight, good resistance to corrosion, ease of installation and its ability to adhere to different structural sections. The major idea of this research is to provide a full understanding of the dynamic bond behaviour between CFRP laminates and steel structures. Structural engineers can use the results of the current research for suitable, safe and economic design tips for strengthening steel structures under impact loading.

The literature review considers studies of different applications of CFRP bonded steel structures by different researchers. As the bond between CFRP and steel members is the key to understanding the bond properties, the summary focusses on research that investigated the bond properties using various parameters, such as surface preparation methods, CFRP dimensions, adhesive thickness and bond area. It also shows the effect of the material properties on the bond behaviour, including CFRP modulus, adhesive shear strength and type of CFRP.

The literature review illustrates both experimental and analytical studies of the bond between CFRP and steel under static flexural bending, tension and compression forces. Steel structures are normally subjected to both static and dynamic loadings, and most previous studies have not considered the effect of dynamic loadings on the bond between CFRP and steel, due to the fact that dynamic tests need high-speed data acquisition facilities and accurate load cell readings to capture data in milliseconds. As a result, far fewer studies have been reported on the bond behaviour between CFRP and steel under dynamic loading than static loading. No experimental and analytical research was found on the effect of high loading rates on the bond between CFRP laminates and steel plates. Therefore, this research has minimised the gap by studying the dynamic behaviour of CFRP laminate-bonded steel members forming double strap joints. Different loading rates, sections and material properties were used to find their effect on the bond behaviour. Both experimental and analytical studies were included in this research project.

A series of CFRP-steel double strap specimens were loaded under tension force with a load rate of 2mm/min using an MTS machine with a maximum capacity of 250 kN. The aim of this phase of the research was to investigate the bond characteristics between CFRP laminate and steel. Three types of CFRP, low modulus (165 GPa), normal modulus (205 GPa) and ultra-high modulus (460 GPa), were used in this research. Araldite 420 epoxy was used to bond CFRP laminate to the steel joints. Two different CFRP sections were used, 20× 1.4mm and 10×1.4mm, in order to investigate the effect of CFRP section on the bond characteristics between CFRP and steel in the double strap joints. Bond strength, strain distribution along the bond, effective bond length and failure mode were findings from this testing program. Two methods of capturing strain were used: image correlation photogrammetry and foil strain gauges. The actual material properties of low, normal and ultra-high modulus CFRP, Araldite 420 epoxy and steel plate were found to be close to the manufacturers'‭ claimed properties. The results show that the use of small-sized CFRP laminate with a width of 10mm in double strap joints does not give accurate results. The reason is that the adhesive size is small and its capacity to resist the load is very sensitive to any movement. For 20mm CFRP width in the double strap joints, changing from low to normal modulus CFRP has no effect on the effective bond length, which is found to be 110 mm for both types of CFRP. However, a significant change in the effective bond length for specimens with ultra-high modulus CFRP was observed, and the effective bond length for specimens with ultra-high modulus CFRP is 70 mm.

CFRP width has some influence on the effective bond length. For specimens with low modulus CFRP and 20mm CFRP width, the effective bond length was 110mm, whereas it was found to be 140mm for specimens with low modulus CFRP and 50mm CFRP width. For specimens with ultra-high modulus CFRP and 20mm CFRP width, the effective bond length was 70mm, whereas it was found to be 110mm for the same joint with 50mm bond width. For all types of specimens (low, normal and ultra-high modulus CFRP), the maximum strain was found to be at the joint and decreased away from the joint, and the same strain distribution curve was found or all joints with different values. Changing from low to normal modulus CFRP has insignificant effects on the maximum failure strain and strain distribution. Lower strain values were observed for specimens with normal modulus CFRP compared to those with low modulus CFRP. However, a significant decrease was observed in the ultimate strain and strain distribution along the bond length for specimens with ultra-high modulus CFRP. This decrement is due to the modulus of elasticity of CFRP, which is 450 GPa. Little increment in the maximum joint capacity was found when using normal modulus CFRP in the double-strap joint specimens compared to the low modulus CFRP specimens. However, a significant decrease was observed in the maximum failure capacity for specimens with ultra-high modulus CFRP, due to the low modulus CFRP tensile strength, which is 1500 MPa, and its thickness of 1.2mm. Failure modes for both specimens with low and normal modulus CFRP were quite similar; the failure mode was debonding between steel and adhesive, in addition to some adhesive failure for both types of specimens. However, other failure modes eres observed for specimens with ultra-high modulus CFRP; FRP delamination for specimens with bond lengths below the effective bond length, and FRP rupture for specimens with bond lengths equal to and beyond the effective bond length.

Other tests were carried out in this research program to investigate the bond characteristics between CFRP laminates and steel plates under dynamic load. A series of CFRP-steel double strap joint specimens were prepared and tested under impact tension force with three loading rates (201×10^3, 258×10^3 and 300×10^3mm/min) using a drop-mass machine with a maximum capacity of 200kN. Three types of CFRPs (low modulus (165 GPa), normal modulus (210 GPa) and ultra-high modulus (460 GPa)) were used in this research. Araldite 420 epoxy was used to bond CFRP laminate to the steel joints. Bond strength, strain distribution along the bond, effective bond length and failure mode were determined in this testing program. The actual material properties of the CFRPs and Araldite 420 epoxy under dynamic loadings are higher than those under static loading. The ultimate bond strength of the joints tested under dynamic loadings increases by up to 100% compared to the ultimate strength tested under quasi-static loadings. The higher the load rate, the higher the ultimate bond strength for all types of joints. However there was an insubstantial increase in the bond strength beyond the loading rate of 258×10^3 mm/min, due to the marginal increase in the materials' strength beyond this loading rate. The effective bond lengths for specimens tested under dynamic loading are smaller than for specimens tested under quasi-static loading. The effective bond length is the same for the same joint tested under the three different loading rates. There was a significant decrease in the effective bond length for joints with ultra-high modulus CFRP compared to the joints with low and normal modulus CFRP tested under dynamic loading. This explains the effect of the ultimate strain of

CFRP laminate on the effective bond length. The same effective bond length was observed for low and normal modulus CFRP-steel double strap joints tested under the three different loading rates, because there is little difference in the ultimate strain between the two CFRPs. Less non-linearity of the strain distribution curve was observed for quasi-static loadings than dynamic loadings. The ultimate strain of the CFRP-steel double strap joints under dynamic loadings is higher than that under quasi-static loadings. Insubstantial changes occurred in the ultimate strain values for all types of joints under the last two impact loading rates of 258×10^3 and 300×10^3mm/min. The failure modes for joints tested under dynamic loading were completely different from those tested under quasi-static loading, with most failures in static testing being debonding for low and normal modulus CFRP, whereas FRP failure was observed in specimens tested under dynamic loading. For joints with ultra-high modulus CFRP, the failure mode in static testing was FRP delamination for joints below the effective bond length, and FRP rupture for joints beyond the effective bond length, whereas the failure mode was FRP delamination for all bond lengths for specimens tested under impact loading.

Three-dimensional finite element modelling was utilised to model different CFRP-steel double strap joints. Three types of CFRP were used in order to validate the ability of both ABAQUS/implicit and ABAQUS/explicit to model these types of joints under quasi-static and impact tension load respectively. All components of the double strap joint (steel, CFRP and adhesive) were simulated in both ABAQUS/implicit and ABAQUS/explicit. The steel was modelled as a 3-D stress element, the CFRP was modelled using continuum shell elements and the adhesive was modelled using cohesive elements. ABAQUS/implicit and ABAQUS/explicit are both able to simulate the components of CFRP-steel double strap joints under both quasi-static and dynamic loading. The numerical analysis results for steel, CFRP and adhesive agreed well with those obtained from experimental investigation. ABAQUS/implicit and ABAQUS/explicit are both able to simulate CFRP-steel double strap joints under both quasi-static and dynamic loading and for all different CFRP types. The predictions of bond strength, failure modes, effective bond length and strain distribution along the bond agreed reasonably well with those obtained from the experimental tests, and there was good agreement on the bond strength results based on the numerical simulation and the experimental tests. The numerical analysis results showed slightly higher bond strengths than those from the actual tests, whereas for quasi-static testing the numerical simulation showed slightly lower bond strengths than those from the actual tests. The effective bond length was predicted very well for all types of joints and under the different loading rates (2, 201×10^3, 258×10^3 and 300×10^3 mm/min). The failure modes for all types of joints were also predicted well, although some models could not show adhesive failure because this mode occurs in the middle of the joints, whereas the numerical simulations showed the failure at the joints and the far ends. The trend of strain distribution along the bond length was very close for all types of joint and under all loading rates, although there were slight differences in strain values at the different load levels between the numerical simulation and experimental results. However, these differences are considered to be acceptable.

Genetic programing application was used to predict a formulation of the bond strength of CFRP-steel double strap joints subjected to direct tension load. Extensive elective data from experimental tests and finite element modelling were used to develop a new joint strength formulation. The elective parameters which have direct impact on the joint strength were: bond length, CFRP modulus and the loading rate. Wide range of loading rates was used and four CFRP moduli with different bond lengths. The genetically programmed model prediction was compared with the actual values. The model has a high value of R squared which indicates good accuracy of results.

7.2 RECOMMENDATIONS FOR FUTURE RESEARCH

Considering the state of the art of the bond behaviour between steel and CFRP, a large number of studies have been conducted on CFRP-strengthened steel structures. However, this research studied the effect of impact load on the bond between steel and CFRP laminates, using a number of different parameters. Although the current research has provided comprehensive data on the behaviour of steel structures exposed to sudden high load rates, there are many other conditions that might be studied to achieve a full understanding of the behaviour of CFRP-bonded steel structures. Some suggestions are as follows:

- The bond behaviour between steel and CFRP has been tested under high loading rates and ambient temperature, but more tests are needed to study the effect of different temperatures and humidity (high and low) on the bond, and the effect of temperature and humidity changes on this bond

- The effect of different loading rates on the bond-slip model needs to be investigated. The bond slip model has been proposed by other researchers under static loading.
- A theoretical model could be developed to propose design guidelines for CFRP-bonded steel structures under static and dynamic loadings. Design guidelines for FRP-strengthened concrete structures are available.
- Other analytical techniques could be used to predict bond strength equation, these techniques could be shear lag analysis, fracture mechanics based approaches, numerical simulations or other empirical approaches.

APPENDIX A

Bond length mm	Loading rate mm/min	Elastic modulus of CFRP MPa	Experimental bond strength (N)	Predicted bond strength (N)	% error
30	2	210000	41900	41730.68	-0.40574
50	2	210000	60700	61600.21	1.461369
60	2	210000	69800	69877.42	0.1108
70	2	210000	75000	77056.35	2.668628
80	2	210000	87400	83127.33	-5.13991
90	2	210000	94200	88068.95	-6.96164
110	2	210000	108300	94419.71	-14.7006
120	2	210000	108500	95727.23	-13.3429
130	2	210000	109200	95702.15	-14.104
30	2	165000	41000	47055.78	12.86936
40	2	165000	50700	58949.64	13.99438
60	2	165000	69100	79115.2	12.65901
70	2	165000	76500	87408.6	12.48001
80	2	165000	86800	94496.95	8.145183
90	2	165000	93600	100351.2	6.727537
100	2	165000	100300	104926.2	4.409002
120	2	165000	108700	109978.7	1.162721
130	2	165000	109100	110286.3	1.075683
30	2	450000	31760	33036.77	3.864707
40	2	450000	43300	41239.8	-4.99566
50	2	450000	54400	48490.81	-12.1862
70	2	450000	73200	60154.95	-21.6857
80	2	450000	73100	64564.95	-13.2193
90	2	450000	73000	68016.66	-7.32665
100	2	450000	73200	70496.3	-3.83523
110	2	450000	73400	71985.2	-1.96541

130	2	450000	73200	71891.59	-1.81997
40	201000	165000	93300	102961.4	9.383495
50	201000	165000	105400	113181.4	6.875118
60	201000	165000	111600	121873.7	8.42982
70	201000	165000	119300	129035.3	7.544654
90	201000	165000	134900	138708.3	2.745553
100	201000	165000	134900	141168.9	4.440722
110	201000	165000	134900	141996.9	4.997895
40	225000	165000	98600	108005.9	8.708691
50	225000	165000	111500	118682.6	6.051967
70	225000	165000	127100	135175.4	5.974011
80	225000	165000	138400	140976.8	1.827807
90	225000	165000	144600	145124.4	0.361334
100	225000	165000	143900	147589.8	2.50004
110	225000	165000	144800	148336.2	2.38393
50	258000	165000	119900	125400.6	4.386423
60	258000	165000	130400	134904	3.338696
70	258000	165000	137500	142673.5	3.626106
80	258000	165000	144400	148698.2	2.890545
90	258000	165000	149800	152959.5	2.065553
110	258000	165000	149800	156077.6	4.022132
40	270000	165000	107700	116212.9	7.325224
50	270000	165000	120500	127632.7	5.588449
60	270000	165000	130700	137284.3	4.79609
70	270000	165000	137800	145164.8	5.073396
90	270000	165000	150100	155562.7	3.511583
100	270000	165000	150200	158036	4.958341
110	270000	165000	150100	158649.8	5.389093
40	285000	165000	109400	118642.5	7.790241
50	285000	165000	122100	130282.4	6.280492
70	285000	165000	138700	148122.2	6.36108
80	285000	165000	145400	154309.1	5.773563
90	285000	165000	151200	158653	4.697678

100	285000	165000	150900	161128.6	6.348082
110	285000	165000	151100	161703.1	6.557163
50	300000	165000	119300	132787.9	10.15749
60	300000	165000	128100	142781.7	10.28261
70	300000	165000	135600	150918.7	10.15028
80	300000	165000	141300	157188.9	10.10817
90	300000	165000	146900	161575.2	9.082575
110	300000	165000	146200	164590.4	11.17343
40	201000	210000	94500	85879.15	-10.0383
50	201000	210000	106300	94403.54	-12.6017
60	201000	210000	112300	101653.8	-10.473
70	201000	210000	121500	107627.1	-12.8897
90	201000	210000	135100	115695.3	-16.7722
100	201000	210000	135100	117747.7	-14.7368
110	201000	210000	135100	118438.3	-14.0678
40	225000	210000	102400	90845.94	-12.7183
50	225000	210000	115600	99826.35	-15.8011
70	225000	210000	129500	113698.7	-13.8975
80	225000	210000	134400	118578.4	-13.3427
90	225000	210000	142000	122067	-16.3295
100	225000	210000	142300	124140.7	-14.628
40	258000	210000	110100	97025.9	-13.4749
50	258000	210000	123500	106573.7	-15.8822
60	258000	210000	123400	114650.4	-7.63156
70	258000	210000	138600	121253.4	-14.3061
80	258000	210000	146300	126373.6	-15.7679
90	258000	210000	150200	129995.1	-15.5428
110	258000	210000	150200	132645.1	-13.2345
40	270000	210000	110300	99107.78	-11.293
50	270000	210000	123800	108846.8	-13.7379
60	270000	210000	125600	117077.8	-7.27913
70	270000	210000	138700	123798.4	-12.037
90	270000	210000	151100	132665.8	-13.8952

100	270000	210000	151200	134775.1	-12.1869
110	270000	210000	151300	135298.5	-11.8268
40	285000	210000	110700	101598	-8.95887
50	285000	210000	124000	111565.6	-11.1454
70	285000	210000	138900	126842.5	-9.50592
80	285000	210000	147000	132140.6	-11.2452
90	285000	210000	151900	135860.4	-11.8059
100	285000	210000	152000	137980.3	-10.1606
110	285000	210000	152200	138472.3	-9.91364
50	300000	210000	124200	114157.3	-8.79728
60	300000	210000	133600	122748.9	-8.84011
70	300000	210000	140100	129744.2	-7.9817
80	300000	210000	147300	135134.7	-9.00234
90	300000	210000	152600	138905.6	-9.8588
110	300000	210000	152500	141497.7	-7.77558
20	201000	450000	37700	34475.99	-9.35147
30	201000	450000	47600	40361.96	-17.9328
40	201000	450000	47900	45563.04	-5.12908
50	201000	450000	47600	50085.63	4.962769
70	201000	450000	47400	57101.39	16.98976
80	201000	450000	47600	59587.73	20.11779
90	201000	450000	47700	61381.96	22.28987
100	201000	450000	47700	62470.83	23.64437
20	225000	450000	39700	37228.5	-6.63872
40	225000	450000	51200	49176.22	-4.11537
50	225000	450000	51300	54037.44	5.065827
60	225000	450000	51100	58161.43	12.14109
70	225000	450000	51200	61546.77	16.81123
80	225000	450000	51200	64188.2	20.23456
100	225000	450000	51300	67199.17	23.65977
20	258000	450000	45100	40813.37	-10.503
30	258000	450000	57400	47760.4	-20.1832
40	258000	450000	57600	53882.01	-6.90024

50	258000	450000	57500	59184.27	2.84581
70	258000	450000	57400	67336.41	14.75637
80	258000	450000	57400	70179.84	18.21013
90	258000	450000	57500	72190.99	20.35017
100	258000	450000	57400	73357.35	21.75289
20	270000	450000	45300	42063.21	-7.69505
40	270000	450000	57700	55522.67	-3.92152
50	270000	450000	57800	60978.69	5.212782
60	270000	450000	57600	65589.9	12.1816
70	270000	450000	57700	69354.94	16.80477
80	270000	450000	57700	72268.79	20.15917
100	270000	450000	57700	75504.36	23.58057
20	285000	450000	45600	43587.4	-4.6174
30	285000	450000	58100	50998.89	-13.9241
40	285000	450000	58100	57523.44	-1.00231
50	285000	450000	58200	63166.97	7.86324
70	285000	450000	58100	71816.53	19.09941
80	285000	450000	58100	74816.26	22.34309
90	285000	450000	58100	76922.37	24.46931
100	285000	450000	58100	78122.64	25.62975
20	300000	450000	45900	45070.81	-1.83975
40	300000	450000	58700	59470.69	1.295912
50	300000	450000	58600	65296.72	10.25583
60	300000	450000	58600	70211.02	16.53732
70	300000	450000	58700	74212.28	20.90258
80	300000	450000	58800	77295.59	23.92839
90	300000	450000	58600	79452.48	26.24522
100	300000	450000	58600	80670.88	27.35917

REFERENCES

ABAQUS 2013. Abaqus User's Manual Version 6.13. *Dassault Systemes Simulia Corp, Providence, RI, USA*.

ADAMS, D. & ADAMS, L. 1989. A tensile impact test apparatus for composite materials. *Experimental Mechanics,* 29**,** 466-473.

ADAMS, D. F. & ADAMS, L. G. 1990. Tensile impact tests of AS4/3501-6 and S2/3501-6 unidirectional composites and the 3501-6 epoxy matrix. *Journal of composite materials,* 24**,** 256-268.

AL-MOSAWE, A., AL-MAHAIDI, R. & ZHAO, X.-L. 2015. Effect of CFRP properties, on the bond characteristics between steel and CFRP laminate under quasi-static loading. *Construction and Building Materials,* 98**,** 489-501.

AL-MOSAWE, A., AL-MAHAIDI, R. & ZHAO, X.-L. 2015b. Experimental and numerical study on strengthening of steel members subjected to impact loading using ultra-high modulus CFRP *Composites for Construction,* (Accepted).

AL-MOSAWE, A., AL-MAHAIDI, R. & ZHAO, X.-L. 2015c. Bond behaviour between CFRP laminates and steel members under different loading rates. *Composite Structures,* (under review).

AL-ZUBAIDY, H., AL-MAHAIDI, R. & ZHAO, X.-L. 2012a. Experimental investigation of bond characteristics between CFRP fabrics and steel plate joints under impact tensile loads. *Composite Structures,* 94**,** 510-518.

AL-ZUBAIDY, H., AL-MAHAIDI, R. & ZHAO, X.-L. 2012a-a. Experimental investigation of bond characteristics between CFRP fabrics and steel plate joints under impact tensile loads. *Composite Structures,* 94**,** 510-518.

AL-ZUBAIDY, H., AL-MAHAIDI, R. & ZHAO, X.-L. 2013. Finite element modelling of CFRP/steel double strap joints subjected to dynamic tensile loadings. *Composite Structures,* 99**,** 48-61.

AL-ZUBAIDY, H., ZHAO, X.-L. & AL-MIHAIDI, R. 2011a. Mechanical behaviour of normal modulus carbon fibre reinforced polymer (CFRP) and epoxy under impact tensile loads. *Procedia Engineering,* 10**,** 2453-2458.

AL-ZUBAIDY, H. A.-A. B. 2012. Behaviour of bond between CFRP sheet and steel under impact tensile loading. PhD thesis, Monash University.

AL-ZUBAIDY, H. A., ZHAO, X.-L. & AL-MAHAIDI, R. 2012b. Dynamic bond strength between CFRP sheet and steel. *Composite Structures,* 94**,** 3258-3270.

AL-ZUBAIDY, H. A., ZHAO, X.-L. & AL-MAHAIDI, R. 2012a-b. Dynamic bond strength between CFRP sheet and steel. *Composite Structures,* 94**,** 3258-3270.

AL-ZUBAIDY, H. A., ZHAO, X. L. & AL-MAHAIDI, R. 2011b. Effect of impact tensile load on strength of CFRP bonded steel plate joints. *Procedia Engineering,* 14**,** 1312-1317.

ANDRÉ, A., HAGHANI, R. & BIEL, A. 2012. Application of fracture mechanics to predict the failure load of adhesive joints used to bond CFRP laminates to steel members. *Construction and Building Materials,* 27**,** 331-340.

ARAVINTHAN, T. & MANALO, A. Field applications and case studies of FRP in civil infrastructure: the Australian experience. Proceedings of the 6th International Conference on FRP Composites in Civil Engineering (CICE 2012), 2012 Rome, Italy, 13-15 June International Institute for FRP in Construction (IIFC), 1-8.

ASTORGA, A., SANTA MARIA, H. & LOPEZ, M. 2013. Behavior of a concrete bridge cantilevered slab reinforced using NSM CFRP strips. *Construction and Building Materials,* 40**,** 461-472.

BAMBACH, M., JAMA, H. & ELCHALAKANI, M. 2009. Axial capacity and design of thin-walled steel SHS strengthened with CFRP. *Thin-Walled Structures,* 47**,** 1112-1121.

BARRÉ, S., CHOTARD, T. & BENZEGGAGH, M. L. 1996. Comparative study of strain rate effects on mechanical properties of glass fibre-reinforced thermoset matrix composite. *Composites Part A: Applied Science and Manufacturing,* 27**,** 1169-1181.

BARROS, J. A. O., DIAS, S. J. E. & LIMA, J. L. T. 2007. Efficacy of CFRP-based techniques for the flexural and shear strengthening of concrete beams. *Cement and Concrete Composites,* 29**,** 203-217.
BENZARTI, K., CHATAIGNER, S., QUIERTANT, M., MARTY, C. & AUBAGNAC, C. 2011. Accelerated ageing behaviour of the adhesive bond between concrete specimens and CFRP overlays. *Construction and Building Materials,* 25**,** 523-538.
BOCCIARELLI, M., COLOMBI, P., FAVA, G. & POGGI, C. 2009. Fatigue performance of tensile steel members strengthened with CFRP plates. *Composite Structures,* 87**,** 334-343.
BUYUKOZTURK, O., GUNES, O. & KARACA, E. 2004. Progress on understanding debonding problems in reinforced concrete and steel members strengthened using FRP composites. *Construction and Building Materials,* 18**,** 9-19.
CAMANHO, P. P. & DÁVILA, C. G. 2002. Mixed-mode decohesion finite elements for the simulation of delamination in composite materials. *NASA-Technical paper,* 211737**,** 33.
CANTWELL, W. & MORTON, J. 1991. The impact resistance of composite materials—a review. *composites,* 22**,** 347-362.
CAPOZUCCA, R. 2007. Analysis of the experimental flexural behaviour of a concrete beam grid reinforced with C-FRP bars. *Composite Structures,* 79**,** 517-526.
CEVIK, A. 2007. Genetic programming based formulation of rotation capacity of wide flange beams. *Journal of Constructional Steel Research,* 63**,** 884-893.
CEVIK, A., ARSLAN, M. H. & KÖROĞLU, M. A. 2010. Genetic-programming-based modeling of RC beam torsional strength. *KSCE Journal of Civil Engineering,* 14**,** 371-384.
CHALLITA, G., OTHMAN, R., CASARI, P. & KHALIL, K. 2011. Experimental investigation of the shear dynamic behavior of double-lap adhesively bonded joints on a wide range of strain rates. *International Journal of Adhesion and Adhesives,* 31**,** 146-153.
CHIEW, S., YU, Y. & LEE, C. 2011. Bond failure of steel beams strengthened with FRP laminates–Part 1: Model development. *Composites Part B: Engineering,* 42**,** 1114-1121.
COELLO, C. C., CHRISTIANSEN, A. D. & HERNÁNDEZ, F. S. 1997. A simple genetic algorithm for the design of reinforced concrete beams. *Engineering with Computers,* 13**,** 185-196.
COLOMBI, P. & POGGI, C. 2006a. An experimental, analytical and numerical study of the static behavior of steel beams reinforced by pultruded CFRP strips. *Composites Part B: Engineering,* 37**,** 64-73.
COLOMBI, P. & POGGI, C. 2006b. Strengthening of tensile steel members and bolted joints using adhesively bonded CFRP plates. *Construction and Building Materials,* 20**,** 22-33.
CRUZ, J. S. & BARROS, J. 2004. Modeling of bond between near-surface mounted CFRP laminate strips and concrete. *Computers & Structures,* 82**,** 1513-1521.
CZADERSKI, C. & MOTAVALLI, M. 2007. 40-Year-old full-scale concrete bridge girder strengthened with prestressed CFRP plates anchored using gradient method. *Composites Part B: Engineering,* 38**,** 878-886.
DAWOOD, M., GUDDATI, M. & RIZKALLA, S. 2009. Effective Splices for a Carbon Fiber-Reinforced Polymer: Strengthening System for Steel Bridges and Structures. *Transportation Research Record: Journal of the Transportation Research Board***,** 125-133.
DAWOOD, M. & RIZKALLA, S. 2007. Bond and splice behavior of CFRP laminates for strengthening steel beams. *accepted for publication in the Proceedings of the International Conference on Advanced Composites in Construction (ACIC 07).* United Kingdom: University of Bath.
DENG, J. & LEE, M. M. 2007. Behaviour under static loading of metallic beams reinforced with a bonded CFRP plate. *Composite structures,* 78**,** 232-242.
DESHPANDE, A. B. 2006. Characterization of CFRP and GFRP composite materials at high strain rate tensile loading. PhD thesis, Wichita State University.

FALZON, B. G., HITCHINGS, D. & BESANT, T. 1999. Fracture mechanics using a 3D composite element. *Composite Structures,* 45**,** 29-39.
FAWZIA, S. 2008. Bond characteristics between steel and carbon fibre reinforced polymer (CFRP) composites. PhD thesis, Department of Civil Engineering, Monash University.
FAWZIA, S., AL-MAHAIDI, R. & ZHAO, X.-L. 2006a. Experimental and finite element analysis of a double strap joint between steel plates and normal modulus CFRP. *Composite Structures,* 75**,** 156-162.
FAWZIA, S., AL-MAHAIDI, R. & ZHAO, X. L. 2006b. Experimental and finite element analysis of a double strap joint between steel plates and normal modulus CFRP. *Composite Structures,* 75**,** 156-162.
FAWZIA, S., AL-MAHAIDI, R., ZHAO, X. L. & RIZKALLA, S. 2007. Strengthening of circular hollow steel tubular sections using high modulus CFRP sheets. *Construction and Building Materials,* 21**,** 839-845.
FAWZIA, S., ZHAO, X.-L. & AL-MAHAIDI, R. 2010. Bond–slip models for double strap joints strengthened by CFRP. *Composite Structures,* 92**,** 2137-2145.
FAWZIA, S., ZHAO, X. L., AL-MAHAIDI, R. & RIZKALLA, S. 2005. Bond characteristics between CFRP and steel plates in double strap joints. *Advanced Steel Construction,* 1**,** 17-27.
FERNANDES, P. M. G., SILVA, P. M. & SENA-CRUZ, J. 2015. Bond and flexural behavior of concrete elements strengthened with NSM CFRP laminate strips under fatigue loading. *Engineering Structures,* 84**,** 350-361.
FERNANDO, D., YU, T., TENG, J. G. & ZHAO, X. L. 2009. CFRP strengthening of rectangular steel tubes subjected to end bearing loads: Effect of adhesive properties and finite element modelling. *Thin-Walled Structures,* 47**,** 1020-1028.
FERNIE, R. & WARRIOR, N. A. 2002. Impact Test Rigs for High Strain Rate Tensile and Compressive Testing of Composite Materials. *Strain,* 38**,** 69-73.
GAMAGE, J. C. P. H., AL-MAHAIDI, R. & WONG, M. B. 2006. Bond characteristics of CFRP plated concrete members under elevated temperatures. *Composite Structures,* 75**,** 199-205.
GANDOMI, A. H., ALAVI, A. H. & SAHAB, M. G. 2010. New formulation for compressive strength of CFRP confined concrete cylinders using linear genetic programming. *Materials and Structures,* 43**,** 963-983.
GANDOMI, A. H., TABATABAEI, S. M., MORADIAN, M. H., RADFAR, A. & ALAVI, A. H. 2011. A new prediction model for the load capacity of castellated steel beams. *Journal of Constructional Steel Research,* 67**,** 1096-1105.
GANESH PRABHU, G. & SUNDARRAJA, M. C. 2013. Behaviour of concrete filled steel tubular (CFST) short columns externally reinforced using CFRP strips composite. *Construction and Building Materials,* 47**,** 1362-1371.
GRZEBIETA, R. H. 1990. On the equilibrium approach for predicting the crush response of thin-walled mils steel structures. PhD thesis.
HADI, M. N. S. & LE, T. D. 2014. Behaviour of hollow core square reinforced concrete columns wrapped with CFRP with different fibre orientations. *Construction and Building Materials,* 50**,** 62-73.
HAGHANI, R. 2010. Analysis of adhesive joints used to bond FRP laminates to steel members – A numerical and experimental study. *Construction and Building Materials,* 24**,** 2243-2251.
HARDING, J. & WELSH, L. M. 1983. A Tensile Testing Technique for Fiber-Reinforced Composites at Impact Rates of Strain. *Journal of Materials Science,* 18**,** 1810-1826.
HART-SMITH, L. 1973. Adhesive-bonded double-lap joints. *Technical report.* Washington DC, USA: National Aeronautics and Space Administration CR-112235.
HASHIM, S. 1999. Adhesive bonding of thick steel adherends for marine structures. *Marine Structures,* 12**,** 405-423.
HASHIN, Z. & ROTEM, A. 1973. A fatigue criterion for fibre-reinforced materials. . *Journal of Composite Materials,* 7: 448-464.

HOLLAWAY, L. & CADEI, J. 2002. Progress in the technique of upgrading metallic structures with advanced polymer composites. *Progress in Structural Engineering and Materials,* 4, 131-148.
HOLZER, A. J. 1978. On dynamic mechanical properties of metals and their measurement. PhD thesis, Department of Mechanical Engineering, Monash University, Victoria, Australia.
HOSSEINI, A. & MOSTOFINEJAD, D. 2013. Effect of groove characteristics on CFRP-to-concrete bond behavior of EBROG joints: Experimental study using particle image velocimetry (PIV). *Construction and Building Materials,* 49, 364-373.
HOU, J. P. & RUIZ, C. 2000. Measurement of the properties of woven CFRP T300/914 at different strain rates. *Composites Science and Technology,* 60, 2829-2834.
HUTCHINSON, A. 1987. Surface pretreatment–the key to durability. *Proceedings of the International Conference on Structural Faults & Repair.* University of London-UK.
IMANAKA, M., NAKAYAMA, H., MORIKAWA, K. & NAKAMURA, M. 1995. Evaluation of fatigue life of adhesively bonded CFRP pipe/steel rod joints. *Composite Structures,* 31, 235-241.
JACOB, G. C., STARBUCK, J. M., FELLERS, J. F., SIMUNOVIC, S. & BOEMAN, R. G. 2004. Strain rate effects on the mechanical properties of polymer composite materials. *Journal of Applied Polymer Science,* 94, 296-301.
JIAO, H. & ZHAO, X. L. 2004. CFRP strengthened butt-welded very high strength (VHS) circular steel tubes. *Thin-Walled Structures,* 42, 963-978.
JONES, S. C. & CIVJAN, S. A. 2003. Application of fiber reinforced polymer overlays to extend steel fatigue life. *Journal of Composites for Construction,* 7, 331-338.
KADHIM, M. M. A. 2012. Effect of CFRP plate length strengthening continuous steel beam. *Construction and Building Materials,* 28, 648-652.
KALFAT, R. & AL-MAHAIDI, R. 2010. Investigation into bond behaviour of a new CFRP anchorage system for concrete utilising a mechanically strengthened substrate. *Composite Structures,* 92, 2738-2746.
KALFAT, R., NAZARI, A., AL-MAHAIDI, R. & SANJAYAN, J. 2016. Genetic programming in the simulation of Frp-to-concrete patch-anchored joints. *Composite Structures,* 138, 305-312.
KARA, I. F. 2011. Prediction of shear strength of FRP-reinforced concrete beams without stirrups based on genetic programming. *Advances in Engineering Software,* 42, 295-304.
KARBHARI, V. & SHULLEY, S. 1995. Use of composites for rehabilitation of steel structures-determination of bond durability. *Journal of Materials in Civil Engineering,* 7, 239-245.
KARBHARI, V. M. & ZHAO, L. 2000. Use of composites for 21st century civil infrastructure. *Computer methods in applied mechanics and engineering,* 185, 433-454.
KIM, Y. J. & HARRIES, K. A. 2011a. Behavior of tee-section bracing members retrofitted with CFRP strips subjected to axial compression. *Composites Part B: Engineering,* 42, 789-800.
KIM, Y. J. & HARRIES, K. A. 2011b. Fatigue behavior of damaged steel beams repaired with CFRP strips. *Engineering Structures,* 33, 1491-1502.
KOZA, J. R. 1992. *Genetic programming: on the programming of computers by means of natural selection*, MIT Press.
LIFSHITZ, J. & LEBER, H. 1998. Response of fiber-reinforced polymers to high strain-rate loading in interlaminar tension and combined tension/shear. *Composites science and technology,* 58, 987-996.
LIU, H., ZHAO, X.-L. & AL-MAHAIDI, R. 2009. Boundary element analysis of CFRP reinforced steel plates. *Composite Structures,* 91, 74-83.
LIU, H., ZHAO, X.-L., AL-MAHAIDI, R. & RIZKALLA, S. 2005a. Analytical bond models between steel and normal modulus CFRP. Advances in Steel Structures: Proceedings of Fourth International Conference on Advances in Steel Structures. Elsevier, 1545-1552.

LIU, H., ZHAO, X. & AL-MAHAIDI, R. The effect of fatigue loading on bond strength of CFRP bonded steel plate joints. Proceedings of the International Symposium on Bond Behaviour of FRP in Structures, 2005b Hong Kong, China. 459-464.

LIU, H. B., ZHAO, X. L. & AL-MAHAIDI, R. 2010. Effect of fatigue loading on bond strength between cfrp sheets and steel plates. *International Journal of Structural Stability and Dynamics,* 10**,** 1-20.

MAJZOOBI, G. H., SANIEE, F. F. & BAHRAMI, M. 2005. A tensile impact apparatus for characterization of fibrous composites at high strain rates. *Journal of Materials Processing Technology,* 162–163**,** 76-82.

MATTA, F. 2003. Bond between steel and CFRP laminates for rehabilitation of metallic bridges. PhD thesis, Faculty of Engineering, University of Padua, Padua.

MATZENMILLER, A., LUBLINER, J. & TAYLOR, R. L. 1995. A constitutive model for anisotropic damage in fiber-composites. *Mechanics of Materials,* 20**,** 125-152.

MAYS, G. C. & HUTCHINSON, A. R. 2005. Adhesives in civil engineering. Cambridge University Press.

MILLER, T., CHAJES, M. & HASTINGS, J. 2001. Strengthening of a Steel Bridge Girder Using CFRP Plates. *Journal of Bridge Engineering,* 6**,** 514-522.

NAGAI, M., HIDEKUMA, Y., MIYASHITA, T., OKUYAMA, Y., KUDO, A. & KOBAYASHI, A. 2012. Bonding Characteristics and Flexural Stiffening Effect of CFRP Strand Sheets Bonded to Steel Beams. *Procedia Engineering,* 40**,** 137-142.

NAZARI, A., RAJEEV, P. & SANJAYAN, J. G. 2015. Modelling of upheaval buckling of offshore pipeline buried in clay soil using genetic programming. *Engineering Structures,* 101**,** 306-317.

NGUYEN, T.-C., BAI, Y., ZHAO, X.-L. & AL-MAHAIDI, R. 2011. Mechanical characterization of steel/CFRP double strap joints at elevated temperatures. *Composite Structures,* 93**,** 1604-1612.

NGUYEN, T.-C., BAI, Y., ZHAO, X.-L. & AL-MAHAIDI, R. 2012. Durability of steel/CFRP double strap joints exposed to sea water, cyclic temperature and humidity. *Composite Structures,* 94**,** 1834-1845.

NGUYEN, T.-C., BAI, Y., ZHAO, X.-L. & AL-MAHAIDI, R. 2013. Curing effects on steel/CFRP double strap joints under combined mechanical load, temperature and humidity. *Construction and Building Materials,* 40**,** 899-907.

OKOLI, O. I. 2001. The effects of strain rate and failure modes on the failure energy of fibre reinforced composites. *Composite Structures,* 54**,** 299-303.

PALA, M. 2008. Genetic programming-based formulation for distortional buckling stress of cold-formed steel members. *Journal of Constructional Steel Research,* 64**,** 1495-1504.

PEREIRA, J. M., GHASEMNEJAD, H., WEN, J. X. & TAM, V. H. Y. 2011. Blast response of cracked steel box structures repaired with carbon fibre-reinforced polymer composite patch. *Materials & Design,* 32**,** 3092-3098.

PÉREZ, J. L., CLADERA, A., RABUÑAL, J. R. & ABELLA, F. M. 2010. Optimal adjustment of EC-2 shear formulation for concrete elements without web reinforcement using Genetic Programming. *Engineering Structures,* 32**,** 3452-3466.

RAFI, M. M., NADJAI, A., ALI, F. & TALAMONA, D. 2008. Aspects of behaviour of CFRP reinforced concrete beams in bending. *Construction and Building Materials,* 22**,** 277-285.

SATO, Y., UEDA, T., KAKUTA, Y. & ONO, S. Ultimate shear capacity of reinforced concrete beams with carbon fiber sheets. Non-Metallic (FRP) Reinforcement for Concrete Structures, Proceedings of the Third Symposium, 1997. 499-506.

SAYED AHMAD, F., FORET, G. & LE ROY, R. 2011. Bond between carbon fibre-reinforced polymer (CFRP) bars and ultra high performance fibre reinforced concrete (UHPFRC): Experimental study. *Construction and Building Materials,* 25**,** 479-485.

SCHAFER, B. W. & PEKÖZ, T. 1998. Computational modeling of cold-formed steel: characterizing geometric imperfections and residual stresses. *Journal of Constructional Steel Research,* 47**,** 193-210.

SCHNERCH, D. 2005. Strengthening of steel structures with high modulus carbon fiber reinforced polymer (CFRP) materials. PhD thesis, North Carolina State University, North Carolina, United States.
SCHNERCH, D. & RIZKALLA, S. 2008. Flexural strengthening of steel bridges with high modulus CFRP strips. *Journal of Bridge Engineering,* 13**,** 192-201.
SELEEM, M., SHARAKY, I. & SALLAM, H. 2010. Flexural behavior of steel beams strengthened by carbon fiber reinforced polymer plates–Three dimensional finite element simulation. *Materials & Design,* 31**,** 1317-1324.
SHOKRIEH, M. M. & OMIDI, M. J. 2009. Investigation of strain rate effects on in-plane shear properties of glass/epoxy composites. *Composite Structures,* 91**,** 95-102.
SILVA, M. A. G., BISCAIA, H. C. & MARREIROS, R. 2013. Bond–slip on CFRP/GFRP-to-concrete joints subjected to moisture, salt fog and temperature cycles. *Composites Part B: Engineering,* 55**,** 374-385.
TAKIGUCHI, M., IZUMI, S. & YOSHIDA, F. 2004. Rate-dependent shear deformation of ductile acrylic adhesive and its constitutive modelling. *Proceedings of the Institution of Mechanical Engineers, Part C: Journal of Mechanical Engineering Science,* 218**,** 623-629.
TAVAKKOLIZADEH, M. & SAADATMANESH, H. 2001. Galvanic Corrosion of Carbon and Steel in Aggressive Environments. *Journal of Composites for Construction,* 5**,** 200-210.
WANG, Z.-Y. & WANG, Q.-Y. 2015. Fatigue strength of CFRP strengthened welded joints with corrugated steel plates. *Composites Part B: Engineering,* 72**,** 30-39.
WU, C., ZHAO, X., HUI DUAN, W. & AL-MAHAIDI, R. 2012b. Bond characteristics between ultra high modulus CFRP laminates and steel. *Thin-Walled Structures,* 51**,** 147-157.
XIA, S. & TENG, J. Behaviour of FRP-to-steel bonded joints. Proceedings of the international symposium on bond behaviour of FRP in structures, 2005. 419-26.
YU, Y., CHIEW, S. & LEE, C. 2011. Bond failure of steel beams strengthened with FRP laminates–Part 2: Verification. *Composites Part B: Engineering,* 42**,** 1122-1134.
ZHANG, S. S., TENG, J. G. & YU, T. 2013. Bond–slip model for CFRP strips near-surface mounted to concrete. *Engineering Structures,* 56**,** 945-953.
ZHAO, X.-L. & ZHANG, L. 2007. State-of-the-art review on FRP strengthened steel structures. *Engineering Structures,* 29**,** 1808-1823.